Journal of Science & Technology

About the Journal

Pertanika is an international peer-reviewed journal devoted to the publication of original papers, and it serves as a forum for practical approaches to improving quality in issues pertaining to tropical agriculture and its related fields. *Pertanika* began publication in 1978 as the Journal of Tropical Agricultural Science. In 1992, a decision was made to streamline *Pertanika* into three journals to meet the need for specialised journals in areas of study aligned with the interdisciplinary strengths of the university. The revamped Journal of Science & Technology (JST) aims to develop as a pioneer journal focusing on research in science and engineering, and its related fields. Other *Pertanika* series include Journal of Tropical Agricultural Science (JTAS); and Journal of Social Sciences and Humanities (JSSH).

JST is published in **English** and it is open to authors around the world regardless of the nationality. It is currently published two times a year, i.e. in **January** and **July.**

Goal of *Pertanika*
Our goal is to bring the highest quality research to the widest possible audience.

Quality
We aim for excellence, sustained by a responsible and professional approach to journal publishing. Submissions are guaranteed to receive a decision within 12 weeks. The elapsed time from submission to publication for the articles averages 5-6 months.

Indexing of *Pertanika*
Pertanika is now over 30 years old; this accumulated knowledge has resulted in *Pertanika* journals being indexed in SCOPUS (Elsevier), EBSCO, AGRICOLA, and EconLit. etc. JST is indexed in EBSCO.

Future vision
We are continuously improving access to our journal archives, content, and research services. We have the drive to realise exciting new horizons that will benefit not only the academic community, but society itself.

We also have views on the future of our journals. The emergence of the online medium as the predominant vehicle for the 'consumption' and distribution of much academic research will be the ultimate instrument in the dissemination of research news to our scientists and readers.

Aims and scope
Pertanika Journal of Science and Technology aims to provide a forum for high quality research related to science and engineering research. Areas relevant to the scope of the journal include: *bioinformatics, bioscience, biotechnology and biomolecular sciences, chemistry, computer science, ecology, engineering, engineering design, environmental control and management, mathematics and statistics, medicine and health sciences, nanotechnology, physics, safety and emergency management,* and related fields of study.

Editorial Statement
Pertanika is the official journal of Universiti Putra Malaysia. The abbreviation for *Pertanika* Journal of Science & Technology is *Pertanika* J. Sci. Technol.

Editorial Advisory Board

Pertanika Editorial Office

Publisher

Pertanika Journal of Science & Technology
Vol. 18 (2) Jul. 2010

Contents

Review Article

Selected Articles from the 9th National Symposium on Polymeric Materials 2009
Guest Editors: Mohd Sapuan Salit, Mohd Khairol Anuar Mohd Ariffin and Aidy Ali
Guest Editorial Board: Edi Syams Zainudin, Zulkiflle Leman, B.T Hang Tuah Baharudin,
Azmah Hanim Mohamed Ariff, Nur Ismarrubie Zahari, Nuraini Abdul Aziz and Faieza Abdul Aziz

Short Communications

Preparation and Characterization of Glass-Ceramic Synthesized from Soda Lime Glass and Wastewater Sludge

Zaidan Abdul Wahab[*], Syaharudin Zaibon, Khamirul Amin Matori, Norfarezah Hanim Edros, Thai Ming Yeow, Mohd Zul Hilmi Mayzan, Mohd Sabri Mohd Ghazali and Mohd Norizam Md Daud

Department of Physics, Faculty of Science, Universiti Putra Malaysia,
43400 UPM, Serdang, Selangor, Malaysia
[*]E-mail: zaidan@science.upm.edu.my

ABSTRACT

This paper reports an alternative method for making glass-ceramic from disposal waste water sludge and soda lime silica (SLS) glass. The glass ceramic samples were prepared from a mixture of wastewater sludge and SLS glasses, melted at 1375°C for 3 hours and quenched by pouring into water to obtain a coarse frit. The frit glass was then crushed and sieved to 106µm before it was pressed to a pellet. The sintering process was performed at various temperatures between 700-1000°C for 2 hours and morphologically characterized with XRD, SEM, and EDX. Overall results showed the crystalline phase of diopside sodian-critobalite glass-ceramic is depending on thermal treatment process and making them attractive to industrial uses such as in construction, tiling, and glass-ceramic applications.

Keywords: Soda lime silica glass, wastewater sludge, glass-ceramic, vitrification, diopside sodian

INTRODUCTION

The industrial development in Malaysia over the last decades has generated large amount of waste and by-products such as sewage sludge, coal ashes and mud, which contain significant amounts of heavy metals. Nowadays, wastewater sludge is mostly dumped in landfills; however, suitable sites are limited in many states and furthermore, this disposal method is considered to be environmentally unfriendly (Francis *et al.,* 2004). Disposal of wastewater sludge is becoming an increasing economic and environmental burden.

Wastewater sludge contains large amounts of Fe_2O_3, P_2O_5, SiO_2 and ZnO which are glass network formers and glass network intermediates. Therefore, it serves as a raw material source for the glass-ceramic production. The recycling of by-products and waste from industry in glass-ceramic production is an effective way to reduce the amount of wastes and to immobilize the element of their heavy metals (Erol *et al.,* 2007; Zhang *et al.,* 2007; Leroy *et al.,* 2001).

Glass-ceramics have significant advantages over traditional powder-process ceramics. Among other, the flexibility and ease of forming is afforded by high speed processes such as rolling, pressing, blowing, and drawing. Meanwhile, the uniformity of microstructure and reproducibility of properties, which depend on structural consistency, are other major advantages resulting from

the homogenous nature of the melting process (Swain *et al.,* 1994). Glass-ceramic materials are fine grained polycrystalline solids containing residual glass phase, produced by melting glass and forming it into products that are subjected to controlled crystallization (Karamberi and Moutsatsou, 2007). Controlled crystallization or heat treatments usually consist of a two-stage heat treatment, namely a nucleation stage and crystal growth stage. In the nucleation stage, small nuclei are formed within the parent glass. After the formation of stable nuclei, crystallization proceeds by growth of a new crystalline phase. The nucleation and crystallization parameters of glasses are important in the preparation of glass-ceramics with desired microstructures and properties (Zhang *et al.*, 2007). The aim of this research is to present the utilization of soda lime silica (SLS) glass and wastewater (WW) sludge in order to transform this waste to more stable and less toxic materials as glass-ceramics.

EXPERIMENTAL PROCEDURE

The raw material used in this study were SLS glass obtained from KFC Holdings (Malaysia) Bhd. Seri Serdang, and WW sludge from the water treatment plant, Hitachi Air-Conditioning, Bangi, Malaysia. In order to dry the waste, the WW sludge was heated in an oven at a temperature of 120°C for 24 hours. Later, both the SLS and WW sludge were crushed and sieved to106μm. The chemical compositions of SLS and WW sludge were determined by Shimadzu energy dispersive X-Ray fluorescence Spectrometer EDX-720 under vacuum condition.

Meanwhile, the glass ceramics were prepared from mixtures of 95-75 wt% SLS glass and 5-25 wt% WW sludge, as shown in Table 1. All samples batches were dry milled for 24 hours to ensure thorough and homogeneous mixing before they were melted in an alumina crucible at 1375°C in air at a heating rate of 10ºC min^{-1} for three hours in an electrically heated furnace. The melted material was poured into water and allowed to cool. Then, it was crushed and sieved to 106μm, and pressed into a 14 mm diameter pellet without any binders under a pressure of 3 tones. All pellets were sintered at various temperatures between 700-1000ºC for two hours at 100ºC intervals with heating and cooling rates of 2ºC min^{-1}.

TABLE 1
The composition of the prepared samples

SLS glass (wt%)	WW sludge (wt%)
95	5
90	10
85	15
80	20
75	25

The density of the samples was measured by using Archimedes principle with acetone as buoyant liquid using the relation, $\rho_s = (W_a/W_{ac})\rho_{ac}$, where ρ_s is the density of the sample, ρ_{ac} is the density of the acetone, W_a is the weight of the sample in air and W_{ac} is the weight of the sample in acetone. All the weights were measured with a digital balance.

XRD was used to identify the crystalline phases which occurred in all the samples, before and after sintering by using a Philips X'Pert XRD model PW3040/60 operating at 40 kV and 30 mA utilizing Cu Kα radiation. The detector was scanned over a range 2θ from 10 to 90° with 0.001° step size. The resulting diffraction patterns were analyzed using X'Pert HighScore software.

The microstructures were investigated by Scanning Electron Microscope (SEM) model LEO 1455 Variable Pressure attached with Energy Dispersive X-Ray (EDX). Selected pellet surface was ground on 600, 800, and 1200 grit abrasive paper (Buehler Silicon Carbide) and polished to obtain a flat and mirror surface. The polished samples were thermally etched at 100°C below their sintered temperature and gold coated using a Sputter Coated Baltec SCD 005.

RESULTS AND DISCUSSION

The chemical compositions of the SLS glass and WW sludge are shown in Table 2. The main elements of the SLS glass are SiO_2, Al_2O_3 which are categorized as glass network formers and CaO, Na_2O as glass modifiers. The WW sludge also contained SiO_2, Al_2O_3 along with P_2O_5 as a glass network formers but it also contained higher Fe_2O_3 which could act as a glass network intermediates. The presence of these glass network formers and modifiers clearly suggests that both the SLS glass and WW sludge have great potentials for the glass-ceramic preparation.

TABLE 2
Chemical composition of the tested soda lime silica glass and wastewater sludge in terms of oxide contents

Oxides	SLS glass	WW sludge
	wt% ± 0.01	wt% ± 0.01
SiO_2	66.50	6.07
CaO	26.00	2.30
Fe_2O_3	0.38	56.78
P_2O_5	0	10.86
ZnO	0.01	5.14
NiO	0	4.48
Al_2O_3	2.12	4.47
MnO	0	3.02
SO_3	2.22	2.98
Na_2O	1.43	0
MgO	0.63	1.78
TiO_2	0	1.64
K_2O	0.29	0
Sc_2O_3	0.27	0
ZrO_2	0.07	0.24
PbO	0.06	0.03
SrO	0.04	0.02
CuO	0	0.13
Cr_2O_3	0	0.08

TABLE 3
Density and sintering temperature of (85% SLS+15% WWS) glass ceramic

Samples	Sintering temperature (°C)	Density ρ (g/cm^3± 0.01)
A	700	2.58
B	800	2.60
C	900	2.64
D	1000	2.68
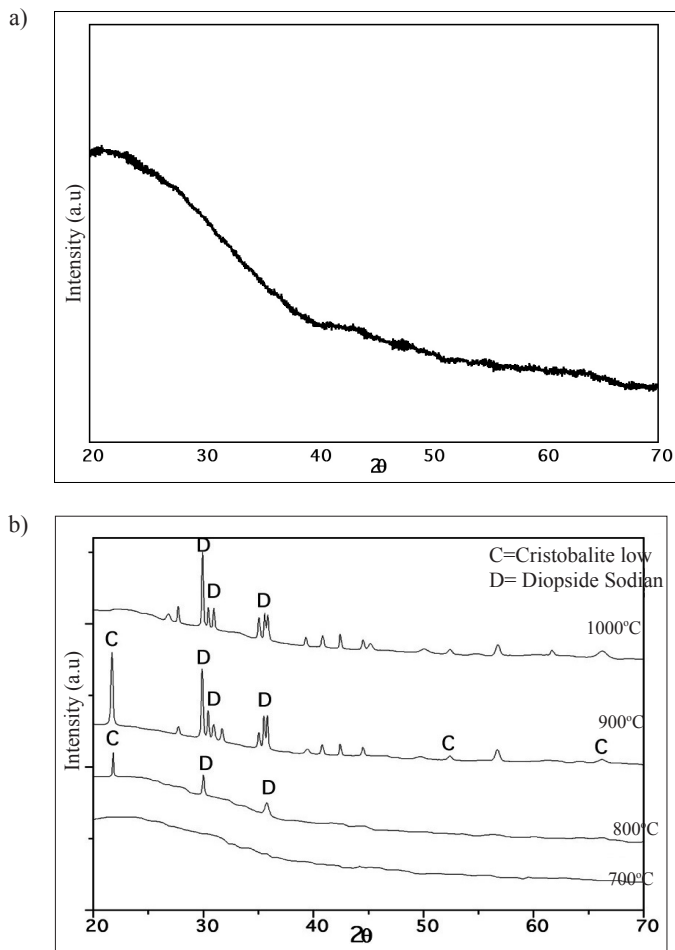
Fig. 1: a) XRD pattern of the untreated (SLS-WW sludge) glass; b) XRD patterns of the produced glass-ceramics indicating the presence of diopside sodian phases (ICSD code: 69702) and cristobalite low phases (ICSD code: 34931)
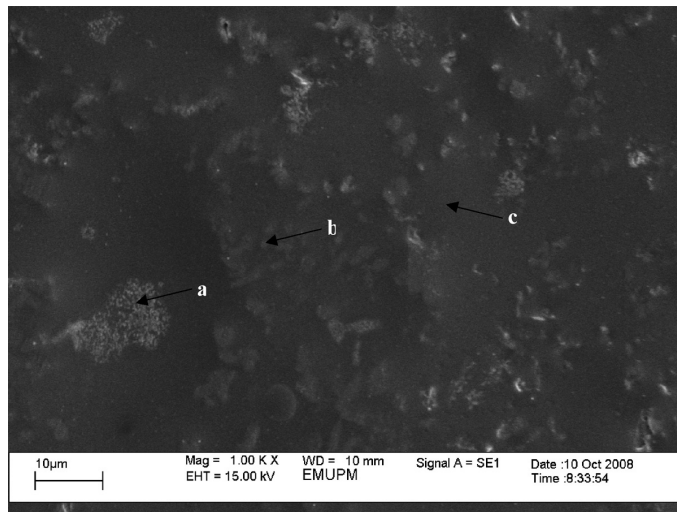
Fig. 2: SEM micrograph of 1000°C sintered glass-ceramic, Sample D

Table 3 shows the density of the produced glass-ceramic for the 85% SLS 15% WWS sample sintered from 700°C to 1000°C. It can be seen that the density of glass-ceramic increases with an increasing sintering temperature (Karamanov and Pelino, 1998). The produced glass containing 85 wt% of SLS glass and 15 wt% WW sludge was selected for this study, based on their basic processing characteristics such as ease of melting and ease to pour into water.

Fig. 1 (a) shows the XRD spectrums of glass frit that reveals the amorphous nature of the mixture of SLS glass and WW sludge which can be used to form glass. *Fig. 1 (b)* shows the XRD patterns from the glass-ceramic produced powder that had been heat treated at different temperatures ranging from 700°C to 1000°C for a constant time of 2 hours. The XRD scans verified that the glass-ceramic sintered at 700°C was an amorphous material. Nevertheless, there is no significant effect of heat below 700°C.

Glass-ceramic sintered at 800°C contained diopside sodian ($Al_{0.06}Ca_{0.91}Fe_{0.11}Mg_{0.9}Na_{0.05}O_6Si_{1.97}$) as the main crystalline phase and minor amount of cristobalite low (SiO_2). Glass-ceramic sintered at 900 °C had a similar mineral content as that of glass-ceramic sintered at 800°C. Diopside sodian was the principal crystalline phase together with cristobalite low.

The XRD analysis of glass-ceramic sintered at 1000°C showed that diopside sodian was the only crystalline phase occurred. In a crystallization study of the glasses produced from similar industrial wastes by Erol *et al*. (2007), diopside was reported as the predominant crystalline phase, especially at a heat treatment temperature of around 900°C. Hence, it is observed that a higher sintering temperature leads to the increment of crystalline diopside phase in the samples, as depicted by the XRD spectrums in *Fig. 1 (b)*. In addition, the presence of a variety of metals (even in small quantities) in these samples probably favours crystallization as well (Karamberi and Moutsatsou, 2007).

The results from the XRD analysis are strongly supported by the SEM observations. The SEM examinations were conducted to get a better understanding of the micro structural morphology. *Fig. 2* shows the SEM image of sample D glass-ceramics, while the EDX analyses on the surface of sintered glass-ceramics is shown in *Fig. 3*. The crystallized microstructure is divided into 3 groups: a) the small rounded crystals, b) cube-like crystals, and c) glassy surface. The EDX analysis shows

a)

b)

c)
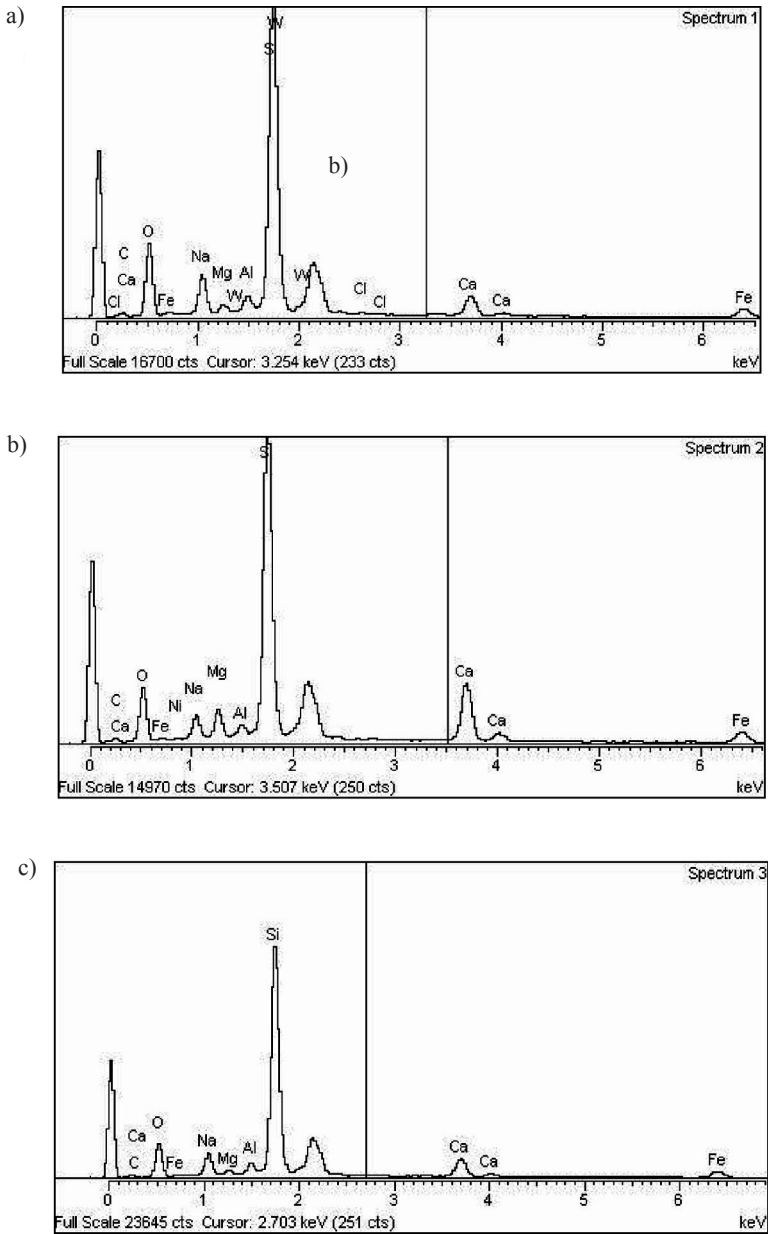
Fig. 3: EDX analyses of 1000°C sintered glass-ceramic, Sample D at 3 spectrum
(a) small rounded crystal, (b) cube-like crystal, and (c) glassy surface

that the small rounded crystals contain high Si, Na, Fe, and Ca. There are no significant differences between the compositions of the glassy phase surrounding with two types of crystals. Thus, both crystalline phases grow from the same parent glass and the XRD results indicate that the peaks of spectrum correspond to crystallized diopside sodian.

CONCLUSIONS

The wastewater sludge from the industrial waste water treatment plant was successfully vitrified by adding 85% of soda lime silica glass as a glass network former. Diopside sodian-cristobalite low glass-ceramics can be produced at relatively 800°C to 900°C via sintering and crystallization of glass powder compact.

ACKNOWLEDGEMENT

REFERENCES

Erol, M., Kucukbayrak, S. and Ersoy-Mericboyu, A. (2007). Production of glass-ceramics obtained from industrial wastes by means of controlled nucleation and crystallization. *Chemical Engineering Journal*, *132*, 335 – 343.

Francis, A.A., Rawlings, R.D., Sweeney, R. and Boccaccini, A.R. (2004). Crystallization kinetic of glass particles prepared from a mixture of coal ash and soda-lime cullet glass. *Journal of Non-Crystalline Solids*, *333*, 187–193.

Karamanov, A. and Pelino, P. (1998). Evaluation of the degree of crystallisation in glass-ceramics by density measurements. *Journal of the European Ceramic Society*, *19*, 649-654.

Karamberi, A. and Moutsatsou, A. (2007). Vitrification of lignite fly ash and metal slags for the production of glass and glass ceramics. *China Particuology*, *4*, 250-253.

Leroy, C., Ferro, M.C., Monteiro, R.C.C. and Fernandes, M.H.V. (2001). Production of glass-ceramics from coal ashes. *Journal of the European Ceramic Society*, *21*, 195-202.

Swain, M.V., Cahn, R.W., Haasen, P. and Kramer, E. J. (1994). Structure and properties of ceramics. *Materials Science and Technology*, *11*, 267-294.

Zhang, J., Dong, W., Li, J., Qiao, L., Zheng, J. and Sheng, J. (2007). Utilization of coal fly ash in the glass ceramic production. *Journal of Hazardous Materials*, *149*, 523-526.

Pertanika J. Sci. & Technol. Vol. 18 (2) 2010

229

Design and Development of Eggplant Harvester for Gantry System

Wan Ishak W.I.[*]**, W. H. Kit and Awal M. A.**

Department of Biological and Agricultural Engineering,
Faculty of Engineering, Universiti Putra Malaysia,
43400 UPM, Serdang, Selangor, Malaysia
[*]*E-mail: wiwi@putra.upm.edu.com*

ABSTRACT

This paper describes the design and development of harvesting system for the gantry system to harvest eggplants. For this purpose, the harvesting robot was successfully designed and fabricated for the gantry system to harvest eggplants. The operation of the harvester was controlled by Programmable Logic Controller (PLC). Basically, the limit switches, DC motor, and relay are connected to the PLC. Meanwhile, a PLC ladder diagram was designed and developed to control the operation of the eggplant harvester. A visual basic programme was developed to interface the harvester with a greenhouse gantry control system. A videogrammetry method was employed to calculate the distance between the stems of eggplants and the cutter of robot end effector. The end effector used electric as its power source and it was controlled via Programmable Logic Controller (PLC). Visual Basic Programme was developed to interface the harvester with the gantry control system. The accuracy of the videogrammetry was tested to be 67.2% for X-axis, 88.2% for Y-axis and 84.7% for Z-axis. Meanwhile, the speed of the end effector for harvester is 2.4 km/h and it could lift up to 55 cm. In order to determine detachment force of eggplant, 16 samples of mature eggplants were tested in a greenhouse, and as a result, more than 22.76 N force was needed to detach a mature eggplant inside the gantry system.

Keywords: Design, eggplants, harvester, gantry system

INTRODUCTION

A solution to solve acute shortage of labour in the plantation and agricultural sectors is to mechanize all operations. In particular, mechanization or the use of machines for all the operations will reduce manpower, lighten most burdens, increase productivity, as well as make agricultural work more interesting. The increasing use of modern technologies and production processes to increase productivity can reduce dependency on labour force, which is very important for both the agricultural and industrial sectors. Thus, in order to increase the productivity of agricultural products, engineering technology such as mobile robots, machine vision, artificial intelligence, mechanization, automation and robotic, remote sensing, global information system, and global positioning system must be introduced. In more specific, automation and robotic system should be introduced and developed immediately in the agricultural sector, particularly in solving harvesting, collection and transportation of agricultural products. Nonetheless, this technology is relatively new in the agricultural sector and thus, it still requires a lot of research to be carried out. For example, recent activities in the mechanization of harvesting of agricultural products have brought about significant reliance on the engineering properties of agricultural materials. Sound knowledge of the engineering properties of

_____
[*]Corresponding Author

agricultural materials should be of value not only to engineers, but also to food technologists and scientists who may find new uses for these products (Wan Ishak *et al*., 2007).

In some agricultural systems, robots have been used for various operations in static applications under controlled environment such as milking, shearing, harvesting, sorting, grading, micro propagation, as well as in some field operations. In the latter cases, literature offers a fair number of robotic systems which were developed to perform operations such as harvesting fruits and vegetables (oranges, tomatoes, and melons), pruning, etc. Some others which have been mentioned represent the opportunities to be better explored, including weed detection and control, and agrochemical applications (Hirakaw *et al*., 1998). Hayashi *et al*. (2002) developed an intelligent robot that could automatically harvest eggplants. The developed system comprised of a machine vision unit, a manipulator control unit and an end-effector unit, which could automatically perform basic harvesting operations like recognition, approach, and picking tasks. The system showed a successful harvesting rate of 62.5%, although the end-effector cut the peduncle at a slightly higher position from the fruit base. The execution time for harvesting of an eggplant was 64.1 seconds. Kondo *et al*. (1995) developed harvesting robots for tomatoes, petty-tomatoes, cucumbers, and grapes in Japan. These robots consist mainly of manipulators, end effectors, visual sensors, and travelling devices. The robots must work automatically by themselves in greenhouses or fields. Murakami *et al*. (1998) designed and developed a harvesting robot for cabbages. The robot consists of a 4-link hydraulic drive manipulator and a gripper to harvest efficiently without degrading the quality of the products, and a machine vision system which measures the size and locations of cabbages in the field. Meanwhile, Bulanon, Kataoka and Hiroma (2001) developed an algorithm for the automatic recognition of Fuji apples on trees for a robotic harvesting system. This system is used to differentiate the fruit from the other portions of the trees, such as the leaves and the branches, as well as to locate the fruit centre and the abscission layer of the fruit's peduncle. The location of the fruit centre and the abscission layer were determined using a geometrical approach and basic image processing procedures.

The objectives of this project were to design a suitable eggplant harvester for the gantry system and to operate the eggplant harvester using a computer control system. Thus, a Visual Basic programme was developed to interface the harvester with the gantry control system. In the project on the eggplant harvesting system, the gantry movement and robot end effector were controlled vertically, horizontally, and in the forward direction by the PLC. A web cam was mounted on the manipulator as the camera captures the image of eggplants and determines the locations of the vegetable by using the videogrammetry method. Through this particular method, the coordinates of the object targets were calculated using the triangulation principle based on the video scene of two different locations of cameras (Mohd. Hudzari *et al*., 2005). The manipulator will move forward to the eggplants and start the harvesting task. The robot arms will be lifted up to push the eggplants upward until they are detached from the tree. Finally, the fruit was transferred into a plastic bag which was placed beside the manipulator.

HARVESTER DESIGN

The fruit harvesting robotic system consists of four basic components, namely a manipulator, an end effector, a power source, and a controller. The manipulator is the arm of the robot which comprises of a system of mechanical linkages and joints that can move in different directions. The end effector is a device which is connected to the wrist flange of the manipulator's arm. In the fruit harvesting operation, the end effector is very important, since it has to meet different criteria for fruit detachment. The main function is to detach the fruit from the tree. The robot arm consists of an arm and a cutter. The robot arm lifts up and pushes the eggplants upward and the cutter will
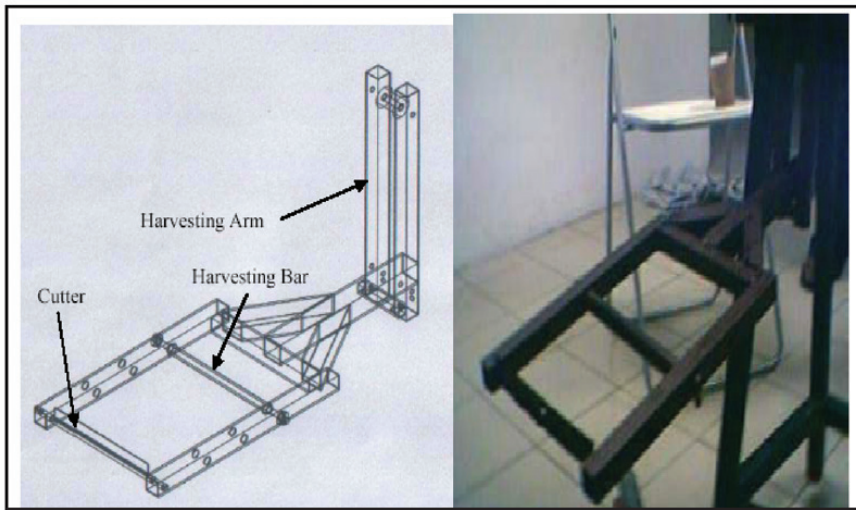
Fig. 1: The structure of end effector

then cut the peduncle of the eggplants during harvesting process. *Fig. 1* shows the design and fabrication of the robot arm harvester end effector. It consists of a cutter, a harvesting bar, and a harvester arm.

The power supply is the unit that supplies power to the controller and the manipulator. The controller is used to control the manipulator movements of the robot, as well as to communicate and control the peripheral components such as machine vision for fruit identification and sensor. Unlike most industrial robots, the fruit harvesting robot will not be stationary. Rather, it will be mounted on a platform, and is able to move in the orchard under various soil and topographic conditions.

Mechanical components such as lead screw, belt, pulley, gears, and chains are used as means of transmitting power from the motor and parts that move on the robot. Lead screw is the more common types of drive mechanisms found in any linear motion machinery. This screw comprises of threaded rods that are fixed with a nut. The basic function of a screw is to convert rotary input motion to linear output motion. The nut is constrained from rotating with the screw, so that when the screw is rotated, the nut travels back and forth along the length of the shaft. Industrial motors are used to convert electrical energy to mechanical energy and they are neither precision speed nor precision positioning devices. For many automated devices and systems, precise positioning is required. Stepper motors are unique because the motion of the rotor is precisely determined by the input signals of the motor. The stepper motor input signals consist of a series of pulses, with the rotor advances one step for each pulse. The motors of the stepper do not require any encoder and servo-control system to achieve the precise positioning required in robotic applications because of the fixed relationship between input signals and rotor motion.

DC servo-driven type robots invariably incorporate feedback loops from the driven components back to the driver. Thus, the control system continuously monitors the positions of the robot components, compares these positions with the positions desired by the controller, and notes any differences or error conditions. The DC current is applied to each motor to correct error conditions until the error goes to zero. In this project, 24 VDC was required for most parts of the equipment. A switching power supply unit was used to convert the AC voltage from the main source to 24 DC voltages. A 12v, 40rpm DC motor was used to connect to the lead screw. The motor rotates

clockwise and counter-clockwise to push the robot arm forward and reverse. Meanwhile, a lead screw was used to transmit power from the DC motor to the end effector. Limit switches were used to start, stop, slow down, speed up, or reboot the robot operations. The DC motor was installed to the lead screw to move it forward and backward as well as to push the robot arm for lifting up and down movements.

At the designing stage, the following limitations were considered: (1) working space of the gantry robot were 300m x 600m x 220m; (2) the maximum height of the end effector was 762 mm; (3) the system should be able locate the position of eggplants; (4) the end effector should be able to detach the eggplant from tree; (5) the accuracy of videogrammetry method; and (6) detachment force of eggplants. *Fig. 2* below illustrates the design and development of the Automatic Eggplant Harvesting System.
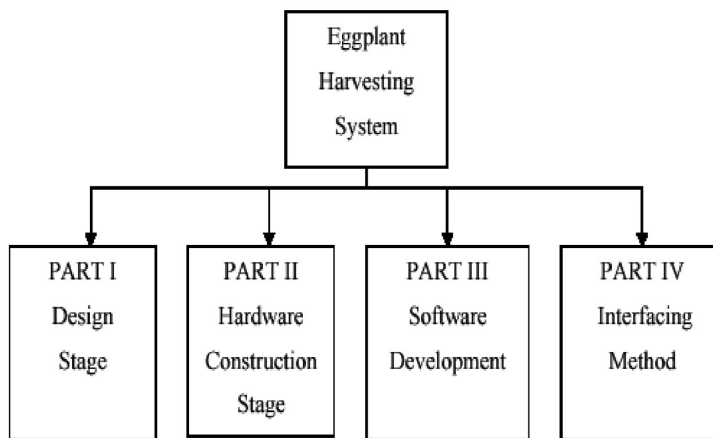
Fig. 2: Four project activities for the development of an
automatic eggplant harvesting system

Programmable Logic Controller (PLC)

A programmable logic controller is defined as a digital-operated electronic apparatus that uses a programmable memory for the internal storage of instructions to implement specific functions such as logic, sequencing, timing, counting, and arithmetic, as well as to control various types of machines or processes through digital or analogue input/output modules (Keramas, 1999). The control of the gantry system is operated by a computer and PLC. The PLC consists of the input interface which receives and converts signals from the process into a form that can be understood by the central processing unit. The Central Processing Unit (CPU) interprets the input signals and carries out the control actions according to the programme stored in its memory. It also communicates the decisions as action signals to the output interface. The function memory section is to store the logic control circuit and fundamental operating data for the logic control circuit. It also acts as a scratch pad for the CPU to store external data for future use or immediate actions. The programming language was used to write a logic control programme into the PLC. The logic control programme such as the ladder diagram language represents relay logic control scheme, coils, and contacts. The programming tool provides the connection between the programmer and the PLC. The programmer

designs the necessary control circuit and programmes it in a language used by the PLC. The output interface takes signal from the CPU and converts the digital signals into forms that are appropriate to produce control actions. The signals are then fed to external devices such as motors, pumps, valves, and heaters. In this project, NAIS PLC model FP2 was used to control the system. This PLC comes with a power supply, central processing unit (CPU), input modules, output modules, RS232 communication ports, and a special function module to control motor drivers which support a maximum of four axes. It has a maximum of 768 points for both the inputs and outputs.

Machine Vision System

The first major task of a fruit harvesting robot is to identify fruit on the tree and determine its location. While humans can recognize familiar objects from almost any angle, it is difficult to replicate this intricate process by machine vision. Fruit are objects of various shapes, sizes and colours, existing in random positions in trees of various sizes, volumes, and limb structures. The common objective was to develop a computer vision system to obtain a digital image of the fruit in the trees, and develop an image-processing algorithm capable of identifying and determining the locations of fruits in these images (Sarig, 1990). Machine vision is often thought of as having the capability to sense, store, and reconstruct a graphic image that matches the original image as closely as possible. It has specific tasks such as checking for proper orientation, identifying parts, searching for specific defects, or checking alignment for assembly (Asfahl, 1992).

Videogrammetry is *per se* fully three dimensions, and works in a non-contact mode to determine and track even very complex point clouds with a high number of particles, delivers very precise and reliable results, and can be fully automated. Two parallel webcams are used to determine the distance between the object and the camera. A Lifeview FlyCam USB 1.00 camera was used as a machine vision system in this project. The webcam has an image resolution of 352x 288 pixels.

Software Development

Robot programming language is a set of words and rules governing their use, employed in constructing a programme. The programme provides the control instruction required for the robot to perform its tasks. The robotic programme instructs a robot how to execute some motions. In other words, this programme supplies the intelligence that enables the robot to receive, understand, and carry out any given tasks.

The PLC programme development software was used to create, edit, store, and monitor PLC user programmes. The environment of FP WIN GR was developed by Matsushita Electric Works LTD. FP WIN GR provides 3 programming styles, namely Ladder Symbol Mode, Boolean Ladder Mode, and Boolean Non-Ladder Mode. In this project, the ladder symbol mode was used to create the PLC programming Ladder diagram. The PLC performs its task after a user programme is loaded into the CPU internal memory. This programme was developed by a personal computer, Visual Basic, and PLC programming software. The programme was downloaded to the PLC via a communication cable through the RS232 port. The software used in this project is known as the FPWIN GR. The first step in the software development is to do a sequence of the processes involved in the whole system. A flowchart should be developed in such a way that it can represent the total programme logic. A programme called 'Eggplant Harvester' was developed to control the end effector operations and videogrammetry. Using this particular programme, an operator can use it to give instructions to the gantry and harvester so as to perform the tasks. *Fig. 3* shows the flowchart of the software development for this project.
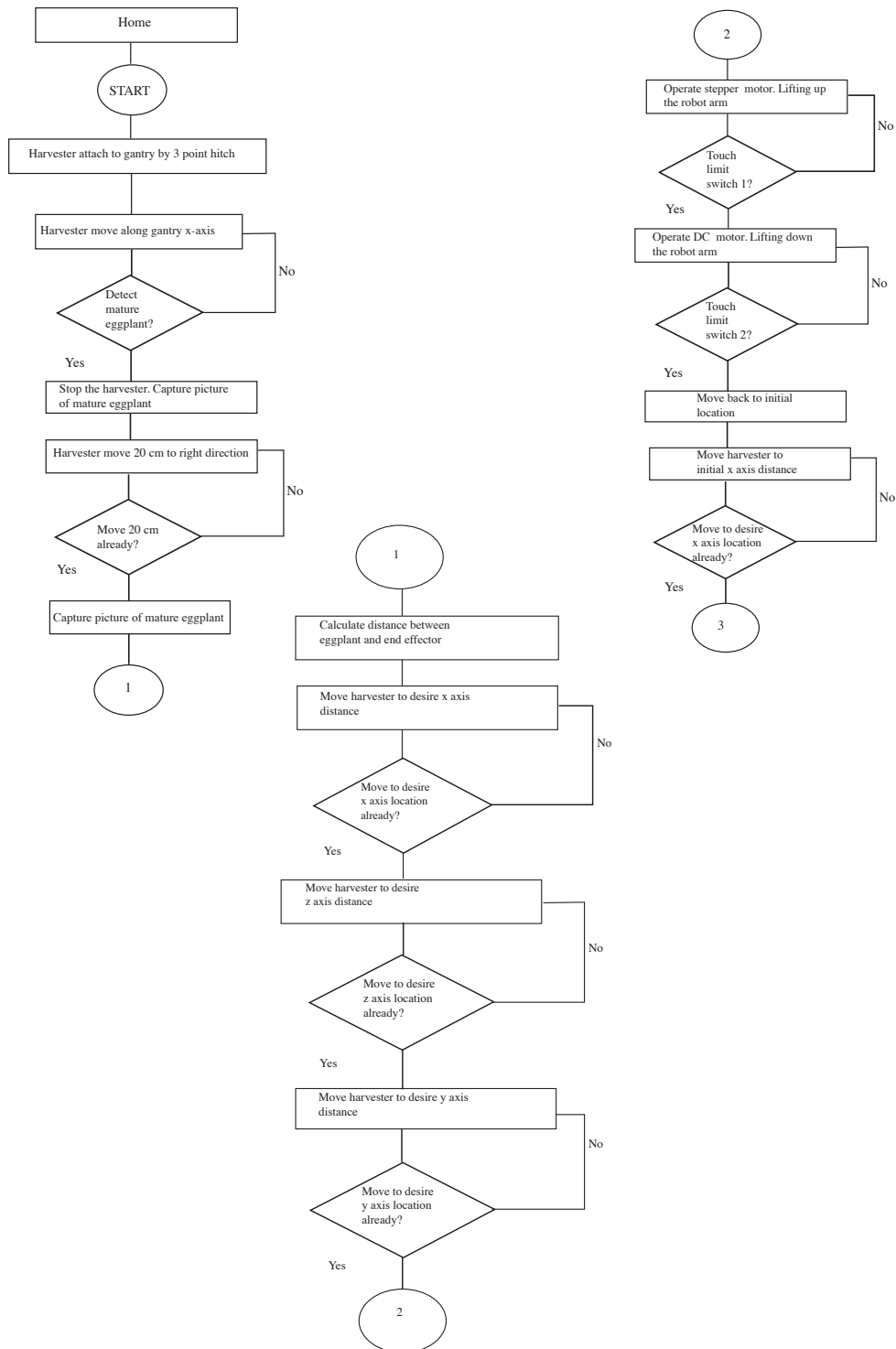
Fig. 3: Flowcharts of the programme

236

Pertanika J. Sci. & Technol. Vol. 18 (2) 2010

Harvester Operations

Initially the harvester was in home position. The harvester was then attached to the three-point hitch of the gantry. The gantry and the harvester moved along the X axis, while the operator monitor the eggplant tree used a webcam which was attached to the harvester. If the operator detects any mature eggplants in tree, he would stop the movement of the gantry by clicking the stop button and automatically capture the picture of mature eggplant by clicking the capture button. The harvester would automatically move to the right, i.e. about 20 cm in distance, and the operator would then recapture the picture of the same egg plant. When the picture appears on the screen, the operator has to click on the peduncle of the mature eggplant in the same location. After that, the programme will automatically calculate the distance between the peduncle eggplant and the robot end effector cutter. After the location of the mature eggplant is determined, the harvester will move to the desired X axis, Z axis, and Y axis distance. Then, the DC motor will operate in the counter-clockwise direction and the robot arm will be lifted up to cut the peduncle of the eggplant. The motion of the robot arm is stopped when it touches the limit switch 2. The relay changes the polarity of the motor when the limit switch 2 is activated. The motor will then turn in a clockwise direction and the robot arm will move down until it touches the limit switch 1. If the limit switch 1 is activated, the DC motor will be stopped. After the eggplant has been detached from tree, the harvester will move back to the initial position. The harvester will move to another row to perform another harvesting process.

1. The harvester is attached to the gantry robot by the three-point hitch.
2. The harvester moves along the gantry x-axis and the operator monitors the eggplant tree through a video which is captured by a camera.
3. If any mature eggplant is detected, the operator will stop the harvester manually.
4. The operator captures a picture of the mature eggplant, and the harvester will then move 20 cm to the right of the tree and recapture the eggplant picture.
5. The operator clicks the peduncle of the mature eggplant on both pictures to make sure that the same object is pictured.
6. The distance between the peduncle mature eggplant and the end effector is then calculated.
7. The gantry will move the harvester to the desired location.
8. The DC motor will operate and push the robot arm upward as its lifting operation. The cutter at the end effector will then cut the peduncle of eggplant during the process.
9. Mature eggplant is then detached from tree and dropped into a plastic bag.
10. The gantry will move the harvester to its initial place and repeat step 2.

RESULTS AND DISCUSSION

The average detachment force for a mature eggplant inside the gantry system was determined to be 22.76N. *Fig. 4* shows the output data for this particular project.

Sample No	Diameter of eggplant (cm)	Length of eggplant (cm)	Weight of eggplant (g)	Pulling strength (kg)	(N)	Angle of pulling
1	4	13	160	2.5	24.53	0°
2	3	19	70	2	19.62	0°
3	3	15	60	2.3	22.56	0°
4	3	10	80	3	29.43	0°
5	3	27	100	5	49.05	0°
6	2.5	15	40	1	9.81	0°
7	2	14	40	3	29.43	0°
8	2.5	18	60	2.5	24.53	0°
9	2.5	18	80	2	19.62	0°
10	2.5	15	50	2.5	24.53	0°
11	2.3	18	60	2.5	24.53	0°
12	2	10	30	1.5	14.72	0°
13	2	11	30	2.3	22.56	0°
14	2	12	40	2.5	24.53	0°
15	2	12	40	1	9.81	0°
16	2	11	30	1.5	14.72	0°

Fig. 4: The output data to determine the pulling strength of peduncle eggplant

Based on the data presented in *Fig. 4*, the average detachment force is calculated as:
= (2.5+2+2.3+3+5+1+3+2.5+2+2.5+2.5+1.5+2.3+2.5+1+1.5) kg / 16
= 2.32 kg
= 22.76 N

For the videogrammetry accuracy test, the average relative error in the X axis, Y axis, and Z axis was found to be 32.8%, 11.8% and 15.3%, respectively. The accuracy of the videogrammetry varies significantly due to several reasons such as the resolution and quality of the camera, size of the object measured, the number of video used, and the location of the camera.

The End Effector Test

In this study, the end effector was successfully tested in the laboratory. During the operation of the DC motor, the lead screw pushes the robot arm to move in either forward or backward direction. The maximum height of the lift was found to be 55 cm from the initial position. The average time for the robot arm to be lifted up and pulled down for the harvesting operation was 42 seconds. Visual Basic Programme and ladder diagram were also tested. The 'Eggplant Harvester' software was developed to capture images and to monitor the harvesting system.
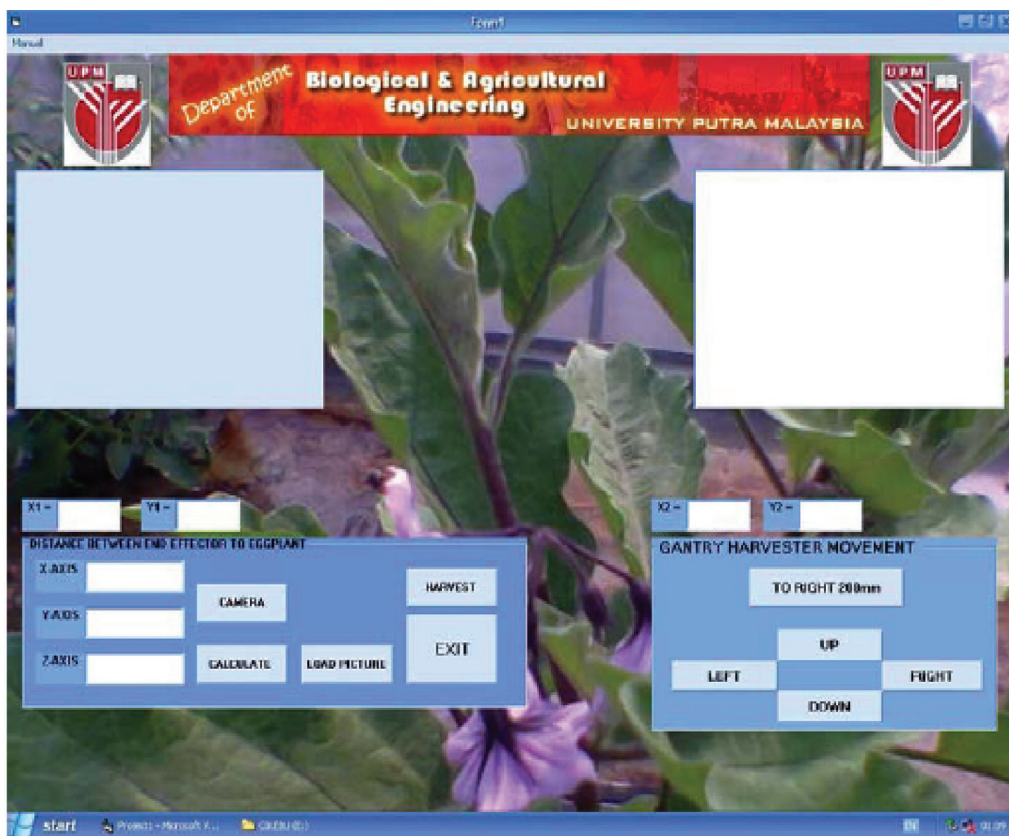
Fig. 5: User interface of eggplant harvester programme

The Software Test

The operator started the Gantry Control programme and the main form of the window was then displayed. The operator pushed or pressed the "Monitoring" click button to proceed to the next page programme. In this window, the operator selected the crop followed by the harvesting operation. If the operator clicked on "Exit" button, this programme would then be terminated.

Firstly, the operator has to connect this programme to the webcam. Then, he has to click on the button "CAMERA" to load the webcam software and video. If a mature eggplant is detected and shown in the video, the operator has to capture the image using the webcam software. He will then click on the button "second camera" for the camera to capture the image to be used by the second camera which is situated 20 cm away from the first camera. The operator clicks on the button "LOAD PICTURE" to load both images on the picture box. The "CALCULATE" button is then selected count the distance between the end effector to the mature eggplant. *Fig. 5* and *6* show the developed graphical user interface for this project.

A programmable logic controller programme was developed to control the sequence of movements and operations of the harvester. For this purpose, the programme was downloaded to the PLC through a communication cable between the PLC and the computer. *Fig. 6* shows a sample of the output data from the computer programme for this project.
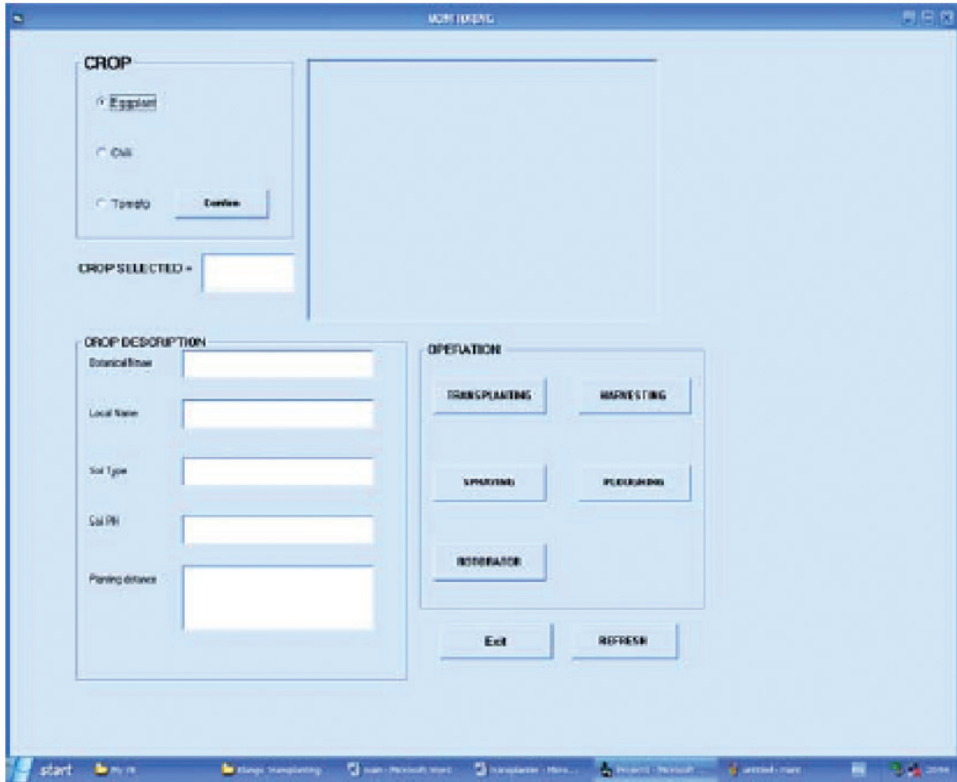
Fig. 6: Selection form of the programme
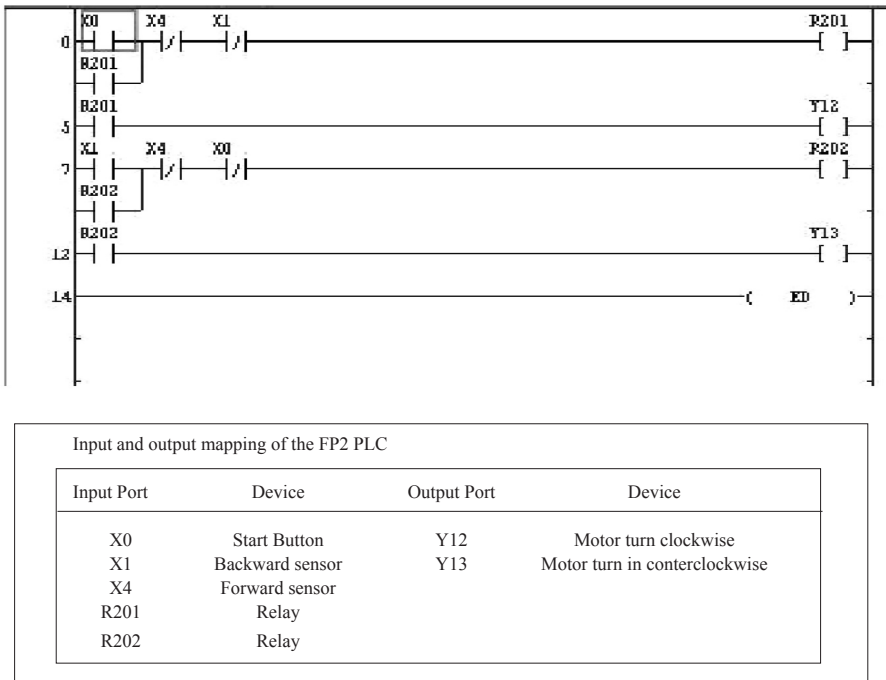
Fig. 7: The sample output of ladder diagram

CONCLUSIONS

The eggplant harvester for the gantry system of the green house was successfully designed, fabricated, and tested. The operation of the harvester is controlled by PLC. Basically, the limit switches, DC motor and relay are connected to the PLC. A PLC ladder diagram was then designed and developed to control the operation of the eggplant harvester. The speed of the end effector was 2.4 km/h and it could lift up to 55 cm.

A machine vision system programme was developed using Microsoft visual basic. The function of this programme is to determine the three dimension axis location of eggplants. The videogrammetry method was employed to calculate the distance between the stem of eggplants and the cutter of the robot end effector. The accuracy of the videogrammetry was tested to be 67.2% for the X axis, 88.2% for the Y axis, and 84.7% for the Z axis. Thus, the maximum absolute error measured in the three dimensional locations was 42.3 mm (X axis), 93.79 mm (Y axis), and 20 mm (Z axis). The minimum absolute errors for X axis, Y axis, and Z axis were 15 mm, 18 mm, and 14 mm, respectively.

REFERENCES

Bulanon, D.M., Kataoka, T., Ota, Y. and Hiroma, T. (2001). A segmentation algorithm for the automatic recognition of Fuji apples at harvest. Silsoe Research Institute.

Hayashi, S., Ganno, K., Ishii, Y. and Tanaka, I. (2002). Robotic harvesting system for eggplants. *JARQ*, *36*(3), 163 – 168. Retrieved from http://www.jircas.affrc.go.jp.

Hirakawa, A.R., Saraiva, A.M. and Cugnasca, C.E. (1998). Wireless robust robots for application in hostile agricultural environment. University of Sao Paulo, 62.

Keramas, J.G. (1999). *Robot Technology Fundamentals*. Delmar Publishers.

Kondo, N., Monta, M. and Fujiura, T. (1996). *Fruit Harvesting Robots in Japan*. Pergamon Press.

Murakami, N., Otsuka, K., Inoue, K. and Sugimoto, M. (1998). Robotic cabbage harvester. Department of Farm Mechanization, National Agricultural Research Center, Kammondai 3-1-4 Tsukuba Science City, Japan.

Mohd. Hudzari Razali, Wan Ishak W.I., I. Napsiah, S. Nasir and S. Rashid. (2005). Videogrammetry technique for arm positioning of bio-production robot. *International Advanced Technology Congress 2005* (Atci 2005). 6-8 December, Putrajaya, Malaysia.

Sarig, Y. (1990). Robotics of fruit harvesting: A state-of-the-art review. Agriculture Research Organization, Institute of Agriculture Engineering, Israel.

Ting, K.C. and Kondo, N. (1998). Robotics for bioproduction systems. ASAE.

Wan Ishak W.I. (2007). Mechanization strategies and challenges in Malaysian agricultural sector. *International Conference on Control, Instrumentation and Mechatronics Engineering, CIM 07*. 28-29 May, Johor Bharu, Johor.

Software Development for Real-Time Weed Colour Analysis

Wan Ishak W. I[*] and Khairuddin Abdul Rahman
Department of Biological and Agricultural Engineering,
Faculty of Engineering, Universiti Putra Malaysia,
43400 UPM, Serdang, Selangor, Malaysia
[*]E-mail: wiwi@eng.upm.edu.my

ABSTRACT

The application of computer and machines for agricultural production has been one of the outstanding developments in Malaysian agriculture, especially in overcoming labour shortages in Oil Palm plantations. The on-line automated weedicide sprayer system was developed at Universiti Putra Malaysia to locate the existence and intensity of weeds in real-time environment and to spray the weedicides automatically and precisely. During the start of the spraying operation, the web camera will initially capture the image of weeds. The computer programme will compute the red, green, blue (RGB) values in the form of computer pixel. These values will be used as reference RGB values to be compared with the RGB values of the weeds captured real-time during the spraying operation. The sprayer nozzle will be turned 'on' or 'off', depending on the percentage or intensity of the green colour pixel value of weeds. The sprayer valve will open the nozzle/s when the camera detected the presence of weeds. The purpose is to reduce wastage, reduce labour, reduce cost, and control environment hazard.

Keywords: Weeds, sprayer nozzle, chemical spray, WEB cam, automation, outdoor vision, image processing

INTRODUCTION

Weeds compete with crops for water, light, nutrients and space, and therefore, it reduces crop yields as well as affects the efficient use of machinery. Manual weeding is a laborious operation, thus mechanical or chemical applications are the best options. The most widely used method for weed control is to use agricultural chemicals (herbicides and fertilizer products). In fact, the success of U.S. agriculture is attributable to the effective use of chemicals. Chemical sprayer is the most popular method to eradicate weeds in Malaysia, but this causes hazardous and harmful effects to the environment, crops and human. Weed detection at the time of spraying could be very valuable, particularly to reduce costs involving the uses of chemicals and in reducing environmental contamination. Thus, an on-line automated sprayer was introduced to farmers in Malaysia so as to locate in the real time environment the existence and intensity of weeds and to spray the weedicides automatically and precisely. Many researchers have attempted to detect weeds in crop fields with machine vision system (Choo *et al*., 1990; Tillet, 1991). The purpose of the smart sprayer is to reduce wastage, labour, and cost, control environment hazard and to attract younger generation to have the interest in the agricultural sector.

The advent of computer and camera vision has given a valuable tool for researchers to develop automation systems to increase mechanization technology in the agriculture sector. In particular, vision is the most powerful and complicated sense. It provides us with a remarkable amount of information of our surroundings and enables us to interact intelligently with the environment.

Vision systems are a new field of research in the agricultural sector. Research on machine vision has been applied to agriculture to identify weeds. Many researchers have tried various image processing methods, and worked in different environments; however, most of the work has been done indoors (Abdul Malik Hamid, 1998; Hazlina Hamdan, 2005). Most of the work in outdoor lighting conditions has been associated with robotic fruit harvesting (Kondo and Ting, 1998). In this research, a machine vision technology was developed to identify weeds in the outdoor environment. There is a practical need for a real time machine for weed detection and to reduce the use of and dependency on agricultural chemicals.

In this project, the ATV Polaris 500 ATP vehicle was installed with a commercial boom sprayer. The commercial sprayer was modified with an automation system guided with a web camera to detect the presence of weeds. The commercial sprayer was modified and installed with 2 cameras for 6 nozzles spaced at a distance of 45 cm. The sprayer was installed with the web camera, portable computer, ICPCON I-7042, and SST-2400 radio modem. Module ICPCON I-7042 and radio modem (SST-2400) were selected as data acquisition and control. SST-2400 radio modem is the heart of the PC based control system. They provide digital input/output and other functions. The radio modem that was set as a receiver receives the signals and transfers them to the ICP modules (I-7042) via RS-485 bus. The ICPCON I-7042 and SST-2400 were later replaced with locally made 'parallel port controller board'. The purpose of this study was to develop an automated sprayer using a camera vision for the application of chemicals on an autonomous all terrain vehicles (ATV). The specific objective of this project was to detect the presence of weeds in real-time and to spray chemicals precisely to eradicate weeds.

METHODOLOGY

In this project, the commercial sprayer was modified. The normally close (NC) solenoid valve was mounted at the nozzles for the purpose of switching ON/OFF the nozzles. The nozzles will be turned 'ON' when the camera detects weeds and turned off when the camera does not detect any weed. These switching ON/OFF functions will reduce the amount or volume of chemicals to be sprayed and therefore help to reduce hazards to the environment and production cost. The normally open (NO) solenoid valve was installed at the chemical tank. If there was nothing to be sprayed, the NO solenoid valve would by-pass the chemical liquid back to the tank. This is meant to avoid the high-pressure build-up in the main sprayer line. *Fig. 1* shows the ATV mounted with an automatic sprayer.

Two PC web cameras were installed to the left and right sides of the boom sprayer. The camera on the left will display the image of the weeds to be sprayed by three nozzles labelled as nozzles 1, 2 and 3, whereas the camera on the right is meant for the other 3 nozzles, namely nozzles 4, 5 and 6. Each camera covers 3 segmented displayed images for the 3 specific areas of applications from the 3 nozzles. These cameras control the area of spraying. The respective nozzles will trigger the spray solution when the weeds appear in green at their respective areas. In addition, selective spraying can be carried out whereby only respective nozzle will spray the chemicals in the presence of the weeds. The respective nozzle will be closed when the green colour of the weeds is not detected.

The variation of the daylight of the outdoor environment changes the light intensity, and thus changes the RGB of the agriculture products. Therefore, the values of RGB of the images captured vary according to the time of the day and to the presence of clouds. In order to avoid the variations of light intensity of the outdoor environment, the RGB values colour of the weeds were captured in real time. These values were saved and used as a reference RGB colour. During the spraying operation, the on-line cameras captures and analyzes the image of weeds in real-time and compares with the reference RGB colour of the weeds which is captured on the real-time basis. In short, the

Fig. 1: A web camera and communication devices installed to the automatic sprayer

spray nozzle will be opened or closed based on the presence and intensity of weeds captured on the camera.

Image Processing

In computer, the intensity of the colours is based on bits. A 24-bit colour is required to represent a non-normalized RGB co-ordinated with a decimal value from 0 to 255 (Rafael and Richard, 2002). *Fig. 2* shows the RGB 24 bit colour cube to demonstrate the above. A colour in the RGB colour model can be described by indicating how much of each of the red, green, and blue color is included. A full intensity red in the RGB colour model is (255, 0, and 0). A colour camera output can be decoded into three images to represent the RGB components of the full image. The three components of the colour image can be recombined in the software or hardware to produce intensity, saturation and hue images, which can be more convenient for subsequent processing.
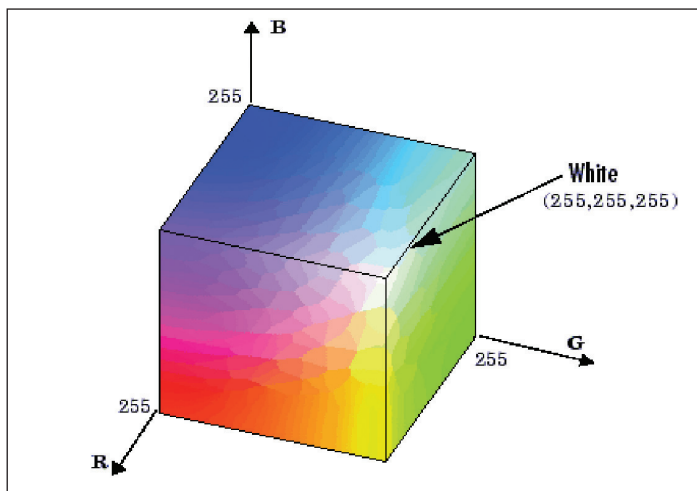
Fig. 2: RGB 24 bit colour cube

This spraying system uses USB webcam to capture the images of weeds. The image is sampled into a rectangular array of pixels. Each pixel has x and y coordinates that correspond to its location within the images. *Fig. 3* shows a sample of the image captured using the USB web camera. The x coordinate is the pixel's horizontal location, whereas the y coordinate is the pixel's vertical location. The pair of coordinates (x, y) is called the intensity or grey level of the images of the point. The grey level images are then calculated by linear combination of an RGB vector of the colour images. The Visual Basic programme (VB) reads the RGB values of each pixel of the total area of the image. The RGB colour pixels range from 0 to 255. The basic API pixel routines obtained from the VB programming language is used to read the RGB value pixel by pixel of the image. The function reads one by one from the first pixel to the end of the pixel coordinate. The algorithm used to read all the pixels of the images is shown in *Fig. 4*. This algorithm shows all the pixel values for each coordinate of the image. Each coordinate will extract the RGB colour pixel which ranges from 0 to 255. When the user clicks on the camera for a specified piece of weed, the programme will then compute the RGB pixel values.
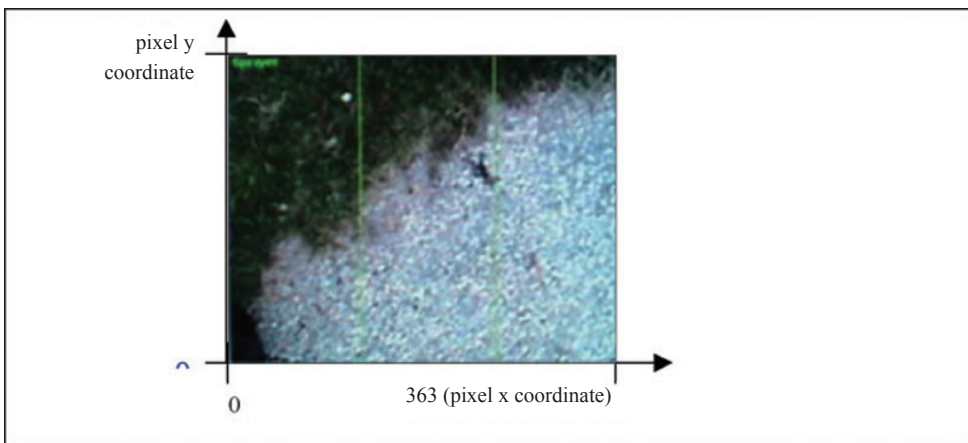
Fig. 3: Sample images captured and analyzed

From two-dimension function, f(x,y);
      Read for f(x) = 0 until image width value
         Read for f(y) = 0 until image height value
            Get pixel value on coordinate pixel, f(x,y);
        End loop
      End loop

Fig. 4: Algorithm to extract pixel value from an image

During the start of the spraying operation, the web camera will initially capture the image of weeds and analyze the red, green, blue (RGB) values in terms of computer pixels. Through appropriate real-time image processing algorithm, which is based on colour image as raw data, the information pertaining to weeds locations and their densities is therefore extracted. The image is sampled into a rectangular array of pixels. Each pixel has x, y coordinates that correspond to their locations within the images. The green weed colour is selected as a reference point and set at the range of plus and minus 10 from the RGB selected pixel values. The programme illustrated in *Fig. 5* shows that the range of plus and minus 10 values from the RGB selected pixel value are set. These values are used as the reference to compare with the values of the RGB of weeds captured real-time during the spraying operation. The information of the reference point will be sent to a sprayer controller. When the camera captures the real time image of weeds, the computer will then calculate the percentage of the green pixels available in the frame and compare with the RGB pixel of the reference point. The pump and nozzles will open or close based on the percentage or intensity of the green colour pixel value of the weeds. In the real-time system, the respond time is a critical parameter. Therefore, the overall system must be well visualized and designed for a successful integration.

R pixel value range
= (R > R pixel value selection -10) and (R < R pixel value selection +10)
G pixel value range
= (G > G pixel value selection -10) and (G < G pixel value selection +10)
B pixel value range
= (B > B pixel value selection -10) and (B < B pixel value selection +10)

Fig. 5: Algorithm for the colour pixel range from the pixel selected

Software Development

In this project, Microsoft Visual Basic 6.0 was used to develop the graphical user interface (GUI) to monitor the parameters controlling the autonomous sprayer operations. *Fig. 6* illustrates the flow chart of the software showing the algorithm for the automated weedicide sprayer spraying system. The algorithm starts with the camera capturing the image, analyses it, calculates the percentage of RGB and instructs the nozzles to open or close for the spraying operations. *Fig. 7* shows the GUI screen of the monitor which is divided into 3 frames as captured by one camera. The three frames were for the 3 units of the spray nozzles. The camera grabs the image and analyzes the red, green, blue (RGB) values in terms of computer pixels. The sprayer nozzle will be turned on or off, depending on the percentage or intensity of the green colour value of weeds.

Each feature in the GUI has its own special code. Some examples given below illustrate the source code for nozzle 1 which is connected to channel no. 9, and nozzle 2 to channel no. 8.

Source code for the nozzle:
Private Sub Noz1on_Click ()
DCON_X1.ChannelNo = 9
DCON_X1.DigitalOutCh True
End Sub

Private Sub Noz2on_Click ()
DCON_X1.ChannelNo = 8
DCON_X1.DigitalOutCh True
End Sub

Private Sub Noz1off_Click ()
DCON_X1.ChannelNo = 9
DCON_X1.DigitalOutCh False
End Sub

Private Sub Noz2off_Click ()
DCON_X1.ChannelNo = 8
DCON_X1.DigitalOutCh False
End Sub
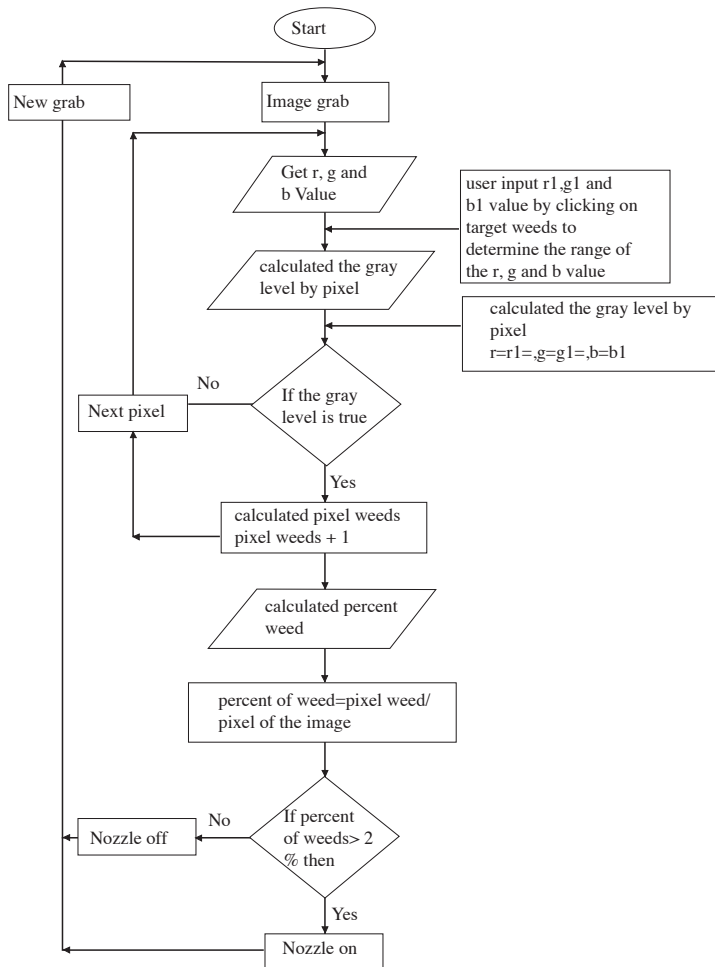
Fig. 6: Flow chart of the software for the automated weedicide sprayer
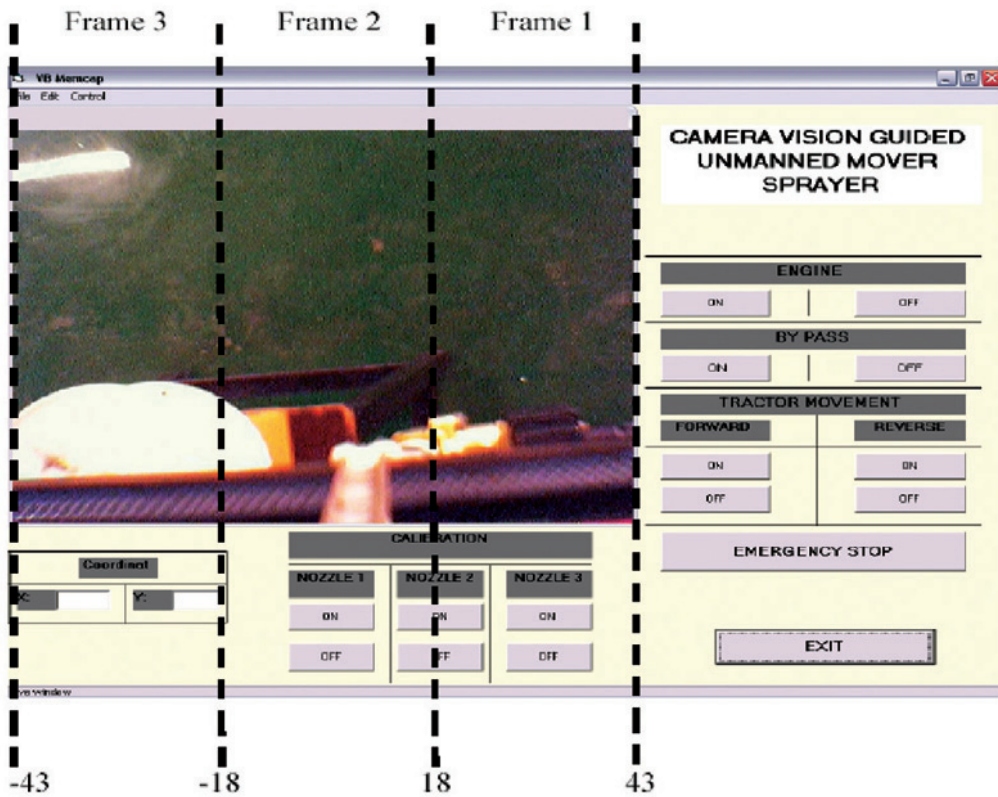
Fig. 7: Boundaries of image frames in GUI

The information presented in Table 1 is useful in determining the task for each output channel of the ICPCON I-87057. The software packages for ICPCON I-7000/8000/87K series module used were I-7000/8000 Utility and NAP 7000X. Table 1 shows the output signals assigned to the ICPCON I-87057. Meanwhile, the source codes were written by referring them to the information given in Table 1. It also helps in the troubleshooting process whenever problems occur.

TABLE 1
Output assigning of the ICPCON I-87057

Module	Channel	Description
	DO0	Bypass
	DO1	Nozzle1
	DO2	Nozzle2
I-87057	DO3	Nozzle3
	DO4	Engine (Ignition)
	DO5	Motor (Forward)
	DO6	Motor (Reverse)

RESULTS AND DISCUSSION

Two web cameras were installed to capture the image of weeds. During the start of the spraying operation, the web camera will initially capture the image of weeds manually and then analyze the red, green, blue (RGB) values in terms of computer pixels. These values will be used as the reference point to be compared with the values of the RGB of weeds captured real-time during the spraying operation. When the camera captures the real time image of weeds, the computer will calculate the percentage of the green pixels available in the frame and compare it with the RGB pixel of the reference point. When the green colour of the weeds matches the reference RGB value stored in the computer, it will trigger the nozzle to spray out chemical solutions to the target area. The green weeds to be sprayed were calculated based on the percentage of their intensity and the percentage of their green pixels.

Table 2 shows the percentage of green grasses which was set to open and close the nozzles and pump of the tank. The sprayer pump and the nozzles will be switched 'ON' at 20 to 100% intensity of weeds and 4 to 100% of pixels of green weeds. The pump and nozzles will be opened or closed based on the percentage or intensity of the green colour pixel value of weeds. In the real-time system, the respond time is a critical parameter. Therefore, the overall system must be well-visualized and designed for a successful integration.

TABLE 2
The status of nozzle based on percentage of rgb and pixel value of weeds

	Sprayer status	
Grass area	0% - 20%	20% - 100%
Pixel percentage of green grass	0.00% - 4.0%	4.0% - 100%
Nozzle status	Off	On
Pump status	On	On
Sprayer status result	Off spraying	On spraying

Spraying system was tested to make sure that the entire components were in a good condition and working perfectly. Calibration was carried out manually for each nozzle using the command button in the Graphical User Interface (GUI). The camera will initially capture the image of weeds and display it on the computer screen. The weeds captured by the camera in each frame were analyzed to activate the respective nozzle, i.e. to either open or close it. The signal from the computer will then be transferred to the PC parallel port which will send the voltage signal to the pump and the nozzle. The GUI screen was divided into 3 frames as captured by one camera. The 3 frames for the 3 units of spray nozzles. The GUI was tested to make sure that it works according to the autonomous sprayer system working process. Each nozzle (nozzle 1, nozzle 2, and nozzle 3) can be operated individually in their respective area of spray. Image which was captured was divided into three frames. The first nozzle can only operate in frame 1, while the second nozzle in frame 2, and the third nozzle in frame 3, respectively. When the user clicks on the region of frame 1, nozzle 1 will be turned ON, while the other nozzles will be turned OFF. The NC solenoid valves mounted on the nozzle will carry out these functions. The Normally Closed (NC) valves were installed on the nozzles for the 'off' un-operated operation. The valve will open the nozzle when the camera detects the presence of weeds. Therefore, the user can select from the image the particular area of weeds to be sprayed. Each application of ON operation will take 2 seconds before

it is turned OFF again. If there is nothing to be sprayed, the NO solenoid valves mounted at the tank is opened to by pass the liquid back to the tank. This is done to avoid the high-pressure build up in the main sprayer line. The GUI was designed to have an emergency stop button if the user needs to immediately stop the autonomous sprayer. *Fig. 8* shows the calculated percentage of the pixel of green weeds for each green weed area captured by the camera. The computer programme was written to activate the pump and the nozzle at a certain percentage of pixel values.
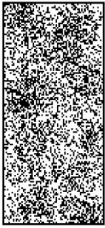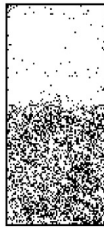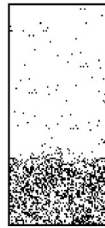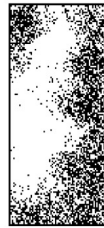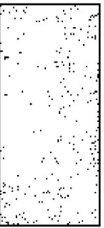
	Percentage of green grass selection					
Area size	X 121	X 121	X 121	X 121	X 121	X 121
Pixel view						
	Percentage of green grass selection					
Grass area	100%	75%	50%	25%	50%	0%
Pixel percentage of green grass	20%	15%	10%	5%	10%	1%
Nozzle status	On	On	On	On	On	Off
Pump status	On	On	On	On	On	On
Sprayer status result	On	On	On	On	On	Off

Fig. 8: The percentages of the green grass selections

Fig. 9 shows a sample of the results gathered from the experiment carried out in this study. It shows the GUI of the weeds captured by the web camera. The image was automatically divided into 3 frames for the operation of the three nozzles which was captured by one camera. Each frame was then analyzed for pixel count. Nozzle 1 was 'off' with the pixel percentage of 13.8, while nozzles 2 and 3 were in the 'on' mode when the percentage of pixel values exceeded 20%.

The concept of the smart sprayer, which includes PC web camera, personal computer, a programmable microcontroller ICPCON and sprayer system, was apparently achieved in this study. This particular project had successfully detected the presence of and intensity of weeds using a camera vision. The normally close (NC) solenoid valve was mounted on the nozzles for the purpose of switching ON/OFF the nozzles. They will be turned 'ON' when the camera detects weeds but turned off when the camera does not detect any weed. These ON/OFF functions help to reduce the amount or volume of chemicals to be sprayed and therefore lower release of hazardous substances into the environment, apart from reducing production cost.
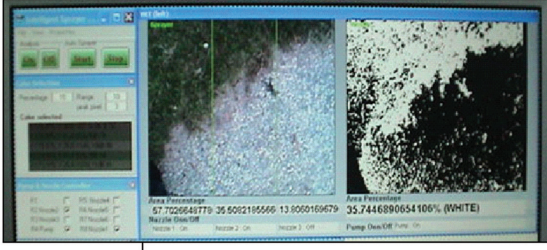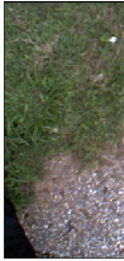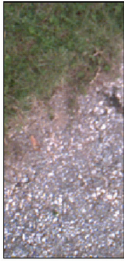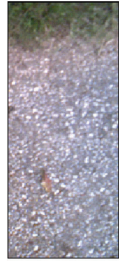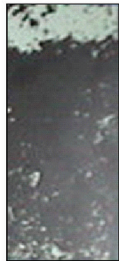
	Image		
Images grab			
Image area	High x 363		
Image weight	X = 0 to x = 363 pixels		
	Create partition		
Partition weight	X > 0 and X <= 121	X > 121 and X <= 232	X > 232 and x <= 363
Size x area	X = 121	X = 121	X = 121
Nozzle	1st nozzle	2nd nozzle	3rd nozzle
	RGB pixel value = 131769		
Grass areas	%	%	%
Image grab			
	Pixels counter		
Pixel view			
Pixel count	76031	46778	18184
	Percentage of grass pixels		
Pixel green grass	52%	35.5%	13.8%
	Pump & nozzle status		
Pump	On	On	On
Nozzle	On	On	Off

Fig. 9: Experimental results for the sprayer system

CONCLUSIONS

The automated sprayer system was successfully developed using the combination of the electromechanical system, controllers, and the software. The controllers consist of I/O module (ICPCON I-7042) and also a pair of (SST-2400) for data transmission. The graphical user interface (GUI) software, which was used to control the whole automatic system, was developed by visual basic programming. The software developed using the GUI has features which enable the user to perform the desired task on the computer instead of manually operating the sprayer.

In the real oil palm plantation environment, the variations of the daylight affect the image analysis of the weeds. The variations of the daylight changes the light intensity and thus changing the RGB values of the weeds. Therefore, the RGB value colour of the weeds is captured in real time so as to reduce the variations of light intensity of the outdoor environment. These values are saved and used as a reference colour. During the spraying operation, the online cameras will capture the image of weeds and compare it with the reference colour of the weeds which is captured on the real-time basis. At the moment, the reference RGB colour was taken at a few hours interval or at times when adverse daylight changes. The researcher of this project is looking forward to installing the third web camera to automatically capture the reference image colour of weeds in the real time.

In this research, a machine vision technology was developed to identify weeds in the outdoor environments. Although there have been efforts to control in row weeds, no system has been completed as a real time implement for field use. Thus, there is a practical need for a real time machine for weed detection, as well as to reduce the use of agricultural chemicals. Weed detection at the time of spraying may be very valuable to reduce chemicals costs and prevent environmental contamination. Similarly, much of the machine vision weed detecting research has been done with control lighting rather than variable lighting associated with outdoor field conditions.

REFERENCES

Abdul Malik B. Hamid. (1998). Camera vision to identify and recognize the colours oil palm fruit bunch. Final year Thesis, Universiti Putra Malaysia.

Choi, C.H., Choi, D.C., Erbach and Smith, R.J. (1990). Navigational tractor guidance system, *Transactions of ASAE, 33*(3), 699–706.

Hazlina Hamdan. (2005). Design and development of camera vision guided unmanned mover sprayer. Final year Thesis, Universiti Putra Malaysia.

Kondo, N. and Ting, K.C. (1998). Robotics for bio production systems. ASAE. St. Joseph, Michigan. USA.

Gonzalez, R. C. and Woods, R. E. (2002). *Digital Image Processing.* New Jersey: Prentice Hall.

Tillet, N.D. (1991). Automatic guidance sensors for agricultural field machines: A review. *Journal of Agricultural Engineering Reasearch, 50*(3), 167–187.

Growth Performance of Fingerlings of the Indian Major Carp, *Catla catla* (Ham.) Fed with Feeds Supplemented with Different Seaweeds

Savita Kotnala[1], Puspita Dhar[1], Partha Das[1] and Anil Chatterji[1, 2*]
*[1]Biological Oceanography Division,
National Institute of Oceanography, Dona Paula, Goa-403 004
[2]Institute of Tropical Aquaculture, Universiti Malaysia Terengganu,
21030 Kuala Terengganu, Terengganu, Malaysia
E-mail:anilch_18@yahoo.co.in

ABSTRACT

The growth performance of Indian major carp (*Catla catla,* Ham.) was assessed over a period of six months through formulated feeds consisting of three seaweeds, namely *Chlorodesmis fastigiata*, *Padina tetrastomatica* and *Stoechospermum marginatum*. A relatively slow average growth rate (6.48 g/month) in fishes was observed in the control group. Meanwhile, the maximum and rapid growth rate (13.38 g/month) was observed with Feed-A supplemented with *C. fastigiata*. Similarly, a comparable growth rate was also observed with Feed-B (11.56 g/month) with *P. tetrastomatica*. However, the growth rate in fishes was relatively lower (9.05 g/month) with Feed-C containing seaweed *S. marginatum*. The growth rate in each month was also compared. The maximum attainable growth rate was found to be 12 g in the control group, whereas this was 30 g with Feed-A. The attainable growth was 20 g and 15 g with Feed-B and Feed-C, respectively. In the control group, the maximum increments in weight was recorded in the third (September) and fifth (November) months of rearing, and the increment was considerably reduced after that. The maximum increment in weight was in the second month (August) with Feed-A, and this was followed by a considerable decrease in subsequent months. A similar trend was observed with Feed-B and Feed-C. The biochemical composition of all the four feeds used in the present study showed approximately the same protein (0.45-0.50 mg/ml) and lipid contents (0.6 mg/ml). Carbohydrate was the only parameter which showed a relatively significant effect ($p<0.05$) on the growth rate (0.107 mg/ml). The average Food Conversion Ratio (FCR) calculated for all the different feeds showed the maximum value with control (2.54$\pm$2.72), followed by Feed-C (1.77$\pm$1.54) and Feed-B (0.67$\pm$0.13). Meanwhile, the minimum value of FCR was obtained with Feed-A (0.57$\pm$0.39) indicating its high efficiency. The data of the present study clearly demonstrated that seaweeds, such as *C. fastigiata* and *P. tetrastomatica*, could be used in commercial formulated feed to get better growth of the fingerlings of major carps.

Keywords: Growth performance, *Catla catla,* seaweeds

INTRODUCTION

Fish form one of the most important components of Asian diets (Ayyappan and Jana, 1997). In Bangladesh, Indonesia and Philippines, it comprises of 50% of animal protein intakes, while in Thailand and Vietnam, it contributes about 40% of the diets (Delagado *et al*., 2003). The demand for fish has increased worldwide with the growing population. It is estimated that by 2050, when world population will approximately increase to 9 billions, and the demand for fish and fish products will also increase to 130.1 million tones, in which aquaculture practices are expected to contribute 41% to the total production of fish (Delagado *et al*., 2003).

---

*Corresponding Author

The most essential and major operational input in successful aquaculture is the feed and hence cheap and nutritionally balanced effective artificial feeds need to be developed. From historical times, carrageen and alginates from seaweeds are used for medicinal purposes. In spite of their usefulness, unfortunately only a little work has been done on the incorporation of seaweed in formulated feeds of freshwater cultivable fishes. Therefore, an attempt has been made in this study to incorporate seaweed as one of the ingredients in pelleted feed and to evaluate the efficacy of the feeds on the growth of Indian major carp (*Catla catla,* Ham.). The main objective of this study was mainly to produce cost effective**,** cheap, and efficient feed for a better growth of carps. Since foraging carps readily accept artificial pelleted feeds under any culture conditions, *Catla catla* belonging to the same group was selected to study the performance of feed developed in his study.

MATERIALS AND METHODS

In the present study, small, healthy, disease-free fries (18-22 mm) of *Catla catla* (Ham.) were procured from the carp hatchery at Anjunam Dam of Goa (India). These live animals were brought to the laboratory in polythene bags filled with oxygen. The polythene bags were kept for 2-3 hours in the experimental tanks for acclimatization of the fries before commencement of the experiment. Initially, a static indoor rearing system, consisting of four rectangular glass aquarium tanks (capacity: 80 L), was used for the study. Before stocking the fish, the tanks were washed thoroughly with freshwater. All the tanks were kept on a cement platform to facilitate better observation and accessibility. These tanks were kept on thermocol sheets to avoid breakage. Adequate level of oxygen in each tank was maintained through aeration. A circular FRP tank of 800 L capacity was also kept separately for regular replenishing of the water. The water of the tank was aerated regularly to eliminate chlorine before it was used for the experiment.

Three different types of artificial feeds incorporated with commonly occurring seaweeds, namely *Chlorodesmis fastigiata* (Feed-A), *Padina tetrastomatica* (Feed-B) and *Stoechospermum marginatum* (Feed-C), were formulated. These seaweeds were collected from Marvel and Anjuna beaches of Goa (India) during low tides. After the collection, the seaweeds were immediately washed with freshwater to remove extraneous materials associated with them. These seaweeds were then allowed to dry under the sun for 6-8 hours and stored in polythene bags for further use. All the three species of seaweed were ground using a mixer and used according to the desired weight, as described in Table 1.

In the above formulation scheme, coconut oil cake was used as a fat substitute, while wheat flour was used as carbohydrate and protein sources. Similarly, rice bran was used as carbohydrate and protein sources whereas tapioca was used as a binder. The ingredients were mixed thoroughly in a mixer with sufficient quantity of water to get the required soft consistency. The material was then hand kneaded. Small pellets (2-3 mm) were prepared with the help of a hand pelletizer. These pellets were dried at 40 °C in an oven for 24 hours. Before use, these pellets were grounded to powder form in a mixture and preserved in airtight containers for further use.

The average weight of fry at the beginning of the experiment was recorded and 40 numbers of randomly selected fries in each experimental tank were transferred. Tank-1 was considered as a control tank where the artificial feed without seaweed was used. In Tank-2, artificial feed with seaweed (*C. fastigiata*), Tank-3 feed with seaweed (*P. tetrastomatica*) and Tank-4 feed with seaweed (*S. marginatum*) were given at the rate of 10% of the biomass. The feed was given twice every day at 0900 hrs and 1700 hrs.

Faeces and uneaten feed was removed from each tank by siphoning before introduction of fresh feed. About 20% of exchange of water was given every day by using freshwater from the circular FRP tanks. Feeding of the fish was done by hand as this method allowed regular inspection of the fish. In each month, a total of ten fish were taken out and their mean average weight was recorded separately for each group. Meanwhile, a monthly sampling was undertaken to record the growth of the fish and also for adjusting the appropriate feed ration. The specific growth rate "G" of the fishes was calculated separately for each group, as follows:

$$G = \frac{W_2 - W_1}{T_2 - T_1} \times 100 \qquad \text{(Chatterji } et\ al.,\ 1979)$$

where W_2 and W_1 are the weights of the juveniles at times, T_2 and T_1, respectively.

Crude protein, crude carbohydrate, and lipid contents in each formulated feed were determined following AOAC (1984). The feed conversion ratio (FCR) was determined as described by Chatterji (1976) to assess the performance of the formulated feed by a simple equation, as:

$$FCR = F / (W_1 - W_0)$$

where F is the weight of food supplied to the fish during the study period, W_0 is the weight of the fish at the beginning of the experimental period, and W_1 is the weight of the fish at the end of the experiment.

TABLE 1
Diet formulation and ingredients used for evaluating growth performance on *C. catla*

Ingredients (weight in gm)	Control (g/500 g)	Feed A (g/500 g)	Feed B (g/500 g)	Feed C (g/500 g)
Coconut oil cake	200	75	75	75
Wheat flour	100	100	100	100
Tapioca	50	50	50	50
Rice bran	150	200	200	200
Seaweed (*Chlorodesmis fastigiata*)	-	75	-	-
Seaweed (*Padina tetrastomatica*)	-	-	75	-
Seaweed (*Stoechospermum marginatum*)	-	-	-	75
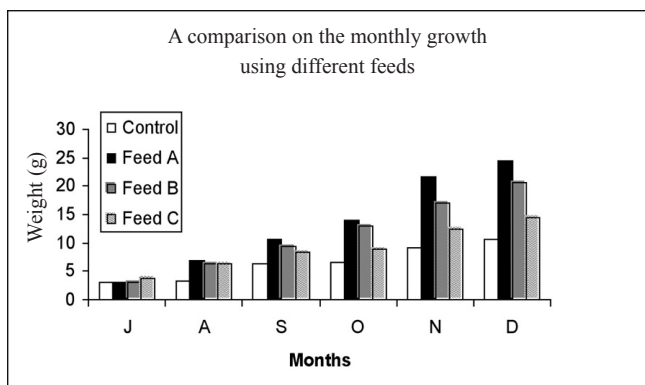
Fig. 1: A comparison on the monthly weight gained using different feeds
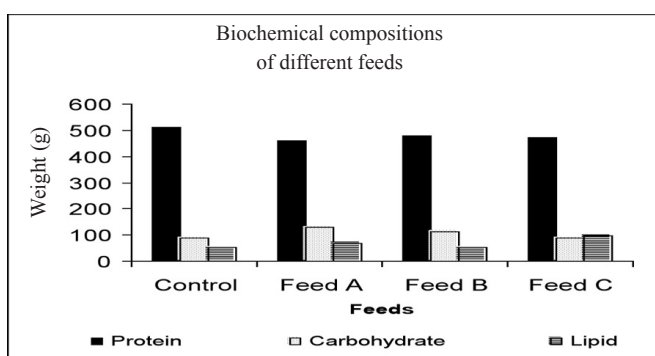
Fig. 2: Biochemical compositions of different feeds

RESULTS

Monthly weights (i.e. from July to December 2005) gained by *C. catla* with different feeds are presented in *Fig. 1*. In the control group, the weight was 6.48 g, whereas the maximum with Feed-A was 13.38 g. With Feed-B and Feed-C, the average growths were 11.56 and 9.05 g, respectively *(Fig. 1)*. In the control group (feed without seaweed), the weight gain of the fish was relatively very low for all the months as compared to the other feed types. The growth rate in terms of weight gain was the maximum and rapid when the fish was fed with Feed- A which was supplemented with seaweed *C. fastigiata*. A more or less similar growth trend was observed with Feed-B supplemented with *P. tetrastomatica*. However, the growth was relatively lower with Feed-C which contained seaweed (*S. marginatum*). In all the groups, except for the control, the growth gained was higher (*Fig. 1*).

The specific growth rate for each group was calculated separately for each month (*see* Table 2). In the control and with Feed-C, the specific growth rate was relatively low with the maximum values in December (10.62 and 14.50%, respectively). The higher SGR values with Feed-A (24.50%) and Feed-B (20.54%) showed consistent growth increments (*see* Table 2). The monthly increment in the weight was also compared in all the four groups. The growth rate in each month was also compared. The maximum attainable growth rate was 12 g in the control group, whereas this was 30 g with Feed-A. The attainable growth was 20 g and 15 g with Feed-B and Feed-C, respectively. In

TABLE 2
Growth performance in *Catla catla* when fed with different feeds

Months	Control		Feed-A *C. fastigiata*		Feed-B *P. tetrastomatica*		Feed-C *St. marginatum*	
	Monthly weight increment (g)	Specific growth rate (%/month)	Monthly weight increment (g)	Specific growth rate (%/month)	Monthly weight increment (g)	Specific growth rate (%/month)	Monthly weight increment (g)	Specific growth rate (%/month)
July	-	2.96	-	2.98	-	2.96	-	3.84
Aug.	8.35	3.23	56.24	6.81	53.01	6.30	13.43	6.34
Sept.	48.20	6.36	35.57	10.57	33.26	9.44	24.16	6.36
Oct.	2.15	6.50	24.28	13.96	27.49	13.02	5.10	8.81
Nov.	53.00	9.25	35.06	21.50	23.85	17.10	29.52	12.50
Dec.	12.71	10.62	12.24	24.50	16.74	20.54	13.79	14.50

TABLE 3
Food Conversion Ratio (FCR) values using different feeds during the experimental periods

Group	Aug	Sept	Oct	Nov	Dec	Average
Control	7.40	0.63	1.41	1.09	2.18	2.54$\pm$2.72
Feed-A	0.52	0.53	1.51	0.39	0.18	0.57$\pm$0.39
Feed-B	0.59	0.63	0.55	0.73	0.87	0.67$\pm$0.13
Feed-C	0.80	0.99	4.41	0.81	1.50	1.77$\pm$1.54

the control group, the maximum increment in the weight was recorded in the third (September) and fifth (November) months of rearing and after that the growth increment was reduced considerably. The maximum increment in the weight was recorded in the second month (August) with Feed-A, which was followed by a considerable decrease in the subsequent months. This showed that in all the experimental groups where seaweeds were incorporated in the feeds, the growth followed the normal trend (*see* Table 2).

The biochemical composition of all the four feeds used for the present study showed that the protein contents of all the feeds were similar (0.45-0.50 mg/ml), as illustrated in *Fig. 2*. Similarly, the lipid content (0.6 mg/ml) of the all the four feeds did not show any significant effect on the growth rate of the juveniles (see *Fig. 2*). Carbohydrate (0.107 mg/ml) was the only parameter which showed a significant effect ($p<0.05$) on the growth, as it was evident with Feed-A.

The average FCR calculated for all the different feeds showed the maximum value with the control (2.54$\pm$2.72), whereas the minimum was with Feed-A (0.57$\pm$0.39), and this was followed by Feed-B (0.67$\pm$0.13). The data presented in Table 3 showed that Feed-A and Feed-B were definitely better as compared to the control and Feed-C (1.77$\pm$1.54).

DISCUSSION

In the traditional carp culture, a mixture of rice bran and groundnut oil cake (1:1) is generally used (Mukhopadhyay, 1997). However, studies pertaining to nutrition in freshwater aquaculture in the recent years have led to the development of new feed formulations for Indian carp (Mohanty *et al*., 1990; Ayyappan and Jana, 1997; Paul *et al*., 1998). However, due to the escalating cost of groundnut oil cake and its increasing demand for aquaculture industry and poultry, there is an urgent need to search alternative sources to replace groundnut oil cake in the carp feeds (Mishra and Samantaray, 2004).

Feeds from plant origin have been reported to be effective and less expensive ingredients to fish diets (Dorsa *et al*., 1982; Robinson *et al*., 1984a, b; Ofojekwu and Ejike, 1984). These feeds are known to have an excellent amino acid profile (Jackson *et al*., 1982). In the recent years, feeds from plant origin have been accepted for Indian major carps as the growth in fishes has been reported to be as good as the traditional feed (Patnaik and Das, 1979). In some cases, aquatic and terrestrial macrophytes have been used as unconventional source of plant proteins to develop suitable fish feeds (Edwards *et al*., 1985; Devaraj *et al*., 1986). In tropical developing countries, where algal production rates are high, algae have been receiving increasing attention as an alternate protein possess relatively high protein contents (50-65%) that may be included in balanced fish feeds (Devaraj *et al*., 1986).

There is a paucity of information concerning the incorporation of seaweeds in fish diets. However, there have always been contradictory results obtained. For examples, inclusion of the brown seaweeds known as *Undaria pinnatifida* and *Ascophyllum nodosum* in the formulated feeds has been found to improve the growth and feed efficiency of red sea bream (Yone *et al*., 1986). The use of red seaweeds (*Eucheuma cottonii*) and *Gracilaria lichenoides* in the diet of juvenile of spotted rabbitfish (*Siganus canaliculatus*) resulted in a negative growth rate (Tacon *et al*., 1990). Hashim and Mat-Saat (1992) investigated the utilization of several seaweed meals by snakehead fry, where a relatively higher growth performance was reported. Considering the above mentioned studies, three species of commonly occurring seaweeds were used to study the growth pattern in *catla* in the present investigation. In this study involving feed with seaweed (*C. fastigiata*), better results were shown as compared to the feed without the seaweeds supporting the fact that the fingerlings of catla preferred food consisting of more carbohydrates as compared to protein. Low FCR value for Feed-A (0.57$\pm$0.39) and Feed-C (0.67$\pm$0.13) shows a better efficiency of the feeds as compared to the control and other feed.

An attempt was also done by Basudha and Vishwanath (1997) to study the growth performance, feed conversion ratio, and protein efficiency ratio of a formulated feed containing *Azolla* powder, fish meal, mineral, vitamin supplements and feed containing rice bran, mustard oil cake in a feeding trial on *O. belangeri*. The growth of fish in the manured ponds, where no supplementary feed was given, was considered as a control group. The growth was compared in all these groups, which showed that the percentage of weight gained by the fish fed with *Azolla* powder was highest. A better growth in the fries in these studies could be attributed to the presence of both plant and animal proteins and probable balance of amino acid composition (Saavedra *et al*., 2008). In the present study, Feed-A, which was formulated with rice bran, groundnut oil cake, tapioca, and seaweeds showed better results. This shows that the incorporation of carbohydrate in feed relatively gives a better growth in common carps as compared to animal proteins. The findings by Keshavnath *et al*. (2002) on common carps have shown that these animals are capable of utilizing high level of dietary carbohydrates, especially when the protein content in the diet is low, and this further supports the findings obtained in the present study.

Krishnanidhi and Shell (1965) recommended 20% carbohydrates as the most efficient level for the feed of channel cat fish. Their study proved that larger carbohydrate contents have also been found to yield a better growth of channel cat fish. In the continuation of other experiments, a 26% carbohydrate in the diet yielded the best growth in carps (Krishnanidhi and Shell, 1965). *Piaractus mesopotamicus* has been reported to use carbohydrates as effectively as lipids and grow better as compared to feeds containing protein (Abimorad and Carneiro, 2007). The specific growth rate and weight gained in juvenile Asian seabass (*Lates calcarifer*) fed with feed containing 20% carbohydrate were higher with better feed conversion ratios as compared to the ones which were fed with feeds containing higher protein and lipid (Catacutan and Coloso, 1997). These observations support the findings of the present study which used carbohydrate-based feed for the juveniles of common carps.

REFERENCES

Abimorad, E.G. and Carneiro, D.J. (2007). Digestibility and performance of pacu (*Piaractus mesopotamicus*) juveniles — fed diets containing different protein, lipid and carbohydrate levels. *Aquaculture Nutrition, 13*(1), 1-9.

AOAC. (1984). Official methods of analysis. In S. William (Ed.), *Association of Analytical Chemist, 14,* 1141. Arlington, Virginia.

Ayyappan, S. and Jana, J.K. (1997). Fresh water aquaculture an upcoming sector in global fisheries. *Fishing Chimes, 17*, 17-21.

Basudha, C. and Vishwanath, W. (1997). Formulated feed based on aquatic weed *Azolla* and fish meal for rearing medium carp *Osteobrama belangeri* (Valenciennes). *Journal of Aquaculture in the Tropics, 12*, 155-164.

Catacutan, M. R. and Coloso, R. M. (1997). Growth of juvenile Asian seabass, *Lates calcarifer*, fed varying carbohydrate and lipid levels. *Aquaculture, 149*(1-2), 137-144.

Chatterji, A. (1976). Studies of the biology of some carps. Ph.D. Aligarh Muslim University, Aligarh, India.

Chatterji, A., Siddiqui, A.Q. and Khan, A. A. (1979). The relative condition factor of bata, Labeo *bata* (Ham.) from the river Kali, Uttar Pradesh. *Indian Journal of Animal Research, 10*(2), 63-68.

Delgado, C. L., Wada, N., Rosegrant, M.W., Miejer, S. and Ahmed, M. (2003). Fish to 2020. World Fish Center Technical Report 62.

Devaraj, K.V., Keshavappa, G.Y. and Manissery, J.K. (1986). Growth of grass *carp*, *Ctenopharyngodon idella* (Val.) fed on two terrestrial fodder plants. *Aquaculture and Fisheries Management, 17*, 123-128.

Dorsa, W.J., Robinson, E.H. and Poe, W.E. (1982). Effect of dietary cottonseed meal and gossypol on growth of young channel catfish. *Transactions of the American Fisheries Society*, *3,* 651-655.

Edwards, P., Kamal, M. and Wee, K. L. (1985). Incorporation of composted and dried water hyacinth pelleted feed for tilapia, *Oreochromis niloticus* (Peter). *Aquaculture and Fisheries Management,* 233-348.

Hashim, R. and Mat-Saat, N.A. (1992). The utilization of seaweed meals and binding agents in pelleted feeds for snakehead (*Channa striatus*) fry and their effects on growth. *Aquaculture, 108,* 299-308.

Jackson, A.J., Capper, B.S. and Matty, A.J. (1982). Evaluation of some plant proteins in compound diets for the tilapia *Sarotherodon mossambicus. Aquaculture, 27*, 97-109.

Keshavnath, P., Manjappa, K. and Gangadhar, B. (2002). Evaluation of carbohydrates rich diets through common carp culture in manured tanks. *Aquaculture*, *8*(3), 169-174.

Krishnanidhi and Shell, E.W. (1965). Utilization of casein and soybean protein by channel catfish, *Ichtalurus punctatus* (Raf.). *Proceedings Annual Conference Southeastern Association Game Fish Commissioners*, *17*, 364-367.

Robinson, E.H., Rawles, S.D., Oldenburg, P.W. and Stickney, R. R. (1984a). Effects of feeding gland less or glanded cottonseed products and gossypol to *Tilapia aurea. Aquaculture, 38,* 145-154.

Robinson, E.H., Rawles, S.D., Oldenburg, P.W. and Stickney, R.R. (1984b). Evaluation of glanded and glandless cottonseed products in catfish diets. *The Progressive Fish-Culturist, 46*, 92-97.

Ofojekwu, P.C. and Ejike, C. (1984). Growth response and feed utilization in the tropical (*Oreochromis niloticus*) fed on cottonseed based artificial diets. *Aquaculture, 4*, 27–36.

Mishra, K. and Samantaray, K. (2004). Interacting effects of dietary lipid level and temperature on growth, body composition and fatty acid profile of rohu, *Labeo rohita* (Hamilton). *Aquaculture Nutrition, 10*(6), 359-269.

Mohanty, S.N., Swamy, D.N. and Tripathi, S.D. (1990). Growth, nutritional indices and carcass composition of Indian major carp by *Catla catla, Labeo rohita,* fed four dietary protein levels. *Aquaculture Hungarica* (Szarras)*, 6*, 211-217.

Mukhopadhyay, P.K. (1997). Recent advances and future strategies in nutrition for freshwater aquaculture. In *Proceedings of VIII Animal Nutrition Research Worker's Conference.* Chennai, (Comp. I) Tamil Nadu Veterinary and Animal Science University, Chennai, 134-143.

Paul, B.N., Nandi, S., Sarkar, S. and Mukhopadhyay, P.K. (1998). Dietary essentiality of phospholipids in Indian major carp larvae. *Asian Fishery Science, 11*, 253-259.

Patnaik, K.S. and Das, K.M. (1979). Utilization of some aquatic weeds as feed for rearing carp spawn and fry. In *Proceedings of the Symposium on Inland Aquaculture.* Central Inland Fisheries Research Institute, Barrackpore, India, 12.

Patra, S. and Ray, A.K. (1988). A preliminary study on utilization of the aquatic weed, *Hydrilla verticillata,* as feed by the carp, *Labeo rohita,* growth and certain biochemical composition of flesh. *Indian Biologist, 20*, 44-50.

Saavedra, M., Pousão-Ferreira, P., Yúfera, M., Dinis, M.T. and Conceição, L.E.C. (2008). A balanced amino acid diet improves *Diplodus sargus* larval quality and reduces nitrogen excretion. *Aquaculture Nutrition*, *15*(5), 517-524.

Tacon, A. G. J., Rausin, N., Kadari, M. and Cornelis, P. (1990). The food and feeding of marine finfish in floating net cages at the National Sea farming Development Centre, Lampug, Indonesia: Rabbit fish, *Siganus canaliculatus* (Park). *Aquaculture and Fisheries Management, 21*, 375-390.

Yone, Y., Furuichi, M. and Urano, K. (1986). Effects of dietery wakame *Undaria pinnatifida* and *Ascophyllum nodosum* supplements on growth, feed efficiency proximate composition of liver and muscle of the red sea bream. *Nippon Suisan Gakkaishi, 52*, 1465-1488.

Chemical Constituents and Antioxidant Activity
of *Cinnamomum microphyllum*

M.A. Norazah[1*], M. Rahmani[1*], S. Khozirah[1], H.B.M. Ismail[2],
M.A. Sukari[1], A.M. Ali[3] and G.C.L. Ee[1]
[1]Department of Chemistry, Faculty of Science, Universiti Putra Malaysia,
43400 UPM, Serdang, Selangor, Malaysia
[2]Centre for Foundation Study in Sciences, Universiti Malaya, 50603 Kuala Lumpur, Malaysia
[3]Department of Biotechnology, Universiti Putra Malaysia,
43400 UPM, Serdang, Selangor, Malaysia
[*]E-mail: mawardi@fsas.upm.edu.my

ABSTRACT

The extract of *Cinnamomum microphyllum* showed strong antioxidant activity when it was tested against auto-oxidation of linoleic acid, superoxide, and DPPH radical scavenging activity. Further detailed investigations of the plant constituents and bioactivity studies led to the isolation and identification of known compounds consisting of three lignans, a coumarin, an ester and β-sitosterol. The structures of the compounds were determined using detailed spectroscopic analysis. The lignans were found to possess a significant antioxidant activity when tested against the three assay systems.

Keywords: *Cinnamomum microphyllum*, pinoresinol, syringaresinol, medioresinol, antioxidant

INTRODUCTION

Cinnamomum of the family *Lauraceae* is an evergreen or decidous shrub or small to large tree which can grow up to 50 meters in height. The genus grows widely in continental Asia, East and Southeast Asia, Australia, the Pacific and in Central and South America. About 21 species are found in Peninsular Malaysia (Kochummen, 1989) alone. Many ethnobotanical studies have reported the traditional uses of *Cinnamomum* species, especially in food, fragrances, fumigants, and traditional medicines (Burkill, 1966; Perry, 1980). Commercially known as cinnamon, it is considered as one of the oldest spices in the world (Wijesekera, 1978) and contains valuable chemicals such as eugenol, cinnamaldehyde, safrole, linalool, camphor and benzyl benzoate. Cinnamon oil and oleoresin are primarily used in the food processing, cosmetic, and pharmaceutical industries, while the cinnamon sticks or powdered form are used as flavourings and in confectionaries (Jayatilaka *et al.*, 1995).

Considerable experimental evidences have supported the view that reactive oxygen radicals play a vital role in an oxidation process which is recognized as the initial stage in the development of many chronic diseases such as cancer, atherosclerosis, diabetes, etc. (Abe and Berk, 1998; Lefer and Granger, 2000). These highly reactive free radicals, in the form of superoxide anion radicals, hydroxyl radicals, and non-free radical species, are unstable molecules and seek other electrons to pair, and thus lead to cell and DNA damages. The roles of antioxidant in food and herbal care products are very important, particularly functioning as free radical scavenger, reducing agents and quenchers for the formation of singlet oxygen (Youdim *et al.,* 1999). These antioxidants

---

[*]Corresponding Author

can neutralize these free radicals and help prevent any damages, as well as increase resistance against diseases and prolong life. Typical antioxidants, which are found in plants, consist mostly polyphenolics such as flavonoids, lignans, xanthones, etc. The objectives of the study were to identify the presence of chemical components in *C. microphyllum* and to evaluate the antioxidant activity of the extracts, essential oils, and pure compounds against linoleic acid autoxidation, superoxide and DPPH free radical scavenging assays. Earlier chemical studies on the plant revealed a rich source of essential oils and some have been shown to exhibit insecticidal, anticandidal, and antidermatophytic activities (Ibrahim *et al.,* 2005; Ibrahim *et al.,* 2008; Mastura *et al.,* 1999). Various types of secondary metabolites have been reported to occur in *Cinnamomum* species and some of the compounds were found to have cytotoxic, antioxidant, anti-platelet aggregation, and antimicrobial activities (Mukherjee *et al.*, 1994; Kwon *et al.,* 1998; Su *et al.*, 1999; Zhu *et al.*, 1994).

EXPERIMENTAL DESIGN

General Experimental Procedures

In this study, melting points were measured on a Kofler hot stage apparatus and uncorrected. The IR spectra were recorded using the KBr discs on a Perkin Elmer FTIR spectrophotometer model 1275X. The UV spectra were recorded in MeOH on a Shimadzu UV 160A spectrophotometer. The ^{1}H-NMR and ^{13}C-NMR spectra were recorded on a JOEL FTNMR 400 MHz spectrometer. Meanwhile, chemical shifts are shown in δ values (ppm) with tetramethylsilane as an internal standard.

Plant Material

The leaf, stem bark, and stem of *Cinnamomum microphyllum* were collected from Gunung Berembun, Cameron Highlands in 1998, and a voucher specimen was deposited at the Herbarium, Forest Research Institute of Malaysia, in Kepong.

Extraction and Isolation

The ground dried bark (2.1 kg) and stem (1.4 kg) were separately and sequentially extracted by cold percolation with hexane, chloroform, and methanol, over a period of two weeks. The bark extracts were concentrated under reduced pressure to give 116.1 g, 82.8 g, and 392.0 g of dark viscous extracts, respectively. A similar treatment of the stem gave 13.4 g, 19.4 g, and 55.0 g of dark viscous extracts, respectively. A portion of the hexane extract of the bark (30 g) was subjected to VLC and eluted with solvent gradient of petroleum ether, ethyl acetate and methanol to afford 22 major fractions of 200 ml each. Further chromatographic separation of fractions 7 and 10-20 gave benzyl benzoate (**1**) as a colourless oil (54 mg) and β-sitosterol (42 mg), respectively. In particular, β-Sitosterol was recrystallised from CHCl₃ as white needles with m.p. 131-133ºC (Hill *et al.*, 1991; m.p. 136-137ºC).

A portion of the chloroform bark extract (30.0 g) was subjected to flash column chromatography using chloroform and ethyl acetate as eluents to afford 83 fractions. Fractions 21-26 were combined and rechromatographed with silica gel to give scoparone (**2,** 75 mg) and recrystallised from chloroform as white plates, m.p. 147-148ºC (Valenciennes *et al.*, 1999; m.p. 143-145ºC). Fractions 51-74 were further separated by a series of silica gel column chromatography and preparative TLC to give pinoresinol (**3,** 38 mg**)** as brownish oil, syringaresinol (**4**, 52 mg**)** as white needle-shaped crystals, while m.p. 172-173ºC (Abe and Yamauchi, 1988; m.p. 173-174ºC) and medioresinol (**5,** 29 mg**)** as white needles, m.p. 170-171ºC (Abe and Yamauchi, 1988; m.p. 170-172ºC).
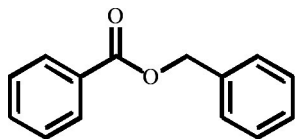
Benzyl benzoate (**1**)
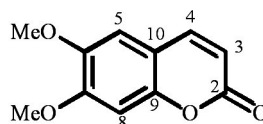
Scoparone (**2**)
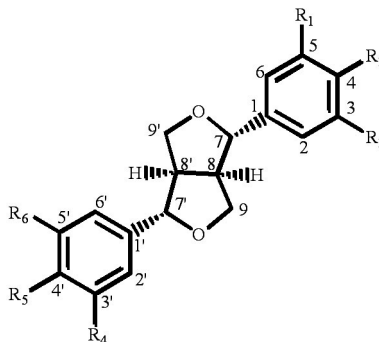
Pinoresinol (**3**) $R_1 = R_6 = H$; $R_2 = R_5 = OH$; $R_3 = R_4 = OMe$
Syringaresinol (**4**) $R_1 = R_3 = R_4 = R_6 = OMe$; $R_2 = R_5 = OH$
Medioresinol (**5**) $R_1 = H$; $R_2 = R_5 = OH$; $R_3 = R_4 = R_6 = OMe$

Benzyl benzoate (1): IR ν_{max} (KBr) cm^{-1}: 1717, 1448, 1324, 1273, 1241, 1199, 978; UV λ_{max} (MeOH) nm (log ε): 208 (2.43); ^{1}H-NMR (400 MHz) δ: 8.07 (1H, *d*, *J*=7.5 Hz, H-4), 7.55 (2H, *t*, *J*=7.5 Hz, H-3, H-5), 7.33-7.45 (7H, *m*, H-3', H-7', H-4', H-5', H-6', H-2, H-6), 5.36 (2H, *s*, H-1');. ^{13}C-NMR (100 MHz) ppm: 166.3 (C=O), 135.9 (C-1), 132.8 (C-4), 129.9 (C-2'), 129.5 (C-2/C-6), 128.2 (C-3/C-5), 128.4 (C-4'/6'), 128.0 (C-3'/C-7'), 127.9 (C-5'), 66.5 (-CH$_2$); MS m/z (%): 212 (M$^+$, 22), 194 (6), 105 (100), 91 (51), 77 (36), 65 (12).

Scoparone (2): IR ν_{max} (KBr) cm^{-1}: 2924, 1623, 1519, 1457, 1385, 1281; UV λ_{max} (MeOH) nm (log ε): 340 (0.43), 291 (0.24); ^{1}H-NMR (400 MHz) δ: 7.64 (1H, *d*, *J*=9.5 Hz, H-4), 6.87 (2H, *s*, H-8, H-5), 6.31 (1H, *d*, *J*=9.5 Hz , H-3), 3.97 (3H, *s*, 6-OMe), 3.94 (3H, *s*, 7-OMe); ^{13}C-NMR (100 MHz) ppm: 161.7 (C-2), 153.2 (C-7), 150.4 (C-9), 146.7 (C-6), 143.5 (C-4), 111.8 (C-10), 113.9 (C-3), 108.5 (C-5), 100.4 (C-8), 56.7 (2xOMe). MS m/z (%):206 (M$^+$, 100), 191 (51), 178 (22), 163 (44), 135 (29), 120 (20), 107 (36), 92 (24), 79 (50).

Pinoresinol (3): IR ν_{max} (KBr) cm^{-1}: 3458, 2997, 1613, 1519, 1462, 1427, 1366, 1343, 1325, 1278, 1245; UV λ_{max} (MeOH) nm (log ε): 289 (1.10), 230 (1.25); MS m/z (%): 358 (M$^+$, 48), 205 (10), 191 (7), 163 (32), 151 (100), 137 (69), 124 (23), 103 (11), 77 (13). ^{1}H-NMR (400 MHz: CDCl$_3$) and ^{13}C-NMR (100 MHz: CDCl$_3$) – *see* Table 1.

Syringaresinol (4); IR ν_{max} (KBr) cm^{-1}: 3472, 3097, 2996, 2947, 2866, 1612, 1521, 1459, 1426, 1368, 1341, 1327; UV λ_{max} (MeOH) nm (log ε): 272 (0.05), 258 (0.04), 208 (1.10); MS m/z (%): 418 (M$^+$, 38), 388 (59), 182 (44), 181 (100), 167 (73). ^{1}H-NMR (400 MHz: CDCl$_3$) and ^{13}C-NMR (100 MHz: CDCl$_3$) – *see* Table 1.

TABLE 1

^{1}H-NMR and ^{13}C-NMR data for pinoresinol (**3**), syringaresinol (**4**) and medioresinol (**5**)

No.	Pinoresinol (3)		Syringaresinol (4)		Medioresinol (5)	
	^{1}H	^{13}C	^{1}H	^{13}C	^{1}H	^{13}C
1	-	133.2	-	132.3	-	132.4
2	6.92, (d, 0.5 Hz)	119.2	6.61 (s)	102.9	6.92 (d, 2.4 Hz)	102.9
3	-	146.9	-	147.4	-	146.9
4	5.63 (s, OH)	145.5	5.94 (s, OH)	134.5	5.50 (s, OH)	146.5
5	6.91 (d, 7.5 Hz)	114.5	-	147.4	6.91 (d, 8.5 Hz)	114.5
6	6.84 (dd, 0.5, 7.5 Hz)	108.8	6.61 (s)	102.9	6.84 (dd, 8.5, 2.4 Hz)	102.9
7/7'	4.76 (brd, 4.0 Hz)	86.1	4.75 (d, 4.0 Hz)	86.3	4.76 (dd, 5.0, 3.2 Hz)	86.4/86.0
8/8'	3.12 (brd)	54.6	3.12 (brd, 1.5 Hz)	54.6	3.13 (m)	54.7/54.3
9a/9'a	4.27 (dd, 9.0, 7.0 Hz)	72.2	4.30 (dd, 7.0, 9.0 Hz)	72.0	4.30 (m)	72.1/71.8
9b/9'b	3.90 (dd, 9.0, 3.2 Hz)	72.2	3.91 (dd, 7.0, 5.5 Hz)	72.0	3.91 (m, 2H)	72.1/71.8
1'	-	133.2	-	132.3	-	133.1
2'	6.92 (d, 0.5 Hz)	119.2	6.61 (s)	102.9	6.60 (s, 1H)	108.8
3'	-	146.9	-	147.4	-	147.4
4'	5.63 (s, OH)	145.5	5.51 (s, OH)	134.5	5.61 (s, OH)	134.5
5'	6.91 (d, 7.5 Hz)	114.5	-	147.4	-	147.4
6'	6.84 (dd, 0.5, 7.5 Hz)	108.8	6.61 (s)	102.9	6.60 (s, 1H)	119.2
OMe	3.93 (s, 6H, 2xOMe)	56.4	3.95 (s, 12, 4xOMe)	56.6	3.93 (OMe)	56.6
					3.95 (2xOMe)	56.2

TABLE 2

Antioxidant activity of *C. microphyllum* extracts and isolated compounds

Extracts/isolated compounds	Inhibition of linoleic acid (%)	Superoxide scavenging activity (%)	DPPH scavenging activity (%)
Hexane (stem)	5.1	95.2	12.5
Chloroform (stem)	34.7	97.0	52.0
Methanol (stem)	38.7	94.6	98.7
Hexane (bark)	16.8	16.7	12.7
Chloroform (bark)	49.2	76.5	76.0
Methanol (bark)	5.4	96.3	86.7
Essential oil (leaf)	-	6.4	-
Essential oil (bark)	-	-	-
Scoparone (**2**)	-	-	-
Pinoresinol (**3**)	84.9	76.8	95.8
Medioresinol (**5**)	79.6	73.4	94.6
Control (5% linoleic acid)	0	-	-
BHT	100		

Medioresinol (5); IR ν_{max} (KBr) cm^{-1}: 3774, 3457, 3139, 3097, 2996, 1612, 1520, 1459, 1368, 1327, 1282, 1204; UV λ_{max} (MeOH) nm (log ε): 279 (0,10), 258 (0.03), 206 (1.12), ; MS m/z (%): 388 (M$^+$, 29), 205 (15), 181 (23), 163 (37), 151 (100), 137 (66), 124 (23), 55 (31). ^{1}H-NMR (400 MHz: CDCl$_3$) and ^{13}C-NMR (100 MHz: CDCl$_3$) – *see* Table 1.

Essential Oil Extraction

The leaf and bark of the plant were subjected to hydrodistillation using Clevenger-type apparatus for 4 hours. The oily layers obtained were separated and dried over anhydrous sodium sulphate. The percentage of essential oils obtained from the leaves and bark were 1.9% and 2.3%, respectively. These were the averaged yield over two experiments and calculated based on the dry weight of the plant materials.

Antioxidant Assays

Autoxidation of linoleic acid in a water-alcohol system. The autoxidation assay was carried out using the method described by Osawa and Namiki (1981), but with a slight modification. 2,6-ditert-Butylphenol (BHT) at 4.0 mg was used as a positive control.

Xanthine/Xanthine oxidase (X/XOD) superoxide scavenging assay. The assay was carried out according to the method described by Chang *et al.* (1996), with a slight modification.

2,2-Diphenyl-1-picrylhydrazyl (DPPH) radical scavenging assay. The effect of *C. microphyllum* extracts on DPPH radical was estimated according to the method proposed by Blois (1958). The plant extracts or compounds (0.5 mg/ml) were added to a solution of DPPH (0.5 mg/ml) in methanol. The mixture was shaken and left to stand at room temperature for 10 minutes. The absorbance of the resulting solution was measured spectrophotometrically at 520 nm.

M.A. Norazah, M. Rahmani, S. Khozirah, H.B.M. Ismail, M.A. Sukari, A.M. Ali and G.C.L. Ee

RESULTS AND DISCUSSION

A positive preliminary screening of crude extracts of *C. microphyllum* against two of the assay systems prompted the researchers to investigate the stem bark and stem extracts of the plant further. The hexane, chloroform and methanol extracts of both parts of the plant were chosen for a detail study.

The chromatographic separation of the hexane extract gave the simple benzyl benzoate (**1**) as colourless oil and the ubiquitous β-sitosterol as white powder with m.p. 131-133°C. The first compound identified from the chloroform extract of the bark was scoparone (**2**), and this was followed by the isolation of pinoresinol (**3**) as brownish oily solid with UV spectrum maximum absorptions at 289 and 230 nm, and molecular ion peak at m/z 358 in the mass spectrum which corresponded to the molecular formula $C_{20}H_{22}O_6$. The mass spectral analysis was consistent with the fragmentation patterns reported for 2,6-diaryltetrahydrofuran lignans (Latip *et al.,* 1999). This was further supported by the ¹H-NMR spectrum which showed the typical characteristic of the symmetrical tetrahydrofuran lignan. A total of six aromatic protons were observed in the range of δ 6.84-6.92 for the two aryl groups, as well as eight protons for the bifuran ring, represented by the resonances at δ 3.12 (H-8, H-8'), 4.76 (H-7, H-7'), 4.27 (H-9a, H-9'a), and 3.90 (H-9b, H-9'b). The chemical shifts observed for the benzylic protons, at H-7 and H-7' appeared at a higher field (δ 4.76), were consistent with the equatorial orientation of the aryl substituents (Pelter *et al.*, 1976).

The correlations in the COSY spectrum strongly supported the connectivity of the 2,6-diaryltetrahydrofuran ring even further. The compound displayed only ten carbon signals in the ¹³C-NMR spectrum (Yang *et al.*, 1999), while the assignments of the individual protons and carbons were supported by DEPT, HSQC, and HMBC spectra. Three pairs quaternary carbons, observed at 146.9, 145.5 and 133.2 ppm, were assigned to C-3/C-3', C-4/C-4' and C-1/C-1', respectively. The two methylene carbons at C-9/C-9' occurred at 72.2 ppm (Table 1). Based on these data and the comparison made with the reported values, the compound was concluded to be pinoresinol (Abe and Yamauchi, 1988; Cowan *et al.*, 2001).

Further separation of the extract gave syringaresinol (**4**) as white needles with m.p. 171-172°C (Abe and Yamauchi, 1988; m.p. 173-174 °C) and molecular ion peak at m/z 418 which corresponded to the molecular formula $C_{22}H_{26}O_8$. A broad band observed at 3472 cm⁻¹ in the IR spectrum indicated the presence of hydroxyl groups. The presence of 2,6-diaryl-3,7-dioxobicyclo[3.3.0]octane system is clearly indicated in the ¹H-NMR spectrum. A sharp singlet integrated for four protons occurred at δ 6.61 and it was assigned to the four equivalent aromatic protons at H-2, H-2', H-6 and H-6', while the other sharp singlet at δ 3.95 was due to the four methoxyl groups. The ¹³C-NMR and DEPT spectra exhibited only 8 carbon resonances indicating the presence of a symmetrical lignan with equivalent aryl carbon signals of each aromatic ring. All the assignments of individual protons and carbons were further confirmed by the HSQC and HMBC experiments.

Subsequently, medioresinol (**5**) was also obtained as white prisms with m.p. 170-171°C (Abe and Yamauchi, 1988; m.p. 170-172°C). The ¹H-NMR spectrum of the compound also showed the characteristics of a pinoresinol-type lignan, which are very similar to the previous two, except the spectrum now showed resonances for five aromatic protons and three methoxyl groups. This suggested a non-symmetrical structure with the two aryl groups having different substitution patterns. The protons in one of the aromatic rings displayed an ABX system, with the occurrence of two doublets at δ 6.91 (*d*, 8.5 Hz) and 6.92 (*d*, 2.4 Hz) and a doublet of doublets at δ 6.84 (*dd*, 8.5, 2.4 Hz). In addition, the presence of 18 carbon resonances in the ¹³C-NMR spectrum, instead of 10 resonances as previously shown by pinoresinol, also supported this deduction. The positions of the hydroxyl and methoxyl substituents were confirmed by *¹J* correlation in HSQC and *²J* and *³J* correlations in the HMBC spectra. These data are in complete agreement with those reported in the literature for medioresinol (Abe and Yamauchi, 1988).

All the extracts of the bark and stem showed a strong superoxides cavenging activity, except the hexane extract of the bark. The antioxidant activity for the hexane, chloroform, and methanol extracts of the stem were found to be 95.2, 97.0, and 94.6%, respectively (*see* Table 2). Meanwhile, the inhibition values for the bark were 16.9, 76.5, and 96.3%. Similarly, all the extracts of the stem and bark indicated a strong activity towards the DPPH scavenging test system, except the two hexane extracts. The strong activity showed by these extracts might be due to the presence of phenolic compounds. When tested against inhibition of linoleic acid, the extracts only displayed a medium to weak activity. Nevertheless, the essential oils extracted from the leaves and bark failed to give any positive results. However, the two pure lignans were found to produce strong antioxidant properties and this finding supports the suggestion that the presence of phenolic compounds is essential for its activity. Lignans such as pinoresinol have been shown to possess strong antioxidant properties (Owen *et al.,* 2000). Hence, the presence of such compounds in *C. microphyllum* could be responsible for the antioxidant activity of the plant.

In summary, the separation of the chemical constituent present in the extracts of *C. microphyllum* had resulted in the isolation of six compounds consisting of three lignans, a coumarin, an ester, and β-sitosterol. Most of the stem and bark extracts were strongly antioxidant against superoxide and DPPH scavenging tests. Two of the lignans, namely pinoresinol (**3**) and medioresinol (**5**), were excellent candidates as antioxidant agents with their strong activities.

ACKNOWLEDGEMENTS

REFERENCES

Abe, F. and Yamauchi, T. (1988). 9α-Hydroxypinoresinol, 9α-hydroxymedioresinol and related lignans from *Allamanda neriifolia*. *Phytochemistry*, *27*, 575-577.

Abe, J. and Berk, B. (1998). Reactive oxygen species as mediators of signals transduction in cardiovascular disease, *Trends Cardiovascular Medicine, 8*, 59-64.

Blois, M.S. (1958). Antioxidant determination by use of a stable free radical. *Nature, 26*, 1199-1200.

Burkill, I.H. (1966). *A Dictionary of the Economic Products of the Malay Peninsula*. Kuala Lumpur: Ministry of Agriculture and Cooperatives.

Chang, W.S., Lim, C.C., Chuang, S.C. and Chiang, H.C. (1996). Superoxide anion scavenging effect of coumarins. *American Journal of Chinese Medicine*, *24*, 11-17.

Cowan, S., Stewart, M., Abbiw, D.K., Latiff, Z., Sarker, S.D. and Nash, R.J. (2001). Lignans from *Strophantus gratus. Fitoterapia, 72*, 80-82.

Hill, R.A., Kirk, D.N., Makin, H.L.J. and Murphy, G.M. (1991). *Dictionary of Steroids*. Great Britain: Chapman and Hall.

Ibrahim, J., Bushra, A.K.M., Santhaman, J. and Jamal, J.A. (2008). Correlation between chemical composition and antifungal activity of the essential oils of eight *Cinnamomum* species. *Pharmaceutical Biology*, *46*, 406-412.

Ibrahim, J., Yalvema, M.F., Ahmad, N.W. and Jamal, J.A. (2005). Insecticidal activities of the leaves oils of eight *Cinnamomum* species against *Aedes aegypti* and *Aedes albopictus*. *Pharmaceutical Biology*, *43*, 526-532.

Jayatilaka, A., Poole, S.K., Poole, C.F. and Chichila, T.M.P. (1995). Simultaneous microsteam distillation/ solvent extraction for the isolation of semivolatile flavor compounds from *Cinnamomum,* their separation by series of coupled-column gas chromatography. *Analytical Chimica Acta, 302*, 147-162.

Kochummen, K.M. (1989). *Family Lauraceae; Tree Flora of Malaya* (Vol. 4). Kuala Lumpur: Longmans.

Kwon, B.M., Lee, S.L., Choi, S.U., Park, S.H., Lee, C.O., Cho, Y.K., Sung, N.D. and Bok, S.H. (1998). Synthesis and in vitro cytotoxicity of cinnamaldehydes to human solid tumor cells. *Archives Pharmaceutical Research*, *21*, 147-152.

Latip, Z., Hartley, T.G. and Waterman, P.G. (1999). Lignans and coumarins from *Melicope hayesii*. *Phytochemisrry, 51*, 107-110.

Lefer, D.J. and Granger, D.N. (2000). Oxidative stress and cardiac disease. *American Journal of Medicine*, *109*, 315-323.

Mastura, M., Norazah, M.A., Khozirah, S., Rahmani, M. and Ali, A.M. (1999). Anticandidal and antidermatophytic activity of *Cinnamomum* species essential oils. *Cytobios*, *98*, 17-23.

Mukherjee, R., Fujimoto, Y. and Kanikawa, K. (1994). 1-(ω-Hydroxyfattyacyl)glycerols and two flavanols from *Cinnamomum camphora*. *Phytochemistry*, *37*, 1641-1643.

Osawa, T. and Namiki, N. (1981). A novel type of antioxidant isolated from leaf wax of *Eucalyptus* leaves. *Agriculture and Biological Chemistry, 45*, 735-739.

Owen, R.W., Mier, W., Giacosa, A., Hull, W.E., Spiegelhalder, B. and Barsch, H. (2000). Identification of lignans as major components in the phenolic fraction of olive oil. *Clinical Chemistry, 46*, 976-988.

Pelter, A., Ward, R.S., Rao, E.V. and Sastry, K.V. (1976). Revised structures for pluviatilol, methyl pluviatilol and xanthoxylol; General methods for the assignment of stereochemistry to 2,6-diaryl-3,7-dioxobicyclo[3,3,0] octane lignans. *Tetrahedron, 32*, 2783-2788.

Perry, L.M. (1980). *Medicinal Plants of East and Southeast Asia: Attributed Properties and Uses*. Cambridge: The Massachussetts Institute of Technology Press.

Su, M.J., Chen, W.P., Lo, T.Y. and Wu, T.S. (1999). Inonic mechanisms for the antiarrythmic action of cinnamophilin in rat heart. *Journal of Biomedical Sciences*, *6*, 376-386.

Valenciennes, E., Smadja, J. and Conan, J.Y. (1999). Screening for biological activity and chemical composition of *Euodia borbonica* var. *borbonica* (Rutaceae), a medicinal plant in Reunion Island. *Journal of Ethnopharmacology, 64*, 283-288.

Wijesekera, R.O.B. (1978). The chemistry and technology of cinnamon. *Critical Review in Food Science and Nutrition, 10*, 1-29.

Yang, S.J., Fang, J.M. and Cheng, Y.S. (1999). Lignans, flavonoids and phenolic derivatives from *Taxus mairei. Journal of Chinese Chemical Society, 46*, 811-818.

Youdim, K.A., Dorman, H.J.D. and Deans, S.G. (1999). The antioxidant effectiveness of thyme oil, α-tocopherol and ascorbyl palmitate on evening primrose oil oxidation. *Journal of Essential Oil Research*, *11*, 643-648.

Zhu, L., Ding, D. and Lawrence, B.M. (1994). The *Cinnamomum* species in China: Resources for the present and future. *Perfumer and Flavorist, 19*, 17-22.

Ergonomic Design of a Computer Keyboard Layout for the *Jawi* Script

Shahrul Kamaruddin[1*], S.C. Beng[1] and Zahid A. Khan[2]

[1]*School of Mechanical Engineering, Universiti Sains Malaysia, Engineering Campus,*
14300 Nibong Tebal, Penang, Malaysia
[2]*Department of Mechanical Engineering, Faculty of Engineering and Technology,*
Jamia Millia Islamia, Jamia Nagar, New Delhi, 110025 India
[*]*E-mail: meshah@eng.usm.my*

ABSTRACT

Due to unavailability of a computer keyboard layout for the *Jawi* script, users of this script make use of the Arabic keyboard layout for typing texts in this particular script. Obviously, the layout of the Arabic script keyboard is not designed for the ancient writing of the *Jawi* script. Keeping this in view, a research was conducted to design a new keyboard layout suitable for the users of the *Jawi* script from an ergonomics point of view, and the outcome of the research is presented in this study. In order to design the *Jawi* script keyboard layout, the relative finger strengths of both male and female subjects were determined experimentally. The relative frequency of the characters and two special characters (full-stop and comma) that appeared in the script were determined by counting their presence in a large number of texts in the script that represent the workload of the fingers. The keys were rearranged in such a way that the workload of each finger was approximately matched with its relative strength. The newly proposed arrangement of the keys was not much different compared to the Arabic script keyboard layout, and hence it is convenient for users to switch between the layouts.

Keywords: Human computer interaction, keyboard layout, ergonomics, product design, the *Jawi* script

INTRODUCTION

Computer is used in various applications and tasks. In the Human-Computer-Interaction (HCI) system, keyboard is an important input device and primary mode for text entry (Shneiderman, 1992). The layout of the keyboard is therefore a crucial variable in determining the speed, accuracy, ease of learning, and efficiency of the interaction between the user and the computer (Hurlburt and Ottenbacher, 1992). Keyboard proficiency is developed in schools since it helps prepare students for the working world, where such skills are used to enhance productivity (Struck, 1999). Although QWERTY keyboard is widely used, many new keyboard layouts have been ergonomically designed to improve the efficiency of specific end users. However, the layouts have been designed merely on the basis of keys arrangements, rather than the shapes or geometries of the keyboard. Among the many keyboard layouts available, the most common design is the DVORAK layout. August Dvorak proposed it in 1932 (Preece *et al*., 1994). The layout is arranged on the basis of the frequency of the usage of letters and the frequency of the letter patterns together with the sequences in the English script. All vowels and the most frequently used consonants are on the home row (Preece *et al*., 1994). The DVORAK keyboard was evaluated by the US Navy in 1944. It was found that

ج jim	ث tha	ت ta	ب ba	ا alif
ذ dzal	د dal	خ kha	چ cha	ح ha
ص shad	ش shin	س sin	ز zai	ر ra
غ ghain	ع ain	ظ dzo	ط tho	ض dhad
ک kaf	ق qaf	ڤ pa	ف fa	ڠ nga
و wau	ن nun	م mim	ل lam	ک ga
ي ya	ء hamzah	لا lam alif	ه ha	و va
				ث nya

Fig. 1: Characters used in the Jawi *script*

typists had improved their relative level of typing efficiency using this keyboard (Tanebaum, 1996). Other keyboard layouts, such as ABCDE, were also designed but studies showed no advantage of this particular style over QWERTY (Shneiderman, 1992).

Although English is the most widely used language internationally, there are still many users who prefer using their own languages. According to Kaplan and Wissink (2003), Microsoft has provided many other keyboard layouts, which were specially designed for different languages/ scripts that are either in the Roman scripts (Danish, French, German, Italian, Portuguese, Finnish, etc.), or non-roman scripts (Arabic, Greek, Russian, Tamil, Thai, Chinese, Japanese, and Korean, etc.). In addition, a computer keyboard layout for the Malay language has been proposed by the authors (Khan *et al.*, 2006). However, an ergonomic keyboard layout has not been designed for the *Jawi* script, even though this language is used widely in the Southeast Asian countries like Malaysia, Indonesia, Brunei, Singapore, and Thailand. Since the total population of these countries is approximately 340 millions, a reasonably large number of people use the *Jawi* script in writing and typing. Consequently, a keyboard layout should be designed for the *Jawi* script for its users' benefits from the ergonomics point of view. Moreover, it is important to mention here that the *Jawi* script is similar to the Arabic script and it uses 36 characters (see *Fig. 1*).

This paper presents a design for a keyboard layout, specifically for the *Jawi* script in order to improve typing efficiency and enhance the work performance and productivity of its users. The keyboard layout was designed by taking into consideration the human factors and linguistic aspects. The relative strength of the fingers was determined for ergonomical reasons. This gave an estimate

of the load that each finger could bear without fatigue. In addition, the relative frequency of each character and two special characters (full-stop and comma), that frequently appear in the *Jawi* script, were obtained by counting their occurrences in a large number of texts printed in the *Jawi* script to represent the workload of the fingers. Subsequently, the keys of the keyboard were rearranged according to the relative strength of each finger and its corresponding workload so that the finger with higher relative strength is utilized to operate key of the alphabet having higher relative frequency. In the following section, the detailed methodology as well as results and discussion are presented. The paper is concluded with the important findings and suggestions for future work.

METHODOLOGY

This section describes the methodology used to find the relative finger strength, the relative frequency of each character and each special character that frequently appear in the *Jawi* script. In addition, the keyboard layout design approach and the method for evaluating alternative keyboard layouts are also discussed.

Procedure for Finding Relative Finger Strength

The procedure adopted in the present study has also been used by other researchers (Khan *et al.*, 2006) for the design of other types of keyboard layout. End users normally make use of only eight fingers for striking the alphabet keys, excluding the thumbs. Matias *et al.* (1996) suggested that a keyboard could be mapped into two halves, and each half could be used by the fingers of each hand for higher typing efficiency. It is advisable to use both hands for typing texts with the keyboard and one hand for spatial inputs to the machine and control panels (Kabbash *et al.*, 1993). Thus, experiments were carried out to determine the relative finger strength of each of the eight fingers for both males and females. Details of the participating subjects and experimental procedure are given below:

Subjects

Initially, 10 male and 10 female subjects were selected to participate in an experiment which was specifically designed to determine their relative finger strengths. In order to verify whether the number of subjects were sufficient for a given level of accuracy and confidence level, the following formula (Barnes, 1980) was used.

$$N' = \left(\frac{2 \times \sqrt{N(\Sigma x^2) - (\Sigma x)^2}}{A \times \Sigma x} \right) \tag{1}$$

where,
N' = number of subjects required,
N = number of subjects used,
A = accuracy level,
x = relative finger strength of an individual finger for all subjects,

In the above formula, A was set at ±10% and the confidence level at 95%. The value N' of was calculated for each finger of both right and left hands. It was found that for the male subjects, the values of N' were less than 10 for all the fingers except for the ring fingers of both right and left hands. On the other hand, the values of N' for all the fingers of the female subjects did not exceed the number of subjects taken ($N' < 10$), so the number of the female subjects were adequate. On the contrary, more male subjects were required. Consequently, five more male subjects were

employed in the experimental study and the new values of N' were calculated using equation (1) on the basis of 15 male subjects.

This time, the values of N' for the right hand index, middle, ring and little fingers were 6.7, 5.9, 10.6 and 8.7, respectively. Similarly, the left hand index, middle, ring and little fingers had values of 4.2, 8.0, 8.6 and 10.0, respectively. It is evident from these values that N' for all the fingers were less than 15, which ensured the fact that 15 male subjects were adequate. Finally, 15 male and 10 female subjects participated in the finger strength experiment. All the subjects were final year mechanical engineering students aged between 22 to 24 years old. Nine of the male subjects were ethnically Chinese but Malaysian nationals, while 6 others were Malaysians by birth. Similarly, four female subjects were ethnically Chinese but Malaysian nationals, while 6 were Malaysians by birth. The mean age, weight, and height of the male subjects were 22.60 years (S.D. $\pm$ 0.74), 59.87 Kg (S.D. $\pm$ 2.07), and 176.80 cm (S.D. $\pm$ 3.05), respectively. Similarly, the mean age, weight, and height of the female subjects were 22.50 years (S.D. $\pm$ 0.71), 51.40 Kg (S.D. $\pm$ 1.96), and 165.90 cm (S.D. $\pm$ 2.60), respectively. The subjects were healthy and none of them had any past record of either physical or mental abnormality.

Experimental Task and Procedure

The experiment used a specially designed load lifting apparatus which was fabricated and mounted on a wooden laboratory table. A schematic view of the experimental set up is shown in *Fig. 2*. The subjects were required to lift a load of 0.5 kg or 5 N (0.5 kg x 10 ms^{-2}) using each finger of both the hands excluding the thumbs. The reasons for choosing 0.5 kg load are that a small load of 0.5 kg enables the subjects to perform the load lifting task with their fingers comfortably without an undue amount of fatigue and to make it more closely simulate the typing task where one exerts almost the same amount of force in striking the keys (Radwin and Ruffalo, 1999). The load was attached to one end of a cotton string, while the other end was attached to the finger of the subjects. The string was put on a frictionless pulley in such a way that the load hung freely. Two knots were made on the string to act as stops to ensure that the load was lifted to the same height by each finger. The distance between the knots was arbitrarily chosen as 10 cm. The subjects performed the lifting task with their fingers in a sitting posture in an air-conditioned room. The lifting task was considered to determine the relative finger strength of the subjects since several studies have indicated that individuals with greater muscular strength (used in the present study) usually have greater muscular endurance in terms of relative striking ability of different fingers (Burke, 1952; Berger, 1960; Eckert and June, 1971). They started the lifting task with the index finger of one hand at a steady speed, and, when they felt fatigued, they switched to the corresponding finger of the other hand. This was done to provide a rest period to the fatigued hand. The same procedure was used for the middle, ring, and little fingers. The number of lifts performed by each finger was counted and recorded by the experimenter using a tally counter. The total number of lifts made by all fingers of a subject was computed by adding the number of lifts made by each finger. The relative finger strength of each of the participants' fingers for a subject was determined by dividing the number of lifts made by that finger by the total number of lifts, and it was expressed as a percentage.

Statistical Hypotheses and Their Test for Significance

After obtaining the relative finger strength for both the male and female subjects, the data were analyzed to test the following null and alternative hypotheses:

H_0: there is no significant difference between male and female relative finger strength.
H_1: there is significant difference between male and female relative finger strength.

Hypotheses testing were done to find out whether the same or different versions of keyboard are required for both males and females. Minitab software was used to perform a 2-sample T-test in order to reject or fail to reject the null hypothesis. In addition, box-plots were also obtained from the software to exhibit the mean and range of relative finger strength of each finger of the right and left hands for the male and female subjects. The first sample consisted of the relative finger strength of each finger of the male subjects, and the second sample comprised of those of the female subjects. The criterion of either rejecting or failing to reject the null hypothesis was the *p*-value. The smaller the *p*-value, the smaller the probability a mistake will be by rejecting the null hypothesis. A cut-off value which is often used is 0.05. The null hypothesis is rejected when the *p*-value is less than 0.05; otherwise, it is accepted (Ryan and Joiner, 1994).

Determination of Relative Frequency

The frequency of each character and each special character was found by counting their presence in a large number of the *Jawi* script articles which were taken from websites having printed articles in the *Jawi* script. Then, their relative frequencies were calculated using the following formula:

$$F_n = \left(\frac{f_1 + f_2 + f_3 + \ldots + f_n}{T_1 + T_2 + T_3 + \ldots + T_n} \right) \times 100$$

or

$$F_n = \left(\sum_{n=1}^{m} f_n \Big/ \sum_{n=1}^{m} T_n \right) \times 100 \qquad (2)$$

where, F_n = relative frequency of a particular alphabet or a special character,
  f_n = frequency of a particular alphabet or a special character in the article n,
  T_n = total number of the characters in article n,
  n = number of articles, ($n = 1, 2, 3\ldots, m$),
  m = total number of articles analyzed.

In order to get a stable value of the relative frequency, a line graph was plotted to observe the variation in the cumulative number of the characters in the articles analyzed until it stabilized. This final stable value actually represented the true value of the relative frequency.

Keyboard Layout Design Approach

Since keyboard layout is important in enhancing speed and accuracy, it is important to use a keyboard that meets an individual's needs (Poole, 1995). As mentioned earlier, eight fingers of both hands are normally used for striking various keys. *Fig. 3* illustrates how each finger is used to strike different keys. It can be seen from this figure that the left little finger is used to strike the keys for "Q", "A", and "Z", while the left ring finger is for "W", "S", and "X", the left middle finger for "E", "D", "C", the left index finger is for "R", "F", "V", "T", "G", and "B", the right index finger for "Y", "H", "N", "U", "J", and "M", the right middle finger for "I", "K", and ","; the right ring finger for "O", "L", and "."; the right little finger for "P" and the other three (empty) yellow coloured keys.

The first step in designing a keyboard layout for the *Jawi* script was to evaluate the existing Arabic script keyboard layout to determine whether the work load of the fingers matched with their relative strength. *Fig. 4* shows the keyboard layout for the Arabic script considered in this study. Based on the evaluation, a rough idea for the possible *Jawi* script keyboard layout was visualized. Then, the keys were rearranged so as to match as much as possible the relative fingers' strengths
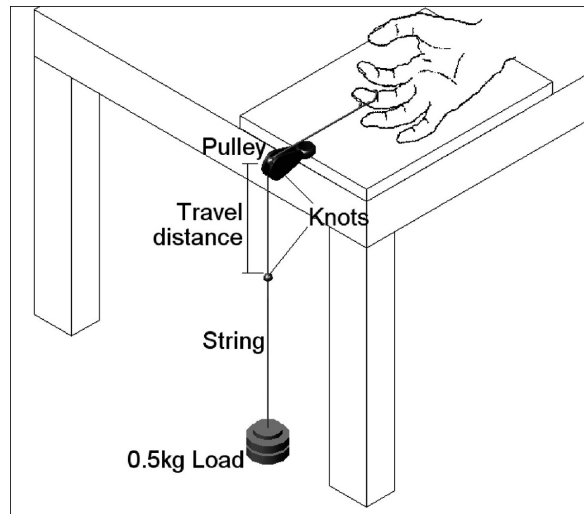
Fig. 2: Schematic view of the experimental setup
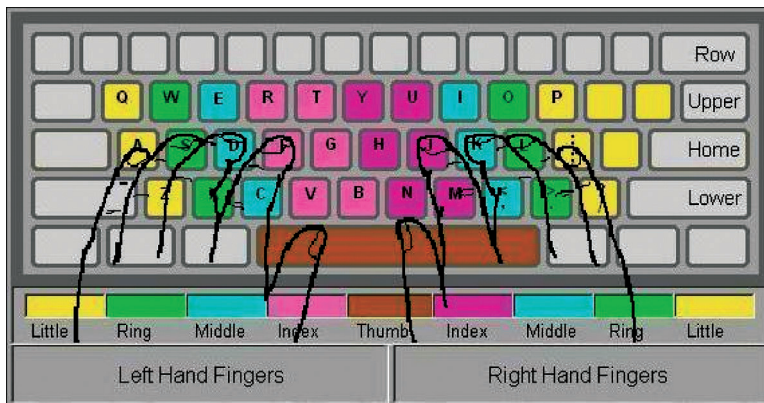
Fig. 3: QWERTY keyboard with typing fingers position

with the relative frequencies (workload) of the characters. In addition, some other features like the total workloads of the right and left hands were also taken into consideration. The keys were arranged in such a way that the right hand fingers would bear a relatively higher workload since most users are right handed. As shown in *Fig. 3*, the three rows of keys in a keyboard layout are the upper, home, and lower rows. The fingers rest on the home row and travel a particular distance between the rows to strike the keys while using a keyboard in the normal posture. Greater finger travel between keys may also result in increased fatigue (Kincaid, 1999). Thus, to avoid unwanted travel, the keys for higher frequency characters were arranged in the home row. The rest of the keys were placed either on the upper row or on the lower row with minimum possible change of key positions from the Arabic keyboard. Since the *Jawi* script has 36 characters and the standard QWERTY keyboard has only 33 keys in all the rows, there are therefore not enough keys on the QWERTY keyboard to accommodate all the *Jawi* characters. The extra *Jawi* characters were

Fig. 4: Keyboard layout of the Arabic script

combined with other characters that were represented by the keys on the right hand side of the lower row in such a way that they could be invoked by pressing these keys together with the "Shift" key in the same way as the characters like "<", ">", "?", etc. are typed on the QWERTY keyboard.

Following this approach, various alternative keyboard layouts were designed arbitrarily. In order to select the design which best fulfils the requirements of the *Jawi* script with minimum change in keys positions from the Arabic keyboard, alternative keyboard layouts were evaluated using the same procedure given in the next section.

Evaluation of the Alternative Keyboard Layouts

Five arbitrarily chosen alternatives and an existing Arabic script keyboard layout were considered for evaluation in this study. The evaluation was done on the basis of 12 design criteria. Criteria 1 to 8 were based on the strength of 8 fingers, criteria 9 and 10 were related to the total workload of the right and left hands, while criterion 11 was based on the finger workloads for operating the home row keys, and the last design criterion was based on the number of changes in the key positions of the Arabic keyboard. A pair-wise comparison between these design criteria was made and a weighting score of either 1 or 0 was assigned to each criterion. A weighting score of 1 was assigned if the design criterion was relatively more important and 0 if it was relatively less important. After comparing all possible pairs of the design criteria, the total weighting score of each design criterion was found by simply counting the number of 1s assigned to that particular design criterion. The total weighting score was subsequently converted into a percentage weighting score by dividing the total weighting score of each design criterion by the grand total and then multiplying it by 100.

Next, the concept of competitive benchmarking was used where numerical values of five different alternatives and an existing Arabic keyboard layout were compared with the desired values. It should be noted that the numerical values obtained on the basis of criteria 1 to 11 represented the workload. On the other hand, the numerical values for the last design criterion represented the number of keys positions which are different from the Arabic script keyboard layout. Obviously, all 11 criteria should be as high as possible since the use of the home row keys is preferred. While quantifying criterion 12 is difficult, it should logically be as low as possible since most users are expected to be familiar with the Arabic script keyboard layout.

Finally, a decision matrix was developed and analyzed to select the best keyboard layout. The decision matrix method was effective for comparing alternative designs that were not refined enough for a direct comparison with engineering specifications (Ullman, 1997). This method provides a means for scoring alternative designs relative to the others in its ability to meet the design criteria.

The decision matrix was developed by subjectively assigning either a positive or a negative score to each keyboard layout on the basis of comparison between the numerical value and the corresponding desired value that were obtained in the competitive benchmarking. The following four-level scale was used to assign scores to each keyboard layout in the decision table for criteria 1 to 10:

        +2   for very close agreement with the desired value
        +1   for close agreement with the desired value
        -1   for large deviation from the desired value
        -2   for very large deviation from the desired value

Similarly, the following four-level scale was used to assign scores to each keyboard layout in the decision table for criteria 11:

        +2   if the numerical value is very high
        +1   if the numerical value is high
        -1   if the numerical value is low
        -2   if the numerical value is very low

Finally, the following four-level scale was used to assign scores to each keyboard layout in the decision table for criteria 12:

        +2   if the numerical value is very low
        +1   if the numerical value is low
        -1   if the numerical value is high
        -2   if the numerical value is very high

Next, the total scores were found by adding the scores of each keyboard layout. Then, the overall weighted total score for each keyboard layout was computed by taking the algebraic sum of the product of the percentage weighting score of each criterion and the score assigned for that particular criterion. Finally, the keyboard layout design with the highest weighted total score was selected as the best alternative.

RESULTS AND DISCUSSION

In the following section, the results pertaining to the finger's strength, relative frequency of characters and final design of the keyboard layout are presented.

Relative Finger Strength

Following the methodology discussed in sub-section 2.1, the results for the finger strength were obtained. Tables 1 and 2 present the relative finger strength of individual fingers for all the 15 male and 10 female subjects, respectively. In addition, these tables also show the total relative finger strength of the left and right hand fingers and the average relative finger strength of individual fingers. Table 1 depicts that the relative finger strength of the males varies from 5.2% to 21.6%. Meanwhile, the index finger of the right hand has the maximum average relative strength (17.0%) and the little finger of the left hand has the minimum (6.5%). Table 2 reveals that the relative finger strength of the female subjects varies from 5.1% to 22.7%. The middle finger of the right hand has the maximum average relative strength (17.3%) and the little finger of the left hand has the minimum (5.9%). Table 3 illustrates that the relative finger strengths obtained in the present study are close to those reported by Barnes (1980).

TABLE 1
Relative finger strength for the male subjects

Subject, N	Relative finger strength, % (L-Left; R-Right)									
	Index		Middle		Ring		Little		Total	
	L	R	L	R	L	R	L	R	L	R
1	15.9	16.4	14.9	15.8	11.4	10.5	7.0	8.1	49.2	50.8
2	13.7	20.6	13.9	11.8	8.6	15.2	5.8	10.4	42.0	58.0
3	11.9	18.7	11.8	17.4	10.4	14.7	6.1	9.0	40.2	59.8
4	14.3	15.5	13.6	15.0	13.8	12.6	6.7	8.5	48.4	51.6
5	12.6	16.0	12.7	17.2	10.3	16.2	6.4	8.6	42.0	58.0
6	13.4	15.5	11.1	16.0	10.3	16.7	8.0	9.0	42.8	57.2
7	11.9	18.5	12.1	17.5	10.1	15.0	6.4	8.5	40.5	59.5
8	13.0	15.5	17.1	15.1	13.8	9.4	7.1	9.0	51.0	49.0
9	13.2	13.3	16.0	14.2	11.3	14.1	8.6	9.3	49.1	50.9
10	14.0	17.0	11.0	19.1	8.0	14.2	7.9	8.8	40.9	59.1
11	13.9	14.8	16.9	14.9	10.5	17.7	4.9	6.4	46.2	53.8
12	10.7	21.6	12.7	19.5	11.4	11.6	6.1	6.4	40.9	59.1
13	15.7	15.9	11.6	17.8	9.3	17.0	5.3	7.4	41.9	58.1
14	12.3	16.5	14.5	18.5	11.7	13.9	5.2	7.4	43.7	56.3
15	14.5	19.2	13.7	17.6	9.7	13.2	6.2	5.9	44.1	55.9
Average	13.4	17.0	13.6	16.5	10.7	14.1	6.5	8.2	44.2	55.8
S.D. (±)	1.41	2.27	1.99	2.07	1.63	2.38	1.06	1.25	3.64	3.64

TABLE 2
Relative finger strength for the female subjects

Subject, N	Relative finger strength, % (L-Left; R-Right)									
	Index		Middle		Ring		Little		Total	
	L	R	L	R	L	R	L	R	L	R
1	14.4	17.7	15.2	15.7	11.7	13.6	6.3	5.4	47.6	52.4
2	13.4	16.8	13.2	17.2	10.2	16.0	5.8	7.4	42.6	57.4
3	13.7	19.2	13.5	16.8	8.2	13.7	5.8	9.1	41.2	58.8
4	12.7	16.0	16.1	16.5	11.7	12.9	6.6	7.5	47.1	52.9
5	14.4	16.7	15.7	17.7	9.6	13.5	5.3	7.1	45.0	55.0
6	14.3	18.0	13.8	16.2	10.5	13.1	5.9	8.2	44.5	55.5
7	15.1	15.6	16.1	16.8	11.3	11.8	5.5	7.8	48.0	52.0
8	17.3	15.9	15.1	15.3	10.0	13.4	5.6	7.4	48.0	52.0
9	11.4	18.1	9.4	22.7	6.5	17.6	5.1	9.2	32.4	67.6
10	13.7	16.7	13.4	18.0	9.8	13.0	6.9	8.5	43.8	56.2
Average	14.0	17.1	14.1	17.3	9.9	13.9	5.9	7.8	43.9	56.1
S.D. (±)	1.55	1.15	2.02	2.07	1.61	1.68	0.57	1.10	4.72	4.72

Pertanika J. Sci. & Technol. Vol. 18 (2) 2010

279

TABLE 3
Comparison of relative finger strength

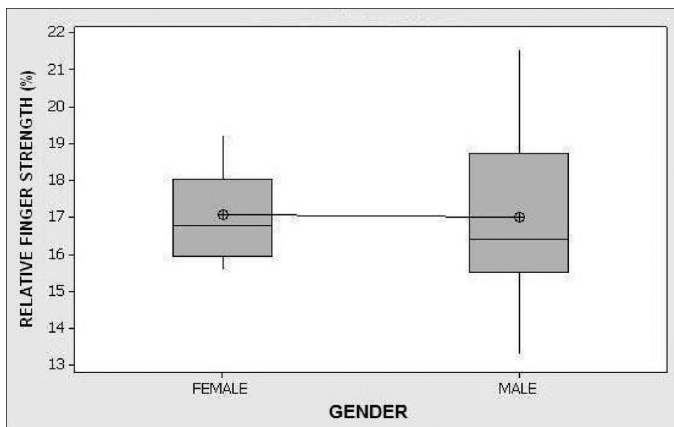| | Relative finger strength, % | | | | | | | |
	Left hand				Right hand			
	Index	Middle	Ring	Little	Index	Middle	Ring	Little
Present study	13.4	13.6	10.7	6.5	17.0	16.5	14.1	8.2
Barnes (1980)	14.2	12.8	8.8	8.1	18.5	15.3	13.4	8.9

Fig. 5: Box-plot of the right hand index finger relative strength for males and females
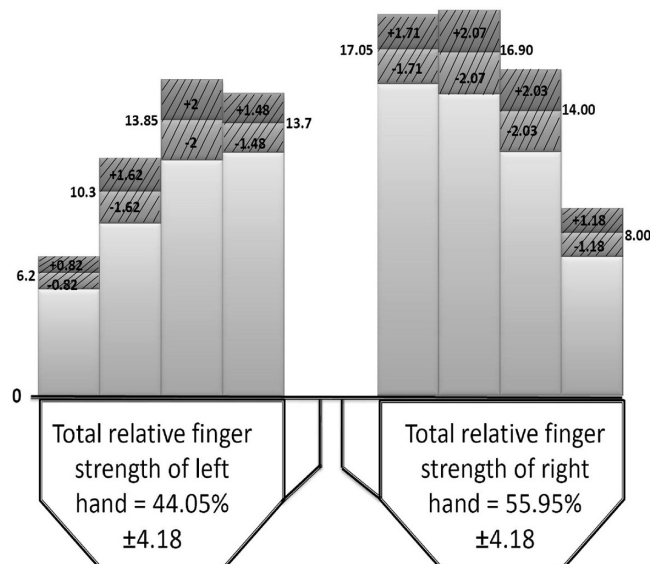

Fig. 6: Average relative finger strength of the left and right hand
fingers with error values shown by hatched bars

TABLE 4
Number of male subjects required, N'

Subject, N	Right hand								Left hand							
	Index		Middle		Ring		Little		Index		Middle		Ring		Little	
	x	x^2	x	x^2	x	x^2	x	x^2	x	x^2	x	x^2	x	x^2	x	x^2
1	16.4	268.96	15.8	249.64	10.5	110.25	8.1	65.61	15.9	252.81	14.9	222.01	11.4	129.96	7.0	49.00
2	20.6	424.36	11.8	139.24	15.2	231.04	10.4	108.16	13.7	187.69	13.9	193.21	8.6	73.96	5.8	33.64
3	18.7	349.69	17.4	302.76	14.7	216.09	9.0	81.00	11.9	141.61	11.8	139.24	10.4	108.16	6.1	37.21
4	15.5	240.25	15.0	225.00	12.6	158.76	8.5	72.25	14.3	204.49	13.6	184.96	13.8	190.44	6.7	44.89
5	16.0	256.00	17.2	295.84	16.2	262.44	8.6	73.96	12.6	158.76	12.7	161.29	10.3	106.09	6.4	40.96
6	15.5	240.25	16.0	256.00	16.7	278.89	9.0	81.00	13.4	179.56	11.1	123.21	10.3	106.09	8.0	64.00
7	18.5	342.25	17.5	306.25	15.0	225.00	8.5	72.25	11.9	141.61	12.1	146.41	10.1	102.01	6.4	40.96
8	15.5	240.25	15.1	228.01	9.4	88.36	9.0	81.00	13.0	169.00	17.1	292.41	13.8	190.44	7.1	50.41
9	13.3	176.89	14.2	201.64	14.1	198.81	9.3	86.49	13.2	174.24	16.0	256.00	11.3	127.69	8.6	73.96
10	17.0	289.00	19.1	364.81	14.2	201.64	8.8	77.44	14.0	196.00	11.0	121.00	8.0	64.00	7.9	62.41
11	14.8	219.04	14.9	222.01	17.7	313.29	6.4	40.96	13.9	193.21	16.9	285.61	10.5	110.25	4.9	24.01
12	21.6	466.56	19.5	380.25	11.6	134.56	6.4	40.96	10.7	114.49	12.7	161.29	11.4	129.96	6.1	37.21
13	15.9	252.81	17.8	316.84	17.0	289.00	7.4	54.76	15.7	246.49	11.6	134.56	9.3	86.49	5.3	28.09
14	16.5	272.25	18.5	342.25	13.9	193.21	7.4	54.76	12.3	151.29	14.5	210.25	11.7	136.89	5.2	27.04
15	19.2	368.64	17.6	309.76	13.2	174.24	5.9	34.81	14.5	210.25	13.7	187.69	9.7	94.09	6.2	38.44
Total	255.0	4407.20	247.4	4140.30	212.0	3075.58	122.7	1025.41	201.0	2721.50	203.6	2819.14	160.6	1756.52	97.7	652.23
N'	**6.7**		**5.9**		**10.6**		**8.7**		**4.2**		**8.0**		**8.6**		**10.0**	

TABLE 5
Number of the female subjects required, N'

Subject, N	Right hand								Left hand							
	Index		Middle		Ring		Little		Index		Middle		Ring		Little	
	x	x^2	x	x^2	x	x^2	x	x^2	x	x^2	x	x^2	x	x^2	x	x^2
1	17.7	313.29	15.7	246.49	13.6	184.96	5.4	29.16	14.4	207.36	15.2	231.04	11.7	136.89	6.3	39.69
2	16.8	282.24	17.2	295.84	16.0	256.00	7.4	54.76	13.4	179.56	13.2	174.24	10.2	104.04	5.8	33.64
3	19.2	368.64	16.8	282.24	13.7	187.69	9.1	82.81	13.7	187.69	13.5	182.25	8.2	67.24	5.8	33.64
4	15.9	252.81	16.5	272.25	12.9	166.41	7.5	56.25	12.7	161.29	16.1	259.21	11.6	134.56	6.6	43.56
5	16.8	282.24	17.7	313.29	13.5	182.25	7.1	50.41	14.4	207.36	15.7	246.49	9.7	94.09	5.3	28.09
6	18.0	324.00	16.2	262.44	13.1	171.61	8.2	67.24	14.3	204.49	13.8	190.44	10.5	110.25	5.9	34.81
7	15.6	243.36	16.8	282.24	11.8	139.24	7.8	60.84	15.1	228.01	16.1	259.21	11.3	127.69	5.5	30.25
8	15.9	252.81	15.3	234.09	13.4	179.56	7.4	54.76	17.3	299.29	15.1	228.01	10.0	100.00	5.6	31.36
9	18.1	327.61	22.6	510.76	17.6	309.76	9.2	84.64	11.4	129.96	9.4	88.36	6.5	42.25	5.1	26.01
10	16.7	278.89	18.0	324.00	13.0	169.00	8.5	72.25	13.7	187.69	13.4	179.56	9.8	96.04	6.9	47.61
Total	170.7	2925.73	172.9	3028.17	138.6	1946.48	77.6	613.12	140.4	1992.70	141.5	2038.81	99.5	1013.05	58.8	348.66
N'	**1.6**		**5.2**		**5.3**		**7.3**		**4.4**		**7.3**		**9.3**		**3.4**	

TABLE 6
p-values obtained from the 2-sample T-test

Finger	*p*-value	
	Right hand	Left hand
Index	0.920	0.308
Middle	0.358	0.490
Ring	0.740	0.266
Little	0.386	0.067

The required number of the male and female subjects' was determined according to the procedure described in sub-section 2.1.1. Tables 4 and 5 show the values of the relative finger strength, *x* of each finger for the 15 male and 10 female subjects, N' respectively. They also show the squared values of x (x^2), sum of x (Σx) and x^2 (Σx^2), and the value of N' for each finger. It can be seen from these tables that the value of N' for each finger is less than 15 for the males and less than 10 for the females. Thus, 15 male and 10 female subjects were adequate for the present study.

As stated earlier, a 2-sample T-test was used to test the statistical significance of the null hypothesis, H_0, and the alternative hypothesis, H_1. The *p*-values for each finger were found to be much higher than 0.05 (Table 6) and therefore, the null hypothesis was accepted. This indicated that there was no significant statistical difference between the male and female relative finger strength. *Fig. 5* shows a typical box-plot for the relative strength of the right hand index fingers of the male and female subjects. The box-plot shows that the range of the relative finger strength of the male is wider than that of the female, but the mean relative finger strength of both male and female is almost the same.

Meanwhile, the average relative strength of each finger of left and right hands is summarized in *Fig. 6* which shows the total relative finger strength of both hands. It should be noted that the relative finger strength is the mean of the average relative finger strength of both the males and females derived from Table 1 and Table 2, respectively. The right index finger has the maximum relative strength (17.05%), while that of the left has the minimum (6.20%).

Relative Frequencies of Alphabets and Special Characters

As outlined in sub-section 2.3, the relative frequency of each character and two special characters was determined. *Figs. 7* and *8* illustrate how the relative frequencies of *alif* ("ا") and full-stop, "." respectively vary with the cumulative number of the characters in the articles. In the beginning, the relative frequency of the alphabet *alif* ("ا") varies considerably but it stabilizes after almost 110×10^3 characters. Thus, the relative frequency of alphabet *alif* ("ا") is 14.90%, as illustrated in *Fig. 7*. Similarly, *Fig. 8* shows that the relative frequency of the special character full-stop, "." is 1.40%.

The relative frequency of other characters and two special characters were determined in a similar manner. Table 7 shows the relative frequency of each character and two special characters considered in the present study. The relative frequency of the alphabet *alif* ("ا") is the highest (14.90%), and that of *dzo* ("ظ") and *ghain* ("غ") are the lowest (0.01%). In addition, the relative frequency of the special character comma "،" is 0.10% and that of the full-stop "." is 1.40%.
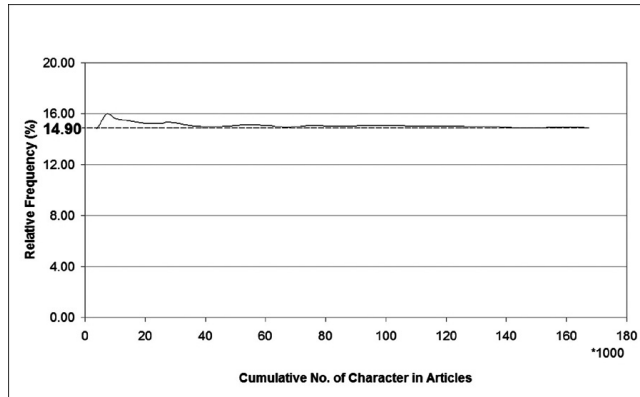
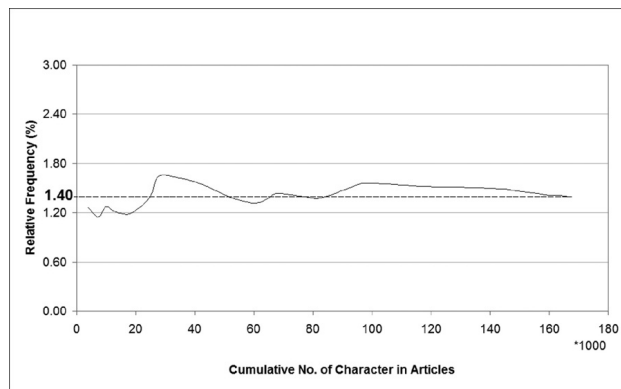Fig. 7: Graph of the relative frequency for alphabet alif, "ا"

Fig. 8: Graph of the relative frequency for the special character full-stop, "."

Alternative Keyboard Layout Designs

As mentioned in sub-section 2.4, the keyboard layout of the Arabic script was first evaluated in terms of finger strength and the corresponding total workload to find its suitability for the *Jawi* script. *Fig. 9* shows the keyboard layout of the Arabic script with the relative frequencies (indicated on the keys) and the total workload of each finger and hand. The total workload of each finger was obtained by adding the relative frequency of the corresponding keys. The total workload of the right index finger is 22.35%, whereas its relative strength is only 17.05%. Thus, this finger is not strong enough to strike the keys and they should be changed. Similarly, other fingers have the total workloads that do not match the corresponding relative finger strength. Thus, it can be concluded that the Arabic script keyboard layout is not suitable for the *Jawi* script. Consequently, other alternative keyboard layouts were considered and evaluated so as to find the best possible layout. *Fig. 10* shows an alternative keyboard layout with the relative frequency of characters, special characters and the total workload of each finger. This layout shows that the finger workloads are relatively close to the corresponding relative finger strengths. It should be noted that the changes in the key position are indicated by putting a dot sign on the lower right corner of the keys.

TABLE 7
Relative frequency of each character and two special characters

Alphabet	ا	ب	ت	ث
Relative frequency (%)	14.90	3.78	5.67	0.07
Alphabet	ج	ح	چ	خ
Relative frequency (%)	2.35	0.47	0.43	0.15
Alphabet	د	ذ	ر	ز
Relative frequency (%)	5.21	0.04	5.46	0.12
Alphabet	س	ش	ص	ض
Relative frequency (%)	5.42	0.23	0.15	0.03
Alphabet	ط	ظ	ع	غ
Relative frequency (%)	0.06	0.01	0.58	0.01
Alphabet	ک	ف	ڤ	ق
Relative frequency (%)	3.01	0.34	3.51	1.27
Alphabet	ى	گ	ل	م
Relative frequency (%)	0.04	1.44	5.20	5.67
Alphabet	ن	و	ژ	ه
Relative frequency (%)	9.55	8.53	0.03	3.00
Alphabet	ال	ء	ي	پ
Relative frequency (%)	1.19	0.31	9.58	0.69
Alphabet	،	.		
Relative frequency (%)	0.10	1.40		

Evaluation of the Alternative Keyboard Layouts

As described in the sub-section 2.5, five arbitrarily chosen alternatives and an existing Arabic keyboard layout were evaluated on the basis of 12 design criteria. Table 8 shows the design criteria and the results of the pair-wise comparison between them. It also shows the total weighting score and the percentage weighting score of each design criterion. The percentage weighting scores were found vary from 4% to 12%. Next, the concept of competitive benchmarking was applied as discussed in sub-section 2.5. The results which show the numerical values obtained for each design criterion for each keyboard layout and the targeted values are presented in Table 9.

The final step in the evaluation process was to develop a decision matrix in order to select the best keyboard layout. The procedure for developing the decision matrix was described in sub-section 2.5. The results which indicate the design criteria, percentage weighting score of each criterion, scores assigned to each keyboard layout, as well as total positive and total negative scores, overall total score, and overall weighted total score for each of the keyboard layouts are presented in Table 10. Clearly, the Arabic keyboard layout is not an ideal choice for the *Jawi* script since its overall weighted total score is very low (+10), whereas the alternative keyboard layout 5 is the best choice

TABLE 8
Pair-wise comparison

Criterion number	Design criteria	Weighting score (1 or 0)											Total weighting score	Percentage weighting score (%)
1	Relative right hand index finger workload	1	1	0	1	0	0	0	1	0	1	1	6	9
2	Relative right hand middle finger workload	0	-	1	0	1	0	0	1	0	1		4	6
3	Relative right hand ring finger workload	0	0	-	0	1	0	0	1	1			4	6
4	Relative right hand little finger workload	1	-	1	0	1	1	1	1				8	12
5	Relative left hand index finger workload	0	1	0	1	1	0	1	0	1	0		6	9
6	Relative left hand middle finger workload	0	0	-	0	1	0	1	0	1			4	6
7	Relative left hand ring finger workload	1	1	1	0	0	-	1	0	1			5	8
8	Relative left hand little finger workload	1	1	1	0	1	1	-	1	0	1		8	12
9	Relative right hand workload			1	1	1	0	0	0	-	1	1	0	6	9
10	Relative left hand workload				0	0	0	1	1	1	0	-	1	0	5	8
11	Relative home row workload					1	1	1	1	1	0	0	-	0	7	11
12	Number of changes in the keys positions compared to the Arabic keyboard					0	0	0	0	0	0	1	1	1	3	4
Grand total														66	100

TABLE 9
Competitive benchmarking for six alternative and three existing keyboard layouts

Criterion number	Design criteria	Alternative keyboard layout					Existing Arabic script keyboard layout	Desired value
		1	2	3	4	5		
1	Right hand index finger workload (%)	22.64	22.41	22.39	19.95	17.63	22.35	17.05
2	Right hand middle finger workload (%)	14.34	15	15.44	15.57	15.57	21.18	16.90
3	Right hand ring finger workload (%)	16.17	12.71	12.6	15.81	15.81	7.34	14.00
4	Right hand little finger workload (%)	8.16	7.12	7.9	7.46	7.54	11.65	8.00
5	Left hand index finger workload (%)	11.4	17.44	16.98	13.83	16.07	17.24	13.70
6	Left hand middle finger workload (%)	16.68	13.75	14.08	12.65	12.65	11.09	13.85
7	Left hand ring finger workload (%)	6.84	11.24	6.84	8.66	8.57	5.88	10.30
8	Left hand little finger workload (%)	3.77	0.33	3.77	6.07	6.16	3.27	6.20
9	Right hand workload (%)	61.31	57.24	58.33	58.79	56.55	62.52	55.95
10	Left hand workload (%)	38.69	42.76	41.67	41.21	43.45	37.48	44.05
11	Workload for striking home row keys (%)	41.19	59.44	49.18	60.69	69.1	60.1	*AHAP**
12	Number of changes in the keys positions compared to the Arabic keyboard (#)	30	25	29	34	34	0	*ALAP**

(*AHAP*- As High As Possible; ALAP*- As Low As Possible*)

TABLE 10
Evaluation matrix to select the best alternative keyboard layout

Criterion number	Design criteria	Percentage weighting score (%)	Alternative keyboard layout					Existing Arabic script keyboard layout
			1	2	3	4	5	
1	Right hand index finger workload	9	-2	-2	+1	+2	-2	-2
2	Right hand middle finger workload	6	+2	+2	+2	+2	-2	-2
3	Right hand ring finger workload	6	+1	+1	+2	+2	-1	-1
4	Right hand little finger workload	12	+1	+2	+2	+2	-1	-1
5	Left hand index finger workload	9	+1	+1	+2	+1	+1	+1
6	Left hand middle finger workload	6	+2	+2	+2	+2	+1	+1
7	Left hand ring finger workload	8	+2	+1	+2	+2	-1	-1
8	Left hand little finger workload	12	-2	+1	+2	+2	+1	+1
9	Right hand workload	9	+2	+1	+1	+2	+1	+1
10	Left hand workload	8	+2	+1	+1	+2	+1	+1
11	Workload for striking home row keys	11	+2	+1	+2	+2	+2	+2
12	Number of changes in the keys positions compared to the Arabic keyboard	4	-1	-2	-2	-2	-	-
Total of positive score			12	15	13	19	21	7
Total of negative score			-5	-3	-4	-2	-2	-7
Overall total score			7	12	9	17	19	0
Overall weighted total score		100	63	77	85	158	175	10
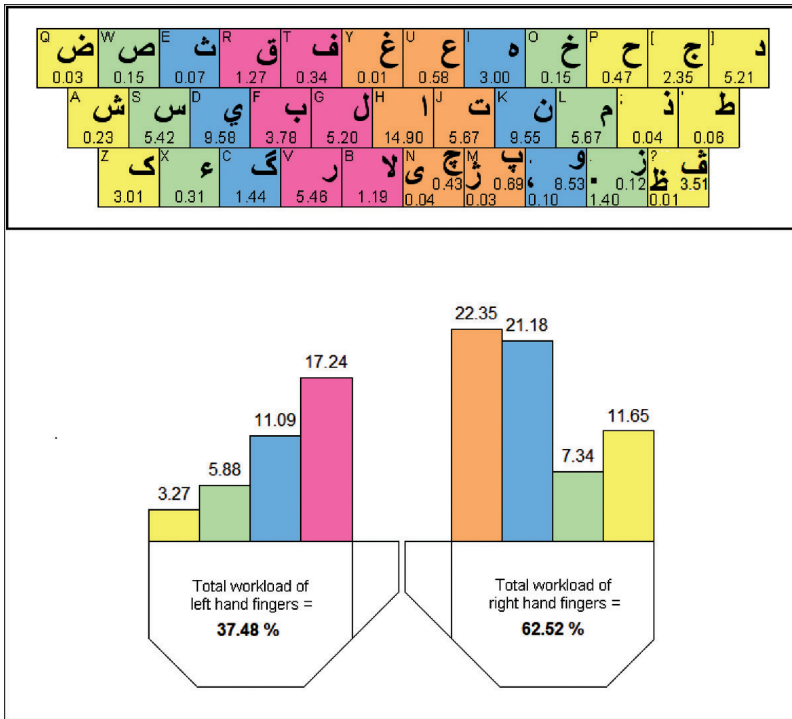
Fig. 9: Keyboard layout of the Arabic script with the relative frequencies and finger workloads
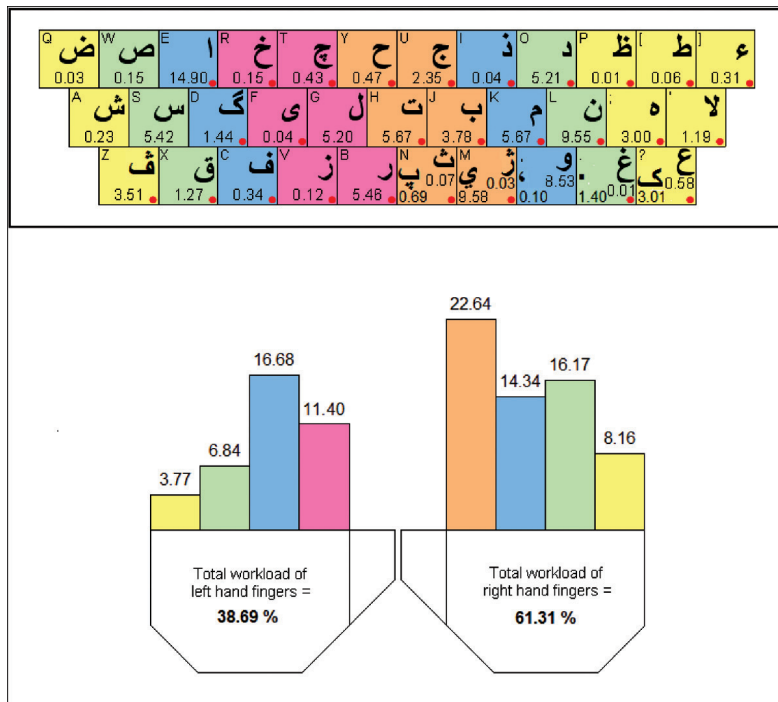

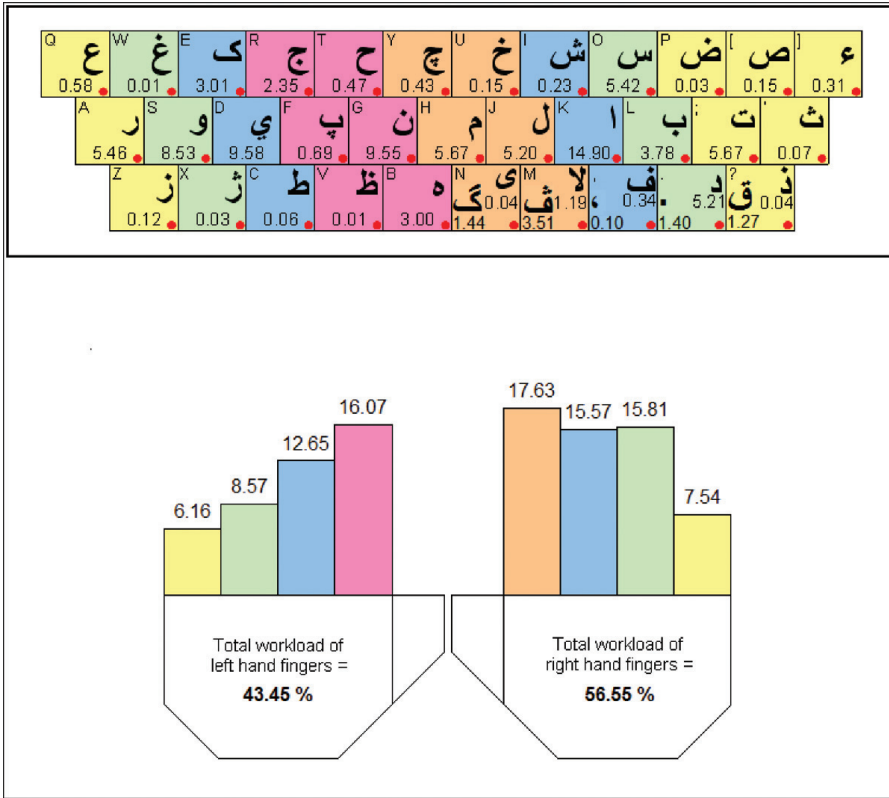*Fig. 10: Alternative keyboard layout*

Fig. 11: Proposed keyboard layout for the Jawi *script*

with the maximum overall weighted total score of +175. *Fig. 11* shows the layout of this particular keyboard with the relative frequency of the characters as well as the total workload of each finger and hand. This figure shows that the relative finger strength matches well with the corresponding total workload. The keys with the dot sign at the lower right corner of the keys indicate the change in the key position.

CONCLUSIONS

This paper presented a systematic approach for designing of a computer keyboard layout for the *Jawi* script from an ergonomics point of view. The relative finger strength of the male and female subjects was experimentally designed through a simple load lifting task performed by their fingers. Meanwhile, a 2-sample T-test method was used to investigate whether different versions of the keyboard were required for the two genders. The results indicated that there was no significant difference between the relative finger strength of the males and females, so both genders could efficiently use the same keyboard. In addition, the relative frequencies of the characters, including two special characters (comma and full-stop) that frequently appeared in this script, were found by counting their presence in a sufficiently large number of the printed articles from various sources. The relative frequency represented the finger workload for striking the keys. Five alternative and an

existing Arabic keyboard layouts were evaluated on the basis of 12 design criteria using the concept of competitive benchmarking and a decision matrix. The Arabic keyboard layout was found to be unsuitable for the *Jawi* script since the arrangement of the keys does not match the finger workloads and relative strengths. Consequently, an alternative keyboard layout is proposed. Although the proposed keyboard layout does not provide 100% matching between the finger workloads and relative strengths, it is the best layout obtained from the evaluation of different alternatives. One limitation of this research is that the relative finger strength has been determined by simply counting the number of lifts performed by the fingers which may not be as accurate as desired. Therefore, the relative finger strength should be measured with sophisticated and accurate instruments like an electromyogram (EMG). Nevertheless, the approach outlined in this paper could be used to design keyboard layouts for other languages as well.

REFERENCES

Barnes, R. M. (1980). *Motion and Time Study Design and Measurement of Work*. Canada: John Wiley & Sons, Inc.

Berger, R. A. (1960). The effect of varied weight training program as strength and endurance. Microcarded Master's Thesis, University of Illinois, USA.

Burke, W. E. (1952). A study of the relationship of age to strength and endurance – Gripping. Microcarded Ph.D. Thesis, University of Iowa, USA.

Eckert, H. M. and June, D. (1971). Relationship between strength and workload in push-ups. *Research Quarterly*, *38*, 380-383.

Hurlburt, M. and Ottenbacher, K. J. (1992). Spinal cord: Wounds and injuries. *Journal of Rehabilitation Research and Development*, *29*, 54-64.

Kabbash, P., MacKenzie, I. S. and Buxton, W. (1993). Human performance using computer input devices in the preferred and non-preferred hands. *Proceedings of the INTERCHI '93 Conference on Human Factors in Computing Systems* (pp.474-481). ACM, New York.

Kaplan, M. S. and Wissink, C. (2003). Unicode and keyboards on Windows, Windows Globalization, Microsoft Corporation. *Proceedings of the 23rd Internationalization and Unicode Conference*. Prague, Czech Republic, March.

Khan, Z. A., Kamaruddin, S. and Beng, S. C. (2006). Ergonomic design of a computer keyboard layout for Malay language. *Asian Journal of Ergonomics, 7*(1 & 2), 81-100.

Kincaid, C. (1999). Alternative keyboards. *Exceptional Parent*, *2*, 34-35.

Matias, E., MacKenzie, I. S. and Buxton, W. (1996). One-Handed Touch-Typing on a QWERTY Keyboard. *Human-Computer Interaction*, *11*, 1-27.

Poole, C. J. M. (1995). Computers and the handicapped. *British Medical Journal*, *311*, 1149-1152.

Preece, J., Rogers, Y., Sharp, H., Benyon, D., Holland, S. and Carey, T. (1994). *Human-Computer Interaction*. Great Britain: Addison-Wesley.

Radwin, R. G. and Ruffalo, B. A. (1999). Computer key switch force-displacement characteristics and short-term effects on localized fatigue. *Ergonomics*, *42*, 160-170.

Ryan, F. B. and Joiner, B. L. (1994). *Minitab Handbook*. Belmont, California, USA: Duxbury Press.

Shneiderman, B. (1992). *Designing the User Interface: Strategies for Effective Human-Computer Interaction*. USA: Addison-Wesley Publishing Company.

Struck, M. (1999). Focus on one handed keyboarding options. *OT Practice*, *4*, 55-56.

Tanebaum, D. (1996). Dvorak keyboards: The typist's long-lost friend. *Technology Review*, *July,* 21-23.

Ullman, D.G. (1997). *The Mechanical Design Process*. Singapore: McGraw-Hill Companies.

Numerical Modelling of Tidal Circulation and Sediment Transport in the Gulf of Khambhat and Narmada Estuary, West Coast of India

P.C. Sinha[1*], G.K. Jena[2], Indu Jain[2], A.D. Rao[2] and Mohd Lokman Husain[1]

[1]*Institute of Oceanography, Universiti Malaysia Terengganu,*
21030 Kuala Terengganu, Terengganu, Malaysia
[2]*Centre for Atmospheric Sciences, Indian Institute of Technology,*
New Delhi-110016, India
[*]E-mail: p_c_sinha@yahoo.co.in

ABSTRACT

A depth-averaged numerical model was developed to study tidal circulation and suspended sediment transport in the gulf of Khambhat along the west coast of India. The spatial resolution of the model is 750m x 750m. A 2-D fine resolution (150 m x 150 m) model for the lower part of the Narmada estuary is coupled with the coarser gulf model to simulate the flow features in the lower estuary. The model dynamics and basic formulation remain the same for both the gulf model and the estuary model. The models are barotropic, based on the shallow water equations and neglect horizontal diffusion and wind stress terms in the momentum equations. The models are fully non-linear and use a semi-explicit finite difference scheme to solve mass, momentum, and advection-diffusion equation for suspended sediments in a horizontal plane. The erosion and deposition have been computed by an empirically developed source and sink term in the suspended sediment equation. The tide in the gulf is mainly represented in the model by the semi-diurnal M_2 constituent. Meanwhile, fresh water discharge from the rivers joining the gulf had also been considered. Numerical experiments were carried out to study the circulation and suspended sediment concentrations in the gulf and estuarine region.

Keywords: Tidal circulation, suspended sediment, numerical model, M_2 constituent, gulf of Khambhat, Narmada estuary

INTRODUCTION

In the recent years, the importance of sediment transport to marine environment and coastal engineering has been widely recognized. Johns *et al.* (1990) used a numerical model to determine changes in bed morphology resulting from bed load and suspended transport of sand in the Taw estuary, England. Podsetchine and Hutulla (1994) developed a 2-D vertical flow and suspended matter transport model for Lake Karhijiarvi, Finland. A coupled hydrodynamic/suspended sediment transport model, including waves and currents, was developed by Lou and Ridd (1997). The model system has been applied to Cleveland Bay, Australia. Wu *et al.* (2000) used a numerical model for calculating flow and sediment transport in open channels. In their model, the water level is determined from a 2-D Poisson equation derived from depth-averaged momentum equations. Suspended load transport is simulated through the general advection-diffusion equation with an empirical settling velocity term. Tattersall *et al.* (2003) applied 2-D depth-averaged models to simulate the tidal currents and suspended sediment concentrations in the Tamar estuary located in the south west coast of England. Recently, Gleizon *et al.* (2003) developed a model of vertically resolving sediments
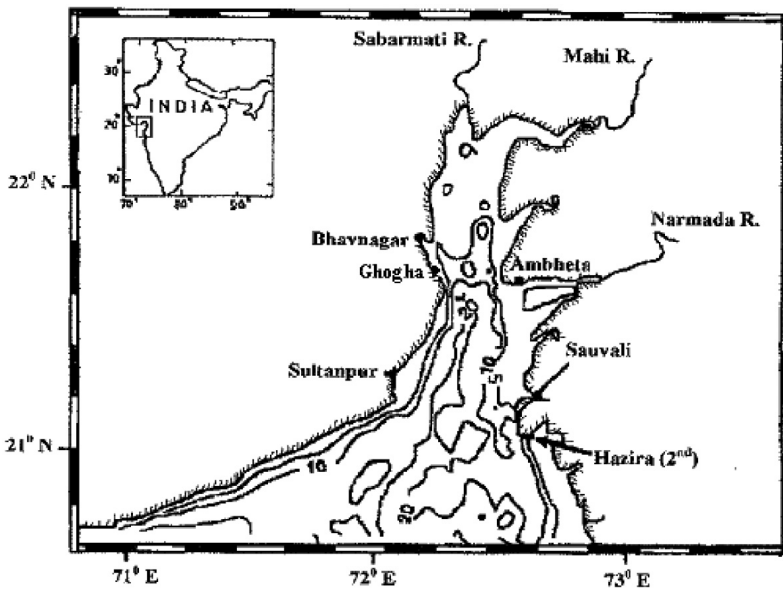
---

*Corresponding Author

Fig. 1: Map of the gulf of Khambhat

in estuaries (VERSE) to simulate water, sediment, and sediment-bound contaminant transport in vertically stratified and relatively narrow microtidal estuary (Ribble estuary).

The gulf of Khambhat (*Fig. 1*) is an inverted funnel-shaped indentation on the western shelf of India, between the Saurashtra Peninsula and the mainland of Gujarat. The north-south extent of the analysis region is approximately 145 km, while its width varies between 20 and 110 km. The gulf has an area of about 3120 sq. km and a maximum depth of 35 m. The important characteristic of the gulf is its high tidal range. In the gulf, tidal currents dominate the flow. The tides are of semi-diurnal type with a large diurnal inequality and varying amplitudes, which increase from the south to north along the gulf coast. The height of the tide increases tremendously from the mouth to the upstream end because of the funnel-shape of the gulf and the semi-enclosed nature at the head and resonance. Meanwhile, tidal currents are fairly strong and bimodal in nature with two dominant directions; towards upstream during flood and downstream during ebb in all encompassing oscillatory motions. The maximum currents occur during mid-tide, which is around 2.5 m/s in the gulf, and associated with high wave energy (Sen Gupta and Deshmukhe, 2000). The gulf is more or less homogeneous displaying a one layer structure. This is caused by the shallowness of the depths and medium to high tidal amplitudes associated with tidal currents and turbulence.

The rivers draining into the gulf of Khambhat carry enormous amount of sediments in their discharges. It receives drainage from Sabarmati, Mahi, and Narmada rivers. These rivers discharge a large volume of sediments as also the suspended load. The bottom consists of mainly the river-borne fine- to coarse-grained sand. The western and northern parts of the gulf consist of largely soft sediments of Quaternary rocks. On the eastern side of the gulf, the river Narmada carries a large volume of suspended sediments. At the estuarine mouth of the river Narmada, the alluvium gets deposited creating deltaic islands like Alia Bet. Keeping this in view, the researchers developed a depth-averaged numerical model to study the tidal flow and suspended sediment transport in the gulf of Khambhat. Nevertheless, the gulf model could not simulate the realistic circulation pattern and suspended sediment concentration near the river mouths. Compared to the other two rivers,

Narmada is a major river in the region. Therefore, a 2-D fine resolution model for the lower part of the Narmada estuary is coupled with the gulf model to simulate the flow features in the lower estuary. The model dynamic and basic formulations remain the same for both the gulf and estuary models. The model equations in the depth-averaged form include non-linear terms and the solution was obtained using a conditionally stable semi-explicit finite difference scheme on a staggered grid.

FORMULATION OF THE MODEL

In the formulation of the model, two-dimensional vertically integrated shallow water equations are used. Neglecting the sphericity of the earth's surface, a system of rectangular Cartesian coordinate is used in which the origin 'O' is within the equilibrium level of the sea surface. Ox points eastward, Oy points northward and Oz is directed vertically upwards. The displaced position of the free surface is given by $z = \zeta(x, y, t)$, and the position of the seal floor by $z = -h(x, y)$.

Assuming hydrostatic approximations, the resulting equations of continuity and momentum are given by:

$$\frac{\partial \zeta}{\partial t} + \frac{\partial (Hu)}{\partial x} + \frac{\partial (Hv)}{\partial y} = 0 \tag{1}$$

$$\frac{\partial u}{\partial t} + u\frac{\partial u}{\partial x} + v\frac{\partial u}{\partial y} - fv = -g\frac{\partial \zeta}{\partial x} + A\nabla^2 u + \frac{1}{H}\left[\frac{F_s}{\rho} - \frac{gu(u^2 + v^2)^{\frac{1}{2}}}{C^2}\right] \tag{2}$$

$$\frac{\partial v}{\partial t} + u\frac{\partial v}{\partial x} + v\frac{\partial v}{\partial y} + fu = -g\frac{\partial \zeta}{\partial y} + A\nabla^2 v + \frac{1}{H}\left[\frac{G_s}{\rho} - \frac{gv(u^2 + v^2)^{\frac{1}{2}}}{C^2}\right] \tag{3}$$

where H ($\zeta + h$) is the total depth, f is the Coriolis parameter at 22° N, g is the acceleration due to gravity, while u and v are the x and y components of depth averaged velocity, respectively, F_s and G_s are the surface shear stress due to wind in the x and y directions, and A is the horizontal eddy viscosity coefficient.

Here, the researchers neglected horizontal diffusion terms in the momentum equations, as their effect was very small as compared to other terms. In addition, the surface stress terms were also neglected as their effect was found to be very small on the tidal circulation in the gulf. The bottom stress terms are parameterized by conventional quadratic laws, and the Chezy coefficient is evaluated by:

$$C = n^{-1}h^{\frac{1}{6}}; \text{ where, } n = 0.025$$

For the sediment transport prediction, a depth-averaged form of the advection-diffusion equation was used to represent the deposition and erosion rates, together with the source and sink terms.

$$\frac{\partial (HC_{ss})}{\partial t} + \left[\frac{\partial (uHC_{ss})}{\partial x} + \frac{\partial (vHC_{ss})}{\partial y}\right] = \frac{\partial}{\partial x}\left[HKc\frac{\partial C_{ss}}{\partial x}\right] + \frac{\partial}{\partial y}\left[HKc\frac{\partial C_{ss}}{\partial y}\right] + \gamma w_S (C_e - C_{ss}) \tag{4}$$

where C_{ss} is the depth-averaged suspended sediment concentration, w_s is the particle settling velocity,

K_c = 150 m²/s is the horizontal diffusivity coefficient of the sediment and C_c is the depth-averaged equilibrium concentration. The profile factor γ is given as (Johns *et al.*, 1990)

$$\gamma = \frac{C_{ss-h}}{C_{ss}} \tag{5}$$

Numerical experimentation has shown that the concentrations of the sediment are in the observed range for the value of γ close to 1. Hence, the value of γ was taken as 1 in the present study.

In determining the equilibrium sediment concentration, the formula suggested by Engelund and Hansen (1967) was used.

Boundary Conditions and Methods of Solution

Tidal boundary condition

The gulf has an open boundary at the seaward end connecting 71.75^0 E and 72.64^0 E at 21^0 N (*Fig. 2*). At the landward end, there are three open boundaries of the analysis area connecting Sabarmati, Mahi, and Narmada rivers. A realistic tidal boundary condition, used at the southern boundary and freshwater discharges from the three rivers, is provided at the river mouths.

The observations of the amplitude and phase of M_2 tide (Unnikrishnan *et al.*, 1999) at the
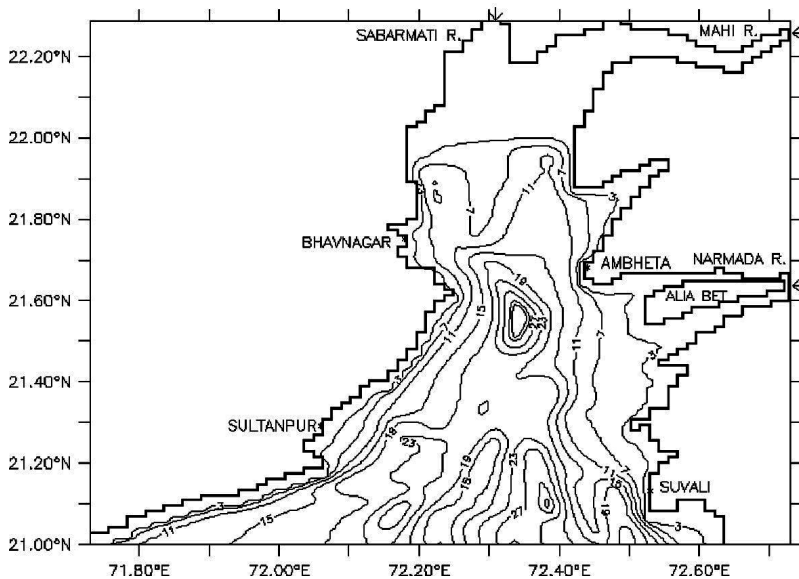
Fig. 2: Bathymetry (m) in the gulf of Khambhat

stations located at the extreme left and extreme right ends of the southern boundary are given in the form

$$\zeta = 1.0 \cos (\omega t - 80^\circ) \text{ and } \zeta = 1.75 \cos (\omega t - 90^\circ) \tag{6}$$

Using these values, the amplitude and phase at the remaining grid points of the open boundary are derived from a linear interpolation.

At the river mouth, the fresh water discharge was prescribed based on available observations. The average runoff into the gulf from Narmada river is nearly 800 m³/s (Haskoning Consulting Engineers and Architects, 1990), while Sabarmati and Mahi contribute about 400 m³/s each. Fresh water discharge from the river mouth is given in the following form

$$\bar{u} = \frac{Q}{A} \tag{7}$$

where Q is the discharge at a river mouth and A is the cross sectional area at that point.

Sediment boundary condition

The sinusoidally varying suspended sediment concentrations along the southern boundary were calculated using the observed values at the extreme ends of the boundary, which are given by:

$$C_{SS} = 200 \cos(\omega t - 170°) \text{ and } C_{ss} = 350 \cos(\omega t - 180°) \tag{8}$$

Along the mouth of the rivers, the sediment concentrations are given by:

$$
\begin{aligned}
C_{ss} &= 260 \cos(\omega t - 270°) \quad \text{at Sabarmati river mouth} \\
C_{ss} &= 200 \cos(\omega t - 273°) \quad \text{at Mahi river mouth} \\
C_{ss} &= 520 \cos(\omega t - 214°) \quad \text{at Narmada river mouth}
\end{aligned} \tag{9}
$$

where amplitude is in mg/l, $\omega = \frac{2\pi}{T}$ and T is the tidal time period.

In addition to the no-slip bottom boundary condition, appropriate conditions have to be satisfied along the lateral boundaries of the gulf area under consideration at all times. In the vertically integrated system at the water land interface, the transport normal to coastline and sediment diffusive fluxes are zero. The motion in the gulf is generated from the initial state of rest and constant sediment concentration. Thus, starting from these initial conditions, an oscillatory steady state was achieved after the 8th tidal cycle of integration, while the results of the 9th tidal cycle were also analysed.

The equations of continuity and momentum were solved using a semi-explicit finite difference scheme on Arakawa-C grid (Sinha *et al.*, 1996), while the suspended sediment transport equation was solved using an explicit finite difference method with advective terms which were represented by an upstream finite difference method.

NUMERICAL EXPERIMENTATION

The analysis areas were chosen from $21°$ N to $22° 18'$ N and $71° 45'$ E to $72° 43'$ E (*Fig. 1*) to study the tidal circulation and the suspended sediment transport in the gulf of Khambhat. Meanwhile, the coastline of the gulf which includes the island of Alia Bet is made up of stair steps consisting of straight line segments parallel to x- and y-axes (*Fig. 2*). In this study, the east-west extent of the gulf is 112.50 km and the north-south extent is 143.25 km. A rectangular mesh of (151 x 192) grid points was chosen to give $\Delta x = \Delta y = 750$ m. In order to avoid sharp depth gradients, a smooth bathymetry was used and the depths in the gulf varied from 3 m to 32 m. The bathymetry in the gulf region is quite irregular and there are many shallow zones followed by deep channels on either side (*Fig. 2*).
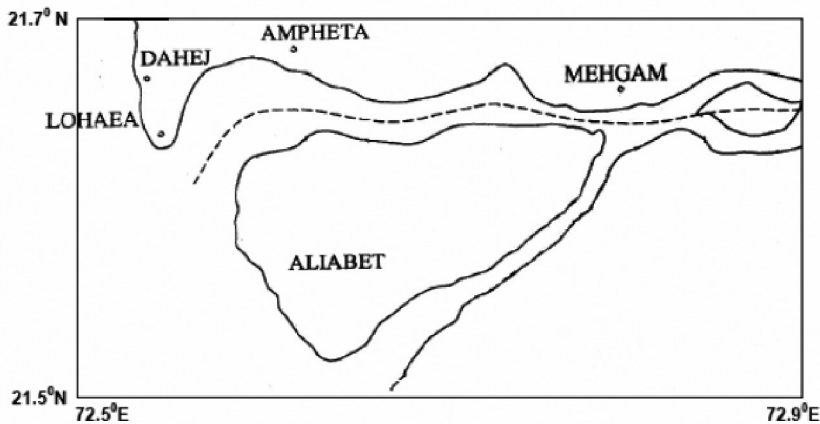
Fig. 3: Narmada river estuary

Compared to the other two rivers, Narmada is a major river in this region. The fresh water discharge from the Narmada estuary is nearly 800m³/s, and it also contributes a higher amount of suspended sediments in the gulf. The coarser gulf model could not compute the tidal flow and sediment transport in the lower part of the Narmada estuary. Hence, a fine resolution model was developed for the lower Narmada estuary, coupled with the coarser gulf model, to compute the flow features in the estuarine region. The gulf and estuary models are dynamically linked together at the interface through the elevation points. The tidal amplitudes and sediment concentrations computed from the coarser model are provided as input to the estuary model.

In order to study the flow features in the lower part of the Narmada river estuary (*Fig. 3*), the estuarine area from Lohaea to Mehgam was chosen. The stair-step boundaries were used to represent the island as well as the irregular coastal boundary of the estuary. Here, the length was taken as 16.65 km, while the breadth as 28.5 km. The area was represented using a mesh of 191 x 112 grid points with a grid interval of 150 m in both x- and y- directions and a constant depth of 6 m was chosen. The time step of the fine resolution estuary model is taken as 10 seconds.

RESULTS AND DISCUSSION

The basic equations, along with appropriate boundary and initial conditions, have been integrated ahead of time till a steady state is reached. During flood, the computed M_2-tidal amplitudes at Suvali and Ambheta were 1.93 m and 2.58 m, respectively. Table 1 provides a comparison of the observed and computed amplitudes at the two stations in the gulf. The computed tidal amplitudes were found to be in agreement with the available observations (Unnikrishanan *et al.*,1999).

The model is able to be used to produce the flood-ebb asymmetry in the gulf region. *Figs. 4a* and *5a* show the computed depth-averaged currents after 3 hours (flood) and 9 hours (ebb) of the 9th tidal cycle, respectively. In the gulf, the currents during flood vary from 0.1 m/s to 2.0 m/s. The tidal currents during ebb are found to vary from 0.1 m/s to 2.21 m/s. It was found that the currents are generally stronger in the central portion of the gulf.

As indicated previously, the coarser gulf model could not simulate the tidal flow near the mouth of the Narmada estuary. Therefore, a fine resolution model for the lower part of the estuary was combined with the coarser gulf model to compute the flow features in this particular estuarine region. *Figs. 4b* and *5b* depict the computed flood and ebb currents in the Narmada river estuary. It was observed that the computed depth-averaged flood currents varied from 0.01 m/s to 1.2 m/s,

TABLE 1
Observed and computed amplitudes (m) of M_2 tide during
flood at two stations in the gulf of Khambhat

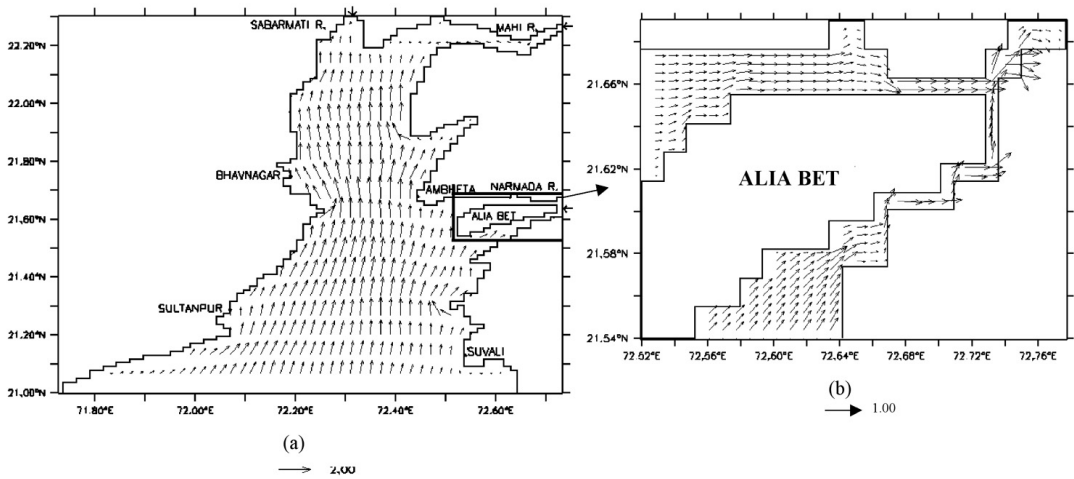| Station	Observed amplitude	Computed amplitude
Suvali	2.05	1.93
Ambheta	2.07	2.58

Fig. 4: Tidal currents (m/s) in (a) the gulf of Khambhat;
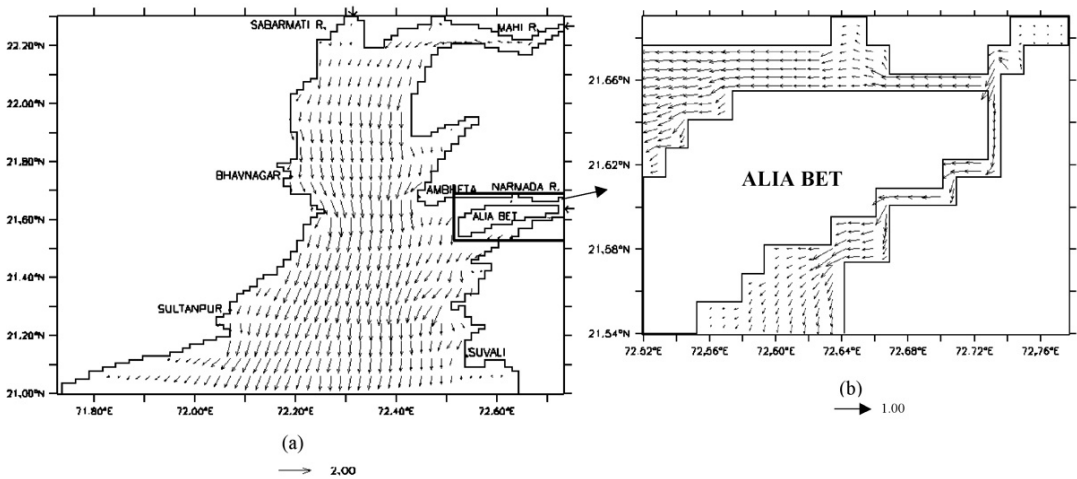(b) the lower part of the Narmada estuary during flood

Fig. 5: Tidal currents (m/s) in (a) the gulf of Khambhat;
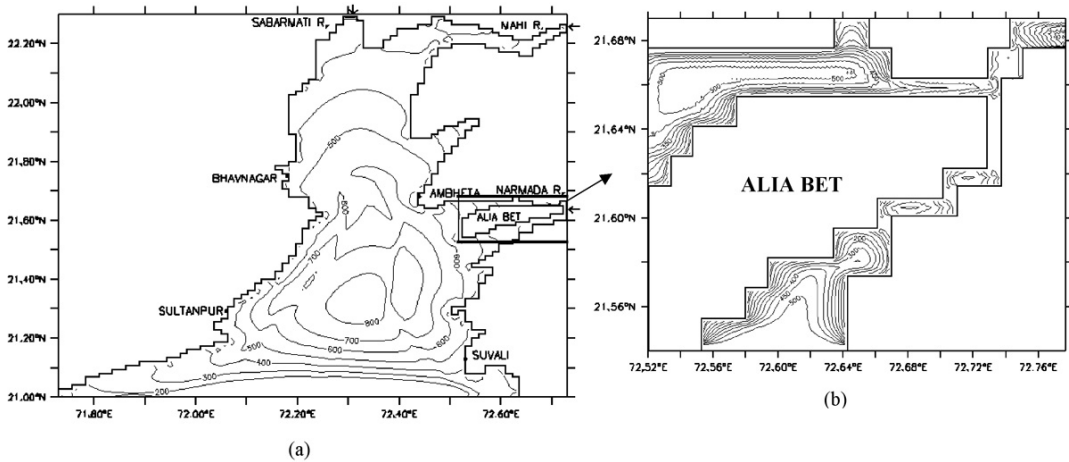(b) the lower part of the Narmada estuary during ebb

(a)

(b)

*Fig. 6: Suspended sediment concentrations (mg/l) in (a) the gulf of Khambhat;
(b) the lower part of the Narmada estuary during flood*

(a)

(b)
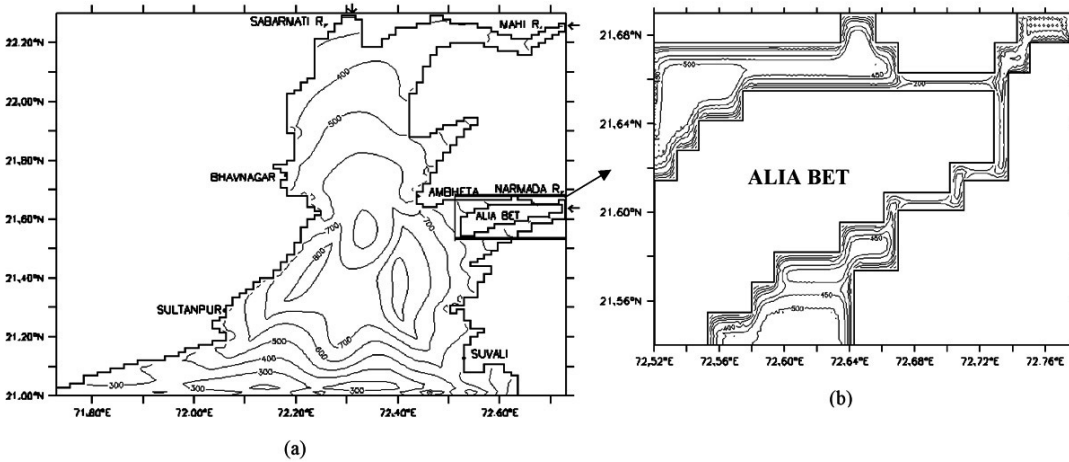
*Fig. 7: Suspended sediment concentrations (mg/l) in (a) the gulf of Khambhat;
(b) the lower part of the Narmada estuary during ebb*

while during ebb it varied from 0.01 m/s to 1.0 m/s. The flow bifurcation near Alia Bet Island was well reproduced in the fine resolution estuary model.

The computed suspended sediment concentrations in the gulf region during flood and ebb periods are shown in *Figs. 6a* and *7a*, respectively. During flood, the sediment concentrations varied from 100 mg/l to 800 mg/l and it varied from 120 mg/l to 920 mg/l during ebb. As expected, the concentrations were higher during the ebb than during the flooding period. This is because of the joining of the three rivers, namely Sabarmati, Mahi and Narmada, in the gulf.

Figs. 6b and *7b* show the computed suspended sediments in the Narmada estuary during flood and ebb periods, respectively. The lower part of the estuary is divided into two parts due to the

TABLE 2
Observed and computed mean suspended sediment concentrations (mg/l) in the Narmada river estuary

Year (Period)	Observed SSC[*]	Computed SSC[*]
1977 (Post-monsoon)	540	-----
1978 (Pre-monsoon)	430	515

[*]SSC – Suspended Sediment Concentrations

presence of Alia Bet Island. During flood, the sediment concentrations were found to vary from 60 mg/l to 500 mg/l in the upper part and from 40 mg/l to 508 mg/l in the lower part. However, the sediment concentrations varied from 110 mg/l to 517 mg/l in the upper part and from 100 mg/l to 530 mg/l in the lower part during the ebb period. The computed mean of the maximum concentration in the lower part of the estuary was found to be 515 mg/l. The computed sediment concentrations in the lower estuary were found to be in the range of available observations, as shown in Table 2 (Borole *et al.*, 1982).

CONCLUSIONS

A depth-averaged numerical model was developed to compute the tidal circulation and suspended sediment transport in the gulf of Khambhat by including three rivers, namely, Sabarmati, Mahi and Narmada. A 2-D fine resolution model for the lower part of the Narmada estuary was combined with the gulf model to simulate the flow features in the lower estuary. The computed M_2-tidal amplitudes, during flood at Suvali and Ambheta, were found to be in reasonable agreement with the available observations. The flow bifurcation near Alia Bet Island was well-reproduced in the fine resolution estuary model. Meanwhile, the computed mean suspended sediments were validated with the available observations in the lower estuary. Reasonable circulation pattern and suspended sediment concentrations have been simulated in the gulf model and the estuary model. However, a better representation of the wind stress terms and the inclusion of horizontal diffusion in the momentum equations would be more appropriate.

ACKNOWLEDGEMENTS

Pertanika J. Sci. & Technol. Vol. 18 (2) 2010

301

REFERENCES

Borole, D.V., Sarin, M. M. and Somayajulu, B. L. K. (1982). Composition of Narmada and Tapti estuarine particles and adjacent Arabian sea sediments. *Indian Journal of Marine Sciences*, *11*, 51-62.

Engelund, F. and Hansen, E. (1967). A monograph on sediment transport to alluvial streams. *Teknik Vorlag*, Copenhagen.

Gleizon, P., Punt, A. G. and Lyons, M. G. (2003). Modeling hydrodynamics and sediment flux within a macrotidal estuary - problem and solutions. *The Science of Total Environment*, 589-597.

Haskoning Consulting Engineers and Architects. (1996). Khambhat Gulf development project. Prefeasibility Survey, Draft Final Report, Narmada & Water Resources Department, Government of Gujarat, Vol. 5, Annex 12-13.

Johns, B., Soulsby, R. L. and Chesher, T. J. (1990). The modeling of sandwave evolution resulting from suspended and bedload transport of sediment. *Journal of Hydraulic Research*, *28*, 355-374.

Lou, J. and Ridd, P. V. (1997). Modeling of suspended sediment transport in coastal areas under waves and currents. *Estuarine, Coastal and Shelf Science*, *45*, 1-16.

Podsetchine, V. and Huttula, T. (1994). Modeling sedimentation and resuspension in lakes. *Water Pollution Resources Journal Canada*, *29*, 309-342.

Sen Gupta, R. and Deshmukhe, G. (2000). Coastal and maritime environment of Gujarat. Gujarat Ecological Society, Vadodara, India.

Sinha, P. C., Rao, Y. R., Dube, S. K., Rao, A. D. and Chatterjee, A. K. (1996). Numerical modeling of circulation and salinity in Hooghly estuary. *Marine Geodesy*, *19*, 197-213.

Tattersall, G. R., Elliott, A. J. and Lynn, N. M. (2003). Suspended sediment concentration in the Tamar estuary. *Estuarine, Coastal and Shelf Science*, *57*, 679-688.

Unnikrishanan, A. S., Shetye, S. R. and Michael, G. S. (1999). Tidal propagation in the Gulf of Khambhat, Bombay High, and surrounding areas. *Proceedings of the Indian Academy of Science (Earth & Planetary Sciences)*, *108*, 155-177.

Wu, W. M., Rodi, W. and Wenka, T. (2000). 3D numerical modeling of flow and sediment transport in open channels. *Journal of Hydraulic Engineering, ASCE*, *26*, 4-15.

Car License Plate Detection Method for Malaysian Plates-Styles by Using a Web Camera

Abbas M. Al-Ghaili[*], Syamsiah Mashohor, Abdul Rahman Ramli and Alyani Ismail
Department of Computer and Communication Systems, Faculty of Engineering,
Universiti Putra Malaysia, 43400 UPM, Serdang, Selangor, Malaysia
[*]E-mail: abbasghaili@yahoo.com

ABSTRACT

Recently, license plate detection has been used in many applications especially in transportation systems. Many methods have been proposed in order to detect license plates, but most of them work under restricted conditions such as fixed illumination, stationary background, and high resolution images. License plate detection plays an important role in car license plate recognition systems because it affects the accuracy and processing time of the system. This work aims to build a Car License Plate Detection (CLPD) system at a lower cost of its hardware devices and with less complexity of algorithms' design, and then compare its performance with the local CAR Plate Extraction Technology (CARPET). As Malaysian plates have special design and they differ from other international plates, this work tries to compare two likely-design methods. The images are taken using a web camera for both the systems. One of the most important contributions in this paper is that the proposed CLPD method uses Vertical Edge Detection Algorithm (VEDA) to extract the vertical edges of plates. The proposed CLPD method can work to detect the region of car license plates. The method shows the total time of processing one 352x288 image is 47.7 ms, and it meets the requirement of real time processing. Under the experiment datasets, which were taken from real scenes, 579 out of 643 images were successfully detected. Meanwhile, the average accuracy of locating car license plate was 90%. In this work, a comparison between CARPET and the proposed CLPD method for the same tested images was done in terms of detection rate and efficiency. The results indicated that the detection rate was 92% and 84% for the CLPD method and CARPET, respectively. The results also showed that the CLPD method could work using dark images to detect license plates, whereas CARPET had failed to do so.

Keywords: Adaptive thresholding, Car License Plate Detection (CLPD), CAR Plate Extraction Technology (CARPET), Vertical Edge Detection Algorithm (VEDA)

INTRODUCTION

Car license plate recognition system is an image processing technology used to identify vehicles by capturing their Car License Plates (CLPs). The car license plate recognition technology is also known as automatic number-plate recognition, automatic vehicle identification, car license plate recognition or optical character recognition for cars. Car License Plate Detection and Recognition System (CLPDRS) became an important area of research due to its various applications such as in the payment of parking fee, highway toll fee, traffic data collection, and crime prevention (Huda, Khalid, Yosuf and Omar, 2007; Thanongsak and Kosin, 1999). Usually, a CLPDRS consists of three parts, namely license plate detection, character segmentation, and character recognition. Among these parts, license plate detection is the most important part in the system because it affects the accuracy of the system (Bai and Liu, 2004).

There are many issues which should be resolved in order to create a successful and fast Car License Plate Detection System (CLPDS); these include poor image quality, plate sizes and designs, processing time, as well as background details and complexity. The need for car identification is increasing for many reasons such as crime prevention, vehicle access control, and border control. In order to identify a car, features such as its model, colour, format, and license plate number can be used (Fukumi, Takeuchi, Fukumoto, Mitsukura and Khalid, 2005; Lee, Kim and Kim, 1994; Parisi, Claudio, Lucarelli and Orlandi, 1998).

In vehicle tracking systems, cameras are used and installed in front of policemen cars to identify those vehicles. Usually, numerous vehicle tracking and pursue systems use outstanding cameras (Naito, Tsukada, Yamada, Kozuka and Yamamoto, 2000), and this leads to cost increment of the system involving both hardware and software. Many methods have been proposed in various Intelligent Transportation System (ITS) applications, but the CLPDRS is usually based on images acquired at a 640 x 480 resolution (Wu, Chen, Wu and Shen, 2006). Enhancing the performance of the CLPD method, such as reducing computation time and algorithm complexity, or even building of License Plate Recognition (LPR) system with lower cost of its hardware devices, will make it more practical and usable than before. This paper proposed a new Vertical Edge Detection Algorithm (VEDA) for detecting vertical edges. In addition, a VEDA-based method was also proposed for car license plate detection in which a web-camera (with 352 x 288 resolutions) was used instead of a more sophisticated one. In this work, the web-camera was used to capture the images and then an off-line process was performed to detect the plate detection from the whole scene image.

This paper is organized as follows: Section 2 includes a brief review of some related work and Section 3 describes the proposed method for CLPD. The experimental results and discussion are presented in Section 4 and the conclusion is given in Section 5.

RELATED WORK

A number of methods have been used for license plate region detection; these include morphological operations (Hsieh, Yu and Chen, 2002; Lensky, Jo and Gubarev, 2006; Martin, Garcia and Alba, 2002), edge extraction (Le, Seok and Lee, 2002; Parker and Federl, 1997; Yu and Kim, 2000; Zhang, Jia, He and Wu, 2006; Zheng, Zhao and Wang, 2005), combination of gradient features (S. Kim, Kim, Ryu and Kim, 2002), a neural network for colour classification (Lee *et al.*, 1994), and vector quantization (Rovetta and Zunino, 1999).

Due to ambient lighting conditions, interference characters, and other problems, it is difficult to detect license plates in complex conditions. Some of the previous license plate detection methods are restricted to work under certain conditions such as fixed backgrounds (Bai, Zhu and Liu, 2003), and known colour (Debi, Chae and Jo, 2008; S. K. Kim, Kim and Kim, 1996; Ron and Erez, 2002; Shahaf, Timor and Erez, 2002).

In the previous years, some researchers have been working on license plate detection in complex conditions. Among other, Kim *et al.* (2002) proposed a license plate detection algorithm using both statistical features and license plate templates. After the statistical features were used to select the Regions of Interest (ROI), the license plate templates were applied to match the ROI. In many cases, general license plate templates are very difficult to be constructed. Moreover, their algorithm could work on a fixed scale. Hence, the application of this algorithm is restricted.

The work by Zheng *et al.* (2005) as well as Thanongsak and Kosin (1998: 1999) made use of image enhancement and Sobel operator to extract the vertical edges of the image of cars. They used an algorithm to remove most of the background and noisy edges. Finally, they searched the plate region using a rectangular window in the residual edge image. Recently, the authors (Abolghasemi and Ahmadyfard, 2007) improved the work by Zheng *et al.* (2005) by enhancing the low quality

input image and then extracting the vertical edges. Then, they used morphological filtering to constitute some regions as plate regions.

Bai *et al.* (2003) proposed an algorithm for license plate detection to monitor highway ticketing systems. Their algorithm presented a linear filter in order to overcome the influence of lights. In addition, the vertical edge detection was also used in order to detect the license plate region. However, their algorithm could only work with fixed backgrounds.

Recently, a CAR Plate Extraction Technology (CARPET), which is used to detect Malaysian car license plate and recognize license numbers, was proposed by Ming (2004a). This method uses a stationary camera in car parking area for capturing the samples. Therefore, this method can process fixed background images.

While the method discussed above processes Malaysian plates, one of the objectives in this work is to compare the proposed CLPD method with this particular method in order to evaluate them. Low quality image produced by a web-camera is one of the problems and difficulties that should be solved. The usage of low quality image in CLPDS can reduce the size of the memory used while processing the input image (Naito *et al.*, 2000). This advantage helps in building applicable hardware system at low cost and with smaller memory size. This paper proposed a new method for CLPDS in which a web-camera is used for acquiring images.

THE PROPOSED METHOD FOR THE CLPD

Overview

In this paper, the proposed CLPD method is introduced and discussed. Then, a comparison between CARPET and the proposed CLPD methods in this study is presented. The proposed CLPD method consists of some processes as follows: First, the colour input image is converted to grey-scale image, and then, adaptive thresholding is applied on the image to constitute the binarized image. After that, an enhancement of the binarized image is performed such as noise removal. Then, the vertical edges are extracted by using VEDA. The details of the plate are highlighted based on the colour information with help of the VEDA output form. Later, some statistical and logical operations are used to detect and search for the true candidate region. Finally, the true plate region is detected in the original image. *Fig. 1* shows the flowchart of the proposed CLPD method.

Adaptive Thresholding (AT)

After colour input image is converted to grey scale values (0-255), an adaptive thresholding process (Bradley and Roth, 2007; Shafait, Keysers and Breuel, 2007) is applied on the grey scale image input to constitute the binarized image. The researchers in (Bradley and Roth, 2007) have recently proposed real-time adaptive thresholding using mean of a local window, where the local mean is computed using an integral image.

First of all, in order to get a good adaptive threshold, the method proposed by Bradley and Roth (2007) is used. The authors proposed the real-time adaptive thresholding method using mean of a local window, where the local mean was computed using an integral image. The integral image is pre-computed for every pixel. The integral image is computed for every pixel g(i,j), as in Bradley and Roth (2007):

$$Intgrl\,Im\,g(i,j) = \begin{cases} sum(i) & if(j = 0) \\ Intgrl\,Im\,ag(i,j-1) + sum(i) & otherwise \end{cases} \tag{1}$$
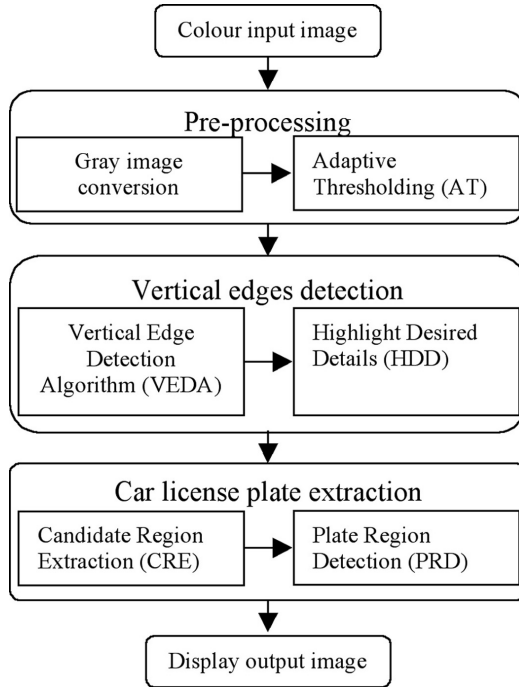
Fig. 1: Flowchart of the proposed method

Where *IntgrlImg(i,j)* represents the integral image for pixel *(i,j)* and *sum(i)* represents the summation of the pixel values for all the *i*-values with one column j^{th}, and these are computed according to Bradley and Roth (2007):

$$sum(i)\big|_{j^{th}} = \sum_{x=0}^{i} g(x,y)\big|_{y=j^{th}} \qquad (2)$$

Whereas *g(x,y)* represents the input value.

By using (2) and (1), the integral image is created. The next step is to perform thresholding for each pixel. In order to get the adaptive threshold value for *(i, j)*, this criterion is tested for all the pixel values according to Bradley and Roth (2007):

$$o(i,j) = \begin{cases} 0 & g(i,j)*S^2(1-T)*sum \\ 255 & otherwise \end{cases} \qquad (3)$$

Where *g(i,j)* represents the input image values, S^2 represents the *SxS* region, where $S = \frac{image\ width}{8}$, *T* is a constant and *T=0.15*, and *sum* represents the summation of the intensities of the grey values for the window size $(i+\frac{S}{2},j+\frac{S}{2}),(i+\frac{S}{2},j-\frac{S}{2}),(i-\frac{S}{2},j+\frac{S}{2})$ and $(i-\frac{S}{2},j-\frac{S}{2})$. Once the integral image is obtained, the intensity summation for any window size can be computed using two subtraction and one additional operation instead of the summation over all the pixel values within that particular window (Porikli and Tuzel, 2006):

$$sum = \left(IntgrlImg\left(i + \tfrac{s}{2}, j + \tfrac{s}{2}\right)\right) - \left(IntgrlImg\left(i + \tfrac{s}{2}, j - \tfrac{s}{2}\right)\right) -$$
$$\left(IntgrlImg\left(i - \tfrac{s}{2}, j + \tfrac{s}{2}\right)\right) + \left(IntgrlImg\left(i - \tfrac{s}{2}, j - \tfrac{s}{2}\right)\right) \tag{4}$$

Once the *sum* in (4) is calculated, the threshold is calculated and tested for each pixel value using Eq. (3).

Fig. 2(a) shows the input image and *Fig. 2(b)* illustrates the results after the application of AT.

(a) Input image   (b) Threshold image

Fig. 2: Adaptive thresholding

Vertical Edge Detection Algorithm (VEDA)

There are two procedures involved in this step. First, thin lines are removed to reduce details of the image. As it is noticeable from the binarized image, some details are not important and contain very thin lines. Therefore, eliminating them could enhance the detection rate and reduce computation time. Second, the vertical lines are extracted.

For removing the lines which are not parts of license plate, the mask in *Fig. 3* is proposed and discussed in (Al-Ghaili *et al.*, 2008).

Each case of *a, b, c* and *d* represents two corresponding grey scale values each time the mask moves through the grey scale value in the threshold image *g(x,y)* values, where *x* and *y* represent the rows and columns locations, respectively.

The binarized image shown in *Fig. 2 (b)* is enhanced by applying the proposed mask (see *Fig. 3*) and the output is shown in *Fig. 4*.

In order to extract the vertical edges, a 2x4 mask was proposed in Al-Ghaili *et al.* (2008), as shown in *Fig. 5*. Basically, the proposed mask consists of 3 smaller masks, namely the left mask 2x1, centre mask 2x2, and right mask 2x1. *Fig. 5* shows the design of the proposed mask, where *(x,y), x,* and *y* represent the current processed pixel location at point (0,1) as the centre of the proposed mask, the rows or the height of the image, and the columns or the width of the image, respectively.

(a)   (b)   (c)   (d)
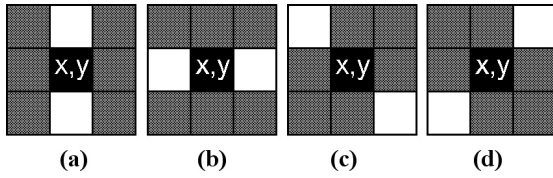
Fig. 3: The mask used for removing too long and thin lines

Fig. 4: The enhanced image after applying the proposed mask

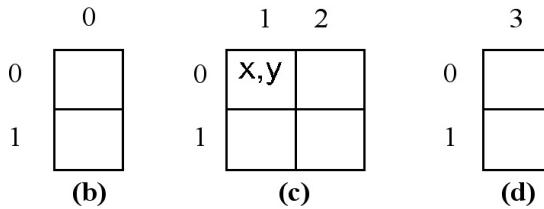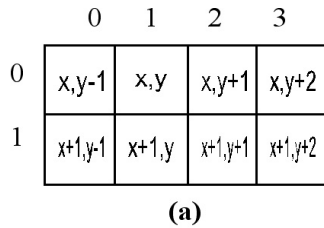
(a)

(b)   **(c)**   **(d)**

Fig. 5: The design of the proposed mask: (a) moving mask; (b) left mask (0,0), (1,0); (c) centre mask (0,1), (0,2), (1,1), (1,2); (d) right mask (0,3), (1,3)

The enhanced binarized image (*Fig. 4*) is scanned by moving the proposed mask *(Fig. 5 (a))* from left to right and from top to bottom. *Fig. 6* shows the output of this process.

Highlight Desired Details Based on VEDA (HDD)

After applying VEDA, the next step is to highlight the desired details such as plate details and vertical edges in the image. HDD performs NAND-AND operation for each two corresponding pixel values taken from both ULEA and VEDA output images. NAND-AND operation for this process is illustrated in *Fig. 7* as shown.

After all the pixels are scanned, the regions which probably contain plate details are then highlighted, as shown in *Fig. 8*.
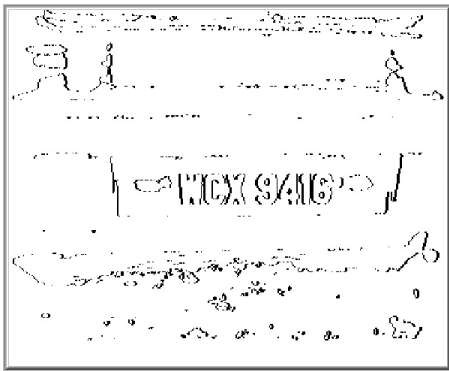
Fig. 6: VEDA output
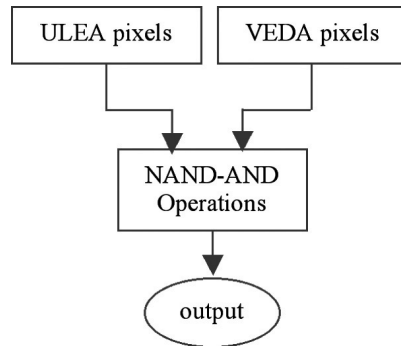
Fig. 7: HDD output generation by using NAND-AND operation
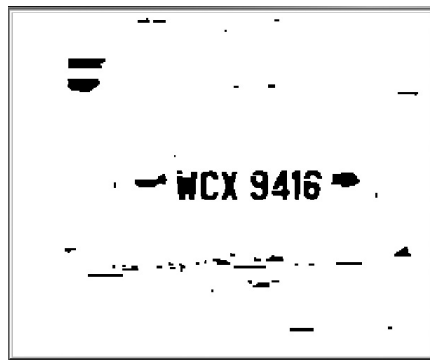
Fig. 8: HDD output

All the pixels in the vertical edge image (for example in *Fig. 6*) are scanned. When there are two neighbour black pixels, followed by one black pixel as in VEDA output form (see *Fig. 6*), the two following tests will be checked to highlight the desired details by drawing black horizontal lines connecting the two vertical edges. First, these two vertical edges should be surrounded by a black background, as shown in the threshold image (see *Fig. 4*). Second, the value of the horizontal distance (hd) should be in range of 2<hd<33, where hd represents the length between the two vertical edges. Prior to this, the hd was computed from the tested images. The hd-length is appropriate to remove very short lines and long lines, as well as to retain details of the plate. This scanning process will be started from left to right and from top to bottom. After all the pixels have been scanned, the regions which probably contain plate details are shown in *Fig. 8*.

Candidate Regions Extraction (CRE)

In this process, the candidate regions are extracted. Some statistical operations are used in this step. First, the number of lines which have been extracted in the HDD process per each row are counted and stored in a matrix variable, *HwMnyLines[a], a=0, 1… height-1*. This process is then repeated for all the pixel values in the HDD image. Then, the image is divided into smaller groups using Equation (5).

$$how\_mny\_groups = \frac{height}{C} \tag{5}$$

In this equation, the total number of groups is equivalent to the total number of rows divided by C, where *how_mny_groups*, *height* and C represent the total number of groups, the total number of image rows, and group-constant, respectively. In the present work, C was chosen to represent one group (set of rows). For the methodology employed in this study, C=10 because each 10 rows could save the processing time and also keep the desired details clearly while processing the images. Probably, more or less than 10, either loses much desired details or wastes much time for processing the image. This particular step helps to distinguish the regions that may have plate details.

Fig. 9 shows an example of the total number of lines vs. each group (for the image shown in *Fig. 8*). In *Fig. 9*, *group* represents values (0-28). This range is calculated using (5), as follows:

$$how\_mny\_groups = \frac{288}{10} \approx 29$$

Where, the total number of image-rows equals to 288, and the total number of groups equals to 29 (0-28) groups. The dimensions of the processed input image are 352 x 288 pixels.
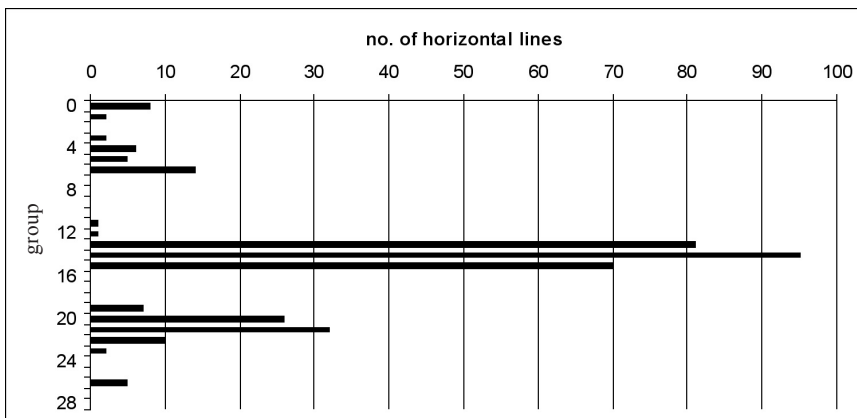
Fig. 9: Number of horizontal lines vs. group

This figure denotes that the highest values of lines frequency are located in the plate region. The second step in this process is performing a threshold in order to eliminate the groups which do not belong to the plate region and to keep others. The remaining groups after the thresholding step should have the plate details. Therefore, the locations of those groups are saved to be processed later by their indexes. While these groups may be one connected region or more than one region, each region is considered as a separate plate region. Thus, this step aims to extract both the upper and lower boundaries for each region that may contain plate region by their indexes. Finally, the horizontal boundaries above and below each candidate region will be drawn in the process. *Fig. 10* shows the result of drawing boundaries of the candidate regions in the input image.
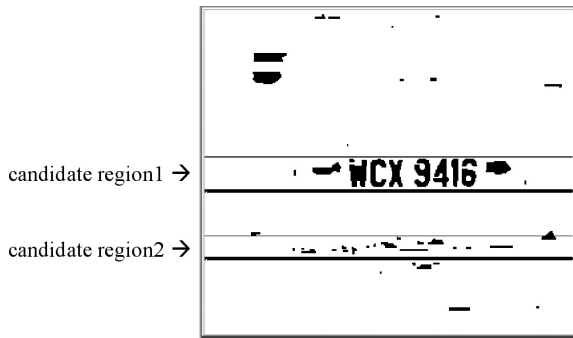
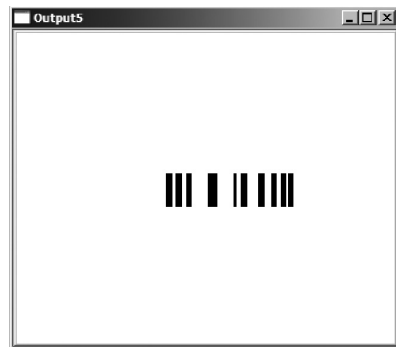Fig. 10: Output of drawing
candidate regions boundaries

Fig. 11: Draw lines for some columns
in candidate regions

Plate Region Selection (PRS)

This process aims to select one region as a plate region and extract the plate region, using the following steps: First, check the blackness-ratio in each candidate region column. Check the ratio of blackness in each column of candidate regions. If the ratio exceeds 50% of the height of the candidate region columns, consider the current checked column as a part of the plate. Then, draw a new black vertical line and replace the current column with the new one. Otherwise, replace the current column with the white background (see *Fig. 11*). *Fig. 11* shows only the vertical lines in which their blackness ratios exceed 50%.

Fig. 12 shows the blackness frequency for both the candidate regions as illustrated in *Fig. 10*. The true candidate region has the blackness frequency more than the others.
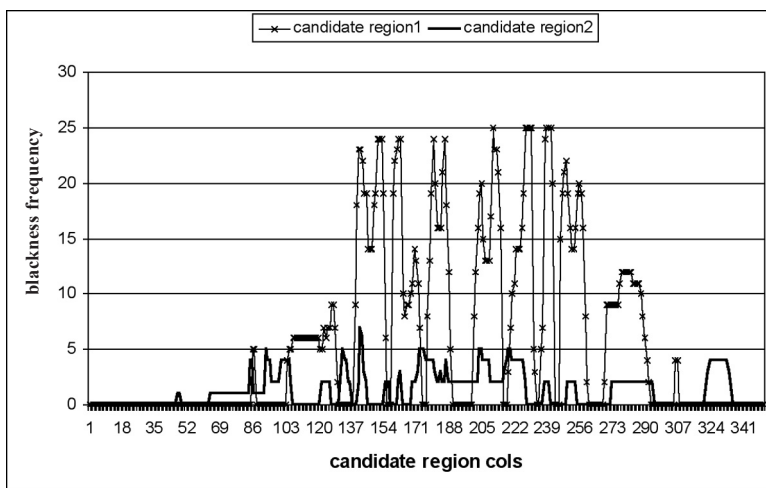
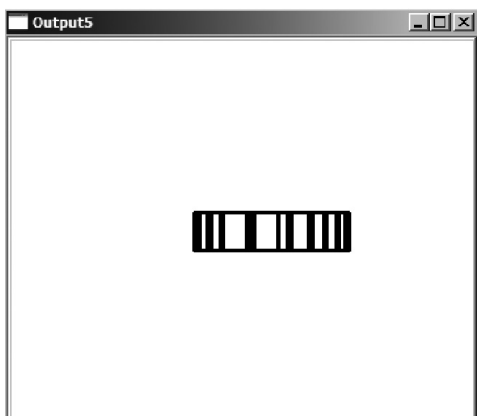Fig. 12: Both candidate region columns vs. blackness frequency

Fig. 13: Extract plate area

Fig. 14: Plate area detection

Next, make a vote for all the candidate regions. As the background colour of the plate is black, the top and down neighbours of the selected columns in the previous step will be checked. If there is enough ratio of blackness, the current checked region will get one vote. The process will be done for all the columns in all the candidate regions and all these candidate regions are compared to select one suitable candidate. Hence, the candidate region with the highest vote values is the selected region as the true license plate. Finally, by tracking the black vertical lines, the plate area can then be detected and extracted as well. The region with the highest value of voting will be detected, while the black vertical lines will be checked and tracked. The region will be detected as the plate area, as shown in *Fig. 13*. *Fig. 14* shows the result derived for the license plate detection after the whole procedure has been performed.

PRS factor (K-factor)

Sometimes, when the images are blurry or the plate region is defected, the ratio value should be dynamically changed. Therefore, *K-factor* is proposed to overcome the problem and this is discussed in this section.

As mentioned above, each column of the candidate regions is checked one by one. If the column blackness ratio exceeds 50%, the current column belongs to the license plate region and this particular column (see *Fig. 10*) can then be replaced by a vertical black line in the resulting image (see *Fig. 11*). Hence, each column is checked using this condition:

If *temp* is greater than or equals to *0.5*cnst*, the current column is then considered as a part of the license plate region, where *temp*, *cnst* represent the total number of the black pixels per each column in the current candidate region and the height of the column of the candidate region, respectively. This condition with a fixed value (0.5) is used with non-blurry images. Unfortunately, some candidate regions will be neglected by the software in case the ratio of blackness to the total length (height) of the candidate region is less than 50%. Therefore, the condition is changed to be less than 50% according to the ratio of the blurry level or the degradation, and then *If (temp≥K*cnst)*, where *K* represents the blurry level factor. The value of *K* must be reduced when the blurry level or degradation is high in order to highlight more important details; on the contrary, *K* must be increased when the blurry level is less.

Fig. 15: K-value (K≥0.5)

Fig. 16: K-value (K≥0.4)

When *K*-value is high (*K*≥0.5), the drawn black columns are extracted and shown from non-blurry image. In this case, if the processed image is blurry, the black pixels will be reduced and the candidate regions will be neglected to be detected and the plate region will be missed or inefficiently detected, as shown in *Fig. 15*.

Using the same example (*K*-value≥0.4), more required details will be shown, as illustrated in *Fig. 16*.

It is clear that the result presented in *Fig. 16* is better than the one in *Fig. 15*. However, it still needs a little bit of enhancement to improve it. *Fig. 17* shows the result for detection when *K*-value≥0.3.

By comparing the three results obtained above, it can be stated that the best result is in *Fig. 17*, i.e. when the *K*-value is ≥0.3.

Therefore, *K* is proportional reverse to blurry level or degradation, and thus:

$$K \propto \frac{1}{blurry\,level\,ratio}$$

By controlling the *K* value, some candidate regions will be processed and taken into account. Thus, this procedure will enhance both the detection rate and the whole performance of the CLPD method, as demonstrated in the experimental results.
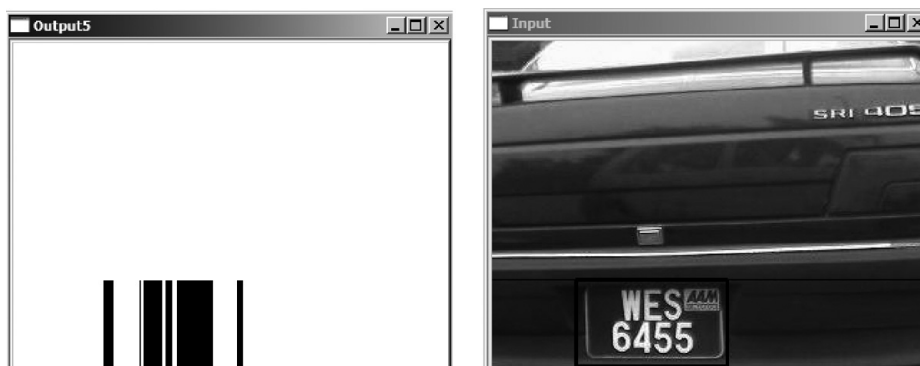
Fig. 17: K-value (K≥0.3)

EXPERIMENTAL RESULTS AND DISCUSSION

This part is divided into two sections; first, an evaluation of the CLPD method is introduced, and second, a comparison between the CLPD and CARPET is discussed.

Evaluation of the Proposed CLPD Method

There were 643 images of Malaysian license plates captured from parking cars using a web camera. The resolution is 352x288. The images were captured at day time and in various weather conditions. These samples were standardized in this experiment. These datasets were selected based on gathering and capturing Malaysian plates from UPM campus.

This experiment had three datasets. There were 100 images in Dataset 1. In this test, 85 images were successfully detected, while 15 images were failed to be detected. The percentage of successful detection was 85%.

Meanwhile, there were also 100 samples for Dataset 2. In this test, 90 images were successfully detected, but it failed to detect 10 other images. The percentage of successful detection was 90%.

For Dataset 3, 404 out of 443 images were successfully detected. The percentage for the car license plate detection accuracy was 91.2%.

From this evaluation, 579 out of 643 images were successfully detected, and thus, the car license plate detection accuracy was 90%.

The datasets were taken using a web camera for many Malaysian car plates which were from UPM Campus. The detection rate in Dataset 1 before PRS-factor was proposed. Meanwhile, the detection rate for Dataset 2 and Dataset 3 was after. Therefore, the PRS-factor was found to have enhanced the whole accuracy of the proposed CLPD method.

Fig. 18 shows the increase in the percentage of detection rate for all the datasets before and after the PRS-factor.

Based on the data presented in *Fig. 18*, the successful detection rate was increased from 87% to 91%. *Fig. 19* shows the average processing time for 100 test images. As illustrated in *Fig. 19*, most of the processed images required 47 ms to be completed, while some images with complex background took more processing time in general because details from their complex background were recorded more and calculated from 100 experimental images. The average processing time for one 352x288 image was 47.7 ms, and this fulfilled the real time processing requirement.
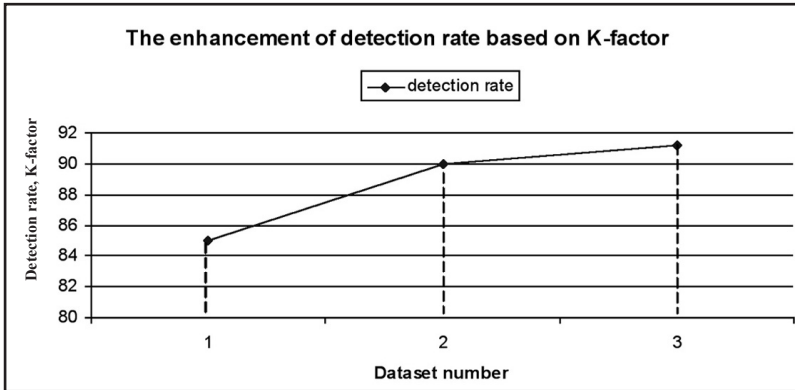
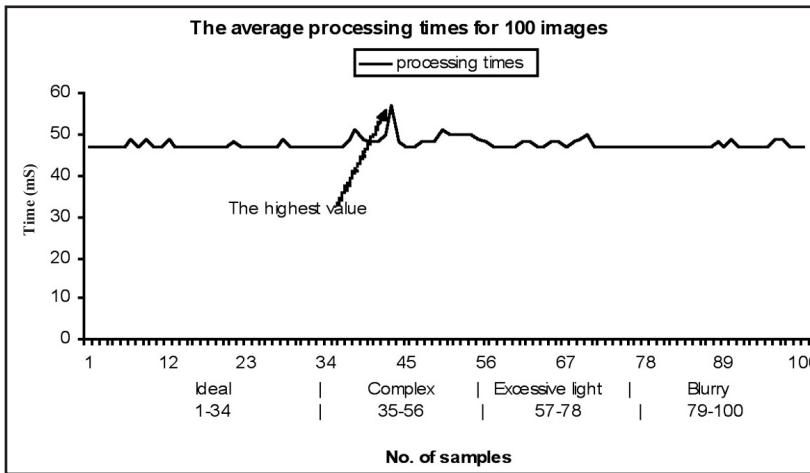*Fig. 18: The increase in the detection rate before and after PRS-factor*

Fig. 19: The average processing time for 100 images

There are seven stages involved in a complete processing of an image in the proposed CLPD method. The average processing time (in msec) for the seven stages of the proposed method is listed in Table 1. A lot of the time is consumed during the second stage, i.e. AT.

TABLE 1
The average processing time for the seven stages involved in the proposed method

Conversion	AT	ULEA	VEDA	HDD	CRE	PRS & PRD	Total time (ms)
1.1	15	5.2	7	7.9	3.3	8.2	47.7

CARPET vs. the Proposed CLPD Method

This section introduces a comparison between CARPET and the proposed CLPD method. As there are a number of images available in the demo version of the CARPET software [1], twenty five images from both the datasets (CLPD & CARPET) were randomly taken and tested using the CARPET software (Ming, 2004b), and then tested by the proposed CLPD in this work.

Detection rate

Table 2 shows the experimental results for the test carried out in this study. From the following table, the proposed method was found to outperform CARPET in terms of detection rate.

TABLE 2
Comparison of detection rates between CARPET and the proposed CLPD method

Methods	Plates detected	Plates not detected	Detection rates (%)
CARPET	21	4	84
The proposed CLPD	23	2	92

In this test, CARPET fails to detect the plate efficiently when the colour of car body is dark. The two missing plates (see Table 2) for the proposed CLPD method were because of the blurry level and the similarity in the colours of the body and plate of the car.

Efficiency

As shown by the data presented in Table 3, CARPET was found to have failed to detect the license plate in four samples, while the proposed CLPD method in two samples. These were samples are 3, 13, 22, and 24. In samples 3 and 13, both the CARPET and CLPD methods had failed to detect the license plates. In samples 22 and 24, the CLPD method detected the license plates correctly whereas CARPET had failed to do so. Samples 3 and 13 were blurred and had similarity in their body-and-plate colours, respectively. Samples 22 and 24 were dark images.

From Table 3, the proposed CLPD method is shown to be insusceptible for changes in image condition such as darkness (as noticeable in samples 22 and 24), while CARPET is found to be sensitive in this case. Therefore, the proposed CLPD method can be used for dark images and it is more efficient than CARPET in such case.

---

[1] Integrated Testing Version 1.0, © 2006. see: "http://www.projekcarpet.com/download/demo.zip"

TABLE 3
CARPET vs. CLPD in different conditions

Method Sample no.	CARPET	CLPD
1	y	y
2	y	y
3	n	n
4	y	y
5	y	y
6	y	y
7	y	y
8	y	y
9	y	y
10	y	y
11	y	y
12	y	y
13	n	n
14	y	y
15	y	y
16	y	y
17	y	y
18	y	y
19	y	y
20	y	y
21	y	y
22	n	y
23	y	y
24	n	y
25	Y	y

CONCLUSIONS

A vertical-edges car license plate detection method has been proposed and discussed in this paper. The vertical edges were detected based on VEDA. The proposed CLPD method was compared with the CARPET system for some tested images. This paper confirmed that the proposed CLPD method has higher detection rate and works more efficiency in different image conditions. From the experimental results, 579 out of 643 images were successfully detected. The CLPD method has a detection rate of 90% for the whole tested images. Using a total of five images, the comparison between CARPET and the proposed CLPD method revealed that the percentage of the detection rate was 92% (the proposed CLPD) and 84% (CARPET), respectively. This paper also showed that the detection rate using the PRS-factor could enhance the accuracy and overall performance of the proposed CLPD method.

REFERENCES

Abolghasemi, V. and Ahmadyfard, A. (2007). Improved image enhancement method for license plate detection. Paper presented at the *Proceedings of the 15ᵗʰ International Conference on Digital Signal Processing* (DSP), Iran.

Al-Ghaili, A. M., Mashohor, S., Ismail, A. and Ramli, A. R. (2008). A new vertical edge detection algorithm and its application. Paper presented at the *IEEE International Conference on Computer Engineering & Systems* (ICCES 2008), Cairo, Egypt.

Bai, H. and Liu, C. (2004). A hybrid license plate extraction method based on edge statistics and morphology. Paper presented at the *Proceedings of the 17ᵗʰ International Conference on Pattern Recognition*, UK.

Bai, H., Zhu, J. and Liu, C. (2003). A fast license plate extraction method on complex background. Paper presented at the *Proceedings of the IEEE International Conference on Intelligent Transportation Systems*, China.

Bradley, D. and Roth, G. (2007). Adaptive Thresholding using the Integral Image. *Journal of Graphics Tools*, *12*(2), 13–21.

Debi, K., Chae, H.-U. and Jo, K.-H. (2008). Parallelogram and histogram based vehicle license plate detection. Paper presented at the *IEEE International Conference on Smart Manufacturing Application*, Korea.

Fukumi, M., Takeuchi, Y., Fukumoto, H., Mitsukura, Y. and Khalid, M. (2005). Neural network based threshold determination for Malaysia license plate character recognition. Paper presented at the *Proceedings of the 9ᵗʰ International Conference on Mechatronics Technology*, Malaysia.

Hsieh, J.-W., Yu, S.-H. and Chen, Y.-S. (2002). Morphology-based license plate detection from complex scenes. Paper presented at the *Proceedings of the 16ᵗʰ International Conference on Pattern Recognition*, Canada.

Huda, S. N., Khalid, M., Yosuf, R. and Omar, K. (2007). Comparison of feature extractors in license plate recognition. Paper presented at the *Proceedings of the IEEE 1ˢᵗ Asia International Conference on Modelling & Simulation* (AMS'07), Thailand.

Kim, S., Kim, D., Ryu, Y. and Kim, G. (2002). A robust license-plate extraction method under complex image conditions. Paper presented at the *Proceedings of 16ᵗʰ International Conference on Pattern Recognition*, Canada.

Kim, S. K., Kim, D. W. and Kim, H. J. (1996). A recognition of vehicle license plate using a genetic algorithm based segmentation. Paper presented at the *Proceedings of International Conference on Image Processing*, Switzerland.

Le, S.-H., Seok, Y.-S. and Lee, E.-J. (2002). Multi-national integrated car-license plate recognition system using geometrical feature and hybrid pattern vector. Paper presented at the *Proceedings of the International Technical Conference on Circuits/ Systems, Computers and Communication*, Thailand.

Lee, E. R., Kim, P. K. and Kim, H. J. (1994). Automatic recognition of a car license plate using color image processing. Paper presented at the *Proceedings of the IEEE International Conference on Image Processing*, USA.

Lensky, A. A., Jo, K.-H. and Gubarev, V. V. (2006). Vehicle license plate detection using local fractal dimension and morphological analysis. Paper presented at the *Proceedings IEEE 1ˢᵗ International Forum Strategic Technology*, South Korea.

Martin, F., Garcia, M. and Alba, J. L. (2002). New methods for automatic reading of VLP's (Vehicle License Plates). Paper presented at the *Proceedings of IASTED International Conference on Signal Processing, Pattern Recognition, and Applications*, Greece.

Ming, C. C. *et al.* (2004a). ProjekCARPET, car license plate extraction & recognition technology. Retrieved on 2008 from http://www.projekcarpet.com/aboutus.asp.

Ming, C. C. *et al.* (2004b). ProjekCARPET, car license plate extraction & recognition technology (Demo Version). Retrieved on 2008 from http://www.projekcarpet.com/download/demo.zip.

Naito, T., Tsukada, T., Yamada, K., Kozuka, K. and Yamamoto, S. (2000). Robust license-plate recognition method for passing vehicles under outside environment. *IEEE Transactions on Vehicular Technology, 49*(6), 2309-2319.

Parisi, R., Claudio, E. D., Lucarelli, G. and Orlandi, G. (1998). Car plate recognition by neural networks and image processing. Paper presented at the *Proceedings of the IEEE International Symposium on Circuits and Systems*, USA.

Parker, J. R. and Federl, P. (1997). An approach to license plate recognition. Paper presented at the *Proceedings of Visual Interface,* Canada.

Porikli, F. and Tuzel, O. (2006). Fast construction of covariance matrices for arbitrary size image windows. Paper presented at the *Proceedings of the International Conference Image Processing*, USA.

Ron, B.-H. and Erez, J. (2002). A real-time vehicle license plate recognition (LPR) system. Retrieved on 2008 from http://visl.technion.ac.il/projects/2003w24/.

Rovetta, S. and Zunino, R. (1999). License-plate localization by using vector quantization. Paper presented at the *Proceedings of the International Conference on Acoustics, Speech and Signal Processing,* USA.

Shafait, F., Keysers, D. and Breuel, T. M. (2007). Efficient implementation of local adaptive thresholding techniques using integral images. Paper presented at the *Document Recognition and Retrieval XV*.

Shahaf, O., Timor, A. and Erez, J. (2002). Real time license plate recognition in a video movie. Retrieved on 2008 from http://visl.technion.ac.il/projects/2002w03/.

Thanongsak, S. and Kosin, C. (1998). Extracting of car license plate using motor vehicle regulation and character pattern recognition. Paper presented at the *Proceedings of the 1998 IEEE Asia-Pacific Conference on Circuit and Systems*.

Thanongsak, S. and Kosin, C. (1999). The recognition of car license plate for automatic parking system. Paper presented at the *Proceedings of the 5th International Symposium on Signal Processing and Its Applications*, Australia.

Wu, H.-H. P., Chen, H.-H., Wu, R.-J. and Shen, D.-F. (2006). License plate extraction in low resolution video. Paper presented at the *Proceedings of the IEEE 18th International Conference on Pattern Recognition*, Hong Kong.

Yu, M. and Kim, Y. D. (2000). An approach to Korean license plate recognition based on vertical edge matching. Paper presented at the *Proceedings of the IEEE Plate Detection in Various Conditions* and the *Proceedings of the International Conference on Systems, Man, and Cybernetics*, USA.

Zhang, H., Jia, W., He, X. and Wu, Q. (2006). A fast algorithm for license. *IEEE International Conference on Systems, Man, and Cybernetics.* Taiwan.

Zheng, D., Zhao, Y. and Wang, J. (2005). An efficient method of license plate location. *Pattern Recognition Letters, 26*, 2431-2438.

Dietary Risk Factors for Colorectal Adenomatous Polyps:
A Mini Review

Ramadas, A.[1], Kandiah, M.[2*], Jabbar, F.[3] and Zarida, H.[4]
[1] *School of Medicine and Health Sciences, Monash University Sunway,*
Bandar Sunway, Petaling Jaya
[2] *Department of Nutrition and Dietetics,*
[3] *Department of Surgery,*
[4] *Department of Pathology,*
Faculty of Medicine and Health Sciences,
Universiti Putra Malaysia, 43400 UPM, Serdang, Selangor, Malaysia
[*]*E-mail: mirna@medic.upm.edu.my*

ABSTRACT

At least 6 million deaths occurred worldwide are due to cancer and this figure is expected to rise to 15 millions by the year 2020. Colorectal cancer is among the most commonly occurring cancers both globally and in Malaysia. Numerous studies have shown significant relationships between various dietary components and the risks for colorectal cancer. Meanwhile, several theories have been suggested as etiological explanations, one of which is the influence of dietary factors on the cell proliferation rate. A higher cell proliferation rate is statistically associated with increased risk of colorectal cancer. However, evidence of a significant relationship between diet and colorectal adenomas, a potential precursor for colorectal cancer, remains insufficient. Colorectal adenomas or polyps are vital in their relationship with colorectal cancers as almost 70% of all colorectal cancers are developed from these polyps. Studying the modifiable risk factors related to polyps will provide an opportunity for the prevention of colorectal cancer even before it develops. This paper reviews the available evidence linking dietary factors with the risk for colorectal adenomas. As the numbers of published studies are limited, of which most are concentrated in Western countries, there is a need for epidemiological studies in Malaysia to strengthen the evidence of a relationship between diet and colorectal adenomas.

Keywords: Colorectal adenomas, risk factors, diet

INTRODUCTION

Cancer is becoming an increasingly important contributor to the global burden of disease. Based on the Globocan 2002 database, Ma and Yu (2006) reported that for the year 2002, there were 10,862,496 new cancer cases (excluding skin cancer) worldwide. Of these, 5,801,839 (53.4 percent) were males and 5,060,657 (46.6 percent) were females. Nearly 45 percent of the new cases were diagnosed in Asia. The World Health Organization (2003) estimated that the number of new cases annually will escalate from ten million in the year 2000 to 15 million by the year 2020.

On a global basis, the number of deaths caused by cancer in 2002 was 6,723,887, among which 3,795,991 were males and 2,927,896 were females (Ma and Yu, 2006). Some 60% of these cases occurred in the less developed parts of the world. Yet, with the existing knowledge, at least one-third of cancer cases, such as lung, colorectal and breast cancers, could be prevented through lifestyle changes (World Cancer Research Fund, 2007).

Worldwide, colorectal cancer (CRC) was estimated to be the third most common cancer among men and fourth in women in the year 2002 (International Association for Cancer Registries, 2002). Among Malaysians, colon cancer ranked the third among all cancers reported in 2003 accounting for 7.6% and 6.0% in males and females, respectively (National Cancer Registry [NCR], 2004). The incidence of colon cancer was highest among Chinese, and the cumulative lifetime risk for Chinese males was 1 in 36, and 1 in 42 for Chinese females. Cancer of the rectum ranked fifth among the cancers reported in males (6.6%) and females (4.1%), respectively. Once again, the Chinese had the highest incidence of rectal cancer, and this was followed by Indians and Malays. The cumulative lifetime risk for developing rectal cancer for Chinese males was 1 in 48, while it was 1 in 71 for Indian males, and 1 in 91 for Malay males (NCR, 2004). A recent report on cancer incidences between 2003 and 2005 in Peninsular Malaysia (NCR, 2008) showed that colorectal cancer, which included cancer of the colon and rectum, was the most frequent cancer among men, accounting for 14.5% of all cancers. In women, CRC accounted for 9.9% of all cancers.

Having a risk factor for a certain cancer contributes to a higher chance of getting cancer, but it does not always lead to that particular cancer. On the other hand, the absence of any risk factor or having a protective factor does not necessarily protect any individual against cancer. It is important to note that different types of cancer have different risk factors. Factors that may lead to cancer can be classified into external factors, which include environmental toxins, viruses, radiation and chemicals, and internal factors such as hormones, immune setting and inherited mutations and behavioural factors such as diet and lifestyle (Chace and Keane, 1996; American Cancer Society, 2004).

Colorectal Adenomas or Polyps

Colon polyps are vital in their relationship with CRC. Polyps are benign growths involving the lining of the bowel (American Society for Gastrointestinal Endoscopy, 2006). They appear as small bumps that protrude from the lining of the bowel into the lumen. Polyps may vary in size, and can be 1 mm or more in diameter. The two common types of polyps are hyperplastic polyps and adenomas. Hyperplastic polyps do not pose risk for CRC and therefore, are not significant. However, adenomatous polyps are considered to be precursor lesions and may be markers for populations at high risk of CRC (Kahn *et al.,* 1998).

Adenomatous polyps can be sporadic polyps (Calvert and Frucht, 2002). More than 70% of CRC are developed from sporadic adenomatous polyps, and a review of some post-mortem studies have found the incidence of sporadic adenomas to be 30 – 40% in the Western population (Hardy *et al.,* 2000). In a large cohort of Japanese patients, the incidence rate of colorectal adenomas (CRA) in patients with no initial neoplasm (n=4028) was 7.2% per year, whereas the recurrence rates in those with small and advanced lesions (n=1818) were 19.3% and 22.9%, respectively (Yamaji *et al.,* 2004). For advanced colorectal lesions (n=323), the incidence rate was 0.21% per year, whereas the recurrence rates in those with small adenomas and advanced lesions were 0.64% and 1.88% per year, respectively. In general, colorectal neoplasms are more likely to develop in males and older subjects. In Malaysia, the prevalence of colorectal adenomas in a multi-ethnic sample of 311 patients who underwent colonoscopy in a private medical centre was about 11%, based on the only published report (Rajendra, Ho and Arokiasamy, 2005). Meanwhile, the prevalence was highest among the Chinese (62%), followed by the Indians (22%) and Malays (16%). Using logistic regression analysis, only family history ($P = 0.05$) and age ≥ 50 years ($P = 0.011$) were found to be significantly associated with adenomas in this particular sample.

CRA can also develop as a result of DNA mutation. Familial adenomatous polyposis syndrome (FAP) is a genetic condition which affects one in 10,000 people and is caused by a mutation in the

APC gene (Olshwang, 2002). People with FAP develop hundreds of polyps and will almost certainly develop CRC, unless the colon is removed. FAP, which is also known as familial multiple syndrome (FMS) or familial polyposis of the colon (FPC), accounts for only about 1% of all CRCs.

Likewise, hereditary non-polyposis CRC (HNPCC) syndrome is an inherited genetic condition that can also cause CRC even though multiple polyps are not present. It is caused by mutations in mismatch repair genes located on chromosomes two, three, or seven (Burt, 2000). HNPCC mainly affects the right colon compared to the other areas of the gastrointestinal system (Hardy *et al.*, 2000). If a person suffers from this condition, he or she has 80% lifetime risk for developing CRC compared to merely six percent in the general population (Pergament, 2003).

It is important to prevent recurrence of CRA as sufficient evidence links them to incidence of CRC in later life. Identification of dietary risk factors may play an important role in preventing adenomas and their recurrence.

METHODOLOGY

Articles eligible for inclusion met the following criteria: 1) they discussed at least one dietary factor associated with CRA, and/or 2) they studied dietary biomarkers associated with CRA. Since the focus of this review is on the dietary risk factors of CRA, the following factors were excluded: lifestyle factors such as alcohol consumption, tobacco smoking, obesity and non-behavioural risk factors for CRA, such as HPNCC and FAP. CRA outcomes comprised incidence of CRA and/or recurrence of CRA.
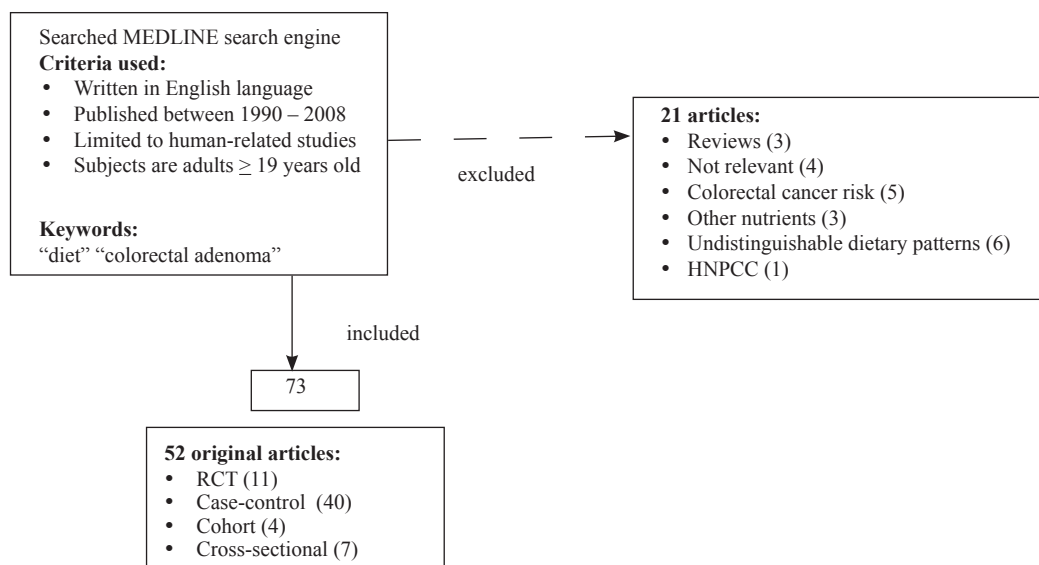
Fig. 1: Flow chart showing article selection process

Fig. 1 shows the flow chart of the article selection. For this purpose, the research papers, written in the English language and published from 1990 to 2008, were reviewed. Meanwhile, studies were initially identified through the search engine Medline by using the keywords ''diet'' and ''colorectal adenomas''. After excluding irrelevant articles, a total of 52 original articles were

selected for this review. Subsequently, the articles were grouped according to the particular dietary component that was studied. A summary of all the selected articles is presented in Table 1.

DIETARY RISK FACTORS

The role of diet in the aetiology of CRA is yet to be elucidated and thus remains an area of active investigation. Dietary risk factors include any type of food, nutrients or other constituents of food that are related to the risk of a disease. Evidence from case-control and cohort studies and some intervention trials suggest a correlation between dietary intake and incidence of CRA. Dietary fat, red meat, fibre, resistant starch, fruits and vegetables in particular, as well as other dietary factors have been associated with the risk for this condition (World Cancer Research Fund, 2007).

Dietary Fat

Epidemiological studies have provided inconsistent data on the role of dietary fats in colorectal cancer, while a few studies have investigated their roles in colorectal adenoma. Mathew *et al.* (2004), in a case-control study from 1994-1996 on 239 cases and 228 control subjects, found an increased risk of seven percent for every five percent increase in energy intake from total fat (OR = 1.07, 95% CI = 0.94 – 1.22). In the same study, the type of fat and sources of fat were also found to influence the risk for CRA. For every additional five percent increase in oleic acid intake, the risk for CRA increased significantly by 115% (OR = 2.15, 95% CI = 1.05 – 4.39). Specifically, red meat fat was found to increase the risk by 20% (OR = 1.20, 95% CI = 0.71 – 2.04), while white meat fat decreased risk by 67% (OR = 0.33, 95% CI = 0.19 – 0.95) for every additional five percent increase in the intake per day.

A randomized, partially double-blind, placebo-controlled trial conducted over four years found that a low fat diet (< 25% of calories from fat) was able to reduce the risk for large adenomas > 10mm in diameter (MacLennan *et al.*, 1995). After 24 months into the trial, the OR for the low fat group was found to be 0.4 (95% CI = 0.1 – 1.1) and after 48 months, it further reduced to 0.3 (95% CI = 0.1 – 1.0). The reduction however was not statistically significant. In another arm of the trial, participants were subjected to both low fat and high fibre (25 g of wheat bran supplementation), and these subjects were found to have zero large adenomas at 24 and 48 months, a statistically significant finding (p = 0.03). These observations suggest that a combination of low fat and high fibre diet may reduce the rate of transition from smaller to larger adenomas. However, affirmative conclusions cannot be made from these findings as only a small number of subjects were enrolled in this study.

In another prospective study on the effect of dietary marine n-3 fatty acids on distal CRA in women, no significant relationship was found between these two variables (Oh *et al.*, 2005). However, higher intakes of dietary marine n-3 fatty acids were inversely but not significantly associated with large adenomas (RR = 0.74, 95% CI = 0.54 – 1.01), but were directly associated with small adenomas (RR = 1.36, 95% CI = 1.02 – 1.81). Once again, the results of this study suggest that higher intakes of marine n-3 fatty acids may reduce the progression of small adenomas to larger ones.

The effect of dietary fat on the risk for CRA continues to be elusive. Diergaarde *et al.* (2005) reported that the high intake of fat seemed to only increase the risk of APC(-) polyps (OR = 1.9, 95% CI = 1.0-3.7). On the other hand, Vinikoor *et al.* (2008) reported that it increased the prevalence of CRA in those in the highest quartile of trans-fatty acid intake as compared to those with the lowest (OR = 1.86, 95% 1.04 – 3.33). A newer study was carried out by Methy *et al.* (2008) to further assess the risks of overall adenoma recurrence associated with dietary consumption of total fat, sub-types of fat, and specific fatty acids (oleic acid, linoleic acid, alpha-linolenic acid). The

study comprised 523 patients with confirmed adenomas at the index colonoscopy, aged between 35 to 75 year old. The overall 3-rear recurrence rate was 22.6%. Nonetheless, this study failed to observe significant associations between overall adenoma recurrences with either total fat, sub-type of fats, or specific fatty acids. Polyunsaturated fatty acids and linoleic acid were both moderately and significantly associated with distal and multiple recurrence. No significant association was observed with the recurrence of proximal or advanced adenomas. The study by Methy *et al.* (2008) did not support the hypothesis of a strong association between dietary fatty acids and the recurrence of colorectal adenomas. It was concluded that the differential role of specific fatty acids according to colorectal subsites deserves further investigation.

As much of the evidence on the role of fat in the CRA risks resulted from case-control studies, more cohort and experimental studies are warranted to examine this association. However, special focus should be placed on determining the ability of dietary fat to influence the progression of smaller adenomas to larger adenomas, and the possible role of dietary fat in the progression of adenomas to carcinoma.

Dietary Fibre

The role of dietary fibre in the prevention of CRC was first proposed by Burkitt (1969), following the clinical observation that colon cancer was rare among the Africans whose diet was high in unrefined foods. Studies on CRA are generally now supportive of a protective association with dietary fibre, although some contradictory results have been published (Fuchs *et al.,* 1999; Schatzkin *et al.*, 2000; Robertson *et al.,* 2005).

Intake of fibre from vegetables and cereals has been associated with a clear reduction in the risk for CRA in a prospective study by Giovannucci *et al.* (1992), where the relative risk for the lowest quintile of dietary fibre intake versus the highest was 8.4 (95% CI = 0.2 – 0.6). This finding was confirmed by a study conducted by Peters *et al.* (2004), which was conducted within the Prostate, Lung, Colorectal and Ovarian (PLCO) Cancer Screening Trial. High intakes of dietary fibre were associated with a 27% lower risk (95% CI = 14 – 38) of CRA, after adjusting for other dietary and non-dietary risk factors. The inverse relationship was strongest for fibre from grains and cereals (OR =0.75), and from fruits (OR=0.58). Risks were similar for advanced and non-advanced adenoma. Risk of rectal adenoma however, was not significantly associated with fibre intake.

Results from the Health Professionals Follow-up Study showed that there was a modest 19% reduced risk of distal colon adenoma with the increase in the intake of fibre from fruits, but not from cereals or vegetables (Platz *et al.,* 1997). The RR comparing the highest intake (median, 8.4 g/day) to the lowest quintile of fibre intake (1.3 g/day) was 0.81 (95% CI, 0.59-1.11). The reduction in risk, however, was observed only for soluble fibre. A latter study within the Prostate, Lung, Colorectal, and Ovarian (PLCO) Cancer Screening Trial (PLCO) by Peters *et al.* (2003) noted a similar finding. Risk of adenoma was lowest at the highest quintile of dietary fibre intake in comparison to the lowest quintile. The inverse association observed was most significant for fibre from grains, cereals, and fruits. Risks were similar for advanced and non-advanced adenomas. These results suggested that soluble fibre might be particularly important in reducing risk of adenomatous polyps of the distal colon. The Wheat Bran Fibre Trial (Jacobs *et al.,* 2002), prior to the Polyp Prevention Trial (Lanza *et al.,* 2007) also found a reduction in risk with the intake of fibre, but the reduction was not statistically significant.

Potential mechanisms that may explain the protective effect of dietary fibre include dilution of faecal carcinogens and procarcinogens, reduction of transit time of faeces through the bowel, production of short chain fatty acids which promote anticarcinogenic action, and binding of carcinogenic bile acids (Lipkin *et al*., 1999).

Pertanika J. Sci. & Technol. Vol. 18 (2) 2010

325

On the other hand, there are studies which have shown no association between dietary fibre and risk for CRA. A prospective study, which was carried out among 88,000 women who had been followed up for 16 years, found the lack of a protective effect of dietary fibre against CRA (Fuchs *et al*., 1999). The Polyp Prevention Trial (PPT), a well-publicised large-scale intervention trial, found no significant association between dietary fibre intakes and recurrence of adenomatous polyps (Schatzkin *et al*., 2000). One of the most plausible explanations for the lack of effect was that the population studied had only low intakes of dietary fibre from cereals (4.8 g/day in the highest intake group). The subjects were further followed up for 4 years and yet no significant association was found between their dietary fibre intakes and recurrence of adenoma (Lanza *et al*., 2007). The authors' explanations for the null observation included inadequate trial length, inappropriate timing in the life course for such a trial, inappropriate end point, and inappropriate intervention.

As some of the recent findings are not encouraging, more studies should be done to establish the relationship between different types of dietary fibre and the risks for CRA at various subsites. Thus, the role of fiber in the etiology of colorectal cancer and precursor adenomatous polyps continues to be controversial.

Red Meat

Western diets containing high amounts of red meat have been associated with a high risk for CRA. A German case-control study, which compared patients with previous adenomas with hospital and population controls, found a positive association between red meat intake and risk for CRA, but not for fat or protein from red meat (Breuer-Katschinski *et al*., 2001). Those in the highest quintile of red meat intake were found to have more than three-fold increase in risk (OR = 3.6, 95% CI = 1.7 – 7.5) as compared to the hospital controls, and over four-fold increase in the risks (OR = 4.4, 95% CI = 1.6 – 12.1) than the control population.

Chiu and Gapstur (2004) reported that the risk for CRA was higher for those with the smallest reduction in red meat intake after the age of 30 years (OR = 2.8, 95% CI = 1.1-7.3). High intakes of red meat appeared to increase the risk of APC(-) polyps only (APC(-) vs. controls OR = 1.8, 95% CI = 1.0-3.1) (Diergaarde *et al*., 2005). Processed meat could specifically contribute to risk at the highest quartile of intake, by a two-fold increase in risk (Ward *et al*., 2007) as compared to the lowest intake.

Sinha *et al*. (1999) suggested that besides total red meat intake, cooking method such as well-done, grilled red meat might also increase the risk of CRA. An increased risk of 11% per 10 g/day of red meat consumption (OR = 1.11, 95% CI = 0.96 – 1.26) while high-temperature cooking methods were reported to increase the risk even further. Consumption of about 10 g/day of grilled red meat was associated with 26% risk (OR = 1.26, 95% CI = 1.06 – 1.50) and 15% per 10 g/day (OR = 1.15, 95% CI = 0.97 – 1.36) for pan-fried red meat. A larger case-control study published six years later confirmed this finding (Sinha *et al*. 2005).

Gunter *et al*. (2005) estimated that an incremental increase of 10 g of barbecued red meat per day might be associated with a 29% increased risk of large adenoma (OR = 1.29, 95% CI = 1.02-1.63). The consumption of oven-broiled red meat was inversely related to adenoma risk compared with non-consumers (OR = 0.49, 95% CI = 0.28-0.85). Furthermore, higher consumption of mutagens from meats cooked at higher temperature and longer duration may be associated with higher risk of distal colon adenoma independent of the overall meat intake (OR highest versus lowest quintile of meat-derived mutagenity = 1.29, 95% CI = 0.97-1.72) (Wu *et al*., 2006). These results are consistent with the hypothesis that carcinogenic compounds, such as heterocyclic amines and polycyclic aromatic hydrocarbons, formed by high-temperature cooking techniques, may contribute to the risk of developing colorectal tumours.

Although an overwhelming number of studies have shown positive correlations between red meat intake and the risk for CRA, Tiemersma *et al.* (2004) reported otherwise. HCAs were present in habitually prepared meat, although meat consumption (7 versus < 5x/week) did not increase the risk of colorectal adenomas (OR = 1.2, 95% CI = 0.8-1.9). Besides, presumed unfavourable preparation habits of meat did not increase adenoma risk (OR = 0.8 and 0.9, respectively).

In recent years, dietary effects on risk of diseases have been studied in relation to genetic polymorphisms in biotransformation genes. A study by Skelbred *et al.* examined the role of dietary factors in combination with genetic factors in the different stages of colorectal carcinogenesis in a Norwegian population. The results suggested an increased risk of colorectal adenomas in individuals for some of the higher ratios of total meat to total fruit, berry, and vegetable intakes. In addition, the study supports the notion that the biotransformation enzymes GSTM1, GSTP1, and EPHX1 may modify the effect of dietary factors on the risk of developing colorectal carcinoma and adenoma.

Evidence continues to mount proving that red meat intake affects risk of developing CRA. Although no study has been reported on Malaysians' risk for adenomas associated with intake of red meat, the current evidence should be taken into consideration, as Malaysian diets are increasingly becoming more westernized coupled with a high demand for animal foods.

Fruits and Vegetables

The presumed beneficial effects of fruit and vegetables have been the core of many large-scale public health campaigns such as the well-known "Five a Day" program and guidelines on cancer prevention, especially CRC (National Cancer Institute 2006). Meanwhile, consumption of fruit and vegetables may confer protection from colorectal adenomas, but the observational and interventional evidence is rather inconclusive.

Witte *et al.* (1996) conducted a case-control study in Southern Carolina and found inverse relationships between high carotenoid vegetables, cruciferous vegetables, high vitamin C fruit, garlic and tofu, and the risk for CRA. This finding supported the hypothesis that high intakes of vegetables, fruit and grains decreased the risk of adenomatous polyps.

A high-fruit, low-meat diet also appears to be protective against CRA compared with a dietary pattern of increased vegetable and meat consumption (Austin *et al.,* 2007). After adjusting for potential confounders, the high vegetable-moderate meat cluster (OR = 2.17, 95% CI = 1.20 – 3.90) and high meat cluster (OR = 1.70, 95%CI = 1.04 – 2.80) were at significantly increased odds of having had an adenoma compared with the high fruit-low meat cluster.

A cross-sectional study within the Nurses' Health Study (Michels *et al.,* 2006) found that a frequent consumption of fruit was inversely related to the risk of being diagnosed with polyps (OR >5 servings vs <1 servings = 0.60, 95% CI = 0.44 – 0.81), whereas little association was found for vegetable consumption (OR = 0.82, 95% CI = 0.65 – 1.05). However, another case-control study reported that individuals in the highest quartile of increased consumption vegetables (OR = 0.5; CI = 0.3-1.1) had a lower risk compared with those with minimal increase in consumption (Chiu and Gapstur, 2004).

On the other hand, Smith-Warner *et al.* (2002) found only juice consumption reduced the risk of CRA, but this was only evident in women subjects (OR = 0.50, 95% CI = 0.27 – 0.92) when cases were compared to negative-controls and (OR = 0.56, 95% CI = 0.30 – 1.06) community-controls. The association was stronger for adenomas with moderate and severe dysphasia.

A three-year endoscopic follow-up study concluded that fruit and vegetables might play an early but weak role in the development of CRC by influencing the growth and recurrence of adenoma (Almendingen *et al*., 2004). Dietary intake which was assessed by a five-day dietary record and food frequency questionnaire (FFQ) revealed a weak inverse association between growth of adenoma

and fruit and berries (adjusted OR = 0.3, 95% CI = 0.1 – 0.9). Moreover, a weak association was found between adenoma recurrence and vegetable intake (crude OR = 0.4, 95% CI = 0.1 – 0.9).

The protective effect of vegetable intake was observed on the recurrence of adenomas but not on the appearance of new adenoma; this suggests that vegetables may have a stronger role in preventing the progression of adenomas to carcinomas rather than in the initial appearance of adenomatous polyps. Meanwhile, research was found an inverse link between high plant-based food intake and the risk for adenomas, but several other studies did not find any relationship. Thus, further investigations are warranted to affirm the protective role of these food items.

Vitamin A

Vitamin A, which is involved in normal tissue growth and differentiation, was one of the earliest vitamins studied with respect to carcinogenesis (Sporn *et al*., 1983). *In vivo* experiments suggested that vitamin A deficiency might enhance the susceptibility of cells to certain chemical carcinogens. The hypothesized mechanisms through which vitamin A may influence carcinogenesis include action on the cell nucleus involving the expression of genetic information that controls cell differentiation. Preformed vitamin A is obtained from animal products, but pro-vitamin A carotenoids are derived largely from fruit and vegetables (Olson, 1994; Ross and Temus, 1993).

Unfortunately, studies indicating the relationship between vitamin A and CRA are few in number and are under-researched compared to research on vitamin A and CRC. An early study by Enger *et al.* (1996) suggested that vitamin A from dietary sources is associated with a decreased risk of CRA (crude OR = 0.60, 95% CI = 0.4 – 0.9) when the highest quartile of intake was compared to the lowest, but the relationship no longer existed after adjusting for potential confounders (adjusted OR = 0.90, 95% CI = 0.5 – 1.5). Nevertheless, the association between supplemented vitamin A and risk was not significant (adjusted OR = 1.4, 95% CI = 0.9 – 2.3). Similarly, Giovannucci *et al.* (1993) found that higher intake of vitamin A did not protect from the risk of CRA (OR = 0.91, 95% CI = 0.69 – 1.19). A case-control study revealed no significant relationship between dietary retinol (vitamin A) and risk of CRA (Lubin *et al.,* 1997). The adjusted odds ratio for the intake of retinol was 0.9 (95% CI = 0.5 – 1.6) when the highest tertile of intake was compared with the lowest, while adjustment was made for energy intake and physical activity. Data from a Japanese cohort study, comprising both male and female subjects, noted a relative risk (RR) of (RR = 1.42, 95% CI = 1.00 – 2.20), indicating an increased risk of adenomas with animal protein and vitamin A intake (RR = 1.51, 95% CI = 1.04 – 2.20) for the highest tertile versus the lowest (Nagata *et al*., 2001).

It is important to note that studies revealing relationships between dietary vitamin A (or even plasma vitamin A) and CRA are sparse. Moreover, very few clinical trials or epidemiological studies have explored the association between vitamin A and its derivates with risk of developing CRA. Thus, the available data are insufficient to conclude any association between vitamin A and risk of CRA, and thus requires further research.

Carotenoids

Carotenoids are pigments found primarily in plants, and the predominant carotenoids in the human diet are β-carotene, lycopene, lutein, β-cryptoxanthin and α-carotene. Carotenoids are related to cancer through their antioxidant properties, modulation of gene expression, regulation of cell growth and possible immune response (Rock *et al*., 1997).

Lubin and co-workers (1997) identified specific nutrients as independent factors which are associated with CRA, while carotene was identified as one of the nutrients with potential benefits. Increased intake of carotene was suggested to reduce the risk of CRA by 40% when the highest tertile of intake was compared with the lowest (OR = 0.6, 95% CI = 0.3 – 1.0).

Senesse *et al.* (2005) investigated the effect of β-carotene on the risk of CRA and the potential interaction with smoking status. The researchers found a significant interaction between β-carotene and smoking habit (p = 0.04). In non-smokers, β-carotene was inversely associated with the risk, of colon adenomas (OR in low vs. high consumers = 0.4, 95% CI = 0.2 – 0.9), whereas in past or current smokers, β-carotene was associated with a non-significant increase in the risk of colon adenomas (OR = 1.9, 95% CI = 0.9 – 4.1). The authors stressed that although β-carotene seemed to be protective in non-smokers, the adverse effect of the nutrient in smokers should be taken as a caution.

Other carotenoids have shown little or almost no significant relationship with the risk of CRA. Enger *et al.* (1996) found that in univariate-matched analysis, α-carotene, β-carotene, β-cryptoxanthin, lutein and zeaxanthin were all associated with decrease in risk, but only β-carotene was found to be significantly associated with adenomas (p = 0.04) after adjusting for potential confounding factors. An observational study carried out among the White subjects with history of hyperplastic polyps and controls revealed that plasma lycopene was the only carotenoid which lowered the risk for CRA (Erhardt *et al.*, 2003). The median plasma lycopene concentration was significantly lower in the adenoma group than in the control group (-35%, p = 0.016). In addition, the median plasma β-carotene was also found to be lower in the adenoma group (-25.5%), but the difference was not significant. In the multiple logistic regression, only smoking (OR = 3.02, 95% CI = 1.46 – 6.25) and plasma lycopene concentration (OR = 2.31, 95% CI = 1.12 – 4.77) were risk factors for adenomatous polyps.

Shikany *et al.* (1997) showed that there is no association between individual plasma carotenoids and the prevalence of adenomatous polyps. This study did not stratify the subjects according to their smoking status but carotenoids were suggested as a probable protective factor only in smokers. This might explain the reason for the non-association found between carotenoids and risk of CRA. In a RCT conducted within Alpha – Tocopherol, Beta–Carotene Cancer Prevention Study (ATBC Study), supplementation with β-carotene had no effect on risk for CRA (RR = 0.98; 95% CI = 0.71 - 1.35) among middle-aged male smokers (Malila *et al.*, 1999).

Even β-carotene, lycopene and lutien, the well-studied carotenoids of all, have shown inconsistent findings. On the other hand, other carotenoids such as zeaxanthin and cryptoxanthin are under-studied. Therefore, future studies should focus on these less studied carotenoids.

Vitamin C

Vitamin C is a water soluble vitamin that occurs mainly in fruit and vegetables. Its potent anti-oxidative properties are thought to contribute to its possible cancer preventive potential. As an antioxidant, vitamin C is considered to have a protective effect on cellular biopolymers, including genetic material and could thus be protective in the initiation and promotional stages of carcinogenesis (Van Poppel and Van Den Berg, 1997).

A high rate of apoptosis has been linked to a reduced risk of CRA in a study conducted within the Diet and Health Study III (Connelly *et al.*, 2003). Among individuals with adenomas, there was an inverse linear association between apoptosis and total vitamin C intake. Similarly, individuals with adenomas in the highest quintile of total vitamin C intake were substantially less likely to have increased colonic apoptosis than those in the lowest quintile (OR = 0.05, 95% CI = 0.01–0.46). High vitamin C intake was associated with reduced colorectal apoptosis, but this was only among individuals with adenomas in this population.

Meanwhile, Benito *et al.* (1993) found higher intake of vitamin C to significantly lower the risk for CRA by 63% (p for trend <0.01), whereas Tseng *et al.* (1996) found a significant reduction in risk exclusively among women subjects. Other studies found insignificant results as well. Enger *et al.* (1996), for example, found that dietary vitamin C only managed to yield a weak association

after adjusting for confounding factors (OR = 0.8, 95% CI = 0.5 – 1.5). This concludes that dietary vitamin C may not always be protective of CRA.

Antioxidant vitamins, such as vitamin C, have been suggested as potential anticancer agents because they fight free radicals which may cause oxidative damage to DNA, possibly leading to development of cancer (Byers and Perry, 1992). The ability of ascorbic acid to inhibit the formation of carcinogenic nitrosamines is the best documented cancer-protecting effect of vitamin C (Block, 1991). This protective mechanism of vitamin C could provide the explanation for numerous studies which found a protective effect of fruit and vegetables against cancer, as vitamin C is one of the most commonly occurring antioxidant vitamins in this particular food group.

Although fruit and vegetables have been consistently shown to be related to the risk of CRA and CRC, the same could not be said about vitamin C per se which is a commonly found micronutrient in these foods. Instability of this vitamin in food and plasma is one of the reasons; thus, methodological and study design may also be partly to be blamed for the inconsistent evidence. More studies which take these issues into account should be done in the future to strengthen the current available evidence.

Vitamin E

Vitamin E is a predominant antioxidant nutrient in the lipid phases of circulating lipoproteins and cell membranes. This potent peroxyl radical scavenger is a chain-breaking antioxidant that prevents the propagation of free radical damage in biological membranes (Traber and Packer, 1995). Just like vitamin C, this vitamin also seems to provide protection from various types of cancer, especially CRC. However, there are some limitations when interpreting the results of plasma vitamin E values in prospective studies. These include person-to-person variation in diet, the effects of non-dietary determinants of blood concentrations and the effects of preclinical disease on blood concentrations.

The use of vitamin E supplements was found to be associated with a lower incidence of recurrent adenomas (OR = 0.62, 95% CI = 0.39 – 0.98) in a population of patients with history of previous colonic neoplasia (Whelan *et al*., 1999). However, Tseng *et al*. (1996) demonstrated a protective effect of vitamin E only among men, whereby those in the highest quartile of vitamin E intake had a risk of 0.35 (95% CI- 0.14 – 0.92) relative to those in the lowest intake.

Plasma α- and γ-tocopherol concentrations for subjects with CRA were compared with healthy controls in order to examine the protective effect of vitamin E in plasma against CRA (Ingles *et al*., 1998). Increasing α-tocopherol and decreasing γ-tocopherol levels were associated with decreased occurrence of large adenomas; however, after adjusting for potential confounding variables, these trends were not statistically significant. Subjects in the highest versus lowest quintile of α-tocopherol:γ-tocopherol ratio had an OR of 0.36 (95% CI = 0.14-0.95) for large adenomas, which had higher probability to progress to CRC. The finding that indicated a high α-tocopherol:γ-tocopherol ratio in association with decreased occurrence of only large CRA is consistent with the previous findings that suggested α-tocopherol might be protective against CRC.

As reported for other antioxidant vitamins, the evidence for vitamin E and its association with CRA is also unequivocal and little. A study focusing on both dietary intake and plasma vitamin E will be able to add more information to the available data, particularly in the Asian community.

Vitamin D and Calcium

There has been a considerable interest in the protective role of vitamin D and calcium. Although evidence exists for the protective effects of vitamin D against CRC, there was no study linking vitamin D, calcium and CRA prior to 1999 (Holt, 1999). However, results of the on-going Nurses'

Health Study indicated that women, whose plasma $1,25(OH)_2D$ concentration was below 26.0 μg/ml, were at increased risk of distal CRA (Platz *et al*., 2000).

Peters *et al*. (2004) showed that serum 25-(OH)D was inversely associated with CRA, in which they found that the risk of CRA decreased by 26% (OR 0.74) with each 10 mg/ml increase of serum 25-(OH)D. However, the inverse association between serum 25-(OH)D and CRA has been suggested to be stronger in subjects with calcium intake above the median. Jacobs *et al*. (2007) also suggested insignificant reduction in the risk with higher serum 25-(OH)D levels.

The findings by Grau *et al. (*2003) indicated a protective role of vitamin D and calcium against CRA. They demonstrated the synergistic effect by looking at the participants' status of vitamin D in a trial which showed that calcium supplements protected against recurrence of CRA. Among people with 25-(OH)D levels at or below the overall median, calcium was found to have no effect on the risk of recurrence of adenomas. However, the risk was lowered in those with high levels of vitamin D. Therefore, vitamin D was associated with a reduced risk only among those taking calcium.

Supplementation with calcium has also been shown to be protective against CRA. The strongest evidence for the use of calcium in preventing CRA came from a trial by Baron *et al.* (1999), where calcium or placebo was given to adenomatous polyp patients for 4 years resulting in a moderate, but significantly reduced risk for adenomatous polyp recurrence in the intervened group. The daily dosage used, 3 g of calcium carbonate, added 1200 mg of calcium ion to the daily intake of dietary calcium. Two other studies showed a significant reduction in adenoma recurrence after given calcium supplements (Hofstad *et al.,* 1998; Bonitton-Kopp *et al.,* 2000).

However, there were studies which did not find any significant association. For instance, Hartman *et al.* (2005) did not find any significant association between adenoma recurrence and dietary calcium, total calcium, and dietary vitamin D intake. Kesse *et al.* (2005) suggested a decreasing trend in risk with the increase in calcium intake (RR = 0.80, 95% CI ==0.62-1.03), but this trend was not significant, and no effect was seen with vitamin D intake. Little association was observed by Miller *et al*. (2007) when they compared total calcium intake of ≥ 900 mg/day to <500 mg/day (adjusted OR = 0.85, 95% CI = 0.53-1.37). However, Miller *et al*. (2007) reported a lower prevalence of adenomas among patients with calcium intake ≥ 900 mg/day and lower fat intake.

The role of vitamin D and calcium have been (but not always) found to be related to adenoma appearance. However, a considerable number of large studies are required before accepting the role of these micronutrients in adenoma appearance.

Folate

Several studies have found a link between lower levels of folate intake and a higher incidence of adenomas, suggesting that folate may play a protective role in the carcinogenic process.

In a case-control study of diet and colorectal adenoma risk, Benito *et al.* (1993) found that subjects with folate intakes greater than 222 μg per day were approximately one fourth as likely to have adenomas as compared to those with intakes below 141 μg per day. Unfortunately, the only dietary factor the data were adjusted for was total calorie intake. Folate seemed to be a risk factor, especially when vitamin B12 intake was low, while vitamin B12 was inversely associated with adenomas, especially with relatively high folate intake (van den Donk *et al*., 2005). The adjusted OR (95% CI) for the highest compared with the lowest sex-specific tertile of intake was 1.32 (95% CI = 1.01 - 1.73) for folate and this was 0.51 (95% CI = 0.36 - 0.73) for vitamin B12. Among non-multivitamin users, Martinez *et al.* (2006) reported results from two major RCTs, namely Wheat Bran Fibre Trial and Ursodeoxycholic Acid Trial, and found that the OR for those in the highest

versus the lowest folate quartile was 0.65 (95% CI = 0.40-1.06) for the WBF study and 0.56 (0.31-1.02) for the UDCA trial.

Tseng *et al.* (1994) pursued this possible cancer-folate connection by conducting a similar case-control study to evaluate the relationship between micronutrients and CRA risk. Although their results did not achieve statistical significance, they observed a gender-specific trend. After adjusting for other dietary factors, their results showed a 60% decrease in the adenoma risk for women in the highest quartile of folate intake compared with the lowest quartile. The cause of the observed sex specificity is unclear, but the authors suggested that there might be other physiological factors involved that changed the risk pattern between men and women.

A prospective study of similar subjects from two large cohorts, namely the Nurses' Health Study and the Health Professionals Follow-up Study, was conducted by Giovannucci *et al.* (1993). They were interested in the association with folate because they found a mechanism by which low folate levels might contribute to the development of adenomas by decreasing the availability of methyl groups. The link including methionine in this equation was suggested because folate is responsible for methylization of homocysteine to methionine. This is particularly important as a low level of folate is hypothesized to disrupt DNA methylation as well.

Similar to other micronutrients studied, the relationship between folate and risk for CRA and CRC needs to be examined further. A prospective study should be able to provide more concrete evidence.

CONCLUSIONS

In conclusion, the dietary intake of an individual may influence the risk of developing CRA. While most of the available evidence suggests a role for certain foods, such as vegetables and fruits especially greens, cruciferous vegetables, citrus fruit and garlic for reducing risk, evidence for other dietary factors remains unequivocal. In addition, international variations in the distribution of the disease may also be a contributing factor to the differences derived in the observations of adenoma status (advanced or small), while position (distal or proximal) may also confound the association. Thus, future epidemiological studies and clinical trials of CRA should take into account the interaction of ethnicity, adenoma size and site into their study design.

REFERENCES

Almendingen, K., Hofstad, B. and Vatn, M.H. (2004). Dietary habits and growth and recurrence of colorectal adenomas: Results from a three-year endoscopic follow-up study. *Nutrition and Cancer, 49*(2), 131 – 138.

American Cancer Society. (2004). Cancer facts and figures 2004. Retrieved from http://www.cancer.org/download/STT?F&F2004.pdf.

American Society for Gastrointestinal Endoscopy. (2006). Understanding polyps and their treatment. Retrieved from http://www.asge.org/nspages/practice/ management/brochures/polyps_ brochure.cfm.

Austin, G. L., Adair, L.S., Galanko, J.A., Martin, C.F., Satia, J.A. and Sandler, R.S. (2007). A diet high in fruits and low in meat reduces the risk of colorectal adenomas. *Nutrition Journal, 137*, 999 – 1004.

Baron, J. A., Beach, M., Mandel, J.S., Van Stolk, R. U., Haile, R. W., Sandler, R. S., Rothstein, R., Summers, R. W., Snover, D.C., Beck, G. J., Bond, J. H., Greenberg, E. R., Frankl, H. and Pearson, L. (1999). Calcium supplements for the prevention of colorectal adenomas. *The New England Journal of Medicine, 340*, 101 – 107.

Benito, E., Cabeza, E., Moreno, V., Obrador, A. and Bosch, F.X. (1993). Diet and colorectal adenomas: A case control study in Majorca. *International Journal of Cancer, 55*, 213-219.

Block, G. (1991). Vitamin C and cancer prevention: The epidemiologic evaluation. *American Journal of Clinical Nutrition, 53*, 270S – 282S.

Bonithon-Kopp, C., Kroborg, O., Giacosa, A., Rath,U. and Faivre, J. (2000). Calcium and fiber supplementation in prevention of colorectal adenoma recurrence: A randomized intervention trial. *Lancet*, *356*, 1300 – 1336.

Breuer-Katschinski, B., Nemes, K., Marr, A., Rump, B., Leiendecker, B., Breuer, N. and Goebell, H. (2001). Colorectal adenomas and diet. *Digestive Dieseases and Sciences, 46*(1), 86 – 95.

Burkitt, D. P. (1969). Related disease, related cause? *Lancet, 2*, 1229 – 1231.

Burt, R.W. (2000). Colon cancer screening. *Gastroenterology, 119*, 837-853.

Byers, T. and Perry, G. (1992). Dietary carotenes, vitamin C and vitamin E as protective antioxidants in human cancers. *Annual Review of Nutrition, 12*, 139 – 159.

Calvert, P. M. and Frucht, H. (2002). The genetics of colorectal cancer. *Annals of Internal Medicine, 137*, 603 – 612.

Chace, D. and Keane, M. (1996). *What to Eat if You Have Cancer: A Guide to Adding Nutritional Therapy to Your Treatment Plan.* United States of America: Contemporary Books.

Chiu, B. C. and Gapstur, S.M. (2004). Changes in diet during adult life and risk of colorectal adenomas. *Nutrition and Cancer*, *49*(1), 49 – 58.

Connelly, A. E., Satia-Abouta, J., Martin, C.F., Keku, T.O., Woosley, J. T., Lund, P.K. and Sandler, R.S. (2003). Vitamin C intake and apoptosis in normal rectal epithelium. *Cancer Epidemiology, Biomarkers and Prevention, 12*, 559-565.

Diergaarde, B., Tiemersma, E.W., Braam, H., Van Muijen, G. N., Nagengast, F. M., Kok, F.J. and Kampman, E. (2005). Dietary factors and truncating APC mutations in sporadic colorectal adenomas. *International Journal of Cancer, 113*(1), 126 – 132.

Enger, S.M., Longnecker, M.P., Harper, M. J., Lee, E.R., Frankl, H.D. and Haile, R.W. (1996). Dietary intake of specific carotenoids and vitamin A, C, and E, and prevalence of colorectal adenomas. *Cancer Epidemiology, Biomarkers and Prevention*, *5*, 147 – 153.

Erhardt, J. G., Meisner, C., Bode, J.C. and Bode, C. (2003). Lycopene, β-carotene and colorectal adenomas. *American Journal of Clinical Nutrition, 78*, 1219-1224.

Fuchs, C. S., Giovannucci, E.L., Colditz, G.A., Hunter, D.J., Stampfer, M.J., Rosner, B., Speizer, F.E. and Willet, W.C. (1999). Dietary fiber and the risk of colorectal cancer and adenoma in women. *The New England Journal of Medicine, 340*, 169-176.

Giovannucci, E., Stampfer, M.J., Colditz, G., Rimm, E.B. and Willet, W.C. (1992). Relationship of diet to risk of colorectal adenoma in men. *JNCI*, *84*, 91 – 98.

Giovannucci, E., Stampfer, M.J., Colditz, G., Rimm, E.B., Trichopoulos, D., Rosner, B.A., Speizer, F. E. and Willet, W.C. (1993). Folate, methionine, and alcohol intake and risk of colorectal adenoma. *JNCI, 85*, 875-884.

Grau, M. V., Baron, J.A., Sandler, R.S., Haile, R.W., Beach, M.L., Church, T. R. and Heber, D. (2003). Vitamin D, calcium supplementation and colorectal adenomas: Results of a randomized – trial. *JNCI*, *95*, 1765 – 1771.

Gunter, M. J., Probst-Hensch, N.M., Cortessis, V.K., Kulldorf, M., Haile, R.W. and Sinha, R. (2005). Meat intake, cooking-related mutagens and risk of colorectal adenoma in a sigmoidoscopy-based case-control study. *Carcinogenesis, 26*(3), 637 – 642.

Hardy, R.G., Meltzer, S. J. and Jankowski, J. A. (2000). ABC of colorectal cancer: Molecular basis for risk factors. *BMJ, 321*, 886 – 889.

Hartman, T. J. *et al.* and Polyp Prevention Study Group. (2005). The association of calcium and vitamin D with risk of colorectal adenomas. *Journal of Nutrition, 135*(2), 252 – 259.

Hofstad, B., Almendingen, K. and Vatn, M. (1998). Growth and recurrence of colorectal polyps: A double-blind 3-year intervention with calcium and antioxidants. *Digest, 5*, 148 – 156.

Holt, P. R. (1999). Dairy foods and prevention of colon cancer: Human studies. *Journal of the American College of Nutrition, 18*, 379S – 391S.

Inges, S. A., Bird, C. L., Shikany, J.M., Frankl, H.D., Lee, E,R. and Haile, R.W. (1998). Plasma tocopherol and prevalence of colorectal adenomas in a multiethnic population. *Cancer Research, 58*(4), 661-666.

International Association for Cancer Registeries. (2002). Globocan 2002: Cancer Incidence, Mortality and Prevalence Worldwide, Version 1.0. Retrieved on http://www-dep.iarc.fr.

Jacobs, E. T., Guiliano, A.R., Roe, D. J., Guillen-Rodriguez, J.M., Hess, L. M., Alberts, D.S. and Martinez, M. E. (2002). Intake of supplemental and total fiber and risk of colorectal adenoma recurrence in the Wheat Bran Fiber Trial. *Cancer Epidemiology, Biomarkers and Prevention, 11*(9), 906 – 914.

Jacobs, E. T., Alberts, D.S., Benuzilo, J., Hollis, B.W., Thompson, P.A. and Martinez, M.E. (2007). Serum 25(oh)d levels, dietary intake of vitamin d, and colorectal adenoma recurrence. *The Journal of Steroid Biochemistry and Molecular Biology, 103*(3-5), 752 – 756.

Kahn, H. S., Tatham, I.M., Thun, M.J. and Heath, C.W. (1998). Risk factors for self – reported colon polyps. *Journal of General Internal Medicine, 13*, 303 – 310.

Kesse, E., Boutron-Ruault, M.C., Norat, T., Riboli, E., Clavel-Chapelon, F. and E3N Group. Dietary calcium, phosphorus, vitamin D, dairy products and the risk of colorectal adenoma and cancer among french women of the e3n-epic prospective study. *International Journal of Cancer, 117*(1), 137 – 144.

Lanza, E. *et al.* (2007). The polyp prevention trial-continued followed up study: No effect of a low-fat, high fiber, high-fruit, and-vegetable diet on adenomas recurrence 8 years after randomization. *Cancer Epidemiology, Biomarkers and Prevention, 16,* 1745 – 1752.

Lee, Y.S. (1987). Adenomas, metaplastic polyps and other lesions of the large bowel: An autopsy survey. *Annals Academy of Medicine, 16*, 412 – 420.

Lipkin, M., Reddy, B., Newmark, H. and Lamprecht, S.A. (1999). Dietary factors in human colorectal cancer. *Annual Reviwew of Nutrition, 19*, 545-586.

Lubin, F., Rozen, P., Arieli, B., Farbstein, M., Knaani, Y., Bat, I. and Farbstein, H. (1997). Nutritional and lifestyle habits and water-fiber interaction in colorectal adenomas etiology. *Cancer Epidemiology, Biomarkers and Prevention*, *6*, 79 – 85.

Ma, X. and Yu, H. (2006). Global burden of cancer. *Yale Journal of Biology, 79*(3-4), 85 – 94.

Mac Lennan, R. *et al.* (1995). Randomized trial of intake of fat, fiber and beta carotene to prevent colorectal adenomas. *Journal of The National Cancer Institute, 87*, 1760 – 1766.

Malila, N., Virtamo, J.,Virtanen, M., Albanes, D., Tangrea, J.A. and Huttunen, J.K. (1999). The effect of α-tocopherol and β–carotene supplementation on colorectal adenomas in middle-aged male smokers. *Cancer Epidemiology, Biomarkers and Prevention*, *8*, 489-493.

Martinez, M. E., Henning, S.M. and Alberts, D.S. (2004). Folate and colorectal neoplasia: Relation between plasma and dietary markers of folate and adenoma recurrence. *American Journal of Clinical Nutrition, 79*(4), 691 – 697.

Martinez, M. E. *et al.* (2006). Folate fortification, plasma folate, homocysteine and colorectal adenoma recurrence. *International Journal of Cancer, 119*(6), 1440 – 1446.

Mathew, A., Peters, U., Chatterjee, N., Kulldorff, M. and Sinha, R. (2004). Fat, fiber, fruits, vegetables and risk of colorectal adenomas. *International Journal of Cancer, 108*(2), 287 – 292.

Methy, N., Binquet, C., Boutron-Ruault, M.C., Pailot, B., Faivre, J. and Bonithon-Kopp, C. (2008). Dietary fatty acids and recurrence of colorectal adenomas in a European intervention trial. *Nutrition and Cancer, 60*(5), 560 – 567.

Miller, E. A., Keku, T.O., Satia, J.A., Martin, C.F., Galanko, J.A. and Sandler, R.S. (2007). Calcium, dietary, and lifestyle factors in the prevention of colorectal adenomas. *Cancer, 109*(3), 510 – 517.

Michels, K. B., Giovannucci, E., Chan, A.T., Singhania, R., Fuchs, C.S. and Willet, W.C. (2006). Fruit and vegetable consumption and colorectal adenomas in the nurses' health study. *Cancer Research, 66*(7), 3942 – 3953.

Nagata, C., Shimizu, H., Kametani, M., Takeyama, N., Ohnuma, T. and Matsushita, S. (2001). Diet and colorectal adenoma in Japanese males and females. *Dis colon rectum 44*(1), 105 -111.

National Cancer Institute. (2006). Eat 5 to 9 servings of fruits and vegetables for better health. Retrieved from http://www.5aday.gov.

National Cancer Registry (NCR). (2004). Cancer incidence in Malaysia 2003. In G. C. C. Lim and Y. H. Halimah (Eds.), *National Cancer Registry*, Kuala Lumpur.

National Cancer Registry (NCR). (2008). Cancer incidence in peninsular Malaysia 2003-2005. In G. Lim, S. Rampal and H. Yahya (Eds.), *Third report of the National Cancer Registry*.

Oh, K. W., Willet, C., Fuschs, C.S. and Giovannucci, E. (2005). Dietary marine n-3 fatty acids in relation to risk of distal colorectal adenomas in women. *Cancer Epidemiology, Biomarkers and Prevention, 14*(4), 835 – 841.

Olschwang, S. (2002). Familial adenomatous polyposis, orphanet encyclopedia. Retrieved from http://orphanet.infobiogen.fr/data/patho/gb/uk-fap.html.

Olson, J. A. (1994). Needs and sources of carotenoids and vitamin. *Annual Review of Nutrition, 52*, 67 – 73.

Pergament, E. (2003). Hereditay nonpolyposis colon cancer. Retrieved from http://wwwintouchlive.com/home/frames.htm?http://www.intouchlive.com/cancergenetics/hnpcc.htm&3.

Peters, U. *et al.* (2004). Calcium intake and colorectal adenoma in a us colorectal cancer early detection program. *American Journal of Clinical Nutrition*, *80*, 1358-1365.

Platz, E. A., Giovannucci, E., Rimm, E.B., Rockett, H.R., Stampfer, M.J., Colditz, G.A. and Willet, W.C. (1997). Dietary fiber and distal colorectal adenoma in men. *Cancer Epidemiology, Biomarkers and Prevention, 6*(9), 661-70.

Platz, E. A., Hankinson, S.E., Hollis, B.W., Colditz, G.A., Hunter, D.J., Speizer, F.E. and Giovannucci, E. (2000). Plasma 1,25-dihydroxy- and 25-hydroxyvitamin d and adenomatous polyps of the distal colorectum. *Cancer Epidemiology, Biomarkers and Prevention, 9*, 1059 – 1065.

Robertson, D. J., Sandler, R.S., Haile, R., Tosteson, T.D., Greenberg, E.R., Grau, M. and Baron, J.A. (2005). Fat, fiber, meat and the risk of colorectal adenomas. *The American Journal of Gastroenterology, 100*(12), 2789-95.

Rock, C. L. (1997). Carotenoids: Biology and treatment. *Pharmacol Therapy*, *75*, 185-197.

Ross, A. C. and Temus, M.E. (1993). Vitamin a as a hormone: Recent advances in understanding the actions of retinol, retinoic acid and carotene. *Journal of the American Dietetic Association, 93*, 1285 – 1290.

Schatzkin, A., Lanza, E., Corle, D., Lance, P., Iber, F., Caan, B., Shike, M., Weissfeld, J., Burt, R., Cooper, M.R., Kikendall, J.W., Cahill, J., Freedman, I., Marshall, J., Schoen, R.E. and Slattery, M. (2000). Lack of effect of a low-fat, high-fiber diet on the recurrence of colorectal adenomas. *The New England Journal of Medicine, 342*, 1149-1155.

Senesse, P., Touvier, M., Kesse, E., Faivre, J. and Boutron-Ruault, M-C. (2005). Tobacco use and associations of β-carotene and vitamin intakes with colorectal adenoma risk. *Journal of Nutrition, 135*, 2468 – 2472.

Shikany, J. M., Witte, J.S., Henning, S.M., Swendseid, M.E., Bird, L.C., Frankl, H.D., Lee, E.R. and Haile, R.W. (1997). Plasma carotenoids and the prevalence of adenomatous polyps of distal colon and rectum. *American Journal of Epidemiology, 145*(6), 552-557.

Sinha, R., Chow, W.H., Kulldorff, M., Denobile, J., Butler, J., Garcia-Closas, M., Weil, R., Hoover, R.N. and Rothman, N. (1999). Well-done, grilled red meat increases the risk of colorectal adenomas. *Cancer Research*, *59*, 4320 – 4324.

Sinha, R., Peters, U., Cross, A.J., Kulldorff, M., Weissfeld, J.L., Pinsky, P.E., Rothman, N. and Hayes, R.B. Meat, meat cooking methods and preservation, and risk for colorectal adenoma. *Cancer Research, 65*(17), 8034 – 8041.

Smith-Warner, S. A. *et al.* (2002). Fruits, vegetables and adenomatous polyps. *American Journal of Epidemiology, 155*(12), 1104 – 1113.

Sporn, M.B. (1983). Retinoids and suppression of carcinogenesis. *Hospital Practice*, *18*(10), 83-98.

Tiemersma, E. W. *et al.* (2004). Risk of colorectal adenomas in relation to meat consumption, meat preparation, and genetic susceptibility in a dutch population. *Cancer Causes Control, 15*(3), 225 – 236.

Traber, M. G. and Packer, I. (1995). Vitamin E: Beyond antioxidant function. *American Journal of Clinical Nutrition, 62*(suppl), 1501 – 1519.

Tseng, M., Murray, S. C., Kupper, I. L. and Sandier, R.S. (1994). Micronutrients and the risk of colorectal adenomas. *American Journal of Epidemiology, 144*, 1005-1014.

Van Den Donk, M. *et al.* (2005). Dietary intake of folate and riboflavin, mthfr c677t genotype, and colorectal adenomas risk: A Dutch case-control study. *Diseases of Colon and Rectum, 42*(2), 212 – 217.

Van Poppel, G. and Van Den Berg, H. (1997). Vitamins and cancer. *Cancer Letters, 114*, 195-202.

Vinokoor, I. C. *et al.* (2008). Consumption of trans-fatty acid and its association with colorectal adenomas. *American Journal of Epidemiology, 168*(3), 289 – 297.

Ward, M. H. *et al.* (2007). Processed meat intake, cyp2a6 activity and risk of colorectal adenoma. *Carcinogenesis, 28*(6), 1210–1216.

Whelan, R. L., Horvath, K.D., Gleason, N.R., Forde, K.A., Treat, M.A., Teitelbaum, S. L., Bertram, A. and Neugut, A.I. (1999). Vitamin and calcium supplements use is associated with decreased adenoma recurrence in patients with a previous history of neoplasia. *Diseases of the Colon & Rectum, 42*(2), 212 – 217.

Witte, J. S., LongneckeR, M.P., Bird, C.L., Lee, E.R., Frankl, H.D. and Haile, R. W. (1996). Relation of vegetable, fruit, and grain consumption to colorectal adenomatous polyps. *American Journal of Epimediology, 144*(11), 1015-25.

World Cancer Research Fund. (2007). Food, nutrition and physical activity and the prevention of cancer: A global perspective. American Institute for Cancer Research, Washington.

World Health Organization. (2003). *Global Strategy on Diet, Physical Activity and Health.* Geneva: WHO.

Wu, K., Giovannucci, E., Byrne, C., Platz, E.A., Fuchs, C., Willet, W.C. and Sinha, R. (2006). Meat mutagens and risk of distal colon adenoma in a cohort of U.S. men. *Cancer Epidemiology, Biomarkers and Prevention, 15*(6), 1120 – 1125.

Yamaji, Y., Mitusushima, T., Ikuma, H., Watabe, Okamoto, M., Kawabe, T., Wada, R., Doi, H. and Omata, M. (2004). Incidence and recurrence rates of colorectal adenomas estimated by annually repeated colonoscopies on asymptomatic Japanese. *Gut, 53*, 568-572.

Pertanika J. Sci. & Technol. Vol. 18 (2) 2010

337

TABLE 1
Summary of studies on dietary factors and risk of colorectal adenomas

Factor	Authors	Year	Study design	Sample size	Results
Dietary fat	Mac Lennan *et al*.	1995	RCT	411 subjects	Low fat diet insignificantly reduced the risk of large adenomas after 48 mo (OR = 0.3, 95% CI = 0.1 – 1.0).
	Mathew *et al*.	2004	Case-control	239 subjects with history of CRA & 238 healthy controls	Total fat (OR = 1.07, 95% CI = 0.94 – 1.22) and red meat fat (OR = 1.20, 95% CI = 0.71 – 2.04) increased the risk. White meat fat reduced the risk (OR = 0.33, 95% CI = 0.19 – 0.95).
	Diergaarde *et al*.	2005	Case-control	278 cases and 414 polyp-free controls	High intake of fat seemed to increase the risk of APC(-) polyps only (OR = 1.9, 95% CI = 1.0-3.7).
	Oh *et al*.	2005	Cohort	34,451 US women followed up for 18 years	Dietary marine n-3 fatty acids reduced the risk of small adenomas (RR = 1.36, 95% CI = 1.02 – 1.81).
	Methy *et al*.	2008	RCT	523 patients with confirmed adenomas	There were no significant associations between overall adenoma recurrence and either total fat, subtypes of fat, or specific fatty acids. Polyunsaturated fatty acids and linoleic acid were both moderately but significantly associated with distal and multiple recurrence.

	Vinikoor *et al*.	2008	Cross-sectional	622 subjects	Increased prevalence of CRA in those with the highest compared to the lowest quartile of trans-fatty acids (OR = 1.86, 95% 1.04 – 3.33).
Dietary fibre	Giovannucci *et al*.	1992	Cohort (part of Health Professionals Follow-up Study)	7284 male health professionals	Low intake of dietary fibre increased the risk (RR = 8.4, 95% CI = 0.2 – 0.6).
	Platz *et al*	1997	Case-control (part of Health Professional Follow-up Study)	159 men with adenomatous polyps, 327 men with hyperplastic polyps and 16,448 healthy men as controls	Reduction in the risk for distal adenomas by 19% with increased intake of soluble fibre from fruit.
	Fuchs *et al*.	1999	Cohort (part of Nurses' Health Study)	88,000 women (16 years follow-up)	Lack of protective effect of dietary fibre (OR = 0.91, 95% CI = 0.71 – 1.16).
	Schatzkin *et al*.	2000	RCT (Polyp Prevention Trial)	2079 subjects with history of CRA	No significant association between dietary fibre and recurrence of adenomas (unadjusted OR = 1.00, 95% CI = 0.90 -1.12). Similar findings after 4 years of follow up (Lanza *et al*., 2007).

Pertanika J. Sci. & Technol. Vol. 18 (2) 2010

339

	Jacobs *et al.*	2002	RCT (Wheat Bran Trial)	1208 subjects	Compared with individuals consuming less than 1.8 g/day of supplemental fibre, the adjusted OR (95% CI) for adenoma recurrence for those consuming greater than 11.0 g/day was 0.94 (0.66-1.33). The OR (95% CI) for participants whose total fibre intake was greater than 30.3 g/day was 0.98 (0.68-1.42) compared with those whose intake was less than 17.9 g/day.
	Peters *et al.*	2004	Case -control (part of PLCO trial)	3696 cases and 34 817 controls	High intake of dietary fibre reduced the risk by 27% (95% CI = 14 – 38).
	Lanza *et al.*	2007	RCT (PPT-Continued Follow-up Study)	405 intervention participants and 396 control participants	RR of recurrent adenoma in the intervention group compared with the control group was 0.98 (95% CI = 0.88-1.09). There were no significant intervention-control group differences in recurrence of an advanced adenoma (RR = 1.06, 95% CI = 0.81-1.39) or multiple adenomas (RR = 0.92, 95% CI = 0.77-1.10).
Red meat	Sinha *et al.*	1999	Case-control	149 cases with history of CRA and 228 healthy controls	Total red meat consumption (OR = 1.11, 95% CI = 0.96 – 1.26), grilled red meat (OR = 1.26, 95% CI = 1.06 – 1.50) and pan-fried red meat (OR – 1.15, 95% CI = 0.97 – 1.36) increased the risk.

	Breuer-Katschinski *et al*.	2001	Case-control (Colorectal Adenoma Study Group)	184 cases with history of CRA and matched controls	Red meat from increase the risk in cases compared to hospital controls (or = 3.6, 95% CI = 1.7 – 7.5) and population controls (OR = 4.4, 95% CI = 1.6 – 12.1).
	Chiu and Gapstur	2004	Case-control	146 colorectal adenomas and 226 controls	Risks were higher for those with the smallest reduction in red meat intake (OR = 2.8, 95% CI = 1.1-7.3).
	Tiemersma *et al*.	2004	Case-control	431 adenoma cases and 433 polyp-free controls	HCAs were present in habitually prepared meat, although meat consumption (7 versus < 5x/week) did not increase the risk of colorectal adenomas (OR = 1.2, 95% CI = 0.8-1.9). Presumed unfavourable preparation habits of meat did not increase adenoma risk (OR 0.8 and 0.9, respectively).
	Diergaarde *et al*.	2005	Case-control	278 cases and 414 polyp-free controls	Red meat consumption was significantly and differently related to polyps with truncating APC mutation (APC(+) polyps) (highest vs. lowest tertile, OR = 0.5, 95% CI= 0.3-1.0). High intake of red meat seemed to increase the risk of APC(-) polyps only (APC(-) vs. controls: red meat, OR = 1.8, 95% CI = 1.0-3.1).

Pertanika J. Sci. & Technol. Vol. 18 (2) 2010

341

	Gunter *et al.*	2005	Case-control	261 cases and 304 controls	Consistent with this finding, an incremental increase of 10 g of barbecued red meat per day was associated with a 29% increased risk of large adenoma (OR = 1.29, 95% CI = 1.02-1.63). Individuals in the top quintile of barbecued red meat intake were at increased risk of large adenoma (OR = 1.90, 95% CI = 1.04-3.45) compared with those who had never consumed barbecued red meat. The consumption of oven-broiled red meat was inversely related to adenoma risk compared with non-consumers (OR = 0.49, 95% CI = 0.28-0.85).
	Sinha *et al.*	2005	Case-control	3,696 left-sided adenoma cases and 34,817 endoscopy-negative controls	Intake of red meat, with known doneness/cooking methods, was associated with an increased risk of adenoma in the descending and sigmoid colon (OR =1.26, 95% CI = 1.05-1.50 comparing extreme quintiles of intake) but not rectal adenoma. Well-done red meat was associated with increased risk of colorectal adenoma (OR = 1.21, 95% CI = 1.06-1.37).

	Wu *et al.*	2006	Cohort (Health Professionals Follow-up Study cohort)	581cases with distal adenoma	Higher consumption of mutagens from meats cooked at higher temperature and longer duration may be associated with higher risk of distal colon adenoma independent of overall meat intake (OR highest versus lowest quintile of meat-derived mutagenity = 1.29, 95% CI = 0.97-1.72).
	Ward *et al.*	2007	Case-control	146 cases of colorectal adenoma and 228 polyp-free controls	Two-fold increased risk in the highest compared to the lowest quartile of processed meat intake (95% CI = 1.0-4.0).
Fruits and vegetables	Witte *et al.*	1996	Case-control	488 matched pairs.	High carotenoid and cruciferous vegetables, high vitamin C fruits, garlic and tofu reduced the risk.
	Smith-Warner *et al.*	2002	Case-control	564 cases with history of CRA, 682 polyp-free controls and 535 community controls	Juice consumption reduced the risk in women (OR = 0.50, 95% CI = 0.27 – 0.92).
	Almendingen *et al.*	2004	Case-control	28 cases with history of CRA and 34 matched controls followed up for 3 years	Weak association between adenomas growth and fruit/berries (OR = 0.3, 95% CI = 0.1 – 0.9) and between adenoma recurrence and vegetable intake (OR = 0.4, 95% CI = 0.1 – 0.9).
	Chiu and Gapstur	2004	Case-control	146 colorectal adenomas and 226 controls	Individuals in the highest quartile of increased consumption vegetables (OR = 0.5; CI = 0.3-1.1) had a lower risk compared with those with minimal increase in consumption.

	Michels *et al*.	2006	Cross-sectional (Nurses' Health Study)	1720 prevalent cases in women	Frequent consumption of fruit was inversely related to the risk of being diagnosed with polyps (OR >5 servings vs <1 servings = 0.60, 95% CI = 0.44 – 0.81), whereas little association was found for vegetable consumption (OR = 0.82, 95% CI = 0.65 – 1.05).
	Austin *et al*.	2007	Case-control	203 cases with history of CRA and 522 controls without CRA	High vegetable-moderate meat cluster (OR = 2.17, 95% CI = 1.20 =- 3.90) and high meat cluster (OR 1.70, 95% CI = 1.04 – 2.80) increased the risk.
Vitamin A	Giovannucci *et al*.	1993	Case-control (using subjects from Nurses' Health Study and Health Professionals Follow-up Study)	564 cases of women with CRA and 15,984 control women. 331 cases of men with CRA and 9490 control men	Higher intake of vitamin A did not protect from the risk (OR = 0.91, 95% CI = 0.69 – 1.19).
	Enger *et al*.	1996	Case-control	488 matched pairs	Dietary vitamin A decreased the risk only before adjusting for confounders (OR = 0.60, 95% CI = 0.4 – 0.9).
	Lubin *et al*.	1997	Case-control	196 cases with CRA and matched healthy controls.	No significant relationship was found between dietary retinol and the risk (OT = 0.9, 95% CI = 0.5 – 1.6).
	Nagata *et al*.	2001	Case-control (part of the cohort of Takayama Study, Japan)	279 cases with CRA and 28361 polyp-free controls	Higher vitamin A intake was significantly associated with increased risk (RR = 1.51, 95% CI = 1.04 – 2.20).

Carotenoids	Enger *et al.*	1996	Case-control	488 matched pairs	Only b-carotene was associated with the risk (p=0.04).
	Lubin *et al.*	1997	Case-control	196 cases with CRA and matched healthy controls	Highest tertile of carotene intake reduced the risk by 40% (OR = 0.6, 95% CI = 0.3 – 1.0) compared to the lowest.
	Shikany *et al.*	1997	Case-control	472 cases with CRA and 502 matched controls	No association between individual plasma carotenoids and the risk.
	Malila *et al.*	1999	RCT (ATBC Study)	15,538 ATBC study participants with 146 cases with CRA	Supplementation with b-carotene had no effect on the risk (RR = 0.98, 95% CI = 0.71 – 1.35).
	Erhardlt *et al.*	2003	Observational study	73 white subjects with history of adenomas, 63 without any polyps, and 29 with hyperplastic polyps	Plasma lycopene significantly lowered the risk by 35%.
	Senesse *et al.*	2005	Case-control	362 cases with CRA and 427 polyp-free controls stratified according to smoking status	β-carotene intake was inversely associated with the risk in non-smokers OR = 0.4, 95% CI = 0.2 – 0.9) but increased the risk in smokers (OR = 1.9, 95% CI = 0.9 – 4.1).

Vitamin C	Benito *et al.*	1993	Case-control	79 cases with history of CRA and 242 healthy controls	Higher intake of vitamin C lowered the risk by 63% (p<0.01).
	Enger *et al.*	1996	Case-control	488 matched pairs	Insignificant weak association between vitamin C intake and the risk (OR = 0.8, 95% CI = 0.5 – 1.5).
	Tseng *et al.*	1996	Case-control	236 cases with CRA or cancer and 409 controls	Significant reduction in the risk only in women.
	Connelly *et al.*	2003	Cross-sectional (within Diet and Health Study III)	503 participants who underwent rectal biopsy	High vitamin C intake was associated with reduced colorectal apoptosis only among individuals with adenomas.
Vitamin E	Tseng *et al.*	1996	Case-control	236 cases with CRA or cancer and 409 controls	Protective effect of vitamin E intake only in men (OR = 0.35, 95% CI = 0.14 – 0.92).
	Ingles *et al.*	1998	Case-control	332 subjects with history of CRA and 363 healthy controls	No significant association with plasma tocopherols and the risk, but higher ratio of α-tocopherol:γ-tocopherol lowered the risk for large adenomas (OR = 0.36, 95% CI = 0.14 – 0.95).
	Whelan *et al.*	1999	Case-control	448 cases with history of CRA and 714 healthy controls	Vitamin E supplements lowered the risk (OR – 0.62, 95% CI = 0.39 – 0.98).

Vitamin D and calcium	Hofstad *et al*.	1998	RCT	42 in the intervention group and 51 in the placebo group. All subjects with history of CRA	Significant reduction in risk with calcium supplementation compared to placebo (Mean difference = 2.3 mm, 95% CI = 0.26-4.36).
	Baron *et al*.	1999	RCT (Polyp Prevention Study Group)	409 in the calcium group and 423 in the placebo group. All subjects with history of CRA	Moderate but significant reduction in risk with calcium supplementation (OR = 0.76, 95% CI = 0.60 - 0.96).
	Bonitton-Kopp *et al*.	2000	RCT (ECPO Study Group)	176 in calcium group, 198 in fibre group and 178 in placebo group. All subjects with history of CRA	Significant reduction in risk with calcium supplementation (OR = 0.66, 95% CI 0.38-1.17).
	Platz *et al*.	2000	Case-control (within Nurses' Health Study)	326 matched women case and control pairs	Plasma $1,25(OH)_2D$ concentration below $26.0\mu g/ml$ increased the risk of distal adenoma.
	Grau *et al*.	2003	RCT	398 in intervention group and 405 in placebo group	High level of vitamin D together with calcium supplementation lowered the risk (RR = 0.71, 95% CI = 0.57 to 0.89, P for interaction=0.012).
	Peters *et al*.	2004	Case-control (within PLCO Trial)	3693 cases with history of CRA and 34 817 healthy controls	The risk decreased by 26% for every 10ng/ml increase in serum 25-(OH)D.

| | Hartman *et al.* | 2005 | Cross-sectional (within PPT) | 754 adenoma cases | There were no overall significant associations between adenoma recurrence and dietary calcium, total calcium and dietary vitamin D intake.

Total vitamin D intake was weakly and inversely associated with adenoma recurrence (OR = 0.84, 95% CI = 0.62-1.13).

Supplemental calcium and vitamin D use during follow-up was also inversely associated with adenoma recurrence (OR for any compared with no use = 0.82, 95% CI = 0.68-0.99; and OR = 0.82, 95% CI = 0.68-0.99 for calcium and vitamin D, respectively). |
| | Kesse *et al.* | 2005 | Case-control | 516 adenoma cases and of 4,804 polyp-free subjects | There was a decreasing trend in the risk of adenoma (p=0.04) with increasing calcium intake (RR = 0.80, 95% CI ==0.62-1.03 in the fourth quartile compared to the first).

No vitamin D effect was identified. |
| | Jacobs *et al.* | 2007 | Cross-sectional | 568 subjects | Insignificant reduction in risk for recurrence of CRA in highest tertile compared to the lowest tertile of serum 25(OH) D levels (OR = 0.78, 95% CI = 0.49 – 1.24).

Insignificant reduction in risk was seen in women (OR 25(OH)D above median vs. below median = 0.59 (95% CI = 0.30 – 1.16). |

	Miller *et al.*	2007	Case-control	222 cases and 479 adenoma-free controls	Little association was observed comparing total calcium intake of ≥ 900 mg/day to < 500 mg/day (adjusted OR = 0.85, 95% CI = 0.53-1.37). Total calcium intake of ≥ 900 mg/day was associated with a lower prevalence of adenomas among patients with lower fat intake (OR = 0.47, 95% CI = 0.25-0.91).
Folate	Benito *et al.*	1993	Case-control	79 cases with history of CRA and 242 healthy controls	Reduction of risk by 25% in those with folate intakes > 222μg/day as compared to those with < 141μg/day.
	Martinez *et al.*	2004	Cross-sectional	1014 subjects	Lower odds of recurrence were shown for higher plasma folate (OR = 0.66, 95% CI = 0.46 -0.97) and higher total intakes (dietary plus supplemental) of folate (OR = 0.61, 95% CI = 0.42 - 0.89).
	Van den Donk *et al.*	2005	Case-control	768 cases with history of CRA and 709 healthy controls	Folate is a risk factor when vitamin B12 intake is low (OR = 1.32, 95% CI = 1.01 − 1.73).
	Martinez *et al.*	2006	RCT (wheat bran fiber (WBF) and the ursodeoxycholic acid (UDCA) trials)	WBF trial – 1014 subjects. UDCA trial – 1111 subjects	Among non-multivitamin users, the OR for those in the highest versus the lowest folate quartile was 0.65 (95% CI = 0.40-1.06) for the WBF study and 0.56 (0.31-1.02) for the UDCA.

Symmetrical Supercapacitor Using Coconut Shell-Based Activated Carbon

Ahmida Ajina[*] **and Dino Isa**
Department of Electrical and Electronic Engineering,
Faculty of Engineering,
University of Nottingham Malaysia Campus,
Jalan Broga, 43500 Semenyih,
Selangor, Malaysia
[*]*E-mail: Keyx7aaj@nottingham.edu.my*

ABSTRACT

Two different supercapacitor configurations were fabricated using coconut shell-based activated carbon. Results for cyclic voltammetry (CV), electrochemical impedance *spectroscopy (*EIS), and charge-discharge measurements are presented and discussed for both configurations. The results show that coconut shell-based activated carbon is viable economical alternative electrode material to expensive activated carbon (AC) and carbon nano tubes (CNT). Meanwhile, the calculations from the charge-discharge characteristics show that the disk-shape supercapacitor, with 10% polyvinylidene fluoride binder (PVdF), has the highest specific capacitance (70F/g). Thus, the testing shows that the flat-laminated super-capacitor with 10% binder (PVdF) has the lowest (10.1ohms). Sources of high equivalent series resistance (ESR) are proposed and methods of reducing it are also discussed in this paper.

Keywords: Symmetrical supercapacitor, coconut shell-based activated carbon

INTRODUCTION

Supercapacitors (EDLCs), as a kind of energy storage devices, have high energy density, great power density and long cycle life (Conway, 1999). Electrochemical double-layer capacitors (EDLCs) are power sources that store energy within the electrochemical double layer which is formed at the solid (active material) and the solution (electrolyte) interface (Nishino, 1996).

Many different types of electrode materials have been intensely studied in the past years for fabricating EDLCs electrodes. Some of the mostly used materials include activated carbon (Kierzek *et al.*, 2004; Frackowaik and Beguin, 2001; Qu, 2002), carbon nano tubes (CNT) (Arabale *et al.,* 2003; Qun *et al.*, 2004; Frackowaik and Beguin, 2002; Emmenegger *et al.*, 2003), carbon aerogels (Probstle, Schmitt and Fricke, 2002), and conducting polymer-based nano composites (Xiao and Zhou, 2003; Chen, Wen and Teng, 2003).

Activated carbons are recognized as an essential component for the electrode of an electric double layer capacitor (EDLC) (Bonnefoi *et al.*, 1999; Qu and Shi, 1998; Oh, Korai and Mochida, 1999; Hal-Bon Gu, Jong-Uk Kim and Hee-Woong Song, 2000). Activated carbon (AC) is the electrode material used most frequently for EDLCs due to the low cost, high surface area, availability, and established production technologies (Nishino, 1996). The activated carbon grains are mixed with binder, cured (stabilized) and carbonized into an activated carbon artifact so as to be connected to the collector. The form should have a large surface area, the correct pore size distribution, as well sufficient electric conductivity and mechanical strength. Such properties appear to be governed by

the activated carbon even when the binder and forming procedure are carefully selected (Wenming, 2002).

At present, because of its stable electrochemical behaviour, good cycling performance, and low cost, activated carbon has become a mainstream electrode material for commercial supercapacitors (Zhou Shao-yun, 2007). The reasons for the use of coconut shell-based activated carbon in this work were because it has a significantly lower price, and it is excellent in term of electrochemical performances.

Carbon materials are available with specific surface areas of up to 500–3000 m^2/g (Shi, 1996). Early electrochemical capacitors were rated at a few volts and had capacitance values measured from fractions of farads up to several farads. The trend today is for cells ranging in size, i.e. from small millifarad-size devices with exceptional pulse power performance up to devices rated at several kilofarads. Some specialized electrochemical capacitors (EC) cells in production at present for traction applications have ratings of more than 100 kilo Farads (kF) (Varakin, 1997).

The purpose of this work was to fabricate a symmetrical (1V, 1F) supercapacitor using coconut shell-based activated carbon with aqueous electrolyte.

EXPERIMENTAL DESIGN

Two supercapacitor configurations were fabricated using coconut shell-based activated carbon (AC), with different packaging and different concentrations of binder.

A: Supercapacitor Cap#1 Disk-shape
B: Supercapacitor Cap#2 Flat-Laminated shape

Two prototypes of supercapacitors of the disk-shape and three prototype of the flat-laminated-shape were fabricated to test the effects of different binder concentrations on the specific capacitance and equivalent series resistance (ESR) in each configuration.

Materials

The materials used in this study are listed in Table 1.

TABLE 1
Materials used for fabrication

No.	Material	Specifications	Company	Role
1	Coconut shell-based activated carbon	LAJU PAC	Laju group	Active material
2	Poly vinylidene fluoride PVdf	182702	*Sigma Aldrich*	*Binder*
3	Isoprobanol	99.5% S42647	*Sigma Aldrich*	*Solvent*

All the materials were used without any further purification

Preparation of Electrode Materials

The coconut activated carbon used in this research is (<u>LAJU PAC</u>) of Laju group, while poly vinylidene fluoride (PVdF) was used as a binder and isoprobanol as solvent for all the supercapacitors with different concentrations.

Supercapacitor Cap#1

This disk-shaped supercapacitor was fabricated using coconut shell-based activated carbon, with 1M potassium chloride (KCl) electrolyte. *Fig. 1* shows the two prototypes of disk-shape supercapacitors labelled as Cap#1.1 and Cap#1.2.
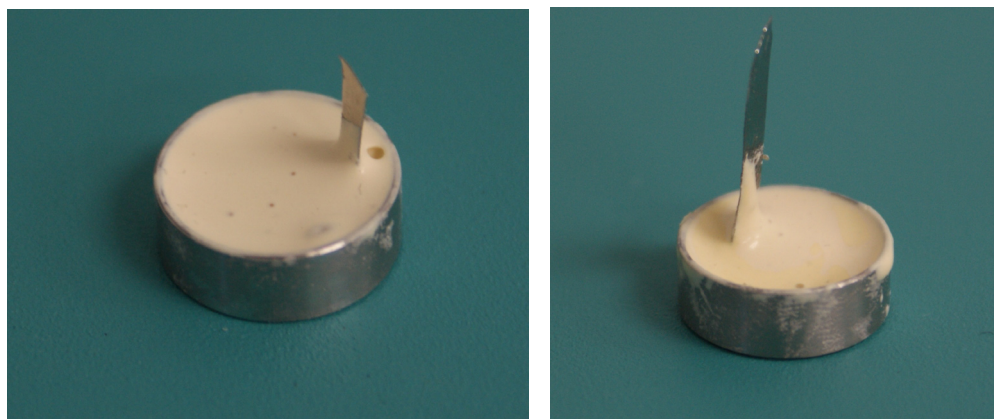
Fig. 1: Picture of supercapacitors (Cap#1.1 and Cap#1.2)

For Cap#1.1, the active material was prepared using coconut shell-based activated carbon (90%) with poly vinylidene fluoride (PVdF) polymer powder (10%). In the case of Cap#1.2, 15% of binder was used. Isopropanol was added to the mixed powders as mixing and solvent solutions. The slurry was then mixed using a mechanical stirrer for 1 hr, and this was followed by an ultrasonic mixing for 30 minutes.

For both samples, the slurry was dried in a vacuum oven at 100ºC to remove all the isopropanol. The dried powder was then used to fabricate the supercapacitor electrode active material. The active material (AC) was pressed using hydraulic press with a die set (13 mm) at 3 tones to form coin-shape electrodes. After that, the two coin-shaped electrodes were sandwiched between the stainless steel mesh current collectors and were separated by porous membrane to allow the transfer of ions through the electrolytes and prevent these electrodes from short circuiting. Later, the electrodes were placed in a can-shaped casing and the whole set was dried again in the vacuum oven for 1hr. One mole KCL solution was impregnated into the pores of the electrodes as electrolyte, and then the set was pressed. An epoxy was used to seal the supercapacitor to prevent the electrolyte from evaporating. The casing and the current collectors mesh were made from stainless steel. *Fig. 2* shows the dimensions of both prototypes. The dimensions of the electrode are as shown.

Current collector mesh thickness = 0.1mm
Electrode diameter = 13mm

0.1mm

13mm
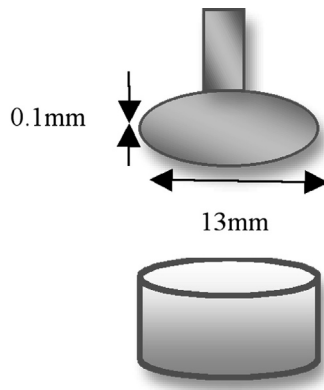
Fig. 2: Dimension of Cap#1

Supercapacitor Cap#2

Three prototypes of flat-shaped supercapacitor were fabricated using coconut shell-based activated carbon. The electrolyte used in this supercapacitor was aqueous (KCl, 1M). *Fig. 3* depicts the three prototypes of Cap#2.
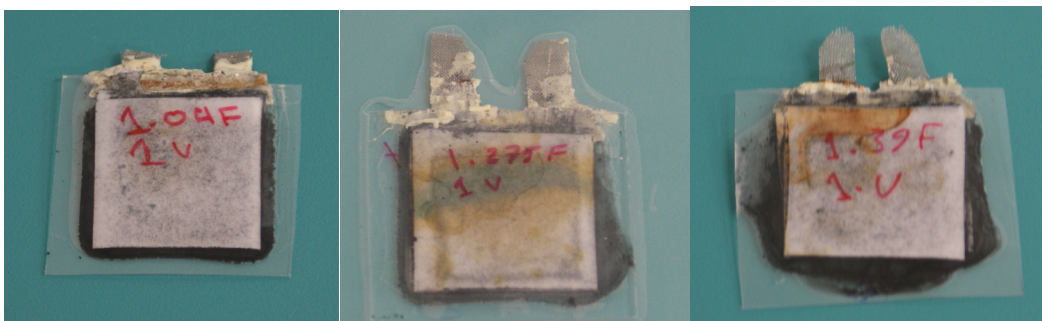
Fig. 3: Supercapacitors (Cap#2.1, Cap#2.2, and Cap#2.3)

As for the previous supercapacitors, the active material used was the coconut shell-based activated carbon mixed with poly vinylidene fluoride (PVdF) polymer powder in the percentages of 10, 15, and 20%. Isopropanol was added to all the samples as solvent and mixing agent. Then, the slurry was mechanically mixed using the mechanical stirrer for 1 hr, followed by an ultrasonic mixing for 30 minutes.

After mixing, the slurry was heated to remove some of the isopropanol solutions and to make thicker slurry. Then, the slurry was spread on the stainless steel mesh current collector to make sure

a uniform layer of the AC was achieved. The set of electrodes was then dried in a vacuum oven for 2 hr. Every set of two electrodes is sandwiched together and separated by a porous membrane which allows the transfer of ions and prevents the electrodes from short circuiting. The electrodes were laminated and the whole set was dried again in a vacuum oven for 1 hr and 1M of KCL was used as electrolyte for this capacitor. Later, the supercapacitors were laminated and sealed to prevent the electrolytes from evaporating. The dimensions of the electrodes are shown in *Fig. 4* below.

Current collector mesh thickness = 0.1 mm
Electrode dimensions = 2x2 cm
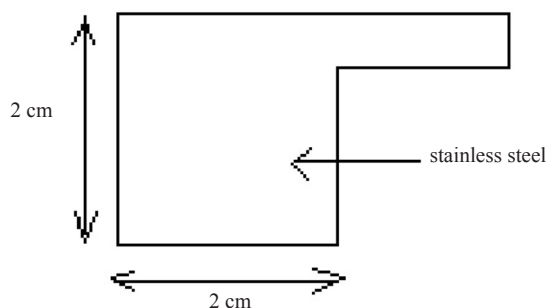
Fig. 4: Dimensions of the supercapacitor (Cap#2)

RESULTS AND DISCUSSION

Cyclic Voltammetry
Cyclic voltammetry (CV) of the unit cells was measured at the scan rate of 10mV/s. *Fig. 5* shows the CV of the (Cap#1.1 and Cap#1.2) supercapacitors.

As it can be seen from the CV in *Fig. 5*, both the cells show capacitor behaviour. According to the principal, specific capacitance keeps a direct ratio with specific current at the same scan rate [22], while Cap#1.1 shows a bigger specific capacitance which that can be attributed to the less percentage of binder (10%) used in this supercapacitor than in Cap#1.2. The more binder is used, the more blockages of the porous of the activated carbon, indicating less usable porous surface area accessible by the electrolyte that leads to less specific capacitance.

Cap#1.2, on the other hand, shows a more ideal rectangular capacitor behaviour which is more close to ideal capacitor CV (rectangular). Table 2 illustrates the specific capacitance and the ESR for both the prototypes. The capacitance measurements were confirmed by CV, charge-discharge curve and EIS measurements, and all the results are closely matched. The equivalent series resistance (ESR) was measured from the drop in the charge-discharge curve.
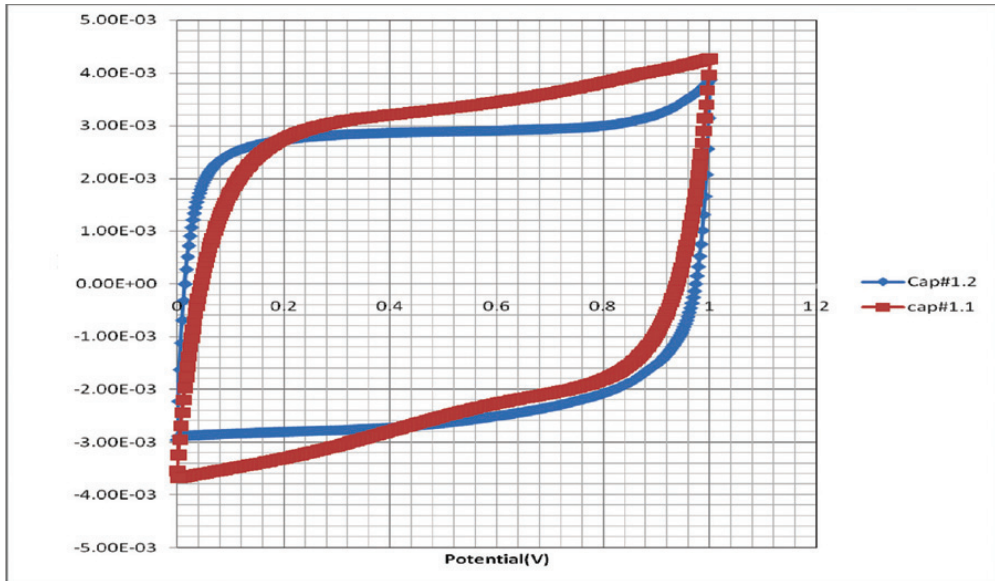
Fig. 5: CV measurement for the supercapacitors (Caps#1.1 and #1.2)

TABLE 2
Specific capacitance and ESR results for Supercapacitor, Cap#1

	Cap#1.1	Cap#1.2
Specific capacitance (F/g)	70F/g	56F/g
ESR (Ohms)	16.5	14.3

In the case of supercapacitor Cap#2 and its variations, namely Cap#2.1 (10%PVdF), Cap#2.2 (15%PVdF) and Cap#2.3 (20%PVdF), *Fig. 6* shows the CV characteristic (Autolab AUT83475) which was used to perform the measurements in this study. The CV was measured at (5mV/s) and it was confirmed that all the cells showed the characteristics of a capacitor. Cap#2.1 shows the most ideal capacitor behaviour, but the Cap#2.3 reveals the highest specific capacitance.
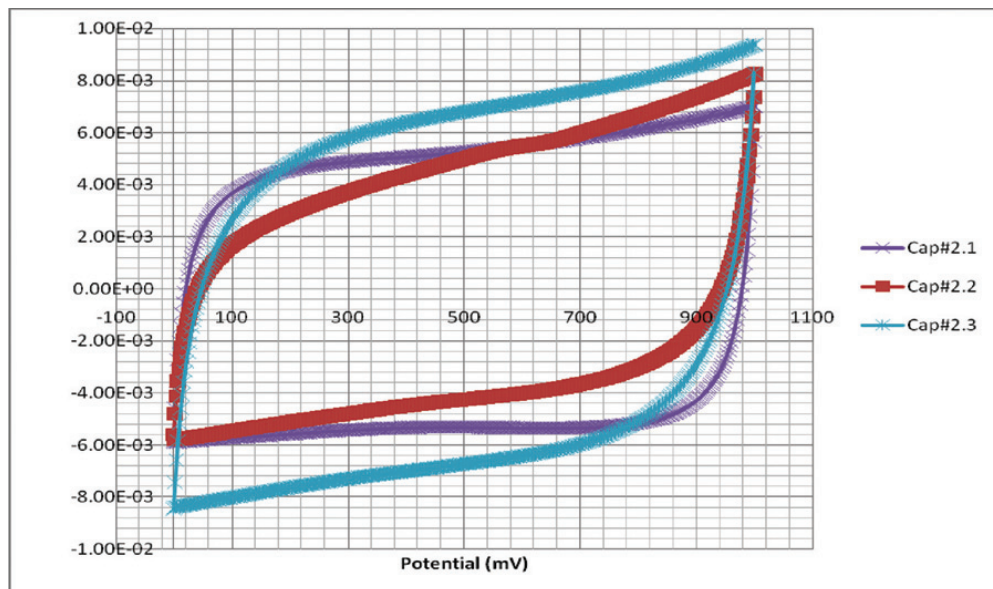
Fig. 6: CV measurements for the flat-laminated supercapacitors (Cap#2.1, Cap#2.2, and Cap#2.3)

TABLE 3
ESR and the specific capacitance of supercapacitors: cap#2.1-2.3

Supercapacitor	Equivalent Series Resistances ESR (Ω)	Specific Capacitance (F/g)
Cap#2.1 %10 PVdF	10.1	40
Cap#2.2 %15 PVdF	11	32.7
Cap#2.3 %20 PVdF	22	44

Table 3 shows the specific capacitance and the ESR measurement for Cap#2.1, Cap#2.2, and Cap#2.3. The capacitance was measured using Autolab AUT83475; by measuring the charge on the capacitor (Q area under the curve) and knowing the voltage applied, the capacitance was calculated using the following equation (Eq1) (Marin, Halper and Ellenbogen, 2006):

$$C = \frac{Q}{V} \qquad \text{(Eq. 1)}$$

The ESR was measured from the drop in the discharge curve at the beginning of discharge, using Eq2. [24]

$$V = ixR \tag{Eq. 2}$$

where;
  V = voltage drop (V)
  i = current = 15mA
  R = ESR

The trend for the specific capacitance depicted in Table 3 might be due to two reasons: the variance in the pressure used to register the two capacitor electrodes together and the inconsistency of the activated carbon particle size used in the three samples. *Fig. 7* shows the voltage drop in the charge-discharge curve used to measure the ESR for all the supercapacitors. Eq. 2 was used to calculate the ESR and the values are listed in Table 3.

(CDC)
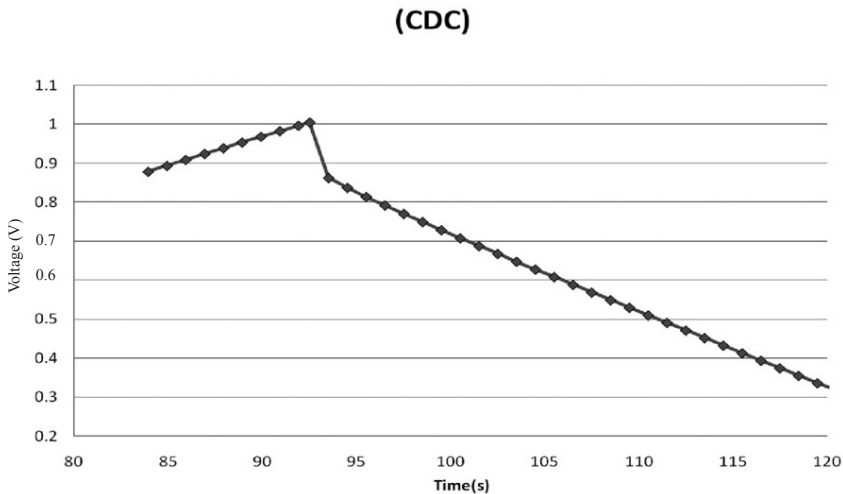
Fig.7: Measuring ESR from the voltage drop in charge-discharge curve Cap#2.1

The measured ESR (Table 3) was found to be bigger than the ones reported (in the range of few ohms) (Kyong-Min Kima, Jin-Woo Hura, Se-Il Junga and An-Soo Kanga, 2004). The authors attributed that to the low conductivity of the coconut shell-based activated carbon, and the lack of any conducting additives (carbon black) to lower the resistance of the active material (AC).

EIS Testing

EIS (Electrochemical Impedance Spectroscopy) testing is an effective method to measure and analyze the parameters of supercapacitors. In this study, a sinusoidal voltage was applied to the supercapacitor at a well-defined frequency range. The amplitude and phase of the voltage were recorded when the signal swept though the range repeatedly and the Nyquist curve was plotted to get the equivalent impedance of the supercapacitor (Namisnyk, 2003; Mullet, 1999).
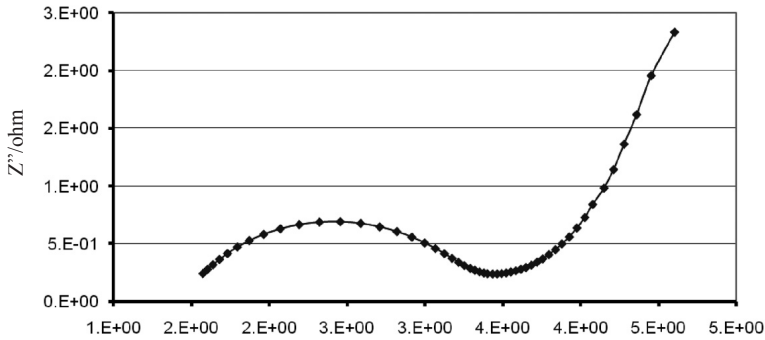
Fig. 8: EIS measurement for Cap#2.1

Fig. 8 shows the Nyquist curve for Cap#2.1. At high frequencies, the imaginary part of the impedance tends to become zero and the resistance measured is related to the ionic resistance of the electrolyte. In the range of medium frequencies, a semi-circle is associated with the resistance of porous structure of the electrodes (Mullet, 1999) with the current collector (Nian and Teng, 2003).

Typical complex plane plots for Cap#1.1 and Cap#1.2 are presented in *Fig. 9*. The double-layer charging, charge-transfer resistance and diffusion-controlled kinetics are all well-separated in the plots. The charge-transfer process, at the electrodes-electrolyte interface, is determined by the semi-circle at high frequencies and the 45° angled straight line represents the diffusion-controlled electrode kinetics at lower frequencies.
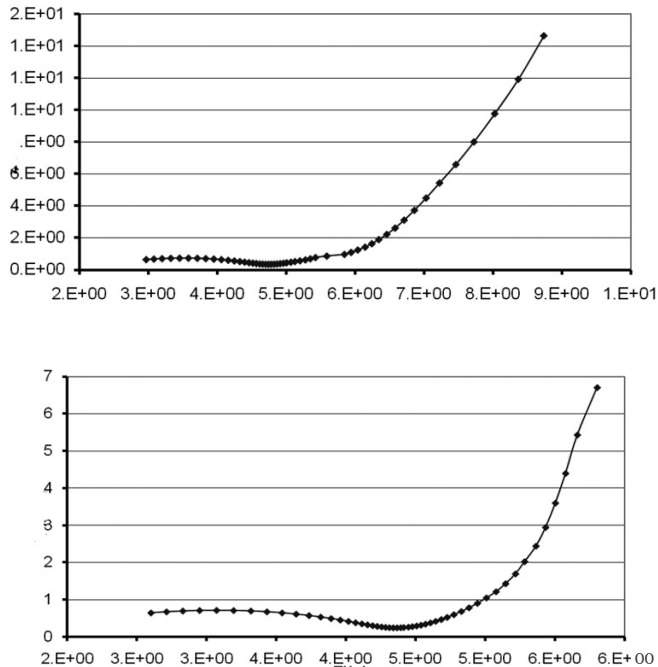
Fig. 9: EIS measurements for the supercapacitors (Cap#1.1 and Cap#1.2)
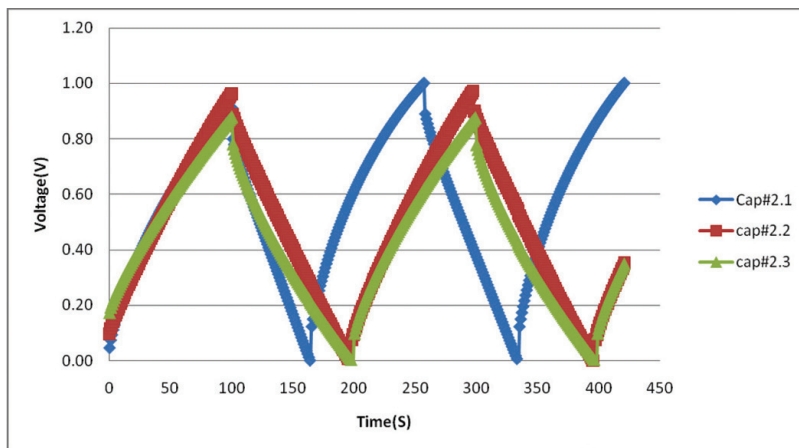
Fig. 10: Charge-discharge curves for the supercapacitors (20mA); Cap#2.1, Cap#2.2, and Cap#2.3
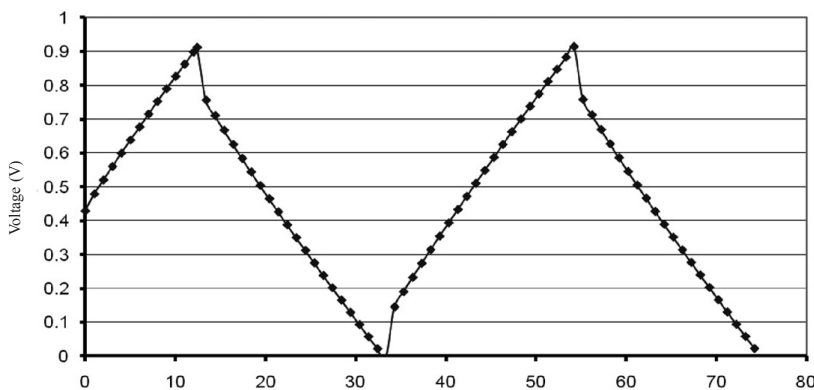
Fig. 11: Constant current (10mA) charge-discharge for Cap#1.2

Fig. 9 shows the EIS measurement for Cap#1.1 and Cap# 1.2 using the (Autolab). The capacitance measurements from EIS (0.2399F) and CV (0.24F) were found to be very close in value.

Charge-Discharge Measurements

The capacity of the supercapacitors was also obtained from the charge-discharge measurement curve to confirm the measurement by CV. The constant current charge-discharge measurements in this research were mainly used to measure the ESR for the supercapacitor. The values of the ESR for all the manufactured supercapacitor were reported earlier in Tables 1 and 2. *Fig. 10* shows the comparison between the charge-discharge characteristics of Cap#2.1, Cap#2.2, and Cap#2.3 at the same constant current (20mA).

From the charge-discharge curve, it is clear that Cap#2.1 (i.e. with the lowest ESR value) is charging and discharging the fastest in the group, and this can be attributed to the lower resistance of the activated carbon because of low binder percentage used in this supercapacitor.
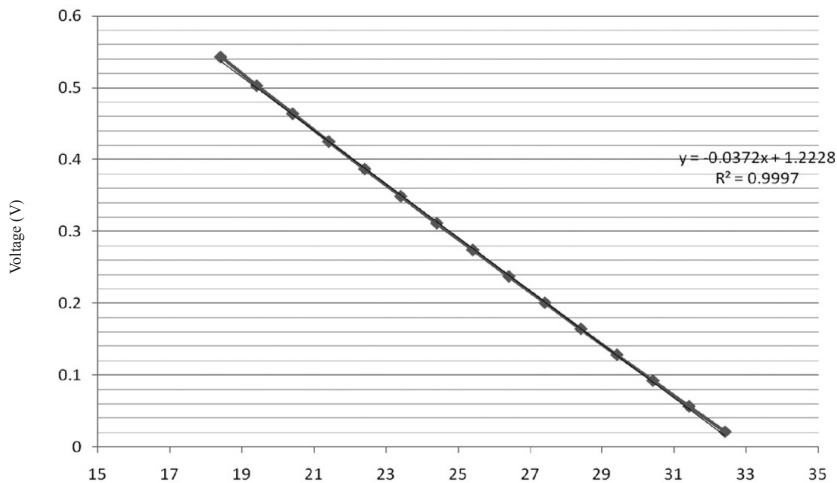
Fig. 12: Measuring the capacitance from the charge-discharge curve Cap#1.2

The constant current charge-discharge characteristics for the Supercapacitor Cap#1.2 are shown in *Fig. 11*. The curve shows the behaviour of supercapacitor charge-discharge characteristics. The constant charging current is 10mA. The voltage drop in the curve, at the beginning of the discharge curve, was used to calculate the ESR, according to Eq 2, while the slope of the straight line was used to confirm the capacitance measurement of the supercapacitor.

Fig. 12 shows a part of the discharge curve that was used to calculate the capacitance for the Cap#1.2. The capacitance was calculated using the following equation:

$$C = i/Slope \qquad\qquad\qquad\qquad (Eq. 3)$$

where,

C is the capacitance of the supercapacitor;
i is the constant charging or discharging current;
Slope is the slope of the discharge line.

In this case, the discharging current was 10mA while the slope (*Fig. 12*) is 0.0372. Using Eq. 3, the capacitance was found to be 0.268F, and the capacitance calculated from the CV was found to be 0.25F.

CONCLUSIONS

Coconut shell-based activated carbon is a good choice for supercapacitor electrode active material compared to the more expensive AC and CNT. In this study, Autolab (AUT83475) was used for all the measurements and all the materials were used without any further purification. The best composition for the electrodes material was found to be 90% coconut shell-based activated carbon and 10% binder, which KCL was employed as electrolyte to give the highest specific capacitance 70F/g at 5mV/s (Cap#1.1). The capacitance measurements were confirmed by CV, EIS, and charge-discharge characteristics and all the results were in close proximity. Meanwhile, the aqueous electrolyte limited the maximum supercapacitor voltage to 1V.

The ESR was calculated from the voltage drop at the beginning of the discharge cycle, and the smallest value was 10.1 Ohms, which was found in the supercapacitor with the lowest binder percentage of 10% (Cap#2.1). The ESR value was somewhat high, and this could be attributed to the low electrical conductivity of the coconut activated carbon. This could be reduced by adding some conductive additives (carbon black).

ACKNOWLEDGEMENTS

REFERENCES

Álvarez, S., Blanco-López, M.C., Miranda-Ordieres, A.J., Fuertes, A.B. and Centeno, T.A. (2005). Electrochemical capacitor performance of mesoporous carbons obtained by templating technique. *Carbon*, *43*(4), 866-870.

Arabale, G., Wagh, D., Kulkarni, M., Mulla, I.S., Vernekar, S.P. and Rao, A.M. (2003). Enhanced supercapacitance of multiwalled carbon nanotubes functionalized with ruthenium oxide. *Chemical Physics Letters, 376*, 207–213.

Bonnefoi, L., Simon, P., Fauvarque, J.F., Sarrazin, C. and Dugast, A. (1999). Electrode optimization for carbon power. *Journal of Power Sources*, *79*, 37–42.

Chen, W.C., Wen, T.C. and Teng, H. (2003). Polyaniline-deposited porous carbon electrode for supercapacitor. *Electrochimica Acta*, *48*, 641–649.

Chu, A. and Braatz, P. (2002). Comparison of commercial supercapacitors and high-power lithium-ion batteries for power-assist applications in hybrid electric vehicles I. Initial characterization. *Journal of Power Sources*, *112*(1), 236-246.

Conway, B.E. (1999). *Electrochemical Supercapacitors*. New York: Kluwer Academic/Plenum Publishers.

Emmenegger, C., Mauron, P., Sudan, P., Wenger, P. and Zuttel, A. (2003). Investigation of electrochemical double-layer (ECDL) capacitors electrodes based on carbon nanotubes and activated carbon materials. *Journal of Power Sources*, *124*(1), 321-329.

Frackowaik, E. and Beguin, F. (2001). Carbon materials for the electrochemical storage of energy in capacitors. *Carbon*, *39*, 937–950.

Frackowaik, E. and Beguin, F. (2002). Electrochemical storage of energy in carbon nanotubes and nanostructured carbons. *Carbon*, *40*, 1775–1787.

Hal-Bon Gu, Jong-Uk Kim and Hee-Woong Song. (2000). Electrochemical properties of carbon composite electrode with polymer electrolyte for electric double-layer capacitor. *Electrochimica Acta*, *45*(8-9), 1533-1536.

Kierzek, K., Frackowiak, E. and Lota, G. (2004). Electrochemical capacitors based on highly porous carbons prepared by KOH activation. *Journal of Electrochimica Acta*, *49*, 515–523.

Kyong-Min Kima, Jin-Woo Hura, Se-Il Junga and An-Soo Kanga. (2004). Electrochemical characteristics of activated carbon/Ppy electrode combined with P(VdF-co-HFP)/PVP for EDLC. *Electrochimica Acta*, 863–872.

Marin, S., Halper, J. and Ellenbogen, C. (2006). *Supercapacitors: A Brief Overview.* Virginia: MITRE McLean.

Maxwell Technology. (2004). How to determine the appropriate size ultracapacitor for your application. Application Note Document 1007236 Rev 2 1 of 9, 2004.

Mullet, P.M., Fiever, P., Szymczyk, A., Foissy, A., Reggiani, J.C. and Pagetti, J. (1999). A simple and accurate determination of the point of zero charge of ceramic membranes. *Desalination*, *121*, 41–48.

Namisnyk, A.M. (2003). A survey of electrochemical supercapacitor technologies. Degree of Bachelor of Engineering, University of Technology, Sydney Faculty of Engineering, June.

Nian, Y.R. and Teng, H.S. (2003). Influence of surface oxides on the impedance behavior of carbon-based electrochemical capacitors. *Journal of Electroanalytical Chemistry*, *450*, 119.

Nishino, A. (1996). Capacitors: Operating principles, current market and technical trends. *Journal of Power Sources*, *60*, 137.

Oh, S.J., Korai, Y. and Mochida, I. (1999). A comparative study on various types of activated carbon fibers. *The 26th Japanese Annual Conference of Carbon Materials*, 132–133.

Probstle, H., Schmitt, C. and Fricke, J. (2002). Button cell supercapacitors with monolithic carbon aerogels. *Journal of Power Sources*, *105*, 189–194.

Qu, D. (2002). Study of activated carbon used in double-layer capacitors. *Journal of Power Sources, 4794*, 1–9.

Qun, X., Durbach, S. and Wu, G.T. (2004). Electrochemical characterization on $RuO_2 \cdot xH_2O$/carbon nanotubes composite electrodes for high energy density supercapacitors. *Carbon*, *42*, 451–453.

Qu, D. and Shi, H. (1998). Studies of activated carbons used in double-layer capacitors. *Journal of Power Sources*, *74*, 99–107.

Shi, H. (1996). Activated carbons and double layer capacitance. *Electrochimica Acta*, *41*, 1633.

Varakin, I.N., Klementov, A.D., Litvienko, S.V., Starodubtsev, S.V. and Stepanov, A.B. (1997). Application of ultracapacitors as traction energy sources. *Proceedings of 7th International Seminar on Double Layer Capacitors and Similar Energy Storage Devices*. Deerfield Beach.

Wenming Qiao, Yozo Korai, Isao Mochida and Yuuichi Hori. (2002). Preparation of an activated carbon artifact: Oxidative modification of coconut shell-based carbon to improve the strength. *Carbon*, *40*(3), 351-358.

Xiao, Q. and Zhou, X. (2003). The study of multiwalled carbon nanotube deposited polymer for supercapacitor. *Electrochimica Acta*, *48*, 575–580.

Zhou Shao-yun, Li Xin-hai, Wang Zhi-Xing, GUO Hua-jun and Peng Wen-jie. (2007). Effect of activated carbon and electrolyte on properties of supercapacitor. *The Transactions of Nonferrous Metals Society of China,* 1328-1333.

Repeated Fed-Batch Cultivation of Nitrogen-Fixing Bacterium, *Bacillus sphaericus* UPMB10, Using Glycerol as the Carbon Source

A.B. Ariff[1*], T.C. Ooi[1], M.S. Halimi[2] and Z.H. Shamsuddin[2]

[1]Department of Bioprocess Technology,
Faculty of Biotechnology and Biomolecular Sciences,
[2] Department of Land Resource Management, Faculty of Agriculture,
Universiti Putra Malaysia, 43400 UPM, Serdang, Selangor, Malaysia
[*]E-mail: arbarif@putra.upm.edu.my

ABSTRACT

The exponential fed-batch cultivation of *Bacillus sphaericus* UPMB10 in 2 l stirred tank fermenter was performed by feeding the initial batch culture with 14 g l^{-1} of glycerol according to the algorithm aimed at controlling the specific growth rate (μ) of the bacterium. Very high viable cell count (1.14 x 10^{10} cfu ml^{-1}), which was four times higher as compared to batch cultivation, was achieved in the fed-batch with a controlled μ at 0.4 h^{-1}. In repeated exponential fed-batch cultivation, consisting of four cycles of harvesting and recharging, a final cell concentration of 1.9 x 10^{11} cfu ml^{-1} was obtained at the end of the fourth cycle (46 h). Meanwhile, acetylene reduction of cell samples collected from repeated fed-batch cultivation remained unchanged and was maintained at around 20 nmol C$_2$H$_2$ h^{-1} ml^{-1} after prolonged cultivation period, and was comparable to those obtained in batch and exponential fed-batch cultivation. Glycerol could be used as a carbon source for high performance cultivation of *B. sphaericus,* a nitrogen fixing bacterium, in repeated fed-batch cultivation with high cell yield and cell productivity. The productivity (0.68 g l^{-1} h^{-1}) for repeated fed-batch cultivation increased about 6 times compared to that obtained in conventional batch cultivation (0.11 g l^1 h^{-1}). A innovative method in utilizing glycerol for efficient cultivation of nitrogen fixing bacterium could be beneficial to get more understanding and reference in manipulating the integrated plans for sustainable and profitable biodiesel industry.

Keywords: Nitrogen fixing bacterium, *Bacillus sphaericus,* glycerol, repeated fed-batch cultivation

INTRODUCTION

Glycerol is an attractive carbon substrate for biological conservation because it is available from renewable resources in large amounts and can be utilized by a number of micro-organisms (Lin, 1976). Moreover, glycerol is produced as a surplus by-product in the growing oleochemical industries for production of soaps, fatty acids, waxes, and surfactants. Crude glycerol is also the principal by-product of biodiesel production, which is about 10% of the weight of vegetables oils (Dasari *et al.*, 2005). The usage of low-grade quality glycerol obtained from biodiesel production is a big challenge as this particular glycerol type cannot be used for direct food and cosmetic uses. Thus, several environmentally friendly processes have been proposed from glycerol utilization based on microbial fermentation. For example, mixed culture fermentation of glycerol synthesizes short- and medium-chain polyhydroxylalkonate blends (Koller *et al.*, 2005). Glycerol has also been used as a carbon source for the production of nitrogen-fixing bacterium, *Azospirillum brasiliense*

(Fallik and Okon, 1996). Meanwhile, nitrogen fixing bacteria have been used for centuries to improve the fertility of soils. The potential and pitfalls of exploiting nitrogen fixing bacteria in agricultural soils as substitute for inorganic fertilizer have been reviewed by Cummings *et al*. (2008). For the preparation of biofertilizer, large-scale production of nitrogen-fixing bacterium is essential before inoculation into suitable solid substrate for composting. The development of a commercially feasible fermentation process for large-scale production involves improvement of yield and overall productivity.

Reduced specific growth rate and yield of *Bacillus shaericus* UPMB10 batch cultivation were observed with increasing glycerol concentration due to reduction in a_w, which greatly repressed the growth (Ooi *et al.*, 2008). The effect of glycerol inhibition to growth could be minimized through fed-batch cultivation technique by controlling the concentration in the culture at low levels through regulation of nutrients feed rates. Several feeding strategies, such as constant feeding, intermittent feeding and exponential feeding, could be applied in fed-batch cultivation. The theory and application of fed-batch cultivation have been well-discussed in the literature (e.g. Lee *et al.,* 1999; Ezequiel and Dirk, 2005). The productivity can be increased by extending the life of the fed-batch fermentation and converting it into repeated fed-batch cultivation. In the repeated fed-batch cultivation, a portion of the reactor content is periodically withdrawn and the residual growing culture in the reactor is used as the starting point for further fed-batch process. This ensures the benefit of high inoculum ratio at the time of fresh feed.

Comparisons between optimal repeated fed-batch cultivation and other cultivation modes have been made for the substrate-inhibited culture systems (Weigand, 1980). Meanwhile, significant improvement in cell productivity was obtained by repeated batch as compared to batch and continuous cultivations. Improvement of the cultivation or fermentation performance, in term of the overall productivity, has been reported for several processes. The productivity of xylitol fermentation by *Candida parapsilosis* in repeated fed-batch was increased by about 40% as compared to the batch fermentation without loss in yield (Furlan *et al.,* 1997). The average productivity of L-sorbose fermentation by *Gluconobacter oxydans* using D-sorbitol as substrate was also improved by the use of repeated fed-batch fermentation (Giridhar and Srivastava, 2001). The production rate of lipase, in the repeated fed-batch fermentation employing *Acinetobacter radioresistens*, was improved by about 3.3 times as compared to the use of fed-batch fermentation (Li *et al.,* 2005). Improvement of biological treatment of pre-treated landfill leachate, using repeated fed-batch technique, has been reported (Kargi and Pamukoglu, 2004), where significant improvement in COD removal was obtained as compared to single-cycle operation.

The objective of this study was to investigate the possibility of using repeated exponential fed batch cultivation technique to improve *Bacillus sphaericus* UPMB10 cultivation using glycerol as a substrate in term of yield ($Y_{x/s}$) and overall cell productivity (P).

MATERIALS AND METHODS

Micro-organism and Inoculum Preparation

The bacterium, *Bacillus sphaericus* UPMB10, was used throughout this study. This bacterium was obtained from the Department of Land Management, Universiti Putra Malaysia. Cell cultures of *B. sphaericus* UPMB10 were suspended in 15% (v/v) glycerol and kept as a stock culture at -80°C. As for the inoculum preparation, the stock cultures were streaked on nutrient agar (NA) slant and incubated at 30°C overnight. A single colony was removed from NA slant and inoculated into 100 ml of Nutrient Broth (NB) in 250 ml Erlenmeyer Flasks. The flasks were agitated in a rotary shaker at 200 rpm and incubated at 30°C for 10 h and used as inoculum for the cultivation. This

inoculum has an optical density of approximately 0.8 measured at 600 nm, which was equivalent to about 1×10^7 cfu ml^{-1}.

Media

All cultivations were carried out using a basal medium consisting of 1.4 g l^{-1} yeast extract, 2.8 g l^{-1}, KH$_2$PO$_4$, 1.12 g l^{-1} Na$_2$HPO$_4$, 0.01 g l^{-1} CaCl$_2$.2H$_2$O, 0.1 g l^{-1} MgSO$_4$.7H$_2$O, 0.004 g l^{-1} MnCl$_2$, 0.003 g l^{-1} FeSO$_4$.7H$_2$O, 0.003 g l^{-1} biotin and 0.03 g l^{-1}thiamine hydrochloride. For the initial batch cultivation, 1.4 g l^{-1} glycerol was added to the basal medium, which was optimal for the growth of *B. sphaericus* UPMB10 (Ooi *et al.,* 2008). High glycerol concentration (14 g l^{-1}) in a basal medium was used as a feeding nutrient for the exponential fed-batch and repeated exponential fed-batch cultivations.

Cultivations

All cultivations of *B. sphaericus* UPMB10 were carried out in a 2 l stirred tank fermenter (Biostat B, B. Braun Germany). The fermenter was equipped with pH, temperature and foam control systems. During the cultivation, agitation speed and aeration rate were maintained at 600 rpm (impeller tip speed = 3.1 m s^{-1}) and 0.5 vvm, respectively. The temperature within the fermenter was controlled at 30ºC. A polarographic dissolved oxygen probe (Ingold, Switzerland) was used to measure the dissolved oxygen tension (DOT) levels. In all the fermentation runs, the initial pH of the culture was set at 7.0 and was not controlled during the cultivation. Meanwhile, the level of foaming was controlled by the automated addition of antifoam A (Sigma Chemical Co., St Louis, MO).

Fed-batch cultivation was initiated as a batch with a working volume of 600 ml in a 2 l stirred tank fermenter. The exponential fed–batch fermentation was started after the glycerol in the initial batch had been depleted. The feeding of the sterile medium was carried out exponentially according to equation (1):

$$F_{i(t)} = (\mu^* X_o V_o) \, e^{\mu^* t} / Y_{x/s} \, S_i, \tag{1}$$

where the kinetic parameter values for all the experiments were as follows: ($X_o = 1.6$ g l^{-1}, $V_o = 0.6$ l, $Y_{x/s} = 0.98$ g cell g substrate^{-1}, $S_i = 14.0$ g l^{-1}, while μ^* was varied according to the requirement of each experiment).

The exponential fed-batch cultivations were carried out at different required μ^* values (i.e. ranging from 0.2 h^{-1} to 0.5 h^{-1}) lower than the maximum specific growth rate (μ_{max}) of B. *sphaericus* UPMB10 (0.53 h^{-1}) for the growth in an optimal concentration of glycerol (Ooi *et al*., 2008). Control of the peristaltic pump was facilitated using autofermenter control system (MFCS)/win software, which is a fermenter supervisory control and data acquisition system (SCADA). This 32-bit PC-based application, using algorithm or a profile inputs, interfaces with a local fermenter control unit for the control of peristaltic pump. The MFCS/win software was also configured for repeated exponential fed-batch cultivation. The fed-batch cultivation was converted into repeated fed-batch mode by rapidly withdrawing three-quarters (1.5 l) of the 2 l culture from the fermenter. Four cycles of culture withdrawal and fresh nutrient medium addition were performed in the repeated exponential fed-batch cultivation experiment.

Analytical Procedure

During the course of cultivation, samples were withdrawn at time intervals for analysis. The sample was centrifuged at 10,000 rpm for 10 min. Cells were washed and re-suspended twice with salt solution for turbidity determination at 600 nm, as well as used for the measurement of dry cell weight

using filtration and oven dry method. The supernatant was used for the chemical analysis. Organic acid such as acetic and lactic acid was measured using high performance liquid chromatography (HPLC) with UV detector (SPD-10A Shimadzu, Japan) at a wavelength of 210 nm. The separation of organic acid was obtained using Biorad aminex HPX-87H cation–exchange resin column (300 x 7.8 mm I.D.) as the stationary phase. The mobile phase was 7 mM H_2SO_4. The flow rate of the mobile phase and column temperature was controlled at 1.0 ml min^{-1} and 50°C, respectively.

Glycerol was determined using a high performance liquid chromatography (HPLC) (ConstaMetric 3000, LDC Analytical, Florida) with a refractive index detector. Sample injection was performed using a sample loop valve equipped with 25 µl loop. The stationary phase was a pre-packed Merck NH_2 column, while the mobile phase was an isocratic mixture of acetonitrile and water (80:20 v/v). The flow rate of mobile phase was 0.7 ml min^{-1} and the reaction was kept at room temperature.

Total nitrogen content in the culture filtrate was quantified using micro-Kjeldahl method. Approximately 1.0 ml of the sample was subjected to Kjeldahl digestion in a 100 ml digestion flask containing concentrated sulphuric acid. The clear digest was analyzed for total N on a Chem Lab autoanalyser. Details of the micro-Kjeldahl and the N determination using an autoanalyser can be found elsewhere (Bremner and Mulvaney, 1982).

Acetylene reduction was estimated for the culture sample at the end of cultivation run. The culture sample was inoculated into 100 ml of nitrogen free broth (NFB) supplemented with 0.05% (w/v) yeast extract in a 250 ml shake flask. Approximately 10 ml of the culture was centrifuged and re-suspended in minimal lactate broth. The re-suspended culture was transferred into a 30 ml McCartney bottles which were sealed with rubber serum stoppers (Thomas Scientific). The McCartney bottles were then flushed with O_2-free nitrogen and shaken for four hours at 30°C. The bottle was injected with 10% acetylene and incubated at 30°C. Periodically (15 min intervals) after incubation, 0.5 ml of gas was tested for the presence of ethylene using gas chromatography (GC) (Autosystem XL, Perkin Elmer) equipped with a flame ionization detector and 1-m Porapak N column. A calibration curve was plotted for each experiment. Rate of N_2 fixation was expressed as the quantity of ethylene accumulated per h.

RESULTS

Batch Cultivation

Fig. 1 shows the typical time course of the batch cultivation of *B. sphaericus* UPMB10 using glycerol as a carbon source. Growth of *B. sphaericus* UPMB10 was found to be very rapid from inoculation to 10 h of cultivation, where lag phase was not observed. During the active growth, glycerol was rapidly consumed for growth. Cells grew to a final cell concentration of 1.62 g l^{-1} or 3.26 x 10^9 cfu ml^{-1} after 14 h with a maximum specific growth rate, μ_{max} of 0.43 h^{-1}. At the end of the fermentation, 0.25 g l^{-1} of glycerol was left unutilized. Dissolved oxygen tension (DOT) level was concomitantly decreased with decreasing glycerol concentration in the culture, indicating that glycerol and oxygen were required for rapid growth. The culture pH was maintained at around pH 7 throughout the cultivation. It was found that the DOT level had dropped to 30% at the end of cultivation, suggesting that the oxygen supply was not limited. Yield ($Y_{x/s}$) and productivity (P) of *B. sphaericus* UPMB10 in batch cultivation were 1.34 g cell g glycerol^{-1} and 0.11 (g l^{-1}h^{-1}), respectively.
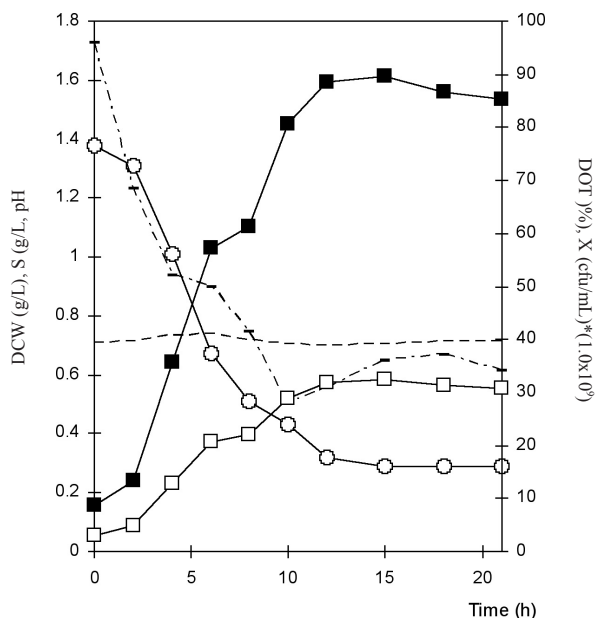
Fig. 1: The time course of batch fermentation using glycerol as the carbon source in a 2 l stirred tank fermenter. Symbols represent (◆) cell count, X (cfu ml⁻¹ x 10⁹); (……) dissolved oxygen tension, DOT (%); (◊) pH/10; (■) dry cell weight, DCW (g l⁻¹); (O) glycerol concentration, S (g l⁻¹)
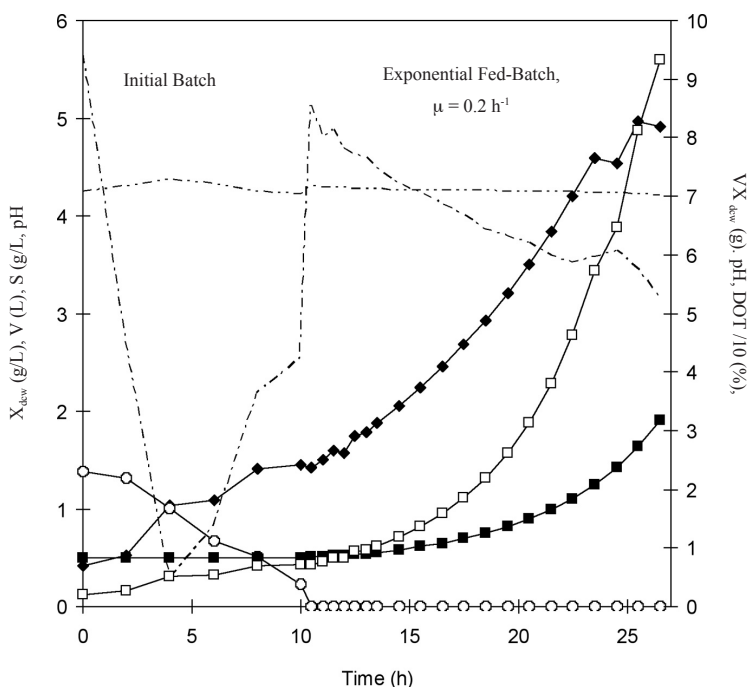
Fig. 2: The time course of exponential fed-batch fermentation at μ = 0.2 h⁻¹ using glycerol as the carbon source in a 2 l fermenter. Symbols represent (◆) X; (O) S; (■) V; (□) VX; (----) pH; (___) % DOT/10. Arrow indicates the start of feeding for the fed-batch fermentation
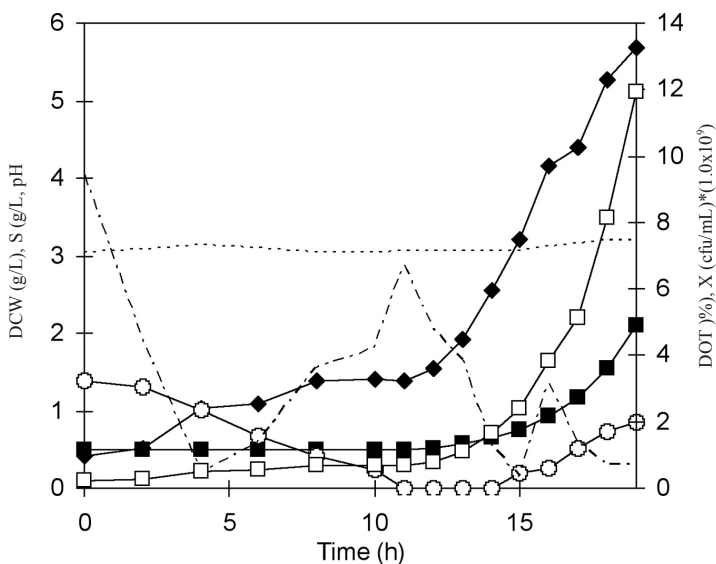
Fig. 3: The time course of the exponential fed-batch fermentation at μ = 0.40 h⁻¹ using glycerol as the carbon source in a 2 l stirred tank fermenter. Airflow was increased to 4 L min⁻¹ at 900 rpm after 17 h. Symbols represent (◆) DCW; (O) S; (■) V; (□) VX; (----) pH; (＿＿) % DOT/10. Arrow indicates the start of feeding for the fed-batch fermentation

Exponential Fed-batch Cultivation

A typical time course of exponential fed-batch cultivation of *B. sphaericus* UPMB10 fed with glycerol is shown in *Figs. 2* and *3*. In the fed-batch cultivation operated at μ^* of 0.2 h⁻¹, the residual glycerol in the culture remained at 0 g l⁻¹. The growth was found to have increased exponentially, according to the feeding rate of glycerol, reached the maximum dry cell weight (X_{dcw}) of 4.96 g l⁻¹ and corresponded to 9.43 x 10⁹ cfu m⁻¹. The DOT level was maintained at very high levels (60-80% saturation), suggesting that the oxygen supply was not limited. On the other hand, residual glycerol in the culture was only maintained at 0 g l⁻¹ up to 14 h for the fed-batch cultivation operated at μ^* of 0.4 h⁻¹. Beyond that, the residual glycerol concentration was gradually increased with cultivation time and reached a value of 0.82 g l⁻¹ at the end of cultivation, indicating that the glycerol feeding rate was higher than the consumption rate. However, the dry cell weight was increased exponentially throughout the fed-batch phase and reached the maximum concentration of 5.67 g l⁻¹. The DOT level was found to drop drastically to around 10% saturation at the later phase of fed-batch, suggesting that the cultivation might be oxygen limited. Similar to the batch, the culture pH in all the fed-batch fermentations was maintained at around pH 7, indicating that pH did not influence the performance of cultivation.

The performance of the fed-batch cultivation of *B. sphaericus* UPMB10, fed with glycerol and controlled at different specific growth rates (μ^*), is summarized in Table 1. The final X_{dcw} obtained at the end of cultivation was slightly increased by increasing μ^* up to 0.4 h⁻¹. On the contrary, a significant reduction in X_{dcw} was observed in the fed-batch operated at μ^* of 0.5 h⁻¹. In this cultivation run, the residual glycerol concentration gradually increased in the fed-batch phase and reached a value of 1.21 g l⁻¹. In addition, the DOT levels dropped to very low levels (i.e. around 5% saturation) during the fed-batch phase (data not shown). High residual glycerol concentration and low DOT levels in the culture were the reason for the reduction in the growth of *B. sphaericus* UPMB10 cultivated in the fed-batch mode at higher μ^* (0.5 h⁻¹).
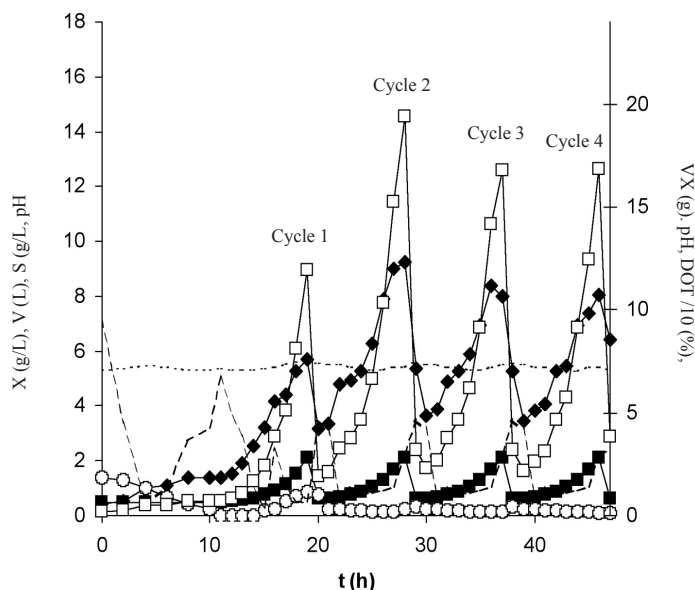
*Fig. 4: Repeated exponential fed-batch culture of Bacillus sp operated at μ = 0.4 h⁻¹. Symbols represent
(◆) X; (O) S; (■) V; (□) VX; (----) pH; (___) %DOT/10. Arrow indicates the start of feeding
for the fed-batch fermentation at each new cycle*

The actual specific growth rate during the fed-batch cultivation was calculated by plotting the logarithmic value of the total cell concentration (ln [VX_{dcw}]) against time (t). The slope of the straight line is the actual specific growth rate of the bacterium during the cultivation. Table 1 also presents a comparison between the required μ^* and the actual μ calculated from the experimental data. In all cases, the actual μ during fed-batch cultivation was closed to the required μ^*, except for μ^* of 0.5 h^{-1}. Meanwhile, the actual μ for fed-batch operated at μ^* of 0.5 h^{-1} was significantly lower and the value was similar to the value of μ_{max} for *B. sphaericus* UPMB10.

The cells produced from all the fed-batch cultivations have almost similar N_2 fixation capacity ranging from 17.4 to 21.4 nmol C_2H_2 h^{-1} ml^{-1}.

Repeated Fed–batch Cultivation

The time course of the repeated exponential fed-batch cultivation of *B. sphaericus* UPMB10 fed with glycerol, conducted for four cycles, is shown in *Fig. 3*. The culture withdrawal and feeding of fresh nutrient to start the new cycle of fed-batch cultivation was done after the maximum volume of the fermenter (2 l) had been reached, which was at 11 h, 20 h, 29 h, and 38 h. For all the cycles, μ^* was set at 0.4 h^{-1}, and the actual μ obtained in all cycles was very closed to 0.4 h^{-1}. The final dry cell weight (X_{dcw}) and cell number obtained at the end of cycles 1, 2, 3, and 4 was 5.67 g l^{-1} (1.09 x 10^{10} cfu ml^{-1}), 9.22 g l^{-1} (1.80 x 10^{10} cfu ml^{-1}), 8.35 g l^{-1} (1.62 x 10^{10} cfu ml^{-1}) and 8.01 g l^{-1} (1.55 x 10^{10} cfu ml^{-1}), respectively. The values were not significantly different for cycles 2, 3 and 4, but it was slightly lower for cycle 1. This result suggests that *B. sphaericus* UPMB10 has increased the adaptation to growth in glycerol after the initial batch and the first cycle of fed-batch phases. The efficiency to grow in glycerol was also maintained up to the fourth cycle of the repeated batch process. In addition, the ability of the cells harvested at the end of each cycle was maintained at

TABLE 1
The growth performance of *Bacillus sphaericus* UPMB10 in the exponential fed-batch fermentation
operated at different required specific growth rates (μ^*)

Required specific growth rate, μ^* (h^{-1})	Actual specific growth rate obtained during the fermentation, μ (h^{-1})	Residual glycerol in the culture in fed-batch phase (g/L)	Cell number, X_{cfu} (cfu ml^{-1} x 10^9)	Dry cell weight, X_{dcw} ($g\ l^{-1}$)	Total dry cell weight, VX_{dcw} (g)	Overall cell productivity, P ($g\ l^{-1}\ h^{-1}$)	Acetylene reduction rate ($nmolC_2H_2\ h^{-1}\ ml^{-1}$)
0.20	0.18	Maintained at 0.00	9.43±0.08	4.96±0.51	9.34	0.19	17.4±1.2
0.25	0.21	Maintained at 0.12	9.69±0.11	4.85±0.38	9.68	0.23	19.8±1.3
0.30	0.31	Maintained at 0.18	10.6±0.25	5.3±0.62	10.52	0.25	18.3±0.4
0.40	0.39	Gradually increased to a final concentration of 0.82	11.4±0.24	5.67±0.52	11.9	0.29	21.4±1.5
0.50	0.42	Gradually increased to a final concentration of 1.21	8.78±0.12	4.39±0.31	6.67	0.25	19.5±2.1

± standard deviation of triplicates

around 20.8 nmol C_2H_2 h^{-1} ml^{-1}. Similarly, the pH of the culture was also maintained at around pH 7 throughout the repeated fed-batch cultivation process.

A comparison of the performance of *B. sphaericus* UPMB10 in the different modes of cultivation is shown in Table 2. The final dry cell weight obtained in the repeated fed-batch cultivation (7.81 g l^{-1}) was about 1.4 and 4.8 times higher than those obtained in the fed-batch and batch cultivations. However, the cell yield for the repeated batch (0.66 g.cell g.glycerol^{-1}) was 2 times lower than the batch, but comparable to the fed-batch cultivation. In term of cell productivity, the values for the repeated fed-batch (0.68 g l^{-1} h^{-1}) was 2.3 and 6.2 higher than those obtained by the fed-batch and batch fermentation. The ability of *B. sphaericus* UPMB10 cells, harvested from the different modes of cultivation, to fix nitrogen was almost similar with the value ranging from 18.5 to 21.4 nmol C_2H_2 h^{-1} ml^{-1}.

DISCUSSION

Microbial fermentation is an important technology for the conversion of renewable sources to valuable products. It can be obtained by microbial fermentation of glycerol, a by-product from biodiesel industry. Glycerol is hygroscopic, which absorbs water from the air. Thus, it will reduce water activity (a_w) in a submerged culture employing glycerol as a substrate. Meanwhile, reduction in water activity led to a disruption of cell tugor pressure and membrane tension, reduced enzyme activity and protein stability, deterioration in integrity and stability of the membranes as well as nucleic acids (Brown, 1990). A number of micro-organisms responded to low-a_w environment by accumulating low-molecular-weight compatible solutes, such as amino acids, amino acid derivatives, trehalose, and polyols (Csonka and Hanson, 1991; Liu *et al.*, 1998).

A number of fermentation processes for the production of chemicals and other valuable products utilizing glycerol as substrate have been developed. Among other, *Klebsiella pneumonia* can be used to ferment glycerol to 1,3-propanediol (Xiu *et al.*, 2004). Meanwhile, Lee *et al.* (2001) reported the production of succinic acid by fermentation of glycerol using *Anaerobiospirillum succiniciproducens*. The production of hydrogen and ethanol from glycerol using *Enterobacter aerogens* HU-101 has also been reported by Ito *et al.* (2005). Polyhydroxyalkonoates can also be produced by a highly osmophilic micro-organism which utilizes glycerol as a substrate (Koller *et al.*, 2005). In all the cases, high glycerol concentrations showed the inhibition effect to growth of the micro-organism employed in the fermentation. This means that the batch culture employing high initial concentration of glycerol is not suitable for high yield and productivity process. Improvement of 1,3-propanediol production was achieved using continuous process, whereby a very low residual glycerol concentration was maintained in the culture (Xiu *et al.*, 2004). The use of continuous process enables the dilution of glycerol with a synthetic medium to increase the rate of glycerol utilization, which in turn, increased hydrogen and ethanol production (Ito *et al.*, 2005).

The inhibition effect of glycerol to growth of *B. sphaericus* UPMB10 in the batch culture has been reported in the researchers' previous study (Ooi *et al.*, 2008). The optimum glycerol concentration for the growth of this bacterium was very low, i.e. 1.8 g l^{-1}. The use of batch culture for commercial production of *B. sphaericus* UPMB10 cells for subsequent use as starter culture in composting may not be economically viable, since large fermenter shall be used for large production. In this study, the cultivation performance of *B. sphaericus* UPMB10 could significantly be improved using fed-batch fermentation, where glycerol in the culture was maintained at a very low concentration to avoid inhibition effect to growth.

Using the repeated fed-batch cultivation or fermentation technique, more volume of substrate could be processed and not limited by the maximum working volume of the fermenter. An infinite

number of cycles of the culture withdrawal and an addition of fresh nutrient could be performed in the repeated fed-batch fermentation, provided that contamination did not occur. The repeated fed-batch cultivation of *B. sphaericus* UPMB10, which was conducted up to four cycles, could be used for further improvement of cell production, which was about six times higher than batch cultivation. The repeated fed-batch fermentation of xylitol by *Candida parapsilosis* was successfully conducted up to four cycles with a slight reduction in yield (Furlan *et al.,* 1997). Four cycles of the culture withdrawal were also achieved in the repeated fed-batch sorbose fermentation by *Gluconobacter oxydans* (Giridhar and Srivastava, 2001). On the other hand, efficient lipase production by *Acinetobacter radioresistens* in the repeated fed-batch fermentation was successfully conducted up to six cycles (Li *et al.,* 2005). By converting the batch or fed-batch into repeated fed-batch fermentation, the non-productive downtime involving cleaning, sterilization, and filling could therefore be eliminated. Thus, the overall productivity of the process could be increased and the production cost could significantly be reduced. It is also important to state that the nitrogen fixing capacity of the harvested cells, measured as acetylene reduction assay (ARA), remained unchanged and was maintained at around 20 $nmolC_2H_2$ h^{-1} ml^{-1} after the prolonged cultivation in the repeated fed-batch process. Innovative utilization of glycerol, for the production of valuable product as reported here, could be beneficial to get more understanding and reference in manipulating the integrated plans for sustainable and profitable biodiesel industry.

CONCLUSIONS

The results gathered in this study have demonstrated that the use of repeated exponential fed-batch cultivation greatly improved the utilization of glycerol for the production of *B. sphaericus* cell, nitrogen fixing bacterium. The viable cell count (1.14×10^{10} cfu ml^{-1}), obtained in the exponential fed-batch cultivation with controlled μ at 0.4 h^{-1}, was four times higher than the batch cultivation. The final cell concentration of *B. sphaericus* was further improved (1.9×10^{11} cfu ml^{-1}) in the repeated exponential fed-batch cultivation consisting of four cycles of harvesting and recharging for a period of 46 h. The overall cell productivity (0.68 g l^{-1} h^{-1}) for the repeated exponential fed-batch cultivation was increased about 6 times compared to the one obtained in the conventional batch cultivation (0.11 g l^{-1} h^{-1}), but more or less the same yields (0.66 g.cell g.glycerol^{-1}). The ability of cell to reduce acetylene after repeated and prolonged cultivation cycles was maintained at around 20 nmol C_2H_2 h^{-1} ml^{-1}, which was comparable to those obtained in the batch and exponential fed-batch cultivations.

REFERENCES

Bremner, J.M. and Mulvaney, C.S. (1982). Nitrogen-total in: Method of soil analysis. In A.L. Pace (Ed.), *Agronomic Monograph No.9* (pp 595-624). American Society Agronomic, Madison, Winsconsin, USA.

Brown, A.D. (1990). *Microbial Water Stress Physiology*. Chichester, UK: John Wiley & Son.

Cummings, S.P., Humphry, D.R., Santos, S.R., Andrews, M. and James, E.K. (2008). The potential and pitfalls of exploiting nitrogen fixing bacteria in agricultural soils as a substitute for inorganic fertiliser. *Environmental Biotechnology, 2,* 1-10.

Csonka, L.N. and Hanson, A.D. (1991). Prokaryotic osmoregulation: Genetics and physiology. *Annual Review in Microbiology, 45,* 569-606.

Dasari, M.A., Kiatsimkul, P.P., Sutterlin, W.R. and Suppes, G.J. (2005). Low-pressure hydrogenesis of glycerol to propylene glycol. *Applied Catalysis A: General, 28,* 225-231.

Ezequiel, F.L. and Dirk, W.B. (2005). Estimation of optimal feeding strategies for fed-batch bioprocesses. *Bioprocess and Biosystem Engineering, 27,* 255-262.

Fallik, E. and Okon, Y. (1996). Inoculants of *Azospirillum brasilense*: Biomass production, survival and growth promotion of *Setaria Italica* and *Zea Mays*. *Soil Biological Biochemistry, 28,* 121-126.

Furlan, S.A., Delia-Dupuy, M.L. and Strehaiano, P. (1997). Xylitol production in repeated fed-batch cultivation. *World Journal of Microbiology and Biotechnology, 13,* 591-591.

Giridhar, R. and Srivastava, A.K. (2001). Repeated fed-batch sorbose fermentation by *Gluconobacter oxydans*. *Chemical Biochemical Engineering Quartely, 15,* 127-129.

Ito, T., Nakashimada, Y., Senba, K., Matsui, T. and Nishio, N. (2005). Hydrogen and ethanol production from glycerol-containing wastes discharged after biodiesel manufacturing process. *Journal of Bioscience and Bioengineering, 100,* 260-265.

Kargi, F. and Pamukoglu, M.Y. (2004). Repeated fed-batch biological treatment of pre-treated landfill leachate by powdered activated carbon addition. *Enzyme and Microbial Technology, 34,* 422-428.

Koller, M., Bona, R., Braunegg, G., Hermann, C., Horvat, O., Kroutil, M., Martinz, J., Neto, J., Pereira, L. and Varilla, P. (2005). Production of polyhydroxylalkanoates from agricultural waste and surplus materials. *Biomacromolecules, 6,* 561-565.

Lee, J., Lee, S.Y., Park, S. and Middleberg, P.J. (1999). Control of fed-batch fermentation. *Biotechnology Advances, 17,* 29-48.

Lee, P.C., Lee, W.G., Lee, S.Y. and Chang, H.N. (2001). Succinic acid production with reduced by-product formation in the fermentation of *Anaerobiospirillum succiniciproducens* using glycerol as a carbon. *Biotechnology and Bioengineering, 72,* 41-48.

Li, C.Y., Chen, S.J., Cheng, C.Y. and Chen, T.L. (2005). Production of *Acinetobacter radioresistens* lipase with repeated fed-batch culture. *Biochemical Engineering Journal, 25,* 195-199.

Lin, E.C.C. (1976). Glycerol dissimilation and its regulation in bacteria. *Annual Review in Microbiology, 30,* 535-578.

Liu, S.Q., Asmundson, R.V., Gopal, P.K., Holland, R. and Crow, V.L. (1998). Influence of reduced water activity on lactose metabolism by *Lactococcus lactis subsp. cremoris* at different pH values. *Applied and Environmental Microbioogy, 64,* 2111-2116.

Ooi, T.C., Ariff, A.B., Halimi, M.S. and Shamsuddin, Z.H. (2008). Growth kinetics of diazotrophic Bacillus sphaericus UPMB10 cultured using different types and concentrations of carbon and nitrogen sources. *Malaysia Journal of Microbiology, 4,* 15-25.

Weigand, W.A. (1980). Maximum cell productivity by repeated fed-batch culture for constant yield case. *Biotechnology and Bioengineering, 23,* 249-266.

Xiu, Z.L., Song, B.H., Wang, Z.T., Sun, L.H., Feng, E.M. and Zeng, A.P. (2004). Optimization of dissimilation of glycerol to 1,3-propanediol by *Klebsiella pneumoniae* in one and two-stage anaerobic cultures. *Biochemical Engineering Journal, 19,* 189-197.

Review Article

A Review of Farm Tractor Overturning Accidents and Safety

Mohammed Shu'aibu Abubakar*, **Desa Ahmad and Fatai Bukola Akande**

Department of Biological and Agricultural Engineering,
Faculty of Engineering,
Universiti Putra Malaysia,
43400 UPM, Serdang, Selangor, Malaysia
*E-mail: abubakarms@gmail.com

ABSTRACT

Tractor rollover occurs when a tractor tips sideways or backwards and overturns, potentially crushing the operator. Rollovers are typically considered to occur more frequently during a sharp turn at a high speed on sloping terrains, although data show that rollovers do occur on flat land after hitting obstacles or through inappropriate use and hitching of implements. It is important to highlight that tractor overturns are the major cause of death in farm operations. The overturns are as a result of interactions between the tractor operator, the tractor and the environment. A review of the relevant literature reveals that more than 800 people are killed each year in tractor accidents, and for every person killed, at least 40 others are injured. This paper focuses on tractor overturns because they account for more than half of all the tractor-related deaths. In addition, farm tractor operational safety principles are also highlighted.

Keywords: **Farm, tractor, overturning, accidents, safety**

INTRODUCTION

Farm tractors are used for farm activities. However, there are serious risks of injuries involved while using tractors as they can either roll over sideways or backwards. At the same time, there is only little chance to prevent tractors from rolling over. Tractor rollover occurs when a tractor tips sideways or backwards and overturns, and it may potentially crush the operator. Rollovers are more frequently reported to have occurred on sloping terrains, often during a sharp turn at high speed, although data show that rollovers do occur on flat land after hitting obstacles or through inappropriate use and hitching of implements (Ashby and Day, 1995; Myers *et al*., 2006). Accident involving an overturning tractor always has serious consequences on the operator. For instance, the tractor driver/operator may be killed or seriously injured and unable to return to work, perhaps for months. The tractor itself and other equipment may be severely damaged and need major repairs. Even when damage is slight, time is lost in repairing the tractor and making it serviceable again. Although the risk of death or injury has certainly been reduced by fitting safety cabs to most agricultural tractors, the safety measure has not eliminated the causes for overturning tractors due to several reasons such as the high centre of gravity and tractors are often used on sloping or uneven ground (Bureau of Labour Statistics, 2005; Owen and Hunter, 1977).

Meanwhile, studies have shown that farm tractors are involved in a high proportion of farm fatalities and severe injuries. Some of the potential hazards are difficult to be eliminated and they have in fact persisted over the years, despite the manufacturers' and engineering efforts to provide

---

*Corresponding Author

better designs (Cole *et al.*, 2006; Melvin *et al.*, 2009). In short, hazards related to farm tractors are related to stability, brakes, access to the workplaces, control, operators, as well as power transmission from the farm tractors, noise and the environment (Carlson *et al.*, 2005; Hwang *et al.*, 2001; Campbell, 1990).

In the United State of America, it is estimated that more than 800 people are killed each year in tractor accidents, and for every person killed at least 40 others are injured (Bureau of Labour Statistics, 2005). Overturns account for more than half of the tractor accidents that lead to death (Liljedahl *et al.*, 1979). According to a personnel at the National Safety Council (NSC, 1992), agriculture had a rate of 44 deaths per 100,000 workers in 1991, making agriculture relatively the most hazardous industry. Consequently, farm tractors have been categorized as the most hazardous of all farm machinery in the United States.

Accidents involving overturning farm tractors are issues of growing concern worldwide, particularly among the farm members' families, farm safety specialists, governments, and researchers. The reasons for concern are attributed to the increase in the occurrence of fatal injuries. In the light of these, this paper highlights the accidents involving overturned farm tractors and provides important information so as to create awareness on the efficient use of farm tractor.

FARM TRACTOR ACCIDENTS

Agriculture is one of the most hazardous industries in the United States, which is only surpassed by mining and construction. No other farm machine has been identified as with potential hazards in agricultural production as the tractor. Tractor-related injuries account for approximately 32% of the fatalities and 6% of the non-fatal injuries in agriculture. More importantly, over 50% of the accidents are attributed to tractor overturns. Farm tractor accidents are the major cause of farm work-related deaths. For example, more than 200 farmers' family members in Indiana died as a result of tractor accidents during the 70's (Carlson *et al.*, 2005; Campbell and Field, 1979). The three major elements responsible for accidents involving farm tractors are:
1. the farm tractor operator,
2. the farm tractor, and
3. the environment (workstation)

The above elements might have control to some extent; among other, setting up fields with adequate turning room at the ends of rows is a safety factor entirely within human control. The speed at which the tractor is operated, as well as if a rollover protective structure (ROPS) and seat belt are used, is another important factor. However, there are some cases in which these elements are beyond humans' control. In such cases, operations must be modified in order to complete the job safely. A particular operator is probably safety-conscious and driving a tractor equipped with safety features, yet the operator may drive into a hazardous environment and because the environment is considered as "safe", the operator may work with an unsafe tractor. Either of these situations is likely to result in an incident. Preventing incidents means recognizing hazards and avoiding them, or at least, taking appropriate precautions if they must be encountered. Falls are also some causes of tractor accidents. Falls involve both tractor operators and extra riders who are often children. Another source of tractor-related injuries and death is entanglement (caught) in rotating power-take off shaft (Cole, 2003; Reynolds and Grovers, 2000; Aherin *et al.*, 1992).

Farm tractor operation, like automobile driving, becomes hazardous with non-stop operation is extended without rest. According to Brauer (1990), drivers should limit themselves to 8-10 hours of automobile driving a day. Exceeding these suggested hours could lead to stress and tiredness, both of which have serious consequences on the operators' ability to function in a safe manner.

Modern tractors have rollover protection systems to prevent an operator from being crushed if the tractor overturns. It is important to remember that the ROPS does not prevent tractor overturns. Rather, it prevents the operator from being crushed during an overturn. This is especially important in open-air tractors, where the ROPS is a steel beam that extends above the operator's seat. For tractors with operator cabs, the ROPS is part of the frame of the cab. A ROPS with enclosed cab further reduces the likelihood of serious injury because the operator is protected by the sides and windows of the cab. In short, farm tractor accidents occur regularly from:

1. Rollovers
2. Power take offs
3. Falls from tractors
4. Hitching equipment
5. Tractor operations and
6. Towing

OVERTURNS/ROLLOVERS

Rollover is one of the main causes of fatalities in using farm tractors. No other machine is identified with hazards of farming more than the tractor. Tractors are often used on sloping or uneven ground as well as towing vehicles. Moreover, tractors have no suspension and this is one of the main reasons for overturning. In particular, it is very hazardous when a tractor is travelling downhill, changing direction, crossing the slope, and climbing uphill. Tractor turnover is by far the major cause of tractor-related deaths. Four reasons can be identified for tractor's overturning; these include tractor being operated on steep side slopes, tractor goes too fast for the sharpness of the turn, power applies to the rear wheels of the tractor too quickly and finally pulling pull a load that is not hitched to the drawbar of the tractor (Melvin *et al*., 2009). In a Johns Hopkins University, a study of tractor-related deaths between 1975 and 1981 revealed that 45 percent or 1,163 of the 2,566 total deaths were caused by roll-over accidents. Similarly, a 12-year study of Colorado agriculture-related deaths (1978 to 1990) revealed that 50 percent of the tractor-related deaths were due to roll-over (Carlson *et al*., 2005). Of the 175 tractor turnover accidents reported in Nebraska from January 1966 to January 1972, 78 involved fatal and 97 non-fatal injuries. According to Etherton *et al*. (1991), tractor overturns were the single most accident accounting for 52 percent of the reported tractor accidents. Rollover protective structure (ROPS) and seat belts were designed to provide overturn protection in the events of tractor rolls over. Tractors with ROPS were first used in New Zealand in the 1960s. The most effective form of protection in the event of a rollover is Rollover Protective Structures in combination with seat belt use. ROPS are structural components, either a roll bar device or crushproof cab, which provide an umbrella of safety in the event of a rollover. The effectiveness of ROPS in preventing tractor rollover deaths has been demonstrated in Sweden, Great Britain and Norway (Springfeldt *et al*., 1998). For example, the tractor rollover fatality rate decreased from 15 per 100,000 tractors to less than 1 per 100,000 tractors as the legal safety requirements moved from ROPS on all new tractors to safety cabins on all new and existing tractors in Sweden (Springfeldt *et al*., 1998).

Many farmers died when their tractors rolled on top of them before tractors with ROPS were introduced and used. Some farmers were killed by rollovers while operating tractors along steep slopes. Others were killed while attempting to pull an excessive load from above axle height, or when cold weather caused tyres of tractors to freeze down; in both cases, tractors were caused to pivot around the rear axle. Goering (1989) reported that early tractors had far fewer safety features than modern ones. Modern tractors are much safer than the ones used 20 or 30 years ago. In more specific, rollover protective structures, and seat belts of the modern tractors used at present prevent

many deaths and injuries during tractor overturns. In addition, these tractors are equipped with improved hitch designs and weight distribution which made them more stable. Moreover, wider wheel bases, better visibility, and other features such as running lights and adjustable seats have given these tractors more safety measures. Despite all these modern safety improvements in design, there are still risks involved while working with or operating a tractor. These risks can be reduced if the tractor operator understands operational safety precautions properly.

Tractors are quite safe when operated properly but they can cause serious injury and even deaths if they are used in improper manner. According to Murphy (1992), farm tractor operators frequently make physical changes to the safety features of the farm tractors. For example, some farmers cut the rollover protective structure (ROPS) off and remove the power take off (PTO) shaft master shield. On the contrary, a few modern features have actually increased the potential dangers. Such dangers include increased rear axle torque which increases the risk of rear overturns, while high speed tractors increase the danger of side overturns due to centrifugal force on curves or corners. High speed tractors increase the danger of losing control during road travel. Tractor upsets or overturns account for more than half of all tractor-related deaths. The side overturn is the most frequent type of overturn. Studies indicated that 75-85 percent of overturns are to the side. A tractor has a high centre of gravity, and this leads to sharp turns or high loads which can cause it to overturn quite easily at a relatively high speed. Meanwhile, centrifugal force can cause a tractor to overturn if the direction of travel is changed. For example, when the right front wheel of a tractor suddenly changes direction into the road ditch, the natural reaction of the operator is to steer it back onto the roadway. However, the forces will pull the tractor over on its side. Similarly, field slope, tractor speed, turning radius, rear axle torque, and centre of gravity are interrelated factors which determine the potential for tractor turnover (Myers *et al*., 2006).

FARM TRACTOR STABILITY

Generally, farm tractor overturn incidents are resulted from changes made to the limiting position of the vertical plane through the centre of gravity of the farm tractor to a position outside the points where any two wheels make contact with the ground. The main limitations of tractors are steep slope, high speed, rough ground, and loss of control. The stability loss on rough ground is more likely than on smooth ground because the wheels of a tractor follow the bumps and hollows of the rough ground which cause steep local slopes. The general ground slope may be small but its roughness can cause local slopes to become steep (Myers, 2008). Thus, it is very useful to design a system that is able to keep tractors stable in various situations. The location of the centre of gravity varies with the make and model of the tractors. It is ahead of the rear axle and midway between the rear wheels on wheel type tractors. As long as the tractor remains level enough (i.e. a vertical line drawn through the centre of gravity falls within the points where the wheels make contact with the ground), the tractor will not tip (Promersberger *et al*., 1979; Spencer, 1978; Spencer and Gilfillan, 1976; Spencer and Owen, 1981). Table 1 shows some classifications of farm tractor overturning accidents and their causes. When tractor stability is the main concern, then a slope of 15° must be classified as steep and a slope of 30° is extremely steep.

Slope and stability limits of some farm tractors are given in Table 2. It is important to realise that overturning tractors can occur on ground which is absolutely flat, such as when they are cornering and driven at a very speed. This is unlike most road vehicles, where skidding usually occurs instead of overturning.

TABLE 1
Classifications of farm tractor overturning accidents and their causes

Category	Cause	Description
Farm tractor related accidents	(1) Loss of stability (when tractor operational safety limit is exceeded) (i) Slope exceeds tip angle (ii) High speed (2) Loss of control	- Tractor overturning rearward - Mostly two wheel-drive tractor sliding downhill before overturning
Operator-related accidents (an operator misjudged width of a head land on which he/she intended to turn and drove into a ditch at low speed and on flat land)	(3) Operator's misjudgement	- Tractor side turning on a flat land

Source: Hunter and Owen, 1983

TABLE 2
Slope and stability limits of some farm tractors

Slope				Unstable tractor
Degree	Percentage	Gradient	Description	
0	0		Flat	Two wheel-drive tractor, turning at high speed
5	9	1 in 11	Gentle	Two wheel-drive tractor, with mounted implement turning at full breaking system lock
10	18	1 in 6	Medium	Two wheel-drive tractor, with heavy ballast on front loader (tipping side ways)
15	27	1 in 4	Steep	Two wheel-drive tractor, with heavy mounted implement
20	36	1 in 3	Very steep	Two wheel-drive tractor, with trailed equipment
25	47	1 in 2	Excessive	Two wheel-drive tractor, with standard wheel tract (1630 mm)
>30	58		Extreme	Four wheel-drive tractor, with wide wheel track (1840 mm)

Source: Murphy *et al*., 1985

TABLE 3

The number of farm tractors in use, the percentage of the farm tractors equipped with ROPS and the number of rollover fatalities per 100,000 farm tractors in some countries

Country	Number of farm tractors	Percentage of farm tractors with ROPS	Fatalities per 100,000 farm tractors per year
Sweden	324000	98	17
Norway	155000	83	24
Finland	240000	75	35
Great Britain	450000	99	14
West Germany	1600000	98	18
New Zealand	120000	65	37
Spain	500000	50	45
USA	4620000	55	60

Source: Bengt, 1996

Hunter and Owen (1983) studied 560 tractors overturning accidents on farms in the UK and found that there were three main conditions leading directly to loss of stability. These were exceeding the tip angle (i.e. exceeding the limit of static stability), travelling at too high a speed, and travelling over rough ground. Loss of stability also occurred indirectly after loss of control, which represented the fourth condition, in which case the tractor skidded downhill on sloping ground before overturning. The above four conditions, which accounted for 55% of total accidents, were seen as exceeding the limitations of the tractor (Myers, 2008). Skidding downhill occurs if the ground is too slippery for the tractor to remain under control, and this is also common on grass fields as well as loose surfaces. Skidding or overturning when cornering usually occurs at a high speed (Hard and Myers, 1999; Behrooz and Hanif, 2009). Sideways overturning often occurs on steep slopes and on rough ground. It is important to note that the manufacturers did not provide any guidelines on safe slope for any of the machines and therefore it was difficult for the tractor operators to prevent any of these accidents. In addition, the fact that a number of accidents caused by tractor operator's misjudgements have also been well accepted.

Table 3 shows the percentage of farm tractors equipped with ROPS and the number of rollover fatalities per 100,000 farm tractors in some countries. Based on the data, it was observed that as the percentage of tractors equipped with ROPS increased, the fatalities caused by farm tractor rollovers per 100,000 per year were decreased (*Fig. 1*).

CONCLUSIONS

Therefore, rollover prevention is an issue of major importance and the subject has become the main focus of several researchers. Rollover protective structure (ROPS) has been one of the most important advances in protecting drivers/operators from tractor overturn accidents. However, one of the most effective ways of minimising farm tractor accidents is through regulation of machinery design, manufacture, supply and operation. In conclusion, the following farm tractor operation safety tips (TOST) are highlighted:

$$y = -0.7547x + 90.026$$
$$R^2 = 0.8766$$
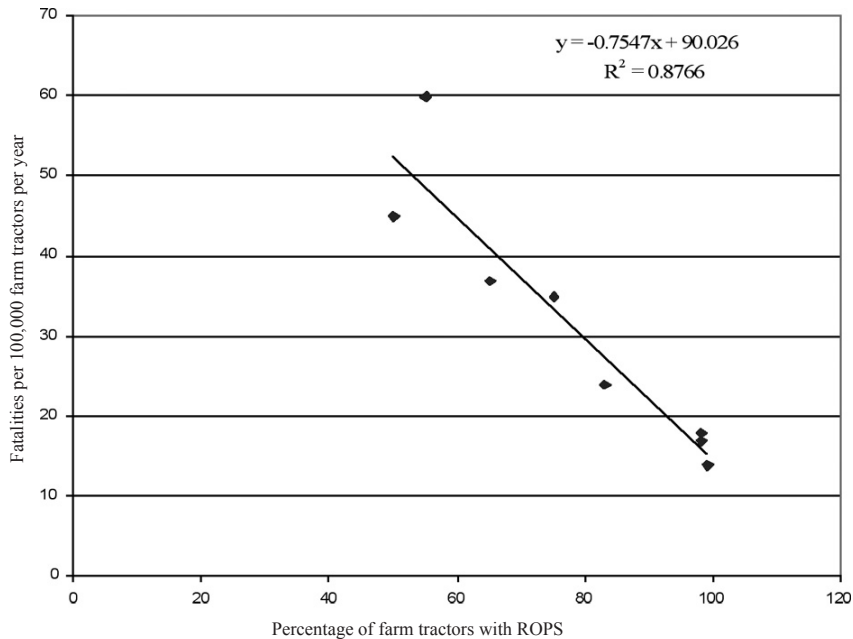
Fig. 1: Fatalities per 100,000 tractors per year against % of tractors with ROPS

1. When a tractor has adjustable wheel width, operate it with the widest wheel adjustment which is rather practical for the task at hand.
2. Add weights to the tractor to make it more stable.
3. Ensure that the shields for the power take off shaft and other moving parts are in place and in good condition.
4. Check the brakes individually and then make sure that the brakes are locked together with the tractor operating at a transport speed to ensure it will make a straight line stop.
5. The rollover protection structures (ROPS) and seat belts, when worn, are the two most important safety devices to protect operators from death during tractor overturns.
6. Slow down at turns and curves. The turning radius of a tractor is much smaller than that of an automobile. Thus, taking a curve too fast can cause an overturn or a jackknife, if machinery is attached.
7. If a tractor must be operated across the slope, use the widest possible wheel adjustment, very slow speeds and extra caution in watching for obstacles that the wheels may hit.
8. Lock break pedals together before driving at transport speed.
9. Four-wheel drive tractor is safer on slopes than two-wheel drive tractor because the former tractor has better front wheels grip.

REFERENCES

Aherin, R.A., Murphy, D.J. and Westaby, J.D. (1992). *Reducing Farm Injuries: Issues and Methods*. St. Joseph, MI: The American Society of Agricultural Engineers.

Ashby, K. and Day, L. (1995). *Tractor Injuries*. Hazard, Edition 24. Victorian Injury.

Surveillance and Applied Research System. (VISAR). Monash University Accident Research Centre, pp. 2- 8.

Behrooz, M. and Hanif, N. (2009). Automatic control of a modified tractor to work on steep side slopes. *Journal of Terramechanics*, *46*, 299–311.

Bengt, S. (1996). Rollover of tractors-International experience. *Safety Science*, *24*(2), 95-100. Elsevier Science Ltd.

Brauer, R.L. (1990). *Safety and Health for Engineers*. New York: Van Nostrand Reinhold.

Bureau of Labor Statistics. (2005). *Census of Fatal Occupational Injuries*. Washington, DC: Bureau of Labor Statistics.

Campbell, B. (1990). Of primary concern: Its getting safer, but farming is still the most dangerous industry. *American Agriculturist*, *187*(9), 10-30.

Campbell, W.P. and Field, W.P. (1992). The condition of safety components on Indiana Farm Tractors. The American Society of Agricultural Engineers. St. Joseph, MI: Paper No. 925506.

Carlson, K.F., Gerberich, S.G., Church, T.R., Ryan, A.D., Alexander, B.H., Mongin, S.J., Renier, C.M., Zhang, X., French, L.R. and Masten, A. (2005). Tractor-related injuries: A population-based study of a five-state region in the Midwest. *American Journal of Industrial Medicine,47*, 254–264.

Cole, H.P. (2003). Farmers' perceptions of ROPS and tractor safety: Studies, stories, and statistics. In *Record of Tractor-related Injury and Death Meeting*, Pittsburgh, PA (pp. 217–218), February 13–14. NIOSH, Morgantown, WV.

Cole, H.P., Myers, M. L. and Westneat, S.C. (2006). Frequency and severity of injuries to operators during overturns of farm tractors. *Journal of Agricultural Safety and Health*, *12*(2), 127-138.

Etherton, J.R., Mayers, J.R., Jensen, R.C., Russull, J.C. and Braddee, R.W. (1991). Agricultural machine-related deaths. *American Journal of Public Health, 81*(6)*,* 850-980.

Goering, C.E. (1989). Engine and tractor power. *The American Society of Agricultural Engineers*, *21*, 235-250. St. Josept, MI.

Hard, D.L. and Myers-Snyder, J.R. (1999). Identifying work-related fatalities in the agricultural production sector using two national occupational fatality surveillance systems. *Journal of Agricultural Safety Health*, *5*(2), 155–69.

Hunter, A.G.M. (1981). Tractor safety on slopes. *Agricultural Engineering, 36*(4), 50-100.

Hunter, A.G.M. and Owen, G.M. (1983). Tractor overturning accidents on slopes. *Journal of Occupational Accidents, 5,* 185-193. Elsevier Science publishers B. V., Amsterdam.

Hwang, S., Gomez, M.I., Stark, A.D., Lowery, St., John, T., May, J.J. and Hallman, E.M. (2001). Severe farm injuries among New York farmers. *American Journal of Industrial Medicine*, *40*, 32–41.

Liljedahl, J.B., Carleton, W.M., Turnquist, P.K. and Smith, D.W. (1979). *Tractors and Their Power Units* (3rd Ed). New York: John Wiley Sons.

Melvin, L.M., Henry, P.C. and Susan, C.W. (2009). Injury severity related to overturn characteristics of tractors. *Journal of Safety Research*, *40*, 165–170.

Murphy, D.J. (1992). *Safety and Health for Production Agriculture*. St. Joseph, MI: The American Society of Agricultural Engineers.

Murphy, D.J., Beppler, D.C. and Sommer, H.J. (1985). Tractor stability indicator. *Applied Ergonomics, 16*(3), 187-191.

Myers, J.R., Snyder, K.A. and Hard, D.L. (1998). Statistics and epidemiology of tractor fatalities – A historical perspective. *Journal of Agricultural Safety and Health*, *4*(2), 95-109.

Myers, M.L., Cole, H.P. and Westneat, S.C. (2006). Seatbelt use during tractor overturns. *Journal of Agricultural Safety and Health*, *12*(1), 43−49.

Myers, M.L. (2008). Continuous overturn control of compactors/rollers by rollover protective structures. *International Journal of Vehicle Safety*, *3*(1), 45−59.

National Safety Council. (1992). *Accident Facts 1992 Edition*. National Safety Council Chicago, III.

Owen, G.M. and Hunter, A.G.M. (1977). Survey of overturning accidents in Scotland, 1964-1976. Dep. Note SIN/238, Scott. Inst. Agric. Eng., Penicuik, Scotland.

Promersberger, W.J., Priebe, D.W. and Bishop, F.E. (1979). *Modern Farm Power* (3rd edn.). Reston, VA: Reston Publishing Company.

Reynolds, S.J. and Groves,W. (2000). Effectiveness of rollover protective structures in reducing farm tractor fatalities. *American Journal of Preventive Medicine*, *18*, 63–69.

Spencer, H.B. (1978). Stability and control of two-wheel drive tractors and machinery on sloping ground. *Journal of Agricultural Engineering Research, 23*, 169-188.

Spencer, H.B. and Gilfillan, G. (1976). An approach to the assessment of tractor stability on rough sloping ground. *Journal of Agricultural Engineering Research*, (21), 169-176.

Spencer, H.B. and Owen, G.M. (1981). A device for assessing the safe descent slope of agricultural vehicles. *Journal of Agricultural Engineering Research,* (26), 277-286.

Springfeldt, B., Thorson, J. and Lee, B.C. (1998). Sweden's thirty-year experience with tractor rollovers. *Journal of Agricultural Safety and Health*, *4*(3), 173-180.

Specific Heats of Neat and Glycerol Plasticized Polyvinyl Alcohol

**Lee Tin Sin[1*], Wan Aizan Wan Abdul Rahman[1], Abdul Razak Rahmat[1],
Noor Azian Morad[2] and Mohd Shahrul Nizam Salleh[1]**

*[1]Department of Polymer Engineering,
Faculty of Chemical and Natural Resources Engineering, Universiti Teknologi Malaysia,
81310 UTM Skudai, Johor, Malaysia
[2]Department of Mechanical Engineering, College of Science and Technology,
Universiti Teknologi Malaysia, International Campus,
Jalan Semarak, 54100 Kuala Lumpur, Malaysia
E-mail: direct.tinsin@gmail.com

ABSTRACT

The specific heats (C_{sp}) of neat polyvinyl alcohol (NPVOH) and 40 phr glycerol plasticized polyvinyl alcohol (PPVOH) were measured using a method known as power compensate differential scanning calorimetry. A high purity sapphire (Al_2O_3) was used as a reference material. NPVOH has a melting temperature of approximately 480 K, while PPVOH has a value of 30 K lower than NPVOH. The amplitude increment of C_{sp} for NPVOH was also higher than PPVOH at melting stage. Overall, C_{sp} of NPVOH is lower than PPVOH because glycerol has reduced the rigidity of PVOH and subsequently induced the motion of molecular structure at an elevated temperature. Based on the specific heat outcomes, neat PVOH and glycerol plasticized PVOH required 1173.544 J/g and 1946.631 J/g, respectively, to heat from 330 to 550 K.

Keywords: Polyvinyl alcohol, glycerol, specific heat, differential scanning calorimetry

INTRODUCTION

Polyvinyl alcohol (PVOH) is one of the most popular biodegradable polymers. When PVOH is exposed to natural environment, it is readily to be consumed by micro-organism. In decades, there has been increasing interest in the use PVOH for the production of disposable plastic articles. However, unlike polyethylene, polypropylene and polystyrene, PVOH is very likely to degrade during processing stage. According to Chiellini *et al.* (2003), the main difficulty in the thermal extrusion of PVOH is the close proximity of its decomposition temperature and melting point. Moreover, PVOH has a high melting point due to the presence of hydrogen bonding interactions among the hydroxyl groups. The hydrogen bond induces crystallization and subsequently requires higher energy to break up the intermolecular forces. According to Tubbs and Ting (1973), the first stage in the degradation of PVOH begins at 200°C which mainly involves dehydration with generation of volatile products; whereas, the melting point of PVOH is 180-240°C (Kuraray, 2003) that includes degradation of temperature. Hence, adding plasticizer is the most effective approach to reduce the melting point of PVOH so that the thermal degradation can be avoided during processing stage. Glycerol is the most common plasticizer (Marten *et al.*, 1991) incorporated with PVOH. This is because glycerol has tri-hydroxyl groups with good compatibility with PVOH in each molecule via hydrogen bond interactions (Kuraray, 2003).

EXPERIMENTAL DESIGN

Fully hydrolysed PVOH of grade BF-17H (viscosity 25-30 cps, hydrolysis 99.4-99.8 mole %, ash < 0.7 %), manufactured by Chang Chun Petrochemical Co., Ltd. Taiwan, was used. Meanwhile, glycerol ($C_3H_8O_3$) at 99.5 % purity was purchased from Fisher Scientific, United States. Calcium stearate (CaS) was supplied by Sun Ace Kakoh Sdn. Bhd., Malaysia. Phosphoric acid at 85% purity was obtained from Merck, Germany. CaS and phosphoric acid were used as internal lubricant and heat stabilizer additive, respectively. All the materials were used in the conditions as they were received. PVOH, glycerol, CaS, and phosphoric acid were pre-mixed in Chyau Long Machinery Co. Ltd. Taiwan, CL-10 a high speed mixer for 15 minutes. After that, the mixtures were compounded using a twin screw co-rotating extruder Sino PSM 30 B5B25 (built by Sino-Alloy Machinery Inc., Taiwan) to produce plasticized PVOH (PPVOH). The composition of PPVOH is shown in Table 1. Side feeder was used to transfer the mixtures into barrel with four heating zones. The heating zones were set at 16ºC, while the screw speed was set to 250 rpm.

TABLE 1
Composition of plasticized PVOH (PPVOH)

Specimen	Glycerol (phr)	PVOH (phr)	CaS (phr)	Phosporic acid (g)
PPVOH	40	100	2	4.18

C_p of the specimens were measured by power compensate differential scanning calorimetry (DSC)-Perkin Elmer United States model DSC 7. The original supplied PVOH was labelled as NPVOH, while PPVOH was used as prepared. Synthetic sapphire disc was used as the standard reference material. The measurements were conducted in the temperature ranging from 330-530 K and at the scanning rate of 10ºC/min with nitrogen purging at 20 ml/min. Sealed aluminium pans were used to encapsulate specimens or sapphire for measurements. The procedure to determine the experimental specific heat was based on three DSC runs, as depicted in *Fig. 1* below:
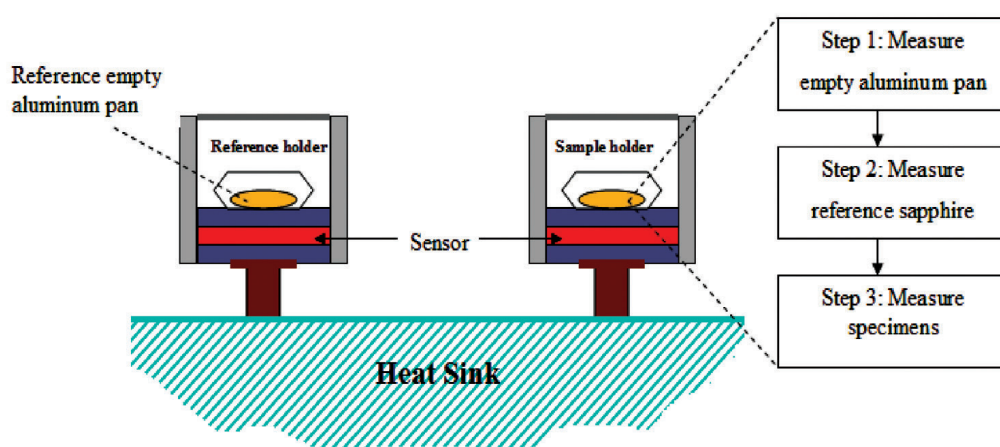
Fig. 1: Procedure of specific heat measurement

Each specimen underwent measurements in duplicate to ensure reproducibility of the results. The specific heat of the specimen is given by:

$$C_{sp} = \frac{M_{rs}}{M_{sp}} \times \frac{\Delta R_{sp}}{\Delta R_{rs}} \times C_{rs} \qquad (1)$$

where C_{rs} is the known specific heat of the sapphire standard reference material in BS ISO 11357-4 (British Standard Institutions, 2005), M_{rs} and M_{sp} are the masses of sapphire reference material and specimen, respectively. ΔR_{rs} is the signal difference between the sapphire reference material and empty aluminium pan ΔR_{sp} and is the signal difference between the specimen and empty aluminium pan.

RESULTS AND DISCUSSION

The C_{sp} of the neat PVOH (NPVOH) and PPVOH are tabulated in Table 2. *Fig. 2* shows the relationships of C_{sp} and temperatures of NPVOH and PPVOH. As illustrated, both C_{sp} of PPVOH and NPVOH increased in an almost proportional manner at the initial stage. After that, C_{sp} increased drastically, but it finally dropped back to the original trend after the melting stage was completed. Two endothermic processes were found to have occurred simultaneously during the melting stage. The first endothermic process utilized the external heat to break up the physical bonds of the specimens to reach the melting stage. Meanwhile, the second endothermic process utilized the external heat to increase the temperatures. The polymer substances have different thermal behaviour over their origin monomers. Mono-disperse low molecular weight substances possess narrow melting range which is mainly due to the similarity of entire intermolecular forces. Poly-disperse high molecular weight polymers have different strengths of intermolecular forces within the entire system. The shorter chain molecules in the polymer melt at a lower temperature and it would continue to absorb the external energy to increase the temperature until the entire polymer system achieved the molten state. Hence, the reported C_{sp} of the specimens have included the enthalpy of melting as well.

As expected, the incorporation of glycerol into PVOH showed a decrement in the onset melting temperature. In more specific, NPVOH has a melting temperature of approximately 480 K, while PPVOH has lower melting temperature at 450 K. The amplitude increment of C_{sp} for NPVOH is also higher than PPVOH at the melting stage. This indicated that glycerol had disrupted the genuine strong interactions and crystallinity structure of PVOH. Thus, PPVOH required lower energy than NPVOH to achieve the melting stage. On the other hand, the overall C_{sp} of PPVOH is higher than NPVOH. This is because the high rigidity of NPVOH limits the molecule structures to mere vibration motion while subjected to thermal effects. However, when glycerol was added to PVOH, it reduced the rigidity of PVOH and induced a number of skeletal vibrations, changed conformational and large-amplitude motion that caused anharmonic interactions, subsequently contributed significantly towards higher C_{sp} (Pyda *et al.*, 2004).

TABLE 2
Specific heat of NPVOH and PPVOH

Temperature (K)	Specific heat, C_{sp} (J/g.K)		Temperature (K)	Specific heat, C_{sp} (J/g.K)	
	NPVOH	PPVOH		NPVOH	PPVOH
330	2.293	3.261	440	6.179	10.885
340	2.656	3.759	450	6.293	11.817
350	3.064	4.405	460	6.438	13.094
360	3.508	5.116	470	6.678	13.471
370	3.986	5.871	480	7.071	12.298
380	4.477	6.620	490	8.914	13.115
390	4.950	7.357	500	11.859	13.560
400	5.310	8.075	510	6.429	13.838
410	5.620	8.765	520	6.993	14.115
420	5.882	9.436	530	7.718	14.677
430	6.044	10.100			
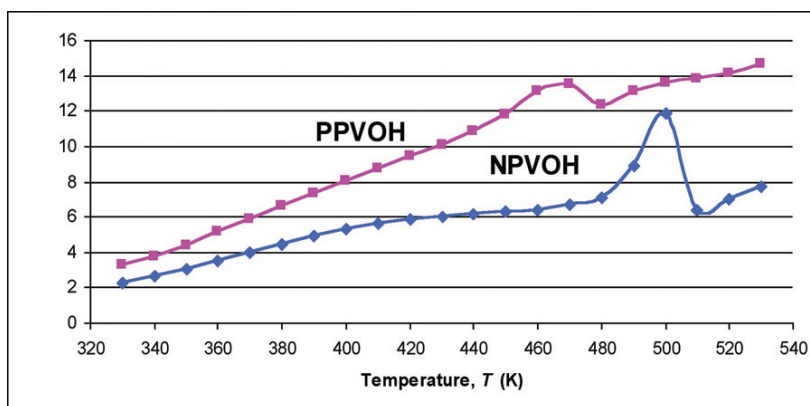
Fig. 2: Specific heat of NPVOH and PPVOH

The overall heat required to increase the temperatures of NPVOH and PPVOH from 330-530 K was calculated as follows:

$$\Delta H = \int_{330}^{530} C_{sp} \, dT \tag{2}$$

$$\Delta H = \frac{1}{2} \sum_{330}^{530} (C_{sp,i+10} + C_{sp,i}) \times 10 \tag{3}$$

390

Pertanika J. Sci. & Technol. Vol. 18 (2) 2010

The calculation outcomes showed that NPVOH and PPVOH required 1173.544 J/g and 1946.631 J/g respectively to heat from 330 to 550 K. This information is very important to predict the energy consumption of PVOH in typical polymer processing techniques such as injection moulding and melt extrusion.

CONCLUSIONS

The measurement of the specific heat of neat PVOH and glycerol plasticized PVOH was conducted using DSC. The following findings were therefore obtained:

1. Both neat PVOH and glycerol plasticized PVOH have the highest specific heat values at the melting stage. These values have included the enthalpy of melting as well.
2. Glycerol plasticized PVOH has an overall specific heat higher than neat PVOH. This is because the incorporation of glycerol has reduced rigidity and induced motion of molecules at an elevated temperature.
3. Neat PVOH and glycerol plasticized PVOH require 1173.544 J/g and 1946.631 J/g, respectively, to heat from 330 to 550 K.

ACKNOWLEDGEMENTS

REFERENCES

British Standard Institutions. (2005). BS ISO 11357-4 Plastics- Differential Scanning Calorimetry (Dsc)- Part 4: Determination of Specific Heat Capacity.

Chiellini, E., Corti, A., D'antone, S. and Solaro, R. (2003). Biodegradation of poly (vinyl alcohol) based materials. *Progress in Polymer Science*, *28*, 963-1014.

Kuraray Specialities Europe Gmbh. (2003). *Specialized in Specialities, Mowiol Polyvinyl Alcohol-Uses of Mowiol*. Frakfut/Main: Kuraray Specialities Europe Kse Gmbh.

Marten, F.L., Famili, A. and Nangeroni, J.F. (1991). *Method for Making Extrudable Polyvinyl Alcohol Compositions, U.S. Patent No. 5,051,222*. Washington D.C.: US Patent and Trademark Office.

Pyda, M., Bopp, R.C. and Wunderlich, B. (2004). Heat capacity of poly(Lactic Acid). *The Journal of Chemical Thermodynamics*, *36*, 731-742.

Tubbs, R.K. and Ting, K.W. (1973). Thermal properties of polyvinyl alcohol. In C.A. Finch (Ed.), *Polyvinyl alcohol-properties and applications* (pp.167-182). Chichester, UK: John Wiley.

Effects of Dynamic Vulcanization on Thermal Properties of Calcium Carbonate Filled Polypropylene/Ethylene Propylene Diene Terpolymer Composites

Siti Rohana Ahmad[1*], Salmah Husseinsyah[2] and Kamarudin Hussin[2]

[1]*Mechanical Section, Universiti Kuala Lumpur Malaysian Spanish Institute (UniKL MSI),
Lot 13-16, Kulim Hi-Tech Park, 09000 Kulim, Kedah, Malaysia*
[2]*School of Material Engineering, Universiti Malaysia Perlis (UniMAP),
02600 Jejawi, Perlis, Malaysia*
[*]E-mail: sitirohana@msi.unikl.edu.my

ABSTRACT

In this study, dynamic vulcanization process was used to improve the thermal properties of calcium carbonate filled composites. The composites were prepared using a Z-blade mixer at 180ºC and rotor speed 50rpm. Thermogravimetric analysis (TGA) and Differential scanning calorimetry (DSC) techniques were used to analyze the thermal properties of the composites. The vulcanized and unvulcanized PP/EPDM composites were filled by $CaCO_3$ at 0, 10, 20, 30, and 40 %wt. Meanwhile, thermogravimetric analysis indicates that the total weight loss of PP/EPDM/$CaCO_3$ composites decreased with increasing filler loading. Dynamic vulcanized composites have higher thermal stability, while the crystallinity of PP/EPDM/$CaCO_3$ composites were increased as compared to unvulcanized composites. Therefore, the thermal properties were improved by the presence of dynamic vulcanization process.

Keywords: Calcium carbonate, polypropylene, dynamic vulcanization, ethylene propylene diene terpolymer, composites

INTRODUCTION

To date, thermoplastic elastomer compositions based on polypropylene (PP)/ ethylene polypropylene diene terpolymer (EPDM) composites have increased tremendously in application. These composites are used for a wide range of products including automotive parts such as rub strips, sight shields, bumper covers, side claddings, etc. PP/EPDM composites have excellent weatheability, low density and impose relatively low cost to make them a common component in a number of exterior and interior automotive applications (De and Bhowmick, 1990).

Mineral filler, such as calcium carbonate ($CaCO_3$), is used in the PP/EPDM composites to reduce cost and improve the properties of the composites. Besides, this type of filler has a primary function as a mechanical property improver; for instance it can slightly increase modulus of elasticity (Zuiderduin *et al*., 2003; Lazzeri *et al*., 2005). In addition, it is also available in different grades, such as dry processed, wet or water ground, and can easily be surface treated (Osman *et al*., 2004) which is usually micron-sized (easier to disperse) with a broad size distribution and irregular shapes (Ismail *et al*., 2004).

Vulcanization or cross-linking is the process in which polymer is mainly converted from a plastic state to an elastic state or a hard rubber state. The process is brought about by linking macromolecules at their reactive sites (Ismail *et al*., 2004). Dynamic vulcanization (DV) is a process of cross-linking the elastomer during its melt mixing with molten plastic. It can improve properties such as mechanical properties (Mehrabzadeh and Delfan, 2000), as well as resistance

to heat and resistance to attack by fluid (Ismail *et al.*, 2001). It is quite obvious that the cross-link density of the dispersed rubber phase plays a key role in achieving higher strength (Mousa *et al.*, 1997; Jain *et al.*, 2000; Katbab *et al.*, 2000). DV also offers several improvements such as reduced set, improved ultimate properties, fatigue resistance, and resistance to hot oils.

Based on the tensile properties, water absorption and morphology analysis in the previous study, the present of dynamic vulcanization on polypropylene/ethylene propylene diene terpolymer/calcium carbonate (PP/EPDM/CaCO₃) composites showed an improvement compared to unvulcanized composites such as the higher tensile strength, elongation at break, and modulus of elasticity of dynamic vulcanized composites than unvulcanized composites. Better filler dispersion and crosslink formation in PP/EPDM matrix resulted in increases of mechanical properties in the dynamic vulcanized (DV) composites. A study on water absorption indicates that the use of dynamic vulcanization reduced the amount of water absorbed by the composites. Therefore, water absorption of DV composites indicates a lower value compared to unvulcanized (UV) composites. The calcium carbonate embedded in the PP/EPDM matrix and less pores of filler pull-out were observed from the SEM analysis (Siti Rohana *et al.*, 2008).

Thermogravimetric analysis (TGA) is one of the members of the family of thermal analysis techniques used to characterize a wide variety of materials. TGA provides complimentary and supplementary characterization information to the most commonly used thermal technique, i.e. DSC. A thermoanalytical technique, in which the difference in the amount of heat required to increase the temperature of a sample and reference, is measured as a function of temperature called Differential scanning calorimetry (DSC).

In this analysis, dynamic vulcanization was used to increase the thermal properties of calcium carbonate (CaCO₃) filled polypropylene/ethylene propylene diene terpolymer (PP/EPDM) composites.

EXPERIMENTAL DESIGN

Materials

Polypropylene used was of grade S12232 G112 from Polypropylene Malaysia Sdn. Bhd. Meanwhile, ethylene propylene diene terpolymer (EPDM) of grade Vistalon 2504N was obtained from Exxonmobile Chemical and Calcium carbonate (CaCO₃) supplied by Ipoh Ceramic Sdn. Bhd., Perak, Malaysia. CaCO₃ with an average particle size of 8.3μm was dried in a vacuum oven at 100°C for 4 hours to remove moisture. The types of curative include stearic acid from Acid Chem. International Sdn. Bhd., zinc oxide from Metroxide Malaysia Sdn. Bhd., N-cyclohexyl-2-benzothiazol-2-sulphenamide (CBS) from Meyors Chemical Inc. Limited, Tetramethyltiuram disulfide (TMTD) from DEUTSCHland CimbH, Germany and sulphur from Taiko Marketing Sdn. Bhd., Selangor. Table 1 shows the formulation of unvulcanized and dynamic vulcanized PP/EPDM/CaCO₃ composites used in this study.

Mixing Procedure

The mixing of composites was prepared in Z-blade mixer machine for 15 minutes at the temperature of 180°C and rotor speed of 50 rpm. For the unvulcanized composites, polypropylene was initially discharged to the chamber and it started the melt. Polypropylene completely melted after 7 minutes. Then, CaCO₃ was added followed by EPDM at the tenth minutes. Mixing was continued for 5 more minutes. This mixing was completed at 15 minutes.

TABLE 1

The formulation of unvulcanized (UV) and dynamic vulcanized (DV) PP/EPDM/CaCO$_3$ composites

Materials	UV	DV
Polypropylene, PP (wt%)	70	70
Ethylene propylene diene terpolymer, EPDM (wt%)	30	30
Calcium carbonate, CaCO$_3$ (wt%)	0, 10, 20, 30, 40	0, 10, 20, 30, 40
Zink oxide (wt%)	-	5
Stearic acid (wt%)	-	2
N-cyclohexyl-2-benzothiazol-2-sulphenamide (CBS) (wt%)	-	2
Tetramethyltiuram disulfide (TMTD) (wt%)	-	2.5
Sulphur (wt%)	-	1

*based on wt% of EPDM
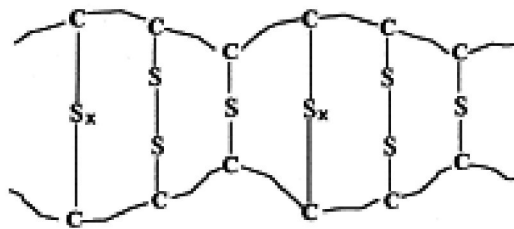
Fig. 1: Schematic representation of the crosslink formed during
the dynamic vulcanization using sulphur

However, for dynamic vulcanized composites, the whole mixing process was conducted in 17 minutes. First, PP was charged into the chamber and allowed to melt, while CaCO$_3$ was charged into the chamber at 7 minutes. Meanwhile, EPDM was charged into the chamber at 10 minutes and mixing was allowed for 5 more minutes. At 15th minute, zinc oxide, stearic acid, CBS, TMTD, and sulphur were added into the chamber and mixing was continued for another 2 minutes.

Finally, the composites were then taken out and sheeted through a laboratory scale, in two roll mills at 2.0 mm nip setting. The samples were compress-moulded in a compression moulding machine (model GT 7014A) to perform 1.0 mm sheet of composites. Hot–press procedures involved a preheating at 180ºC for 6 minutes, followed by compressing for 4 minutes at the same temperature and subsequent cooling under pressure for 4 minutes. The samples were cut from the moulded sheets using Wallace die cutter model S/6/1/4 in order to obtain the dumbbell specimens (ASTM D-638).

Pertanika J. Sci. & Technol. Vol. 18 (2) 2010

395

Measurement of Thermal Properties

Differential Scanning Calorimetry (DSC)

Differential scanning calorimetry (DSC) is a thermo analytical technique. It is used to study what happens to polymer when it is heated and to determine the thermal transitions that take place in a polymer when heated. In addition, DSC measures the difference in the amount of heat required to increase the temperature of a sample and the reference is measured as a function of temperature.

The melting characteristics and crystallization behaviour of the samples composites were carried out using Perkin Elmer DSC Q10 V8.2 Build 268 analyser equipment. The samples in about 10 - 25 mg were heated from 20 to 220°C in nitrogen air flow of 50 ml/min and the heating rate of 20°C/min. The crystallinity percentage of composites (X_{com}) was determined using the relationship in equation (1) below:

$$X_{com} \text{ (\% crystalinity)} = \Delta H_f / \Delta H^0_f \times 100\% \qquad (1)$$

where ΔH_f and ΔH^0_f are enthalpy of fusion of the system and enthalpy of fusion of perfectly (100%) crystalline PP, respectively. As for ΔH^0_f (PP), a value of 209 J/g was used for 100% crystalline PP. X_{com}, which is calculated using this equation. However, it gives only the overall crystallinity of the composites based on the total weight of composites including non-crystalline fractions. Moreover, it is not the true crystallinity of the PP phase. The value of crystallinity for PP phase of the fraction (X_{pp}) was normalized using equation (2):

$$X_{pp} = (X_{com}) / Wf_{pp} \qquad (2)$$

where Wf_{pp} is the weight fraction of PP in the composites.

Thermogravimetric Analysis (TGA)

The thermogravimetric analysis (TGA) is an analytic method with that the change of mass of a sample, as a function of the temperature and time, is measured. The thermogravimetric analysis of the composites was carried out using the Perkin Elmer analyzer equipments. The sample weights between 15 to 25 mg were scanned from 50 to 600°C using a nitrogen air flow of 50 ml/min and a heating rate of 20°C/min. The sample size was kept nearly the same for all the sample tests.

RESULTS AND DISCUSSION

Differential Scanning Calorimetry (DSC)

The DSC curves of dynamic vulcanized of PP/EPDM/CaCO$_3$ composites at 0, 20 and 40 wt% are given in *Fig. 2*. Table 2 indicates the values of T$_m$, $\Delta H^0_{f(com)}$, X_{com} and X_{pp} for the unvulcanized and dynamic vulcanized of PP/EPDM/CaCO$_3$ composites. It can be seen from Table 2 that the values of $\Delta H^0_{f(com)}$ and X_{com} for all the composites decreased with the increase in calcium carbonate loading. Dynamic vulcanized composites exhibit a higher value of enthalpy during crystallization process as compared to the unvulcanized composites. The increasing crystallinity of the DV composites was due to the increasing crosslink between calcium carbonate and matrix that increased the nucleation activity of calcium carbonate.
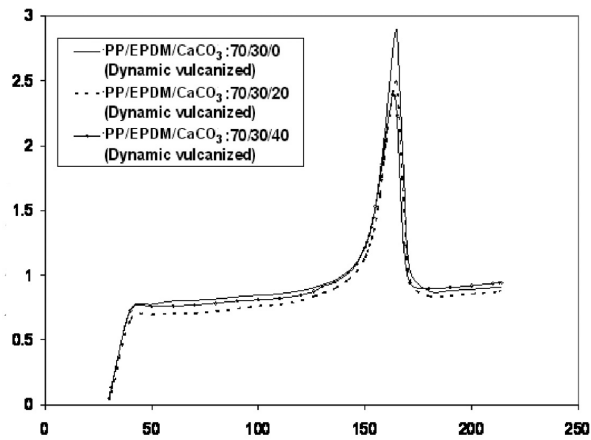
Fig. 2: A comparison of the differential scanning calorimetry (DSC) curve of the unvulcanized and dynamic vulcanized PP/EPDM/CaCO$_3$ composites at 40 php CaCO$_3$

TABLE 2
Parameter DSC for the unvulcanized and dynamic vulcanized PP/EPDM/CaCO$_3$
composites with different filler loadings

Composites	Melting temperature Tm (ºC)	$\Delta H^0_{f(com)}$ (J/g)	X_{com} (% crystalinity)	X_{pp} (%)
PP/EPDM/CaCO$_3$: 70/30/0 (Unvulcanized)	163.33	55.50	26.56	37.94
PP/EPDM/CaCO$_3$: 70/30/20 (Unvulcanized)	163.86	46.49	22.24	38.15
PP/EPDM/CaCO$_3$: 70/30/40 (Unvulcanized)	162.87	43.41	20.73	41.54
PP/EPDM/CaCO$_3$: 70/30/0 (Dynamic vulcanized)	164.78	76.84	36.76	52.52
PP/EPDM/CaCO$_3$: 70/30/20 (Dynamic vulcanized)	164.64	68.20	32.63	55.97
PP/EPDM/CaCO$_3$: 70/30/40 (Dynamic vulcanized)	163.41	61.30	29.33	58.66

The heat of fusion values is dependent on the crystallinity of the material. In the case of compatible blends, the decrease in the melting temperature is related to the extent of interaction between the components. Choudhary *et al*. (1991), George *et al*. (2000), and Xiao *et al*. (2002) reported a similar result in the DSC curves of dynamic vulcanized composites. Ha *et al*. (1986) reported that cross-linking of EPDM in the molten PP restricted the crystallinity of PP.
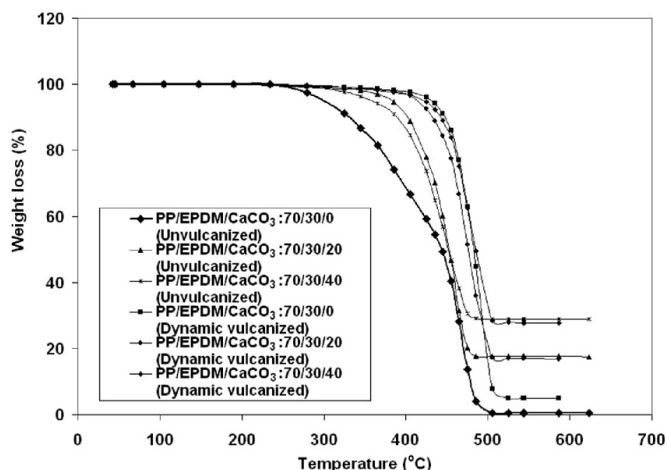
*Fig. 3: A comparison of the thermogravimetric analysis curves of the unvulcanized
and dynamic vulcanized PP/EPDM/CaCO₃ composites at 20 and 40 php CaCO₃*

Thermogravimetric Analysis

The thermogravimetric analysis (TGA) curve of unvulcanized and dynamic vulcanized of PP/
EPDM/CaCO₃ composites at 0, 20, and 40 php of calcium carbonate loading are shown in *Fig. 3*
and summarized in Table 3. It can be seen from Table 3 that the total weight loss of the dynamic
vulcanized composites is lower than the unvulcanized composites. The better thermal stability
of dynamic vulcanized composites might be due to the presence of inorganic curing agents such
as zinc oxide, stearic acid and accelerator, etc. Generally, the vulcanization of rubbers improves
the degradation temperature because more energy is required to break the bonds formed during
vulcanization. All of the PP/EPDM/CaCO₃ composites were vulcanized using the sulphur
system.

TABLE 3

Percentage of weight loss for the unvulcanized and dynamic vulcanized PP/EPDM/CaCO₃
composites at different filler loadings and temperatures

Temperature (°C)	Weight loss (%)					
	Unvulcanized			Dynamic vulcanized		
	70/30/0	70/30/20	70/30/40	70/30/0	70/30/20	70/30/40
50-100	0.00	0.21	0.07	0.05	0.10	0.02
100-200	0.05	0.03	0.03	0.16	0.07	0.01
200-300	0.73	0.47	1.14	0.61	0.78	0.68
300-400	11.91	8.92	12.14	1.41	2.11	2.12
400-500	86.96	73.15	57.68	87.24	77.50	64.20
500-623	0.23	0.05	0.12	5.68	1.45	3.22
Total	99.88	82.83	71.18	95.15	82.01	70.25

CONCLUSIONS

The Differential Scanning Calorimetry analysis indicated that the increasing crystallinity of DV composites was due to the increasing crosslink between calcium carbonate and matrix that subsequently improved the nucleation activity of calcium carbonate. In the thermogravimetric analysis, the total weight loss of the dynamic vulcanized composites was lower than the unvulcanized composites. The better thermal stability of the dynamic vulcanized composites might be due to the presence of inorganic curing agents such as zinc oxide, stearic acid and accelerator, etc. The improvement is dependent on the formation of more crosslinks between rubber chains.

REFERENCES

Choudhary, V., Varma, H.S. and Varma, I.K. (1991). Polyoleofin blends: Effect of EPDM rubber on crystallization, morphology and mechanical properties of polypropylene/EPDM blends. I. *Polymer*, *32*(14), 2534-2540.

De, S.K. and Bhowmick, A.K. (1990). *Thermoplastic Elastomers from Rubber-Plastic Blends*. England: Ellis Horwood.

George, J., Varughese, K.T. and Thomas, S. (2000). Dynamically vulcanised thermoplastic elastomer blends of polyethylene and nitrile rubber. *Polymer, 41*, 1507–1517.

Ha, C.S., Ihm, D.J. and Kim, S.C. (1986). Structure and properties of dynamically cured PP/EPDM blends. *Journal of Applied Sciences*, *78*, 6281-6297.

Ismail, H., Mohamad, Z. and Bakar, A.A. (2004). The effect of dynamic vulcanization on properties of rice husk powder filled polystyrene/styrene butadiene rubber blends. *Iranian Polymer Journal*, *13*(1), 11-19.

Ismail, H., Salmah, A. and Nasir, M. (2001). Dynamic vulcanization of rubber-wood-filled polypropylene/natural rubber blends. *Polymer Testing*, *20*, 819-823.

Jain, A.K., Nagpal, A.K., Singhal, R. and Gupta, N.K. (2000). Effect of dynamic crosslinking on impact strength and other mechanical properties of polypropylene/ethylene propylene diene rubber blends. *Journal of Applied Polymer Science,78*, 2089-2103.

Katbab, A.A., Nazockdast, H. and Bazgir, S. (2000). Carbon black reinforced dynamically cured EPDM/PP thermoplastic elastomers, I. Morphology, rheology and dynamic mechanical properties. *Journal of Applied Polymer Science*, *75*, 1127-1137.

Lazzeri, A., Zebarjad, S.M., Pracella, M., Cavalier, K. and Rosa, R. (2005). Filler toughening of plastic. Part 1 – The effect of surface interactions on physico-mechanical properties and rheological behaviour of ultrafine $CaCO_3$/HDPE nanocomposites. *Polymer*, *46*, 827-844.

Mehrabzadeh, M. and Delfan, N. (2000). Thermoplastic elastomers of butadiene acrylonitrile copolymer and polyamide. VI. Dynamic crosslinking by different systems. *Journal of Applied Polymer Science*, *77*, 2057-2066.

Mousa, A., Ishiaku, U.S., Ismail, H. and Mohd. Ishak, Z.A. (1997). Mechanical properties and thermo-oxidative ageing of dynamically vulcanized PVC/ENR thermoplastic elastomer. *International Rubber Conference*, 1997 (IRC 97), Kuala Lumpur, Malaysia, 756-764.

Osman, M.A., Atallah, A. and Suter, U.W. (2004). Influence of excessive filler coating on the tensile properties of LDPE-calcium carbonate composites. *Polymer*, *45*, 1177-1183.

Siti Rohana, Salmah, H. and Kamarudin, H. (2008). Effects of effects of dynamic vulcanization on the properties of calcium carbonate filled polypropylene/ethylene propylene diene terpolymer composites. *Proceeding Paper: VIIIth National Symposium on Polymeric Materials (NSPM 08)* at Naza Hotel, Penang; 26 & 27 November.

Xanthos, M. (2005). *Functional Fillers for Plastics*. Wiley-VCH Verlag GmbH & Co.

Xiao, H., Huang, S., Jiang, T. and Cheng, S. (2002). Miscibility of blends of ethylene propylene-diene terpolymer and polypropylene. *Journal of Applied Polymer Science, 83*, 315-322.

Zuiderduin, W.C.J., Westzaan, C., Huetink, J. and Gaymans, R.J. (2003). Toughening of polypropylene with calcium carbonate particles. *Polymer, 44*, 261–275.

Preparation and Thermal Behaviour of Acrylonitrile (AN)/Ethyl Acrylate (EA) Copolymer and Acrylonitrile (AN)/Ethyl Acrylate (EA)/Fumaronitrile (FN) Terpolymer as Precursors for Carbon Fibre

Siti Nurul Ain Md. Jamil[*], Rusli Daik and Ishak Ahmad

School of Chemical Sciences and Food Technology,
Faculty of Science and Technology, Universiti Kebangsaan Malaysia,
43600 UKM, Bangi, Selangor, Malaysia
[*]E-mail: nurul_ainjamil@yahoo.com

ABSTRACT

Redox polymerization of acrylonitrile (AN) with ethyl acrylate (EA) and fumaronitrile (FN), as comonomer and termonomer respectively, were carried out using sodium bisulfite (SBS) and potassium persulphate (KPS) as initiators at 40°C. The actual composition of monomers in copolymers and terpolymers has been characterized by gas chromatography (GC). The effects of EA and FN on the glass transition temperature (T_g) and stabilization temperature have been studied by Differential Scanning Calorimetry (DSC). The degradation behaviour and char yield were obtained by thermogravimetric analysis. Meanwhile, incorporation of 10 mol% of EA in homoPAN system was found to greatly reduce T_g to 66°C as compared to that of the homoPAN (T_g=105°C). The initial cyclization temperature (T_i) was found to be higher (264°C) in comparison to that of homoPAN (246°C). In addition, the incorporation of EA was also shown to reduce the char yield of copolymer to 40%. When FN was incorporated as termonomer, the char yield of poly(AN/EA/ FN) 90/4/6 increased up to 44% after the heat treatment with the lowest T_i (241°C).

Keywords: Acrylonitrile, carbon fibre, copolymer, ethyl acrylate, fumaronitrile, redox polymerization, terpolymer

INTRODUCTION

Carbon fibre has excellent properties such as low density, high stiffness, good resistance toward chemical and environment effects, and the ability to withstand high temperature. Hence, carbon fibre has a lot of applications such as in aerospace industry, sporting goods, automobile, defence applications, and ship structure (Gupta *et al*., 1991). Carbon fibres can be made from various materials such as rayon, pitch, and polyacrylonitrile (PAN). At present, PAN in fibre form is the most successful precursor for making high performance carbon fibres (Tsai *et al.,* 1991). In this paper, the focus of the study is on PAN-based precursors, which are commonly used in various applications that require high tensile strength fibres and a high extension to break. The most important process involved in the conversion of PAN fibres into carbon fibres is the stabilization process. This process leads to the formation of a ladder polymer. This stabilization process involves some complex reactions of intra and intermolecular cyclizations of PAN that should yield the highest degree of ladder-like structure formation with minimum adverse effects, such as chain scission and defect on chain structure (Gupta *et al.,* 1995). However, it is well known that the cyclization process of

PAN involves a rapid exothermic process with high heat liberation. The evolution of volatile by products such as H_2O, CO_2, HCN, NH_3 and even nitrogen causes mass loss. The elimination of HCN and NH_3 creates uncyclized gaps in the structure of polymer which retards the process of cyclization (Martin *et al.,* 2001). Hence, it may produce carbon fibre with poor properties after heat treatment. In order to overcome this problem, ethyl acrylate (EA) comonomer was incorporated into the PAN system. EA was used as T_g modifier in AN/EA copolymer system (Jordan *et al.,* 1972). Ester-based comonomers are known to have diluent effect on the exothermic reactions which occur during stabilization of the precursor fibres. Since acrylate comonomer can be randomly polymerized into the PAN system, it acts as defects and helps to reduce the dipole-dipole interactions and long-range order in the PAN system (Rangarajan *et al.,* 2002) that also can be indirectly observed by T_g depression. In addition, this also indicates a low processing temperature of PAN (Rangarajan *et al.,* 2002). However, the incorporation of ester-based comonomer reduces the level of formation of ladder-like structure which further reduces the char yield of PAN that provides a realistic indication of the final carbon content after heat treatment (Tsai *et al.,* 1991). In this study, FN was used as termonomer because it had been shown to increase the char yield of PAN copolymer. In more specific, FN was found to increase the possibility to form ladder-like structure during stabilization and thus lead to a high char yield during carbonization (Jamil *et al.,* 2007). High char yield indicates high carbon content in fibres (Rangarajan *et al.,* 2002), and thus results in carbon fibres with good mechanical properties.

Water is used in the redox method for polymerization, and this gives it some advantages, i.e. polymerization which is carried out in a mild reaction conditions, short reaction time, affords a high conversion and avoids the use of organic solvent (Sarac, 1999).

MATERIALS AND METHODS

The homoPAN, copolymers and terpolymers in this study were synthesized using the redox method. The three-necked flask was fitted with a condenser, stirrer, and nitrogen inlet tube. Deionized water was used as a reaction medium with potassium persulfate (KPS) and sodium bisulfite (SBS) as initiator. Polymerization was carried out at 40°C for 3 hours under a nitrogen atmosphere. The polymer formed was precipitated, filtered, and washed successfully with deionised water and methanol. The polymers obtained were dried under vacuum at 45°C till a constant weight was obtained. The actual composition of ethyl acrylate and fumaronitrile that polymerized was calculated from the residual monomer concentration data. The residual monomer concentrations of the withdrawn samples were obtained using the gas chromatography (GC) system. The polymers obtained were firstly mixed with a defined amount of methanol to precipitate and isolate the polymer from the reaction medium (water). The residual monomer remains in water. A defined portion of supernatant was injected for the GC analysis (Rintoul *et al.,* 2005). In addition, the calibration curves of ethyl acrylate and fumaronitrile were obtained using the GC system. Undecane was used as the internal standard for calibration curve and sample analysis. The peak area served as the calibration parameter. On the other hand, the composition of acrylonitrile that polymerized was calculated using the following equation:

$$Polymerized\ acrylonitrile\ (g) = polymer\ conversion\ (g) - (ethyl\ acrylate + fumaronitrile\ polymerized)\ (g) \tag{1}$$

The fourier transform infrared spectroscopy (FTIR) spectra of homoPAN, copolymers, and terpolymers were recorded on the Perkin Elmer GX infrared spectrophotometer using KBr pellets. Meanwhile, the samples in powder form (~5) mg were used for the DSC analysis. The glass

transition temperatures (T_g) of the samples were evaluated using the Mettler-Toledo differential scanning calorimeter (DSC). The heating rate employed was 10°C/min and the samples were heated from room temperature to 200°C, cooled back to room temperature at the same heating rate, and reheated again to 200°C. The temperature during the stabilization process was obtained by heating the samples from room temperature to 400°C at 10°C/min. The thermogravimetric analysis was carried out using a Mettler-Toledo TGA instrument in nitrogen from room temperature to 950°C at a heating rate of 10°C/min. A sample size of ~15 mg in the form of fine powder was used to determine the weight loss of polymers.

RESULTS AND DISCUSSION

Conversion of Polymerization and Actual Composition

As shown in Table 1, homoPAN achieved the highest conversion (85%). This is due to the non-abnormalities or defects present in the polymer chains since polymerization was not incorporated with other monomer (Jamil *et al.,* 2007). In the case of AN/EA copolymer, the incorporation of EA into copolymer was 86-89%, which is higher as compared to that of the AN (68-76%). In the case of terpolymers, the incorporation of EA into terpolymers was also the highest (82-87%) as compared to that of the AN (62-68%) and FN (77-80%). The rate of copolymerization is greatly influenced by the concentration and polarity of the monomers (Bhanu *et al.,* 2002). In water reaction medium, polymerization was proceeded according to the suspension polymerization mechanism; hence, propagation would mostly occur in oligomeric radicals phase as the number of polymer particles increased (Wan *et al.,* 2005). In this case, it remains in the aqueous phase since FN is more hydrophilic, whereas EA (which is more hydrophobic as compared to FN) is buried in the growing particle core and has a better chance to polymerize into polymer particles.

TABLE 1
Actual composition of PAN, poly(AN/EA) and poly(AN/EA/FN)

Feed (%mol), M AN/EA/FN	Conversion (%)	Composition (%mol), m AN/EA/FN	Reacted monomers (%) m/M x 100 AN/EA/FN	Actual composition (%mol)
100/0/0	85	85/0/0	85/0/0	100/0/0
Copolymer				
95/5/0	77	71.88/4.45/0	76/89/0	94/6/0
90/10/0	76	66.15/8.70/0	74/87/0	88/12/0
85/15/0	73	57.81/12.90/0	68/86/0	82/18/0
80/20/0	-	-	-	-
Terpolymer				
90/2/8	65	55.73/1.74/6.40	62/87/80	87/3/10
90/4/6	69	59.90/3.44/4.62	67/86/77	88/5/7
90/6/4	66	56.25/5.16/3.12	63/86/78	87/8/5
90/8/2	70	60.94/6.56/1.56	68/82/78	88/9/2

FTIR Spectroscopy

A representative FTIR spectrum of homoPAN, together with its copolymer and terpolymer, is shown in *Fig. 1*. In all cases, the bands in the region 2943 cm^{-1} were assigned to C-H stretching in CH, CH$_2$, and CH$_3$. Meanwhile, the bands at 1450 cm^{-1}, 1353 cm^{-1}, and 1204-1199 cm^{-1} appear due to the C-H vibrations of the different modes. The band at 2244 cm^{-1} indicates the absorption of nitrile groups in homoPAN, copolymers, and terpolymers. The band in the 1654 cm^{-1} region may be attributed to the hydrolysis of acrylonitrile units during the polymerization process which was also found by other researchers (Bajaj *et al.,* 1996). The strong band in the range of 1735 cm^{-1} in the copolymer and terpolymer spectra were due to the C=O stretching (Bajaj *et al.,* 1993). The disappearance of bands at 2238-2239 cm^{-1}, which was due to the stretching of unsaturated nitriles of FN (Jensen, 2003), confirmed that FN was incorporated together with AN and EA to form terpolymers.
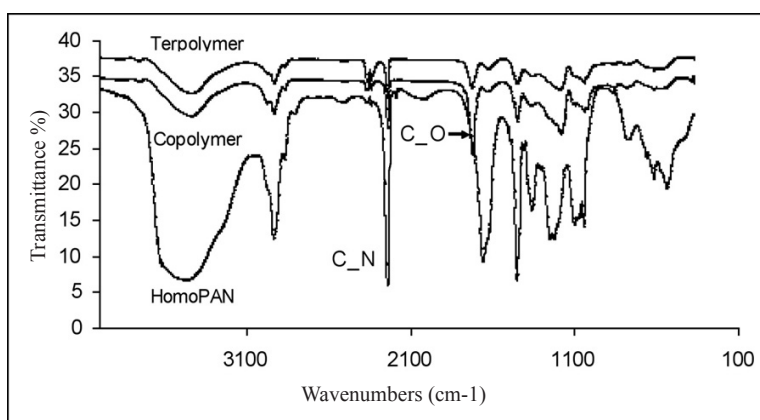
Fig. 1: IR spectrum of homoPAN, copolymer and terpolymer

DSC Analysis

Table 2 shows the glass transition temperature (T_g) of PAN, copolymers, and terpolymers. The T_g of the copolymers is lower as compared to that of the homoPAN (105°C). It is well known that homoPAN has a high T_g, and this is attributed to high chain stiffness resulting from strong dipole-dipole interaction (Min *et al.,* 1994). Meanwhile, AN/EA copolymers exhibited lower value of T_g. This can be ascribed to the introduction of EA that reduces the intermolecular interactions between the polymer chains due to structure loosening (Gupta *et al.,* 1989). From all the samples obtained, the AN/EA copolymer of 10 mol% EA was found to have achieved the lowest T_g (66°C). However, as the amount of EA increased to 15 and 20 mol%, the T_g increased to 68°C and 70°C, respectively. This might be due to the non-optimized amount of EA that hindered the chain mobility sterically, and subsequently increased T_g (Gupta *et al.,* 1989).

In the case of terpolymers, T_g is higher as compared to that of the copolymers. This might be due to the incorporation of FN termonomer with polar nitrile group that further increased the intermolecular interactions in the PAN system (Gupta *et al.,* 1989; Bajaj *et al.,* 2001).

TABLE 2
Glass transition temperature of homoPAN, copolymers and terpolymers

AN:EA:FN (mol %)	Glass transition temperature, T_g (°C)
100:0:0	105
Copolymer	
95:5:0	81
90:10:0	66
85:15:0	68
80:20:0	70
Terpolymer	
90:2:8	81
90:4:6	74
90:6:4	70
90:8:2	67
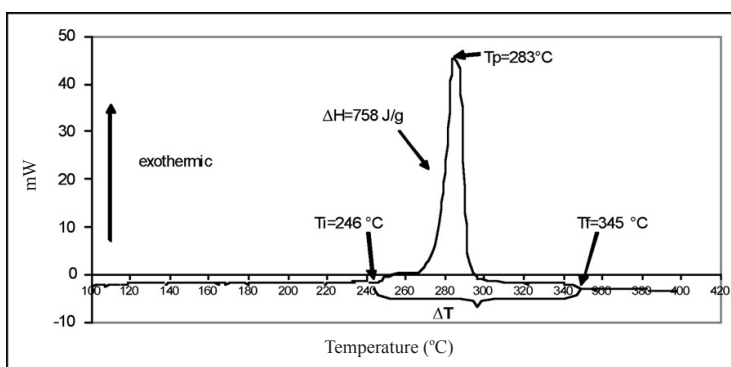
Fig. 2: DSC thermogram of homoPAN
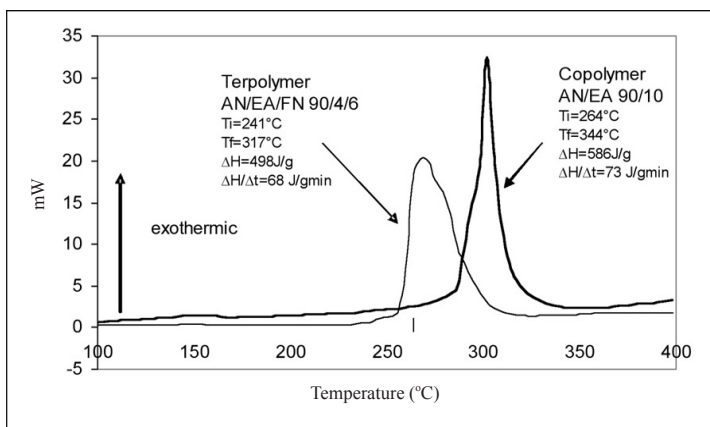
Fig. 3: DSC thermogram of copolymer and terpolymer

Figs. 2 and *3* show a comparison between DSC thermogram of PAN, copolymer, and terpolymer. The exothermic peak of homoPAN has a singlet, sharp, intense, and narrow peak starting from 246ºC to the final temperature, i.e. 345ºC. The heat liberated during the reaction (ΔH) was 758 Jg^{-1}. The singlet, intense, and narrow peak indicates that the rate of propagation is very high after the initiation of cyclization reaction through a radical mechanism (Gupta *et al.,* 1995). On the other hand, the exothermic process that involves heat evolution accomplished at the lowest rate in the case of AN/EA/FN 90/4/6 copolymer (68 $Jg^{-1}min^{-1}$), indicating that the exothermic reaction takes much longer time to be completed with lower heat liberation per time (Bajaj *et al.,* 1993). This is favourable in the production of carbon fibre because it reduces defects in polymer chains and increases the formation of ladder-like structure, and hence produces carbon fibre with good mechanical properties (Bajaj *et al.,* 1993).

Amongst homoPAN, copolymer and terpolymer, the AN/EA/FN 90/4/6 terpolymer achieved the lowest rate of heat liberation (68 $Jg^{-1}min^{-1}$), as compared to homoPAN and AN/EA copolymer. This indicates that FN slightly affects stabilization process by facilitating the cyclization reaction, as reported previously (Jamil *et al.,* 2007).

Thermogravimetric Analysis (TGA)

Table 3 shows the char yield obtained from the TGA thermogram. The char yield of copolymers is lower (40%) as compared to that of homoPAN (48%). The incorporation of EA enhances the level of degradation due to the higher amount of chain scission instead of the formation of the ladder-like structure. According to Rangarajan *et al.* (2002), other researchers have reported that there is an increase in weight loss with the increase in the comonomer content due to the disruption of nitrile sequence which ultimately results in poor char yield of carbon fibre. However, incorporating 6mol% of FN in the case of terpolymers increased the char yield to 46%. There might be a different degradation process of terpolymer as compared to that of copolymer. There are 4 stages in oxidative degradation. In the case of AN/EA 90/10 copolymer (*Fig. 4*), the weight loss in the region 30-100°C involved the vaporization of moisture. The weight loss in the first zone (100-240°C) is only 1.25% due to the evolution of HCN and NH_2 (Bajaj *et al.,* 1993). The second zone (240-350°C) has a rapid weight loss with a maximum weight loss of 31.94%. This is the most important stage because it is associated with the formation of ladder-like structure which produces volatile products (HCN, NH_2 along with other products such as CO_2 and H_2O) and subsequent chain scission (Bajaj *et al.,* 1996). This is followed by little weight loss of about 18.68% in the region 350-480°C. The final zone (480-900°C) showed a steady and slow weight loss (8.01% weight loss) up to 900°C and gave a char yield of 40%.

TABLE 3
Weight loss and char yield of PAN, copolymer and terpolymer

Monomer feed (mol%)	Weight loss (%)				Char yield (%)
	Zone 1 (30-250°C)	Zone 2 (250-350°C)	Zone 3 (350-480°C)	Zone 4 (480-900°C)	
PAN	1.61	23.21	13.17	14.27	47.74
AN/EA/FN					
90/10	1.25	31.94	18.68	8.01	40.12
90/2/8	0.98	27.79	17.65	6.46	47.12
90/4/6	0.36	29.86	14.54	8.87	46.37
90/6/4	0.65	30.14	13.67	10.31	45.23
90/8/2	1.14	31.78	13.41	10.80	42.87
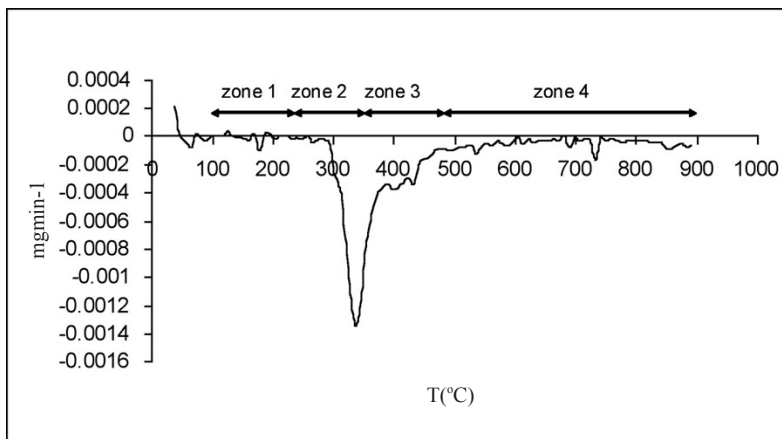
Fig. 4: DTG curve of AN/EA copolymer
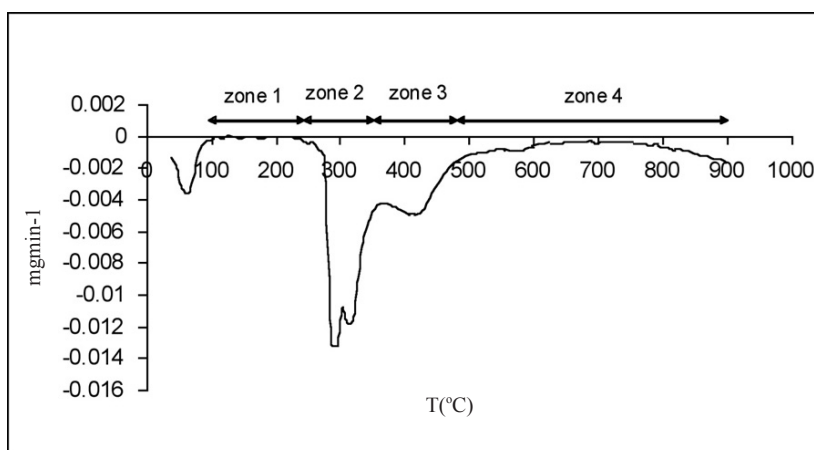
Fig. 5: DTG curve of AN/EA/FN terpolymer

On the other hand, the AN/EA/FN 90/4/6 terpolymer (see *Fig. 5*) has a different degradation pattern. The weight loss in the first zone is 0.36%, followed by 29.86% weight loss in the second zone. The weight loss in the third zone is 14.54% and the weight loss in fourth zone is 8.87%. This gave a char yield of 46% which is higher as compared to that of the AN/EA copolymer. This is due to the incorporation of FN which has increased the formation of ladder-like structure during the stabilization process, and subsequently increases the char yield of terpolymer (Jamil *et al.,* 2007).

CONCLUSIONS

Using the redox method in this study, the polymerization was achieved with a maximum conversion of 77% and 70% in the case of AN/EA copolymer and AN/EA/FN terpolymer respectively. Meanwhile, the introduction of EA had successfully reduced T_g of copolymer to 66°C as compared to that of the homoPAN (105°C). The initial cyclization temperature of copolymer increased

to 264°C as compared to that of the homoPAN (246°C). The incorporation of EA comonomer also reduced the char yield to ~40% which is unfavourable to the mechanical properties of PAN precursors. In order to overcome this problem, FN has successfully been incorporated into the terpolymer system to increase the thermal stability of terpolymers and consequently increase the char yield to 47%. FN was found to facilitate the exotherm process by reducing T_i to 241°C and the rate of heat liberation to 68 Jg^{-1}min^{-1}.

ACKNOWLEDGEMENTS

REFERENCES

Bajaj, P., Paliwal, D.K. and Gupta, A.K. (1993). Acrylonitrile-acrylic acids copolymers. I. synthesis and characterization. *Journal of Applied Polymer Science, 49*, 823-833.

Bajaj, P., Sen, K. and Bahrami, S.H. (1996). Solution polymerization of acrylonitrile with vinyl acids in dimethylformamide. *Journal of Applied Polymer Science, 59*, 1539-1550.

Bajaj, P., Sreekumar, T. V. and Sen, K. (2001). Thermal behavior of acrylonitrile copolymers having methacrylic and itaconic acid comonomers. *Polymer, 42*, 1707-1718.

Bhanu, V.A., Rangarajan, P., Wiles, K., Bortner, M. and Sankarpandian, M. (2002). Synthesis and characterization of acrylonitrile methyl acrylate statistical copolymers as melt processable carbon fiber precursors. *Polymer, 43*, 4841-4850.

Gupta, D.C. and Agrawal, J.P. (1989). Effect of comonomers on thermal degradation of polyacrylonitrile. *Journal of Applied Polymer Science, 38*, 265-270.

Gupta, A.K., Paliwal, D.K. and Bajaj, P. (1991). Acrylic precursors for carbon fibers. *Polymer Reviews, 31*, 1-89.

Gupta, A.K., Paliwal, D.K. and Bajaj, P. (1995). Effect of an acidic comonomer on thermooxidative stabilization of polyacrylonitrile. *Journal of Applied Polymer Science, 58*, 1161-1174.

Jamil, S.N.A.M.J., Daik, R. and Ahmad, I. (2007). Redox copolymerization of acrylonitrile with fumaronitrile as a precursor for carbon fibre. *Journal of Polymer Research, 14*, 379-385.

Jensen, J.O. (2003). Vibrational frequencies and structural determinations of fumaronitrile. *Theory and Computation in Chemistry, 631*, 231-240.

Jordan, E.F., Riser, G.R., Salber, C. and Wrigley, A.N. (1972). Terpolymers. I. The mechanical properties and transition temperature of terpolymers of n-octadecyl acrylate, ethyl acrylate and acrylonitrile. *Journal of Applied Polymer Science, 16*, 3017-3034.

Martin, S.C., Liggat, J.J. and Snape, C.E. (2001). In situ NMR investigation into the thermal degradation and stabilisation of PAN. *Polymer Degradation and Stability, 74*, 407-412.

Min, B.G., Son, T.W., Kim, B.C., Lee, C.J. and Jo, W.H. (1994). Effect of solvent or hydrophilic polymer on the hydration melting behavior of polyacrylonitrile. *Journal of Applied Polymer Science, 54*, 457-462.

Rangarajan, P., Bhanu, V.A., Godshall, D., Wilkes, G.L., McGrath, J.E. and Baird, D.G. (2002). Dynamic oscillatory shear properties of potentially melt processable high acrylonitrile terpolymers. *Polymer, 43*, 2699-2709.

408

Pertanika J. Sci. & Technol. Vol. 18 (2) 2010

Rintoul, I. and Wandrey, C. (2005). Polymerization if ionic monomers in polar solvents: Kinetics and mechanism of the free radical copolymerization of acrylamide/acrylic acid. *Polymer, 46*, 4525-4532.

Sarac, A.S. (1999). Redox polymerization. *Program Polymer Science, 24*, 1149-1204.

Tsai, J.S. and Lin, C.H. (1991). The effect of molecular weight on the cross section and properties of polyacrylonitrile precursor and resulting carbon fiber. *Journal of Applied Polymer Science, 42*, 3045-3050.

Wan, L.S., Xu, Z.K., Huang, X.J., Wang, Z.G. and Wang, J.L. (2005). Copolymerization of acrylonitrile with n-vinyl-2-pyrrolidone to improve the hemocompatibility of polyacrylonitrile. *Polymer, 46*, 7715-7723.

Pertanika J. Sci. & Technol. Vol. 18 (2) 2010

409

Development of Biodegradable Plastic Composite Blends Based on Sago Derived Starch and Natural Rubber

**Kiing Sie Cheong[1], Jaya-Raj Balasubramaniam[1], Yiu Pang Hung[1*],
Wong Sie Chuong[1] and Rajan Amartalingam[2]**
[1]Department of Basic Sciences and Engineering,
[2]Department of Crop Sciences, Faculty of Agriculture and Food Sciences,
Universiti Putra Malaysia Bintulu Campus,
97000 Bintulu, Sarawak, Malaysia
[*]E-mail: yiuph@btu.upm.edu.my

ABSTRACT

Polyethylene is a widely used packaging material, but its non-biodegradable nature can lead to waste disposal problems. This increases the concern in research and development of biodegradable plastics from natural resource as alternatives to petroleum-derived plastics. In this study, biodegradable plastic composites were prepared by blending thermoplastic starch with natural rubber in the present of glycerol as plasticizer. Local sago starch was cast with 0.5 to 10% of natural rubber to prepare the bioplastic. The products were characterized by differential scanning calorimetry (DSC), Fourier transform infrared spectroscopy (FTIR), water absorption test, biodegradable test, hydrolysis test, and mechanical analysis. Meanwhile, composite with natural rubber latex was increased from 0.5 to 10% showing that the melting temperature is in the range of 120 to 150˚C, but with no significant difference. The water absorption characteristics, biodegradability, and tensile strength decreased by 11.21%, 30.18%, and 20.733 MPa, respectively. However, the elongation at break was increased from 26.67 to 503.3%. The findings of this study showed that sago starch has a great potential in bioplastic production with good miscibility and compatibility.

Keywords: Biodegradable, sago starch, thermoplastic starch (TPS), natural rubber latex

INTRODUCTION

Polyethylene is a widely used packaging material due to its good material properties and low cost. However, these qualities have overshadowed its non-biodegradable nature, leading to waste disposal problems. Moreover, this has led to the research and development of biodegradable plastics from natural resources as alternatives to petroleum-derived plastics (Kim *et al.*, 2000).

One biopolymer showing a great promise is starch. Starch, obtained from renewable resources, has many advantages which include low cost, abundant supply, and environmental amity (Takahashi, 1986). Starch is composed of amylose and amylopectin, which are both polysaccharides made up of α-D-glucopyranosy units (French, 1984). Amylose is a linear (1-4) linked α-D-glucan and amylopectin, a highly branched molecule consisting of short chains of (1-4) linked α-D-glucose with (1-6) linked α-linked branches (Kennedy *et al.*, 1983). The ratio of amylase and amylopectin varies with the starch source, but it is typically 20:80 amylose to amylopectin (Orford *et al.*, 1987).

Sago palm is one of the important starch production crops in which *M. longispinum, M. sylvestre, M. microcanthum, M. sagu,* and *M. rumphii* are the important species widely used. Sago starch consists of oval granules with diameters in the range of 20 to 40 μm, and moisture contents ranging between 10.6% and 20.0%. The total amylose contents (lipid free starch) in sago starch

ranged between 24% and 31%, whereas the apparent amylose content (starch with lipid) was slightly lower, i.e. in the range of 24% to 30%. The gelatinization temperature for sago starch is high as compared to corn, peas and potatoes, but low than sweet potatoes, Tania and yam (Tian *et al*., 1991; Veletudie *et al*., 1995). These led to important properties of sago starch such as ease to gelatinize, high viscosity with proper extraction and easily moulded (Takahashi, 1986). Therefore, it shows that starch has a great potential to be produced into biodegradable polymer.

However, starch properties need to be improved with physical and/or chemical additions due to poor mechanical properties, processability, and water sensitivity (Choi and Kim, 1999). Common method used to improve these properties is the use of polymer blending. It is a method designed to generate materials with optimized chemical, structural, mechanical, morphological, and biological properties. Polymer blending can be defined as a mixture of two or more polymers in order to achieve a material that has certain properties of each of the compositions of the blend. Some researchers have previously reported on some polymer blends like starch/synthetic polymer blends which only enable partial environmental degradability (Martina and Herbert, 1996; Evangelista *et al*., 1991).

Due to the increased concern over environmental pollution caused by non-biodegradable materials, the development of biodegradable materials for wide application is on demand. As starch-based materials have been proven to be good biodegradable sources, sago starch (which is readily available in Sarawak) was chosen to be used in developing biodegradable plastic composite with a natural rubber blend. Natural rubber latex is used because it is a renewable resource which can be biodegraded and it contains natural stabilizers (i.e. proteins and lipids) that could help compatibilization with starch (Antoine *et al*., 2004). Therefore, the objectives of the present study were to develop starch-rubber composite using sago starch and biodegradable plastic composite blend with good compatibility, miscibility, and biodegradability.

MATERIALS AND METHODS

Natural rubber latex was extracted from *Hevea brasiliensis* tree in UPMKB field and it was stabilized by adding 2.5% of ammonia solution. Meanwhile, sago starch was supplied by MuiHiong Foodstuff Company. Glycerol (Fisher Scientific) and sodium hydroxides (System) used were analytical grade reagents.

Film preparation

The method used was modified from that of Antoine *et al.* (2004). Sago starch (3% wt/wt) was gelatinized at 75°C and continuous stirred before it was dissolute in an autoclave at 120°C, 110 kPa for 30 minutes. Glycerol was added as plasticizer with 30% w/w relative to starch (dry basis). Thermoplastic starch-latex samples, in the ratios of 100:0, 99.5:0.5, 98.5:1.5, 97.5:2.5, 96.5:3.5, 95:5 and 90:10, were prepared. The mixture was then homogenized using an ultrasonic homogenizer (OMNI Rupter 250) under 30% power for 6 minutes. The products were dried at room temperature for 3 days before they were oven dried at 50°C overnight.

Film Characterization

Mechanical properties

Film products were tested for their tensile strength and elongation at break in accordance with the ASTM D 638M standard.

Differential scanning calorimetry

The film products of 10 mg were encapsulated in Tzeroaluminum pans. The sample pan was then heated at 20˚C/min from 20˚C to 200˚C. The melting temperatures (Tm) were also recorded.

Fourier transform infrared spectroscopy

The fourier transform infrared (FTIR) spectra of the film products was recorded to be between 4000 and 500 cm^{-1} of wavelength.

Water absorption

The method used was according to Chandra and Rustgi's (1996). The film products, in the size of 2.0 x 3.5 cm, were dried for 6 hours at 50˚C before they were cooled and weighed. The samples were soaked in distilled water at 23 ± 1˚C. The samples were periodically weighted every 4 weeks to record any change in their weights. The percentage of the water absorption by films was then calculated using the following formula: $W_f = \dfrac{w_w - w_c}{w_c}$ x 100, where W_C represents conditioned weight, W_w is wet weight, and % W_f represents the % of the final weight increase.

Film Biodegradability

Simple hydrolysis

The method used was according to the one proposed by Arvanitoyannis *et al.* (1997). The samples in the size of 1.5 x 3.0 cm were soaked in 20 ml distilled water at 70˚C. The changes in the weight were measured every 2 hours in order to record the weight losses versus time.

Alkali hydrolysis

The method used was that of Arvanitoyannis *et al.* (1997). The samples with the size of 1.5 x 3.0 cm were soaked in 20 ml sodium hydroxide at 70˚C. The changes in weight were measured every 2 hours to record the weight losses versus time.

Soil burial

The method employed was according to that of Arvanitoyannis *et al.* (1997). For this purpose, some film products, in the size of 3.0 x 4.0 cm, were buried into mineral soil. The films were removed, rinsed with distilled water and dried in an oven at 50˚C for 24 hours before they were weighed. The test was conducted every 30 days up to 90 days of soil burial.

RESULTS AND DISCUSSION

Mechanical Properties

Both the tensile strength and elongation at break of thermoplastic starch/ natural rubber latex blends are summarized in Table 1. The mechanical profiles show that the tensile strength reduced as the percentage of the natural rubber in films increased, whereas the elongation at break was increased with the increase in the percentage of the natural rubber used in the films. Films with natural rubber contents, ranging from 0.5 to 10%, showed significantly less tensile strength as compared to the ones without any natural rubber. In particular, TPS90.0NR10.0 and TPS95.0NR5.0 exhibited a high elongation at break with the values of 420.00 and 503.33%, respectively. The results that showed

natural rubber which was used as a reinforcement agent in starch blends could cause a reverse effect on the mechanical strength. In addition, poor interfacial interaction between natural rubber and starch matrix limits the mechanical solicitation of the blends.

TABLE 1

The effect of NR treatment on the tensile strength and elongation at break of TPS films

Treatment	Mechanical properties	
	Tensile strength (MPa)	Elongation at break (%)
TPS100NR0	25.200[a]	26.67[b]
TPS99.5NR0.5	16.000[b]	30.00[b]
TPS98.5NR1.5	10.233[bc]	23.33[b]
TPS97.5NR2.5	8.600[c]	23.33[b]
TPS96.5NR3.5	7.200[c]	23.33[b]
TPS95.0NR5.0	5.367[c]	420.00[a]
TPS90.0NR10.0	4.467[c]	503.33[a]

Note: The same alphabets (within column) indicate no significant difference between mean using Tukey's test at P=0.05

Water Absorption Properties

The effect of the NR treatment on the TPS films under water absorption test is shown in Table 2. It can be seen that the ability of film to absorb water generally decreases with the (high) amount of NR blended with the TPS film. According to data analysis, however, the water absorption capacity was not significantly affected by the increases in natural rubber content from 0 to 10%. Meanwhile, water absorption capacity plays an important role in the degradability of bio-based materials. The films with a high amount of starch readily absorbed water due to the present of hydroxyl groups. Although water absorption capacity is an advantage for bio-based materials, it also becomes a drawback when applied as packaging materials. According to Zhao *et al*. (2005), this disadvantage could be overcome by methylation of starch molecule where hydrophobic of the films would be increased by replacing the hydroxyl group with the methyl group.

TABLE 2

The effect of the NR treatment on the TPS films under water absorption test

Treatment	Water absorption capacity (%)			
	1st week	2nd week	3rd week	4th week
TPS100 NR0	47.751[ab]	38.882[a]	34.732[ab]	34.656[ab]
TPS99.5NR0.5	47.199[ab]	45.632[a]	44.021[a]	44.095[a]
TPS98.5NR1.5	50.913[a]	44.784[a]	42.454[ab]	42.439[ab]
TPS97.5NR2.5	48.300[a]	38.176[a]	39.328[ab]	42.537[ab]
TPS96.5NR3.5	42.531[ab]	44.386[a]	34.866[ab]	34.983[ab]
TPS95.0NR5.0	41.609[ab]	36.933[a]	34.039[ab]	34.084[ab]
TPS90.0NR10.0	30.314[b]	26.026[a]	23.454[b]	23.446[b]

Note: The same alphabets (within column) indicate no significant difference between mean using Tukey's test at P=0.05

The Thermal Profile

The thermal profile of TPS/NR film is shown in Table 3. The thermal profile of the film products showed no significant difference in melting point with increase in natural rubber content from 0.5% to 10%. TPS films showed the melting points in the range of 120 to 150˚C. Nevertheless, there was no significant difference in the melting points, and this was probably due to the low amount of rubber present in the entire TPS films. However, TPS films without natural rubber also showed the melting points of more than 100˚C. This characteristic may enable the application of TPS films as packaging materials which could be heat over 100˚C.

TABLE 3
Effect of NR treatment on melting point of TPS films

Treatment	Melting temperature (˚C)
TPS100NR0	120.273[a]
TPS99.5NR0.5	129.407[a]
TPS98.5NR1.5	130.397[a]
TPS97.5NR2.5	133.643[a]
TPS96.5NR3.5	131.433[a]
TPS95.0NR5.0	134.250[a]
TPS90.0NR10.0	149.130[a]

Note: The same alphabets (within column) indicate no significant difference between mean using Tukey's test at P=0.05

The FTIR Analysis

The FTIR spectroscopic analysis of the entire TPS films did not exhibit any drastic changes in the spectra. Meanwhile, the FTIR spectrum of films exhibited a wide O-H stretching absorbance centred around 3400 cm-1, a slight C-H stretching band at 2921 cm-1, and a characteristic set of strong C-O stretching bands between 960-1190 cm-1. The TPS films buried in the soil showed a drastic reduction in the absorption of peaks corresponding to both the hydroxyl and fingerprint regions of the spectra. However, the changes in the absorption peaks were comparatively less in TPS97.5NR2.5, TPS96.5NR3.5, TPS95NR5, and TPS90NR10. The FTIR data in this study proved that the loss of starch material was due to biodegradation alone. Meanwhile, natural rubber functions as a coating material that protects the films from degradation. Hence, the films with high amounts of NR showed less change in the FTIR spectra. The weight loss was due to the microbial invasion and not because of the physical action alone. *Fig. 1* shows some FTIR spectra of the films before and after soil burial for 90 days.
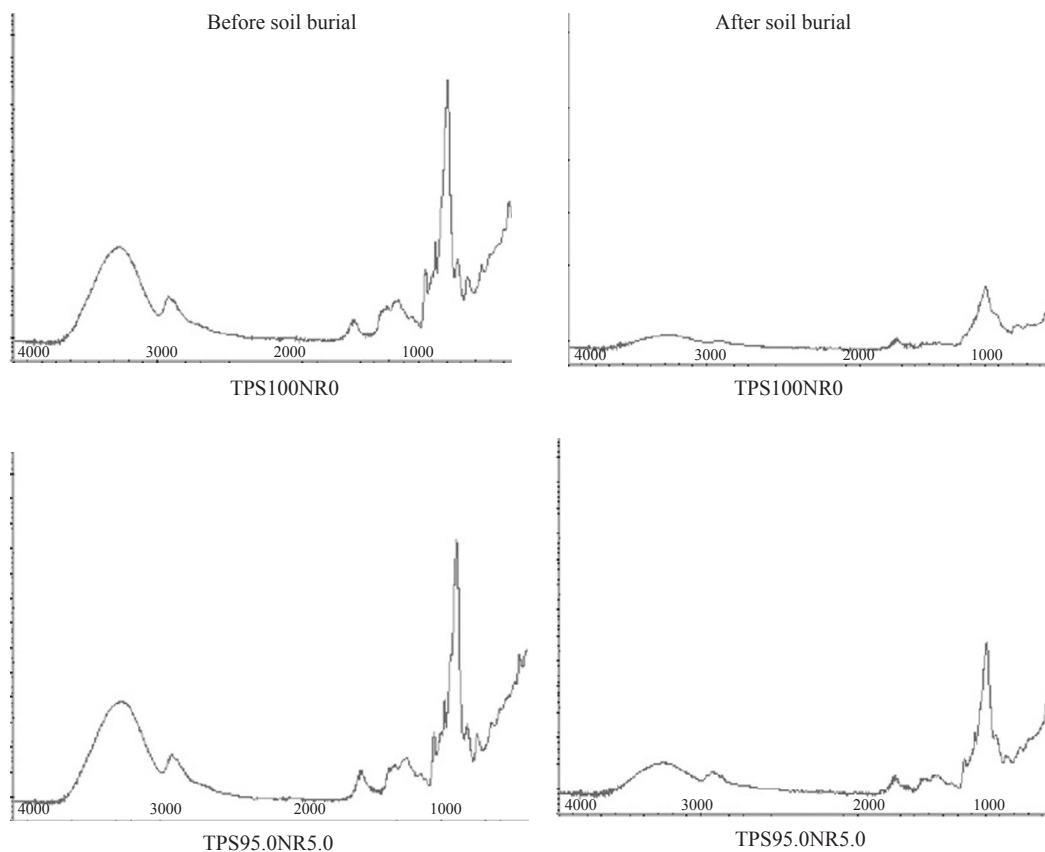
Fig. 1: Fourier Transform Infrared (FTIR) analyses before and after the soil burial for 90 days

Film Biodegradability

The data obtained from the simple hydrolysis test are shown in Table 4. Films with natural rubber content (i.e. from 3.5% to 10%) significantly experienced a slower weight loss as compared to the rest of the films. Films with higher amount of starch showed higher weight losses. This might be due to the loss of starch which got dissolved in water. Table 5 illustrates the results of the alkali hydrolysis test. All the films showed a drastic weight loss, particularly the TPS film without rubber. The alkali hydrolysis caused a higher weight loss as compared to the simple hydrolysis. Thus, NaOH was found to enhance the solubilization of gelatinized starch in the polymer blend (Arvanitoyannis *et al*., 1997). The purpose of using these methods for assessing the biodegradability of film was to prove that the synthesized film could be degraded in water with different values of pH. Higher pH values could accelerate the degradability of starch based film.

TABLE 4
Effect of the NR treatment on the TPS films under simple hydrolysis test

Treatment	Weight loss (%)					
	2 hours	4 hours	6 hours	8 hours	10 hours	12 hours
TPS100 NR0	55.278[a]	58.689[a]	60.849[a]	63.663[a]	66.933[a]	69.679[a]
TPS99.5NR0.5	49.812[a]	53.326[ab]	57.528[ab]	60.981[a]	62.876[a]	64.376[a]
TPS98.5NR1.5	46.342[ab]	49.812[ab]	55.736[ab]	57.709[ab]	58.148[ab]	61.264[ab]
TPS97.5NR2.5	40.198[abc]	42.035[bc]	42.566[bc]	42.590[bc]	42.626[bc]	42.703[bc]
TPS96.5NR3.5	28.599[bcd]	29.262[cd]	29.654[cd]	29.681[c]	29.843[c]	29.891[c]
TPS95.0NR5.0	32.605[bcd]	33.490[cd]	33.711[cd]	33.675[c]	34.032[c]	34.051[c]
TPS90.0NR10.0	21.268[d]	23.574[d]	24.461[d]	28.096[c]	28.270[c]	28.340[c]

Note: The same alphabets (within the column) indicate no significant difference between the mean using Tukey's test at P=0.05

TABLE 5
Effect of the NR treatment on the TPS films under alkali hydrolysis test

Treatment	Weight loss (%)					
	30 min	60 min	90 min	120 min	150 min	180 min
TPS100NR0	100.000[a]	100.000[a]	100.000[a]	100.000[a]	100.000[a]	100.000[a]
TPS99.5NR0.5	41.900[b]	64.773[bc]	71.361[bc]	73.501[b]	75.441[b]	76.843[b]
TPS98.5NR1.5	53.290[b]	75.098[ab]	77.006[ab]	77.542[ab]	78.288[ab]	78.864[b]
TPS97.0NR2.5	43.280[b]	54.983[bc]	57.348[bcd]	58.410bc	59.756bc	60.369bc
TPS96.0NR3.5	52.290[b]	57.241[bc]	58.100[bcd]	58.388[bc]	58.901[bc]	59.238[bcd]
TPS95.0NR5.0	44.140[b]	48.009[bc]	48.558[cd]	48.833[c]	49.101[c]	49.316[cd]
TPS90.0NR10.0	36.410[b]	37.977[c]	38.049[d]	38.174[c]	38.275[c]	38.589[d]

Note: The same alphabets (within the column) indicate no significant difference between the mean using Tukey's test at P=0.05

Kiing Sie Cheong, Jaya-Raj Balasubramaniam, Yiu Pang Hung, Wong Sie Chuong and Rajan Amartalingam

The soil burial test provides a real environment for the polymer to biodegrade. A rapid weight loss was observed in all the films with different compositions during the first 30 days of the experiment as shown in Table 6. After 90 days of exposure to soil, the films were found to have reduced in size and become hard and fragile. The film deterioration was indicated by the loss in their total weight after soil burial for the three-month period. There were black and red spots on the surface of the films indicating the soil microbial invasion. *Fig. 2* shows films without natural rubber which had experienced a rapid degradation as compared to the rest of the films.

TABLE 6
Effect of the NR treatment on the TPS films in the soil burial test

Treatment	Weight loss (%)		
	30th days	60th days	90th days
TPS100.0NR0	44.64[a]	50.46[a]	59.35[a]
TPS99.5NR0.5	23.50[a]	46.58[a]	59.95[a]
TPS98.5NR1.5	20.19[a]	58.59[a]	59.21[a]
TPS97.5NR2.5	24.33[a]	42.34[a]	43.81[a]
TPS96.5NR3.5	21.21[a]	32.30[a]	33.21[a]
TPS95.0NR5.0	26.77[a]	38.59[a]	42.56[a]
TPS90.0NR10.0	18.94[a]	28.29[a]	29.17[a]

Note: The same alphabets (within the column) indicate no significant difference between the means using Tukey's test at P=0.05

TPS100.0NR0

Before soil burial

After 90 days of soil burial

Before soil burial

After 90 days of soil burial
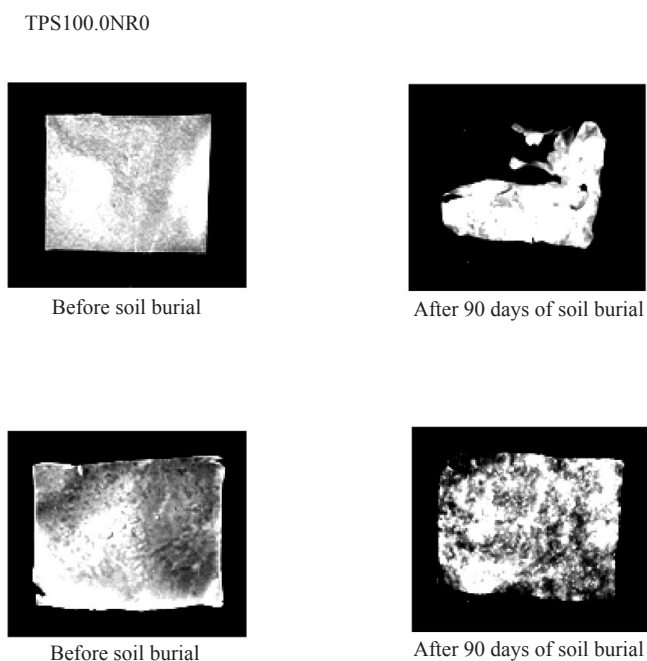
Fig. 2: The evolution of the physical state of the TPS films
before the soil burial during 90 days of the experiment

CONCLUSIONS

Sago starch and rubber latex blends showed a wide range of physical and mechanical properties. This shows that sago starch has a good potential in producing bioplastic with good miscibility and compatibility. Further study using different plasticizers may produce blends with the optimum properties for different applications.

ACKNOWLEDGEMENTS

REFERENCES

Antoine, R., Luc, R. and Robert, G.G. (2004). Synthesis and properties of composites of starch and chemically modified natural rubber. *Polymer, 45*, 7813-7820.

Arvanitoyannis, I., Kolokuris, I., Nakayama, A. and Aiba, S. (1997). Preparation and study of novel biodegradable blends based on gelatinized starch and 1, 4-transpolyisoprene (guttapercha) for food packaging or biomedical applications. *Carbohydrate Polymers, 34*, 291-302.

Chandra, R. and Rustgi, R. (1997). Biodegradation of maleated linear low-density polyethylene and starch blends. *Polymer Degradation and Stability, 56*, 185–202.

Choi, E.J. and Kim, C.H. (1999). Structure-property relationship in PCL/starch blend compatibilized with starch-PCL copolymer. *Polymer Physics, 37*(17), 2430-2438.

Evangelista, R. L., Nikolov, Z. L., Sung, W., Jane, J. L. and Gelina, R. (1991). Effect of compounding and starch modification properties of starch-filled low density polyethylene.Ind. *Reviews in Chemical Engineering, 30*, 1841-1846.

French, D. (1984). *Starch: Chemistry and Technology*. New York: Academic Science.

Kennedy, J.F., Griffiths, A.J. and Atkins. D.P. (1983). The application of hydrocolloids: Recent development, future trends. In G.O. Phillips, D.J. Wedlock and P.A. Williams (Eds.), *Gums and stabilisers for food industries 2* (pp. 430-431). Oxford: Pergamon Press.

Kim, M.N., Lee, A.R., Yoon, J.S. and Chin, I.J. (2000). Biodegradation of poly (3-hydroxylbutyrate), Sky-Green and Mater-Bi by fungi isolated from soils. *European Polymer Journal, 36*, 1677-85.

Martina, W. and Herbert, B. (1996). Influence of natural fibres on mechanical properties of biodegradable polymers. *Industrial Crops and Products, 8*, 105-112.

Orford, P.D., Ring, S.G., Carroll, V., Miles, M.J. and Morris, V.J. (1987). The effect of concentration and botanical sources on the gelation and retrogradation of starch. *Journal of Science Food Agriculture, 39,* 169-177.

Takahashi, S. (1986). Some useful properties of sago starch in cookery science. In N. Yamada and K. Kainuma (Eds.), *Proceeding of the Third International Sago Symposium* (pp. 208-216). Tokyo: Tokyo Press.

Tian, S.J., Rickard, J.E. and Blanshard, J.M.W. (1991). Physicochemical properties of sweet potato starch. *Journal of Science Food Agriculture, 57*, 459-491.

Veletudie, J.C., Guadeloupe, L., Colonna, P., Bouchet, B. and Gallant, D.J. (1995). Gelatinization of sweet potato, Tania and yam tuber starches. *Starch, 47*, 289-306.

Zhao, G., Liu, Y., Fang, C., Zhang, M., Zhou, C. and Chen, C. (2005). Water resistance, mechanical properties and biodegradability of methylated-cornstarch/poly (vinyl alcohol) blend film. *Polymer Degradation and Stability*, *91*(4), 703-711.

Vulcanisation and Coagulant Dipping of Epoxidised Natural Rubber Latex

Dazylah Darji[*] and Ma'zam Md Said
Rubber Research Institute of Malaysia,
Malaysian Rubber Board,
P.O Box 10150, 50908 Kuala Lumpur, Malaysia
[*]*E-mail: dazylah@lgm.gov.my*

ABSTRACT

Epoxidised Natural Rubber (ENR) is now a commercially available polymer produced by chemical modification of natural rubber. Currently, three types of ENR are commercially available, and these are ENR 10, ENR 25, and ENR 50 with 10%, 25%, and 50% mol epoxidation, respectively. Studies on prevulcanisation of ENR 50 and postvulcanisation of the latex films were carried out. The objective of this study was to develop ENR 50 that could be dipped easily in coagulant dipping solution to produce dipped products. Several attempts were made by compounding prevulcanised ENR 50 at various sulphur levels ranging from 0.5 to 3.0 pphr. Using suitable coagulant dipping systems, ENR 50 film could be formed despite the high contents of non-ionic surfactant. It was found that the tensile strength of prevulcanised ENR 50 film decreased with the increase in the sulphur level. The results show that as level of sulphur increased, M_{300} also increased to an optimum value of 1.5 pphr of sulphur. For the postvulcanised ENR 50 film, however, the tensile strength increased and then decreased with the increasing sulphur level. Meanwhile M_{300} increased with the increasing postvulcanization time and sulphur level. The postvulcanisation of ENR 50 film seems to be a more effective way of increasing tensile properties than by prevulcanisation of ENR 50.

Keywords: Epoxidised natural rubber latex, prevulcanisation, postvulcanisation

INTRODUCTION

Natural rubber (NR) latex has invariably become the first choice for the production of most of latex dipped products. However, NR latex films have very poor resistance to rubber solvents and certain oxidising chemicals. As a result, chemical modifications of NR have been carried out to improve these important properties. The chemical modifications of NR were carried out either in latex or in dry phase. Basically, the chemical modifications of NR can be categorised into three main categories, namely grafting copolymerisation of NR, hydrogenation NR, and epoxidised NR (ENR). Epoxidised natural rubber (ENR) was produced by attaching the epoxy groups to NR molecule. The epoxidation reaction involves the addition of oxygen atom to the carbon-carbon double bonds of olefinically unsaturated polymer, thereby converting them to oxirane (epoxide) ring (Gelling, 1991).

Despite the fact that any desired epoxidation level can generally be achieved using this modification route, only three grades of ENR (ENR10, ENR 25, and ENR50) containing 10, 25, and 50% mol epoxidation levels, respectively are produced by the Malaysian Rubber Board (MRB) at present. These three grades of ENR should cover the range of desirable properties for most of the intended applications. ENR has been shown to exhibit beneficial properties, particularly its

oil and chemical resistance, air permeability, and adhesive properties (Gelling, 1991). It would be useful if these desirable properties of ENR could be exploited in latex dipped product applications. In addition, the ENR latex with a polar epoxy group could be expected to confer a certain degree of chemical resistance to products prepared from it.

However, uncompounded epoxidised natural rubber latex has been shown to be incapable of being satisfactorily processed by coagulant dipping due to its inability to gel on the former and because of the formation of a very thin latex deposit. The main reason for this observation is the stabilization of ENR latex by high level of non-ionic surfactant. Whilst the non-ionic surfactant is necessary to keep the latex stable during epoxidation reaction with acetic acid and hydrogen peroxide, it however keeps the latex chemically too stable against the calcium salt coagulant such as calcium nitrate.

ENR latex was compounded with sulphur vulcanising system in the attempts to develop ENR latex that could easily be dipped in coagulant. This process is called prevulcanisation. The prevulcanisation of NR latex, a process of chemical crosslink that takes place inside the particle, is generally performed by using sulphur, peroxide, and γ-radiation system. The vulcanisation of latex was proposed by Schidrowitz (1923) and subsequently by Schidrowitz and Stutchbury (1925). The production of prevulcanised (Gorton, 1979) latex involves heating of raw latex with various compounding ingredients such as accelerators and sulphur until the required degree of crosslinking is obtained as indicated by the relevant parameters. Using this system, this is not be possible and hence, ENR dipped film has to be developed.

EXPERIMENTAL DESIGN

Prevulcanisation of Latex

ENR latex and potassium hydroxide were added into stainless steel container and stirred for 10 minutes at room temperature. As shown in Table 1, sulphur at various levels, zinc dibutyl dithiocarbamate, tetra methyl thiuram disulphide, zinc oxide, and antioxidant were added into the container and stirred for 10min. After that, the latex was heated at 60°C for 3 hours. The vulcanised latex was cooled and then sieved. Later, the latex properties were tested.

TABLE 1
Level of sulphur added to prevulcanisation epoxidised natural rubber latex (ENRL)

Formulation	A	B	C	D	E	F
Level of sulphur (pphr)	0.5	1.0	1.5	2.0	2.5	3.0

Coagulant Dipping Process

The former was first immersed in a 10% coagulant solution. After withdrawing the former from the solution, the solvent was allowed to evaporate, leaving either a very viscous concentrated solution or a dry deposit of calcium nitrate. The coated former was then immersed in the ENR latex compound and allowed to dwell for a predetermined time. This time, the coagulant migrated from the former into the latex and this resulted in the destabilization/gelation of the latex particles adjacent to the former and in the zone of the diffusing ions. The gelled deposit was vulcanized at

100ºC in the oven, postvulcanised for 0.5, 1.0, 1.5, 2.0, 2.5, 3.0, 6.0, and 22.0 hours. The films were cooled and stripped-off from the former. Tensile test was carried out according to ISO 37:1998 test method. Type 2 dumbells were cut parallel to the grain of the films. The test was carried out at room temperature (23±4ºC) using the 'Instron 5565' tensile machine.

RESULTS AND DISCUSSION

The Effect of Sulphur Level on the Tensile Properties of Prevulcanised ENR Latex Films

The prevulcanisation of ENR latex with was prepared at various levels of sulphur and the effects on the tensile properties were evaluated. *Fig. 1* illustrates the increase in the level of sulphur has caused the tensile strength to slightly decrease. However, the value of tensile modulus M300 was slightly increased with 0.5, 1.0, and 1.5 pphr of sulphur levels but decreased at 2.0, 2.5, and 3.0 pphr of sulphur levels. The tensile strength of latex films is largely dependent upon the amount of sulphur added. Thus, it can be stated that increasing the amount of sulphur would theoretically increase the strength of vulcanisate. Based on the result, the abrupt decrease in the tensile strength at 2.0-3.0 pphr sulphur was observed, and this indicated that the level of sulphur had passed the optimum level of sulphur for the maximum tensile strength of vulcanised ENRL film.
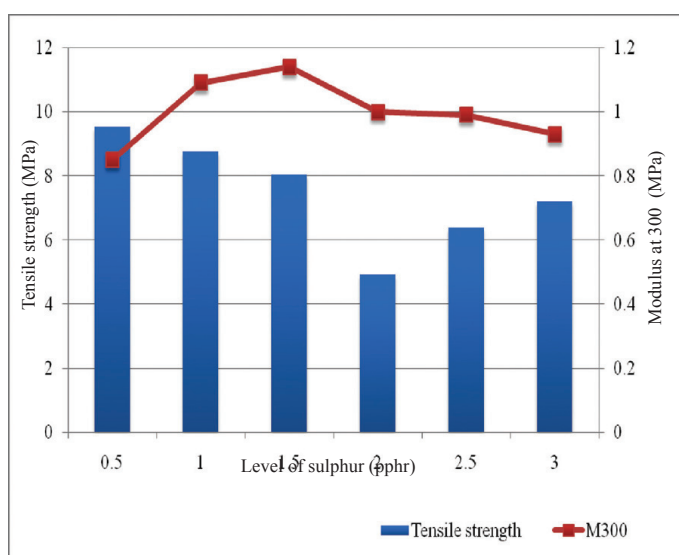
Fig. 1: Effect of the sulphur level on the tensile properties

Effect of Sulphur Levels and Postvulcanisation Time on Tensile Properties of Postvulcanised ENRL Films

The postvulcanisation studies of ENRL films were also carried out in order to improve the tensile properties of prevulcanisation. The tensile strength and modulus at 300 for the postvulcanised ENRL films prepared at various sulphur levels are shown in *Figs. 2* and *3*, respectively. The results of the tensile strength are generally in the range of 3-12 MPa. Meanwhile, the tensile strength for 1.0 pphr and 3.0 pphr of sulphur was higher as compared to the ones for 0.5, 1.5, 2.0, and 2.5 pphr of
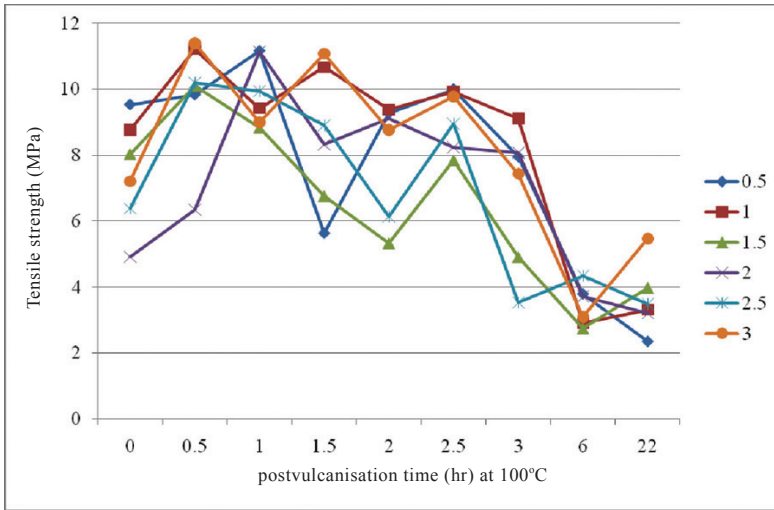
Fig. 2: The effects of postvulcanisation time on the tensile strength of ENRL films at various sulphur levels
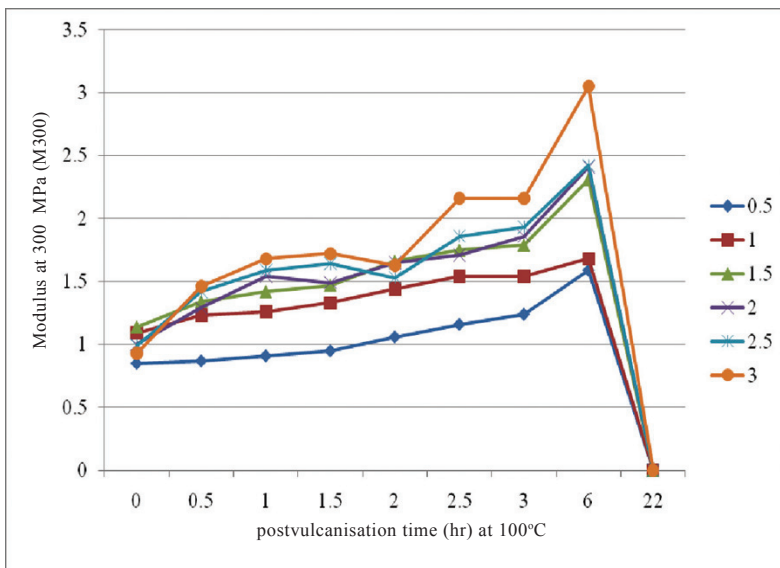
Fig. 3: The effects of postvulcanisation time on the tensile modulus of ENRL films at various sulphur levels

sulphur. When postvulcanised for 0.5 hours, the tensile strength was found to increase but it then decreased with the increasing sulphur content over the range of sulphur levels studied. However, the was a cyclical increase observed while the tensile strength was found to decrease over the range of postvulcanisation time. These results are significant as the changes in the tensile strength values were substantial in the range 2-4 MPa, and were observed for all the studied samples. Nonetheless, the reason for this phenomenon is still not clear.

An interesting feature is that the tensile modulus M300 value increased with postvulcanisation time quite significantly over a wide range of postvulcanisation times for all the compounds containing sulphur. Meanwhile, the postvulcanisation of ENR latex film is much more effective in increasing the degree of crosslinking as compared to prevulcanisation. The range of M300 values obtained for all the samples is 0.8-3.0 MPa. The modulus result showed that when the level of sulphur was increased, M300 also increased. The highest M300 value for ENRL vulcanisate was obtained using 3 phr of sulphur. The M300 value was dramatically reduced to zero after 22 hours of heating, suggesting that an extensive oxidation of the ENR had occurred.

CONCLUSIONS

Coagulant dipped films could be formed from compounded ENRL-50 using suitable coagulant systems. The postvulcanisation of ENRL-50 films is a more effective way of increasing crosslink density as compare to using prevulcanisation of ENRL-50

ACKNOWLEDGEMENTS

REFERENCES

Gelling, Ir. (1991). Epoxidised natural rubber. *Journal of Natural Rubber Research, 6*(3), 184-205.

Gorton, Adt. (1979). The production and properties of prevulcanized natural rubber latex. *Natural Rubber Technology, 10*, Part 1.

Schidrowitz, P. (1923). Prevulcanization of Latex and Its Use to Manufacture Dipped *British Patent 19345.*

Schidrowitz, P. and Stutchbury, P.M. (1925). Manufacture of Rubber *Us Patent 1530164.*

The Effect of Polypropylene Maleic Anhydride (PPMAH) on Properties of Polypropylene (PP)/Recycled Acrylonitrile Butadiene Rubber (NBRr)/ Rice Husk Powder (RHP) Composites

Ragunathan Santiagoo[1*], Hanafi Ismail[1] and Kamarudin Hussin[2]

[1]*School of Materials and Mineral Resources Engineering, Universiti Sains Malaysia,*
Nibong Tebal, 14300 Pulau Pinang, Malaysia
[2]*School of Environmental Engineering, Universiti Malaysia Perlis,*
Kompleks Pengajian Jejawi 3, 02600 Jejawi, Perlis, Malaysia
[*]*E-mail: ragunathan25@yahoo.com*

ABSTRACT

The effect of polypropylene maleic anhydride (PPMAH) on tensile properties and morphology of polypropylene (PP)/recycled acrylonitrile butadiene rubber (NBRr)/ rice husk powder (RHP) composites has been studied. The composites were prepared through melt mixing at 180ºC for 9 minutes using 50 rpm rotor speed. The specimens were analyzed using different techniques, namely tensile test and Scanning Electron Microscopy (SEM). The results obtained showed that the tensile strength and Young's modulus of the modified composites were increased, while the elongation at break showed the opposite trend as compared with the unmodified composites. The morphology results support the tensile properties and these indicated a better interaction between the filler and matrix with the presence of PPMAH as a compatibilizer.

Keywords: Recycled acrylonitrile butadiene rubber, polypropylene, physical properties, PPMAH

INTRODUCTION

Thermoplastic elastomers (TPEs) are advanced polymeric materials with fill the gap between an elastomer and plastomer which is crystalline (Golden *et al*., 1996). Its combined properties in strength and toughness have attracted many researches in this area. Besides, TPE has also been found to be cheap, recyclable, biodegradable, and environmentally friendly (Paul and Newman, 1978). Elastomer, such as recycled acrylonitrile butadiene rubber (NBR), has gained much interest in TPE production due to its availability in market, especially from the surgical glove industries. Meanwhile, cheap fillers from the agricultural wastes such as oil palm empty fruit bunch, rice husk ash, jute fibre, rubber wood powder, and cellulose fibres have been investigated as fillers in elastomers and plastics (Satyanarayana and Arizaga, 2009) due to their vast existence in the agricultural sector.

Lignocellulose materials such as rice husk powder (RHP) from the agricultural waste may serve as a good additive in plastic materials. However, as far as TPEs are concerned, very limited studies have been reported on rice husks as fillers in the PP/NBRr composite. It is because these composites are found to be incompatible or immiscible due to the poor physical and chemical interactions between the phases. This incompatibility may be due to the fact that the polyolefin is non-polar and hydrophobic, whereas lignocelluloses materials such as RHP are polar because of the –OH groups in the cellulose (Satyanarayana and Arizaga, 2009). In this study, surface modification or treatment using compatibilizing agents for the purpose of making the polyolefin chains to become

more hydrophilic had been performed. Morphology studies of the tensile fracture surfaces of PP NBRr/RHP composites, with and without PPMAH, were also carried out to correlate the change in the morphology with properties.

EXPERIMENTAL

Materials

Polypropylene (PP) used in this work was supplied by Titan PP Polymers (M) Sdn. Bhd., in Johor, Malaysia (code 6331). It has a melt flow index and density of 14 g/10 min at 230° C and 0.9 g/cm^3, respectively. The polypropylene maleic anhydride (PPMAH) was supplied by Bayer (M) Sdn. Bhd. in Selangor, Malaysia. The recycle acrylonitrile butadiene rubber (NBRr), with 33% acrylonitrile content and density of 0.98 g/cm^3, was obtained by grinding nitrile rubber gloves retrieved from Juara One Resources Sdn Bhd., Penang, Malaysia. The range of particle size of NBRr used in this study was 300 µm – 500 µm and the density of NBRr was 1.015 g/cm^3. The rice husks, containing 35% of cellulose, 25% of hemicelluloses, 20% of lignin and 17% of ash by weight, were supplied by a rice factory, Thye Heng Chan Enterprise Malaysia Sdn. Bhd., located in Penang. The rice husks were dried at 110ºC for 24 hours in a vacuum oven prior to grinding for a particle size of 300-500 µm and with a density of 1.4702 g/cm^3. *Fig. 1* (*a-b*) show the scanning electron micrograph of recycled NBR powder and rice husk powder at a magnification of 21x.
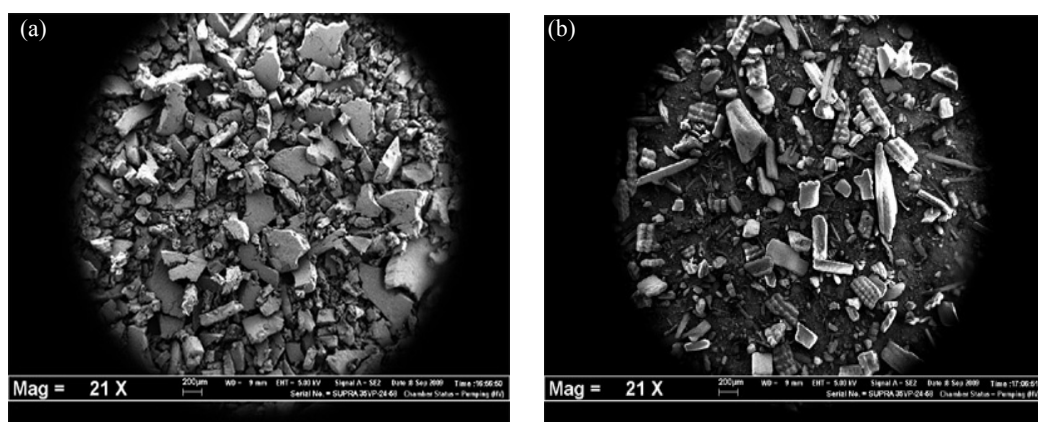
Fig. 1: Scanning electron micrograph at magnification of 21x for
(a) Recycled NBR powder, (b) Rice husk powder

Preparation of the Composites

The formulation of the composites is given in Table 1.

TABLE 1
Formulation for PP/NBRr/RHP/PPMAH composites

Materials (pphr)	Composition											
	1	2	3	4	5	6	1a	2a	3a	4a	5a	6a
PP	100	80	70	60	50	40	100	80	70	60	50	40
NBRr	0	20	30	40	50	60	0	20	30	40	50	60
RHP	15	15	15	15	15	15	15	15	15	15	15	15
PPMAH	-	-	-	-	-	-	5	5	5	5	5	5

The composites were prepared by melt mixing using a Haake Rheomix Polydrive R 600/610 mixer at 180ºC at a rotor speed of 60 rpm. The PP was charged into the mixing chamber and melted for 4 min before the NBR was added. Subsequently, RHP was added at 6 min while mixing was continued for 3 more minutes and a total of 9 min mixing time.

Compression Moulding

Samples of the composites were compress moulded in an electrical heated hydraulic press. The moulding procedure involves a preheating of the samples for 7 min at 180ºC, followed by compressing of the mould for 2 min at the same temperature and subsequently cooling under pressure for another 2 min.

Tensile Properties

The tensile tests were carried out according to ASTM D638 using the Instron tensile machine model no 3366. Specimens in the form of one milimeter thick dumbell tensile were cut from the moulded sheets with a Wallace die cutter S6/1/6.A. A cross head speed of the tensile machine was maintained at 50 mm/min and the tests were performed at 25± 3ºC. Stress at peak (MPa), Young's modulus (MPa) and elongation at break (%) were also measured. All the experimental tests were repeated trice (3 times) and found to be consistent and reproducible.

Morphological Study

The morphology of the tensile fractured surfaces of the samples was analysed using the SUPRA36VP-24-58 Field Emmission Scanning Electron Microscope (FESEM). The fractured ends of the specimens were mounted on aluminium stub and sputter-coated with a thin layer of gold to avoid electrostatic charging during examination.
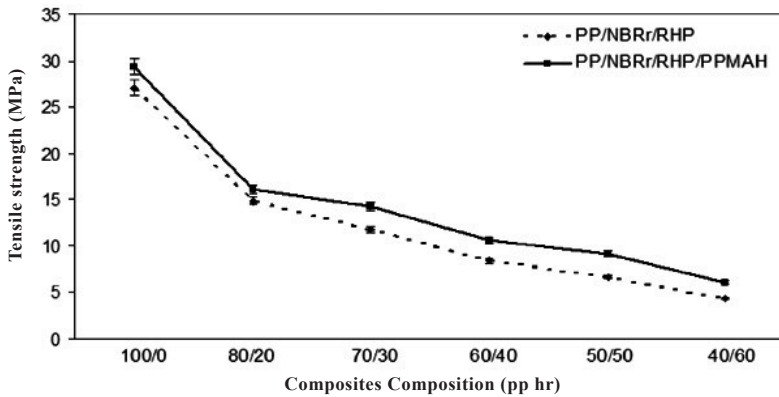
Fig. 2: Tensile strength of PP/NBRr/RHP and PP/NBRr/RHP/PPMAH composites
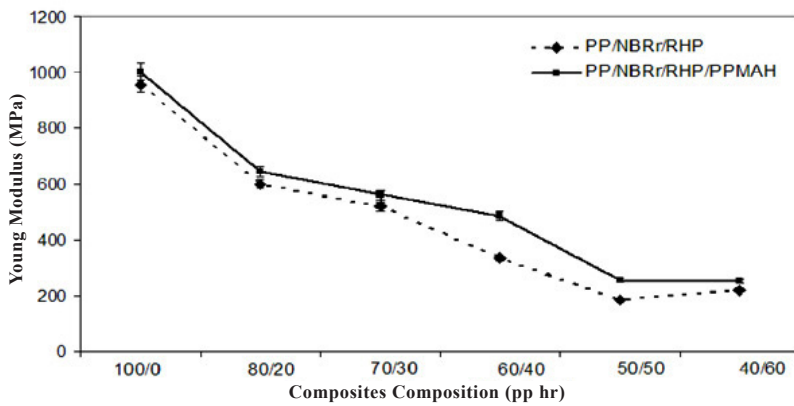
Fig. 3: Young's modulus of PP/NBRr/RHP and PP/NBRr/RHP/PPMAH composites

RESULTS AND DISCUSSION

Mechanical Properties

The effects of composite composition on the tensile properties of PP/NBRr/RHP are shown in *Figs. 2* and *3*. Tensile strength and Young's modulus of composites decrease with increasing amount of NBRr. These are due to the decrease in crystallinity of PP phase in the composite with the addition of NBRr. Similar findings have been reported by many researchers in their studies on thermoplastic elastomer composites (Zhang *et al.*, 2002; Ismail *et al.*, 2004). The stiffness and brittleness of the composite decreases with increasing amount of NBRr in the composite due to increasing content of elastomer which resulted in higher elongation of the material (Ismail *et al.*, 2009). These finding are in agreement with the elongation at break (E_b) for the respective composites as shown in *Fig. 4*. E_b increases with increasing of recycle nitrile rubber content. The compatibilization of PP-MAH in these composites has contributed in higher strength and stiffness as shown in *Figs. 2* and *3*. These are due to good adhesion between the PP and NBRr with RHP in the presence of PPMAH. The relatively low elongation at break for these composites supports the finding that the composite are getting more stiff and stronger after compatibilization.
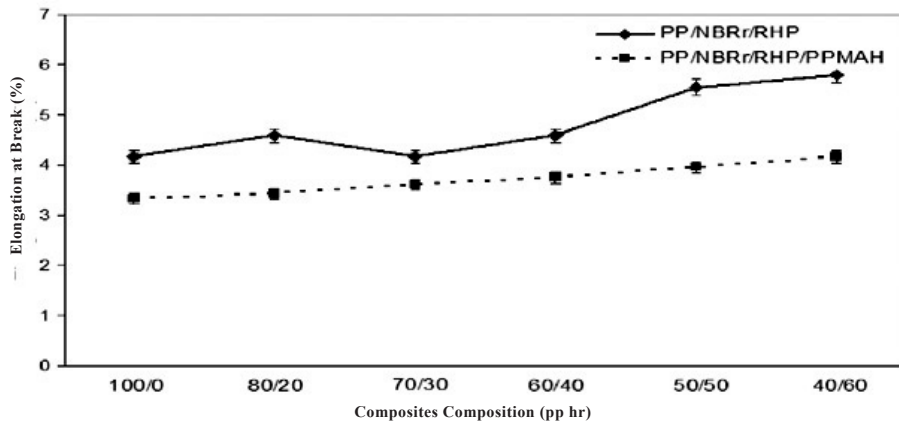
Fig. 4: Elongation at break of PP/NBRr/RHP and PP/NBRr/RHP/PPMAH composites
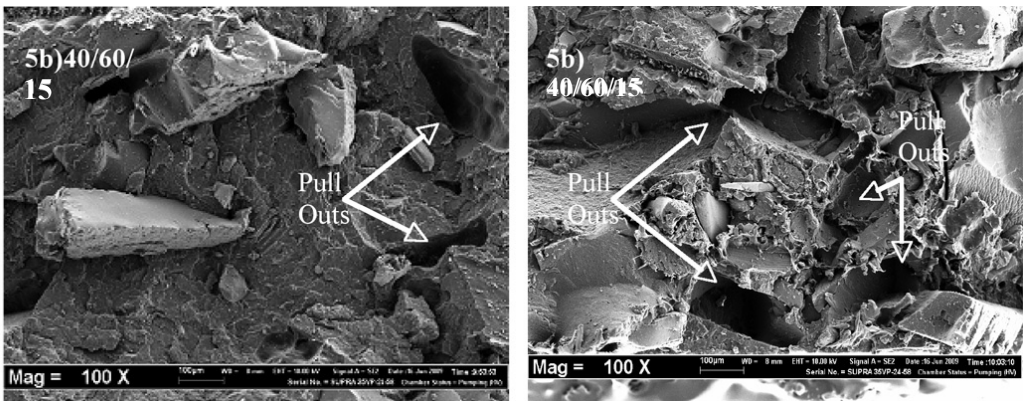
Figs. 5 (*a-b*): Scanning electron micrograph of tensile fractured surface of
PP/NBRr/RHP at magnification of 100x

Morphological Study

Figs. 5 (*a-b*) show the scanning electron micrographs of the tensile fractured surface of PP/NBRr/ RHP at the composition of 80/20/15 and 40/60/15, respectively. It can be clearly seen from the SEM micrographs that the dispersion of NBRr phase in the PP matrix in the presence of RHP has become poor as the NBRr content increases. The increasing number of pull outs indicates that there is low adhesion between the phases. Lower adhesion between the phases gives rise to poor stress transfer across the interface (Ismail *et al*., 2004; Ismail *et al*., 2009).
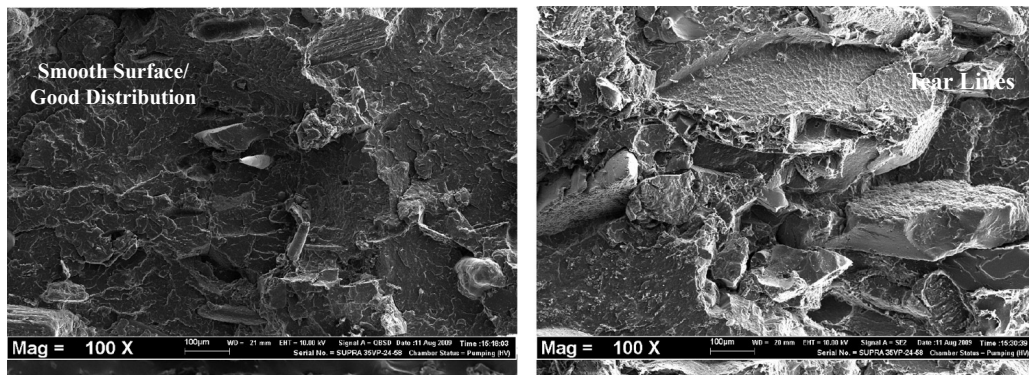
Figs. 6 (*a-b*)*: Scanning electron micrograph of tensile fractured surface of PP/NBRr/RHP/PPMAH composites at magnification of 100x*

Figs. 6 (*a-b*) clearly show even distribution of dispersion of NBRr phase in the PP matrix occurred in the composites which were compatibilized with PPMAH. Less pull outs and more tear lines observed in both composites indicate a high adhesion between the phases. This finding may be due to the attachment of NBRr with –OH radicals from the RHP resulted from compatibilization (Ismail *et al*., 2004; Ismail *et al*., 2009).

CONCLUSIONS

The results obtained showed that the tensile strength and Young's modulus of modified composites increased, while the elongation at break indicated an opposite trend as compared with the unmodified composites. The morphology results support the tensile properties revealing a better interaction between the filler and the matrix in the presence of PPMAH as a compatibilizer. Meanwhile, the scanning electron microscopy (SEM) study reveals a better dispersion of NBRr in the continuous PP matrix.

REFERENCES

Holden, G., Legge, N.R., Quirk, R. and Schroeder, H.E. (1996). *Thermoplastic Elastomers* (2nd edn.). Munich: Hanser Publisher.

Ismail, H. and Supri Yusof, A.M.M. (2004). Blend of waste poly(vinylchloride)(PVCw) /acrylonitrile butadiene rubber (NBR) The effect of maleic anhydride (MAH). *Polymer Testing, 23*, 675-683.

Ismail, H., Galpaya, D. and Ahmad, Z. (2009). The compatibilizing effect of epoxy resin on polypropylene (PP)/recycled acrylonitrile butadiene rubber (NBRr) blends. *Polymer Testing, 28*, 363-370.

Paul, D.R. and Newman, S. (1978). *Polymer Blends*. New York: Academic Press.

Satyanarayana, K.G., Arizaga, G.G.C. and Wypych, F. (2009). Biodegradable composites based on lignocellulosic fibers - An overview. *Progress in Polymer Science*, *34*, 982–102.

Zhang, F., Endo, T., Qiu, W. and Hirotsu, Y.L. (2002). Preparation and mechanical properties of composite of fibrous cellulose and maleated polyethylene. *Journal of Applied Polymer Science, 84*, 1971-1980.

Water Absorption Behaviour of Kenaf Reinforced Unsaturated Polyester Composites and Its Influence on Their Mechanical Properties

Abdalla A. Ab. Rashdi[1], Mohd Sapuan Salit[1*], Khalina Abdan[2] and Megat Mohamad Hamdan Megat[3]

[1]Department of Mechanical and Manufacturing Engineering,
[2]Department of Biological and Agricultural Engineering, Faculty of Engineering,
Universiti Putra Malaysia, 43400 UPM, Serdang, Selangor, Malaysia
[3]Faculty of Engineering, National Defence University of Malaysia,
Kem Sungai Besi, 57000 Kuala Lumpur, Malaysia
[*]E-mail: sapuan@eng.upm.edu.my

ABSTRACT

Fibre reinforced composites have gained use in a variety of applications. The performances of these composites may suffer when the material is exposed to adverse environments for a long period of time. Kenaf fibre reinforced unsaturated polyester composites were subjected to water immersion tests in order to study the effects of water absorption on the mechanical properties. Composites specimens containing (10%, 20%, and 30%) weight percentages of fibre were prepared. Water absorption tests were conducted by immersing these specimens in a distilled water bath at 25ºC for four months. The tensile properties of the specimens immersed in water were evaluated and compared with the dry composite specimens. A decrease in the tensile properties of the composites was demonstrated, indicating a great loss in the mechanical properties of the water-saturated samples compared to the dry samples. The percentage of moisture uptake was also increased as the percentage of the fibre weight increased due to the high cellulose content. The water absorption pattern of these composites was found to follow the Fickian behaviour.

Keywords: Polyester matrix composite, natural fibre, kenaf, mechanical properties

INTRODUCTION

Natural fibres unsaturated polyester composites have become increasingly used in many applications not only because they are environmentally friendly, but also because of their various desirable properties which include high specific strength and high specific stiffness. The use of natural fibres and unsaturated polyester matrix is highly beneficial because the strength and toughness of the resulting composites are greater than those of the unreinforced plastics. Moreover, cellulose-based natural fibres are strong, light, cheap, abundant, and renewable. In recent years, natural fibres reinforced unsaturated polyester materials are used in many applications such as automotive, sporting goods, marine, electrical, industrial, construction, and household appliances (Wallenberger and Weston, 2004). A number of investigations have been conducted on several types of natural fibres such as kenaf, hemp, flax, bamboo, and jute to study the effects of these fibres on the mechanical properties of composite materials (Satyanarayana *et al.,* 1990; Mansur and Aziz, 1983).

Kenaf (*Hibiscus cannabinus*, L. family *Malvaceae*) is an herbaceous annual plant. It is a warm-season annual row crop. Kenaf has a single, straight, and unbranched stem consisting of two parts, namely an outer fibrous bark and an inner woody core. The attractive features of kenaf grow quickly, rising to heights of 4-5m in a 4-5 month growing season and 25-35 mm in diameter (Nimmo,

2002), with high biomass output, broad growth area, strong adaptability to environment, and low cost in cultivated condition. Furthermore, the kenaf fibre composites have excellent strength and renewability. Kenaf has a bast fibre which contains 75% cellulose and 15% lignin, and it offers the advantages of being biodegradable and environmentally safe (Karnani, 1996). In addition, natural plant fibre reinforced unsaturated polyester composite also have some disadvantages such as the incompatibility between the hydrophilic fibres and hydrophobic thermoplastic, as well as thermoset matrices requiring appropriate treatments to enhance the adhesion between the fibre and the matrix (Gassan and Cutowski, 2000; Dhakal *et al.,* 2007).

All polymer composites absorb moisture in humid atmosphere and when they are immersed in water. The effect of moisture absorption leads to the degradation of fibre-matrix interface region which thus creates poor stress transfer efficiencies resulting in a reduction of mechanical properties (Yang *et al.,* 1996). Meanwhile, among the main concerns for the use of natural fibre reinforced composite materials are their susceptibility to moisture absorption and the effects on the physical and mechanical properties (Thwe and Kin, 2002). Therefore, it is important that the problems are investigated so that natural fibre could be considered as a viable reinforcement in the composite materials. Aziz *et al.* (2005) studied kenaf unsaturated polyester composites and observed that their moisture absorption indicated that polyester composites gave the most superior bonding and adhesion, apart from higher storage modulus.

EXPERIMENTAL DESIGN

Materials

Long fibre kenaf were used for the fibre reinforcements. The matrix material used in this study was based on the unsaturated polyester resin trade name Reservol P9509 which was supplied by Revertex (Malaysia) Sdn. Bhd. This type of resin is rigid, and with low reactivity, thixotropic general purpose orthophthalic. The matrix was mixed with curing catalyst, methyl ethyl ketone peroxide (MEKP) at a concentration of 0.01 w/w (weight ratio) of the matrix for curing. Unsaturated polyester has many advantages compared to other thermosetting resins including room temperature and low pressure moulding capabilities which make it particularly valuable for large component manufacturing at a relatively low cost (El-Sayed *et al*., 1995).

Methods

A combination of hand lay-up and compression moulding method was used to prepare kenaf unsaturated polyester composites samples. Long kenaf fibre was first dried at 100ºC to remove stored moisture in an oven. A measured quantity of unsaturated polyester resin was mixed with curing catalyst (MEKP) at a concentration of 0.01 w/w of the matrix for curing was poured on the kenaf fibre, and placed in a mould. The mould was closed and kept under pressure of 5 bar at a temperature of 50ºC for about 1h. The mould was then opened and the composite was removed from the press. The mechanical tensile test and water absorption evaluation test samples were cut in the sizes of 250 mm x 15mm x 2 mm and 62mm x 62mm x 1mm, respectively. The schematic view of a mould press used to consolidate the composite panel is shown in *Fig. 1*.

The water absorption test was carried out as described by ASTM D570. For the purpose of water absorption study, the specimens with a dimension of (62 x 62 x 1) mm³ marked (AD) were immersed in distilled water for four months. The tensile test specimens of dimensions (250 x 15 x 2) mm³ marked (W) were immersed in the same distilled water for the same period of time, and the aim was to study the effect of water absorption in mechanical tensile properties
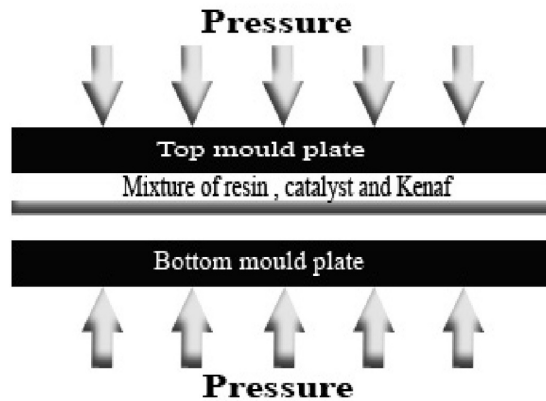
Fig. 1: Schematic of the composite consolidation

(a)   (b)
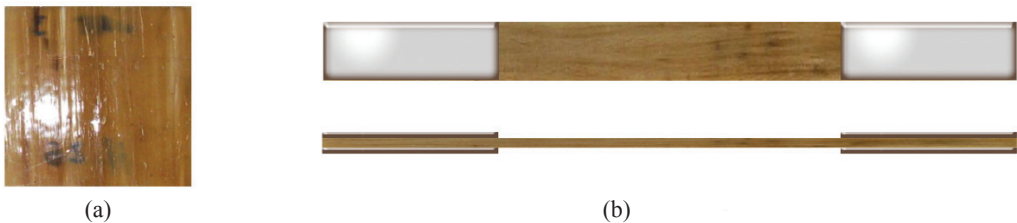
Fig. 2: Schematic view of the (a) water absorption (AD) and (b) tensile composite samples

of composites (*Fig. 2*). The samples were collected every 10 days and dried to a constant weight at 40ºC. The percent of the moisture content or percentage weight gain, M_i is calculated using following equation:

$$M_i = \left(\frac{W_i - W_b}{W_b}\right)100$$

Where
  M_i = Percentage weight gain, g
  W_i = Weight of the specimen at time (t)
  W_i = Baseline mass (oven dry specimen mass), g

Weight-gain was plotted versus the square root of time for all the samples in order to investigate the absorption behaviour of the samples. Fifteen tensile stress samples were used with weight percentages of fibre (10%wt, 20%wt, and 30%wt) to study the tensile properties of the composites. The tensile strength and modulus of kenaf fibre reinforced unsaturated polyester composite after water absorption were carried out using the Instron 5569 Universal Electromechanical Testing System with 50 kN loading capacity, and with a cross-head speed of 2 mm/min. The clamping procedure was performed carefully to ensure that the specimen was aligned with the loading axis.

RESULTS AND DISCUSSION

Water Absorption of Immersed Composites

Fig. 3 shows the weight gain due to the moisture uptake of water absorption samples AD for four months. It is observed that the samples had a significant and sharp linear increase in their moisture absorption and reached their saturation state with the maximum moisture content of 1.7% after 1440 h, following the Fickian diffusion process. Nevertheless, there was not much change observed in the weight. This status can be described by considering the water uptake attributes of kenaf fibre (Dhakal *et al.,* 2007).
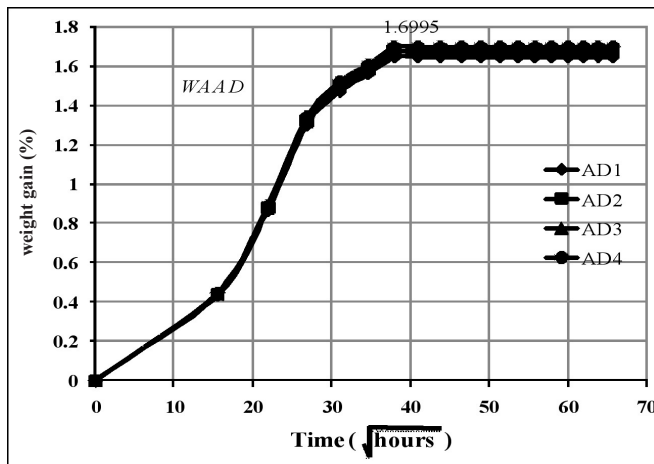
Fig. 3: Weight-gain of AD specimens versus the square root of immersed time
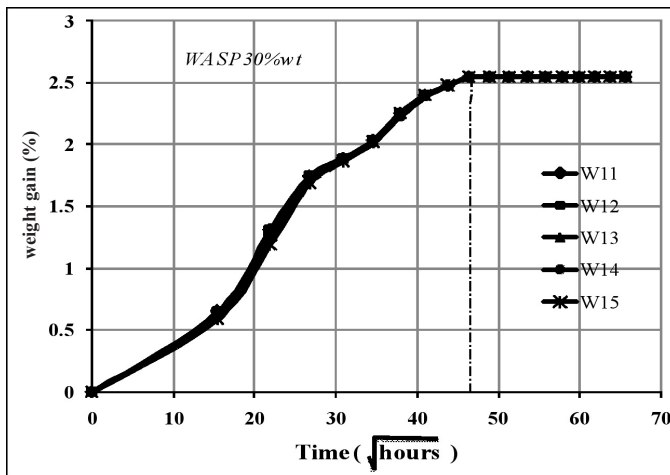
Fig. 4: Weight-gain of 30%wt specimens versus the square root of immersed time

Fig. 4 shows the behaviour of the 30%wt samples after they had been immersed in water for four months. From the process of weight gain due to moisture uptake, it is observed that the samples had a sharp linear increase in their moisture absorption and reached their saturation state with the maximum moisture content of 2.55% after 2160 h (90 days) with linear initial gain. The 20%wt samples, shown in *Fig. 5*, reached their saturated state after a linear increasing region at about 1920h (80 days) of immersion, whereas the moisture content at equilibrium was about 2.46%. In the case of 10%wt samples, the initial linear gain and these samples reached their saturation state with maximum moisture content of 2.32% about 2400 hours (100 days) after immersion (*Fig. 6*).
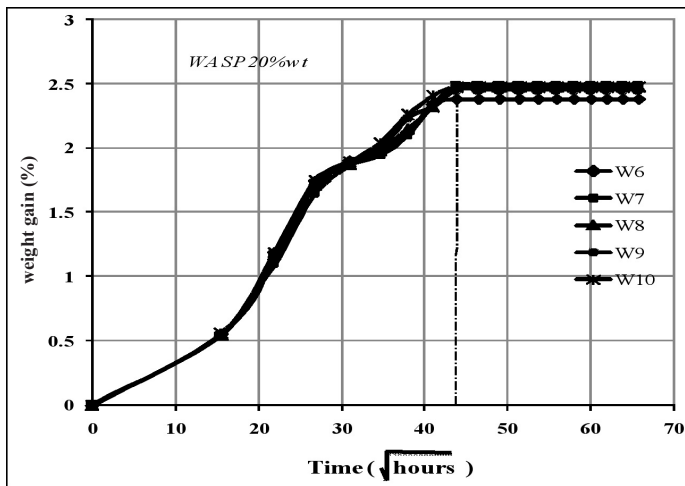
Fig. 5: Weight-gain of 20%wt specimens versus the square root of immersed time
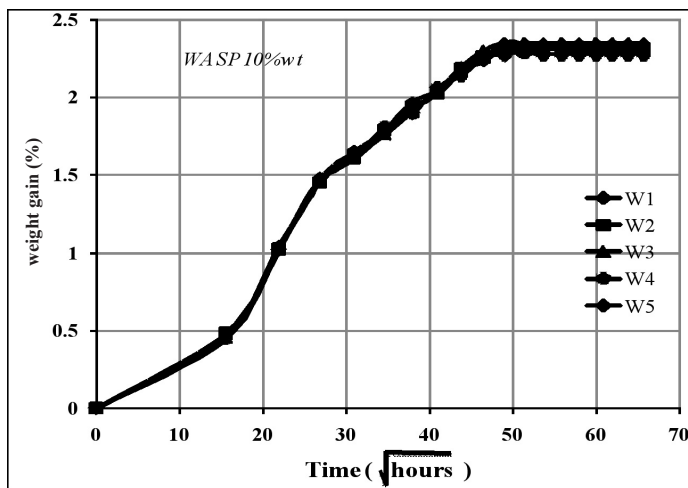
Fig. 6: Weight-gain of 10%wt specimens versus the square root of immersed time

Fig. 7 shows the comparison in the average weight gain between the 10%wt, 20%wt, 30%wt, and the AD specimens. It is observed that the samples with 30%wt gained more moisture and took longer time to reach the maximum moisture content of 2.55% after 2160 h (90 days) as compared with other samples. The high fibre content in the samples enables more water penetration into the interface through the micro cracks induced by the swelling of fibres that created swelling stresses leading to composite failure (Bismarck *et al.,* 2004). The moisture gain for the AD samples was faster as it reached the maximum after 1440 h (60 days). The difference in thickness might lead to a much faster moisture gain for the AD samples.
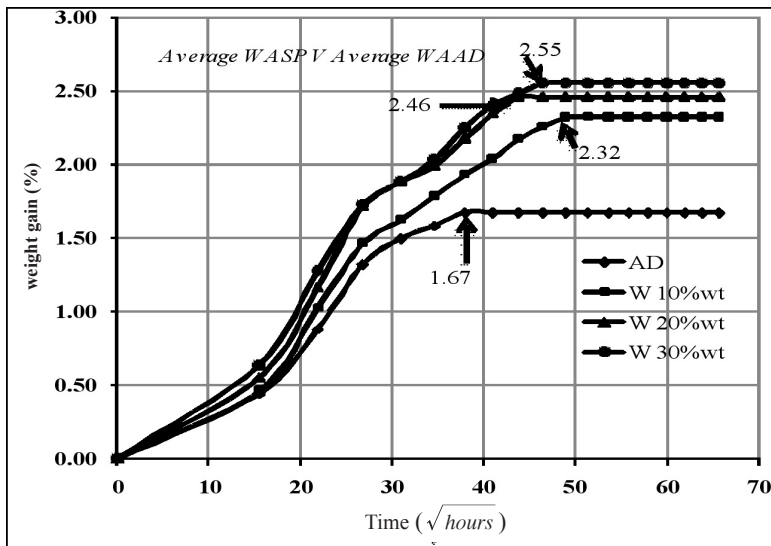
Fig. 7: Comparison of average weight gain between the AD and tensile test
samples (W) versus the square root of immersed time

Effects of Moisture Absorption on the Mechanical Properties of Composites

Most specimens reached their saturation state with the maximum moisture content in about 1920h-2400h. Nonetheless, no significant mass loss was observed. *Fig. 8* shows the tensile stresses results versus the weight percentage of fibre content for both the dry and immersed samples. It was observed that tensile stress was high as the fibre content increased for the dry specimens unlike the immersed specimens where the tensile stress was found to decrease. The same observation was obtained for the other specimen groups (20%wt and 10%wt). The stress-strain curves are linear up to the point of failure for all the specimens. As for the stress at the maximum load, the immersed specimens values were somewhat reduced after water absorption.
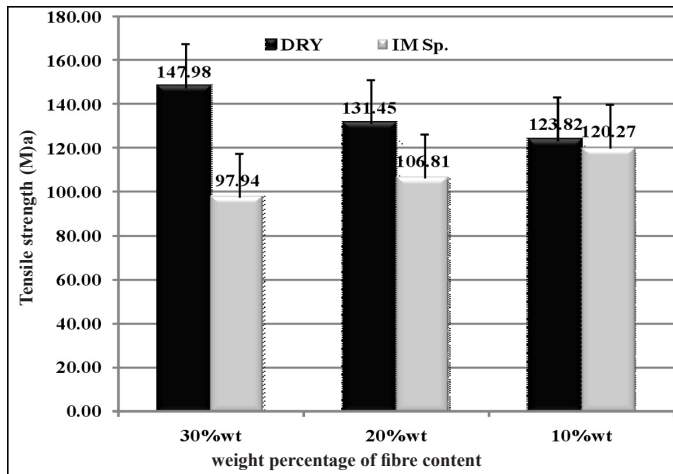
Fig. 8: Tensile stresses versus the weight percentage of the fibre
content for the dry and immersed samples

Fig. 9 shows that due to the moisture uptake, the mechanical properties decreased with the increase of fibre content. It was observed that the 10%wt sample reached the maximum values of Young's modulus (117.7 MPa) and the tensile properties of 120 MPa, whereas the Young's modulus was 114.3 MPa and the tensile stress was 106.8 MPa for the 20%wt samples. However, it is noticed that the ultimate tensile stress is low (97.9 MPa) compared to other samples for the 30%wt reinforced samples. This could be due to the high amounts of water absorption that led to decrease in the mechanical properties for composite with higher fibre content.
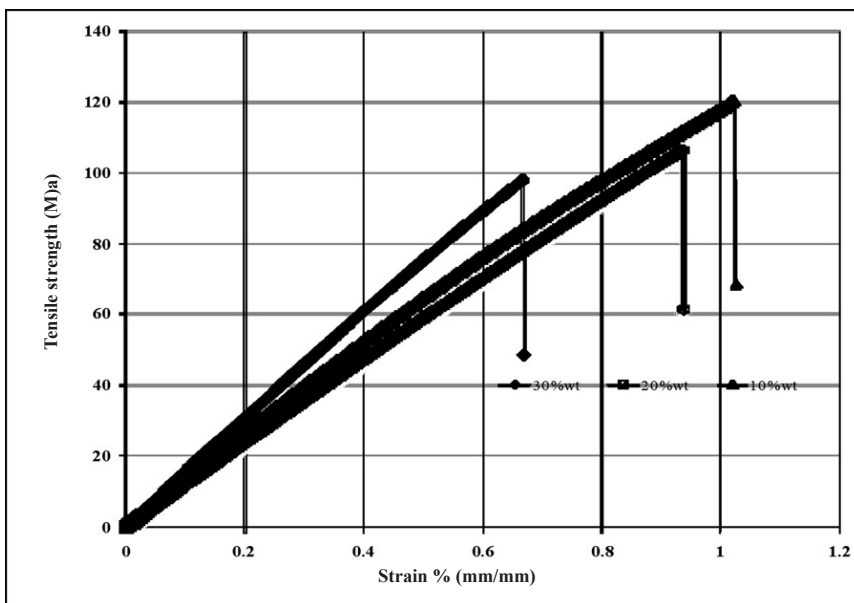
Fig. 9: Average stress strain curve of the tensile stress samples

Abdalla A. Ab. Rashdi, Mohd Sapuan Salit, Khalina Abdan and Megat Mohamad Hamdan Megat

CONCLUSIONS

The effects of water absorption on the mechanical properties of kenaf fibre reinforced unsaturated polyester composite were studied using water immersion samples. It is shown that the moisture uptake increases with the increase in the percentage of the fibre content. The water absorption pattern of these composites was found to follow the Fickian behaviour. Meanwhile, increasing the weight percentage of the fibre content was found to the increase the tensile properties of the composites for the dry specimen, whereas increasing the weight percentage of fibre content could lead to a decrease in the tensile properties of the composites for the immersed specimen.

ACKNOWLEDGEMENTS

REFERENCES

Aziz, S.H., Ansell, M.P., Clarke, S.J. and Panteny, S.R. (2005). Modified polyester resins for natural fibre composites. *Composites Science and Technology*, *65*, 525-535.

Bismarck, A., Aranberri-Askargorta, I., Springer, J., Wielage, T.L.B., Ilja, A.S. and Limbach, H. H. (2004). Surface characterization of flax, hemp and cellulose fibers: Surface properties and the water uptake behavior. *Polymer Composites*, *23*, 872-894.

Dhakal, H.N., Zhang, Z.Y. and Richarson, M.O.W. (2007). Effect of water absorption on the mechanical properties of hemp fibre reinforced unsaturated polyester composites. *Composites Science and Technology*, *67*, 1674-1683.

El-Sayed, A.A., El-Sherbiny, M.G., Abo-El-Ezz, A.S. and Aggag, G.A. (1995). Friction and wear properties of polymeric composite materials for bearing applications. *Wear*, *184*, 45-53.

Gassan, J. and Cutoswski, V.S. (2000). Effect of corona discharge and UV treatment on the properties of jute-fibre epoxy composite. *Compost Science Technology*, *60*, 2857-2863.

Karnani, R. (1996). Kenaf-reinforced polypropylene composites. Master Thesis, Michigan State University.

Mansur, M.A. and Aziz, M.A. (1983). Study of bamboo-mesh reinforced cement composites. *International Cement Composites and Lightweight Concrete, 5*, 165–171.

Nimmo Bert. (November, 2002). Kenaf fibers. *Presentation of the 5th Annual Conference of the American Kenaf Society,* Memphis, TN., 7-9.

Satyanarayana, K. G., Sukumaran, P.S.M. and C.P. & Pillai, S.G.K. (1990). Natural fiber–polymer composites. *Journal of Cement and Concrete Composites*, *12*, 117–136.

Thwe, M.M. and Kin, L. (2002). Effects of environmental ageing on the mechanical properties of bamboo-glass fibre reinforced polymer matrix hybrid composites. *Composites Part A*, *33*, 43-52.

Wallenberger, F. T. and Weston, N. (2004). *Natural Fibers, Plastics and Composites Natural*. Materials Source Book from C.H.I.P.S. Texas.

Yang, G.C., Zeng, H.M., L.J., Jian, N.B. and Wb, Z. (1996). Relation of modification and tensile properties of sisal fibre. *Acta Scientiarum Naturalium Universitatis Sunyatseni, 35*, 53-57.

Durability Simulation of Elastomeric Materials Using Finite Element Method (FEM)

C. W. Chieh, Aidy Ali*, Asmawi Sanuddin and Reza Afshar

Department of Mechanical and Manufacturing Engineering,
Faculty of Engineering, Universiti Putra Malaysia,
43400 UPM, Serdang, Selangor, Malaysia
*E-mail: aidy@eng.upm.edu.my

ABSTRACT

The paper presents a simulation work conducted on the elastomer subjected to cyclic loads. A 3D finite element model of elastomer specimen, in accordance to ASTM D412, was developed using CATIA and ANSYS commercial finite element (FEM) packages. Fatigue life predicted from the simulation was compared with well-documented published data and it showed an acceptable agreement. Meanwhile, the simulated strain-life results are slightly lower than the experimental data. Several factors which potentially influenced the variations of the results were noted. Finally, some recommendations are offered at the end of this study to further improve the simulation.

Keywords: Elastomer, FEM, strain controlled loading, CATIA, ANSYS

INTRODUCTION

Synthetic polymers such as elastomers consist of a large family of amorphous polymers with a low elastic modulus; they can be stretched to at least twice their original length and return quickly to the original length when stress is released (Philip, 2006). These polymeric materials are widely used in applications where low stiffness and a high elastic strain are required. They are commonly used in many demanding applications, from tyres and seals to gloves and medical devices. The failure of rubber products in these demanding applications would cause disaster. In many of these applications, the component experiences cyclic loading and failure is due to a fatigue.

Fatigue is a phenomenon of failure of material under cyclic or long-term stress at stress levels well below their ultimate stress and it is the result of the progressive growth of cracks through the material (Hall, 1979). Generally, elastomers can fail due to either thermal fatigue or mechanical fatigue. The failure is caused by factors such as load frequency, stress level, temperature, and the geometry of the component. The observation carried out showed that the fatigue process involved the following states: (1) crack nucleation, (2) short crack growth, (3) long crack growth, and (4) final fracture. Fatigue starts with crack nucleation and when cyclic loading continues, the crack tends to grow along the plane of maximum shear stress through grain boundary (Lee *et al*., 2005).

In fact, cracks cannot be avoided in many structural applications. The location and size of these cracks will influence the fatigue life of any structure. For elastomers, their fatigue life is affected by some parameters such as the size and distribution of the initial defects, stress concentrations within the sample geometry or it can be caused by processing, molecular distribution, as well as degree of cross-linking in the microstructure, and environmental influences like test temperature and exposure to aggressive chemicals (for example, UV light, oils, ozone) (Hainsworth, 2007). In order to predict the fatigue life of any component, a fatigue analysis is needed to provide a sound basis of lifespan of the designed components.

According to Andriyana and Verron, (2007) two approaches are generally adopted to define end of life (Mars and Fatemi, 2002); the crack nucleation approach and the crack growth approach. The former defines fatigue life as the number of cycles required to create a crack of a given size. This approach, which follows the work of Wohler (1867), was applied to rubber by Cadwell *et al.* (1940), considering the fact that fatigue life of rubbers can be determined from the history of strain and stress at each material point of the body. Meanwhile, the second approach defines fatigue life as the number of cycles required by the pre-existing crack to grow to the point of failure. The idea of considering pre-existing cracks or flaws was introduced by Inglis (1913) and Griffith (1920), but it was Rivlin and Thomas (1953) who first applied it to rubber (Andriyana and Verron, 2007; Fetemi and Mars, 2002).

Fatigue life prediction under loadings is crucial in structure design. Therefore an appropriate fatigue life criterion is necessary to prevent their fracture in service (Saintier *et al.*, 2006). In the previous studies, fatigue life prediction in metallic materials has been largely investigated over the past decades and it is still of major concern (Papadopoulus *et al.*, 1997; Doblare, 2002; Liu *et al.*, 2005; Makkonen, 2009). However, fatigue life prediction in rubbers has limited investigation as compared to metallic materials, despite the growing use of rubbers in a wide range of industrial applications (Saintier *et al.*, 2006). Therefore, the objectives of this work are: (1) to develop a finite element model (FEM) of natural rubber under cyclic loadings, and (2) to predict the life of elastomer specimens under cyclic loads through the developed FEM model.

FINITE ELEMENT METHOD (FEM) AND ELASTOMERIC FATIGUE MODELLING

The Finite Element Method (FEM) is a numerical procedure that can be used to obtain solutions to a large class engineering problems involving stress analysis, heat transfer, vibration, deflection, buckling behaviour, and many other phenomena (Osman, 2004; Marcus *et al.*, n.d.; Lira *et al.*, 2002). This method can be used to analyze either small or large-scale deflection under loading or applied displacement. The simulation is required because of the astronomical number of calculations needed to analyze a large structure. The finite element analysis is a way to deal with structures which are more complex than can be dealt with analytical solution using classical theories (Chan *et al.*, 2006; Hertzberg, 1996). The key idea of the finite element method is to discretize the solution domain into a number of simpler domains called elements. An approximate solution is assumed over an element in terms of solution at selected points called nodes (Bhatti, 2005).

There are several forms of strain energy potentials available to model the incompressible and isotropic elastomers. They are the Mooney-Rivlin model (Green and Addkins, 1970), the Ogden (1984) model, the Yeoh (1993) model, the Arruda and Boyce (1993) model, the Van der Waals model (Kilian *et al.*, 1996), the neo-Hookean model, the polynomial model, and the reduced polynomial model (Weber and Anand, 1990). By comparing these options after performing hyperelastic material curve fitting, the Ogden was chosen since it provides the best approximation to a solution at larger strain levels. In the Ogden model, the strain energy potential is represented as:

$$U = \sum_{i=1}^{N} \frac{2\mu_i}{\alpha_i^2}\left(\overline{\lambda}_1^{\alpha_i} + \overline{\lambda}_2^{\alpha_i} + \overline{\lambda}_3^{\alpha_i} - 3\right) + \sum_{i=1}^{N} \frac{1}{D_i}(J-1)^{2i} \tag{1}$$

Where,

$\overline{\lambda}_i^i = J^{-\frac{1}{3}}\lambda_i =$ deviatoric principal stretches

$\lambda_i \quad =$ principal stretches

$J \quad =$ Jacobian determinant of the deformation gradient

$N \quad =$ number of terms in the series

$\mu_i, \alpha_i, D_i =$ temperature dependent material parameters

By assuming the material is incompressible, therefore, in the uniaxial stress state, the principal stretches λ_i are represented by:

$$\lambda_1 = \lambda_u, \quad \lambda_2 = \lambda_3 = \frac{1}{\sqrt{\lambda_u}} \quad (2)$$

The nominal strain in the loading direction is given by:

$$\varepsilon_U = \lambda_U - 1 \quad (3)$$

Where,

λ_u = stretch in the loading direction
ε_u = nominal strain in the loading direction

The uniaxial nominal normal stress, T_U, is determined by considering the principle of virtual work (Ogden, 1984) in the form of:

$$T_U = \frac{\partial U}{\partial \lambda_U} \quad (4)$$

By letting $N=1$ and substituting equation (2) into equation (1), the strain energy potential for the uniaxial stress state is represented by:

$$U = \frac{2\mu_1}{\alpha_1^2}\left(\lambda_U^{\alpha_1} + 2\lambda_U^{-\alpha_1/2} - 3\right)$$

$$= \frac{2\mu_1}{\alpha_1^2}\left[(1 + \varepsilon_U)^{\alpha_1} + 2(1 + \varepsilon_U)^{-\alpha_1/2} - 3\right] \quad (5)$$

From equations (4) and (5), the nominal stress and strain relation under uniaxial tension is expressed as:

$$T = \frac{2\mu_1}{\alpha_1}\left(\lambda_U^{\alpha_1 - 1} - \lambda_U^{-(\alpha_1/2 + 1)}\right)$$

$$= \frac{2\mu_1}{\alpha_1}\left[(1 + \varepsilon_U)^{\alpha_1 - 1} - (1 + \varepsilon_U)^{-(\alpha_1/2 + 1)}\right] \quad (6)$$

In order to define the hyperelastic material behaviour, such as constitutive relation, experimental test data are required to determine material parameters in the strain energy potential (Wang *et al.*, 2002; Kim *et al.*, 2004). Therefore, material parameters, α_1 and μ_1, can be determined by fitting the experimental nominal stress-strain curve into Equation (6) (Wang *et al.*, 2002).

SIMULATION WORK

In this study, an elastomer material under uniaxial zero based cyclic loading of strain ratio, r = minimum strain/maximum strain = 0 with strain controlled, was analyzed. A 0.1 Hz frequency of triangular strain wave was used. The strain amplitude was measured by dividing the cross-head displacement and the gauge length of the specimen. The geometric modelling and simulation are respectively performed by CATIA and ANSYS Multiphysics. For the experimental work, the material used is a carbon-filled natural rubber with 65 parts of carbon black mixed with 100 parts of natural rubber having an international rubber hardness degree (IRHD) of 72 (Wang *et al.*, 2002).

Geometry Modelling in CATIA

In simulation, all dimensions in CATIA were measured in mm. The nominal dimensions of the ASTM D412 specimens are shown in *Fig. 1*. The geometry of model shown in the figure is symmetry at horizontal and vertical. Since then, a quarter part of the specimen was drawn on YZ plane and this was followed by creating the full image. The 3D drawing was obtained by extruding the full image to 1.9 mm in x direction and perpendicular to YZ plane.
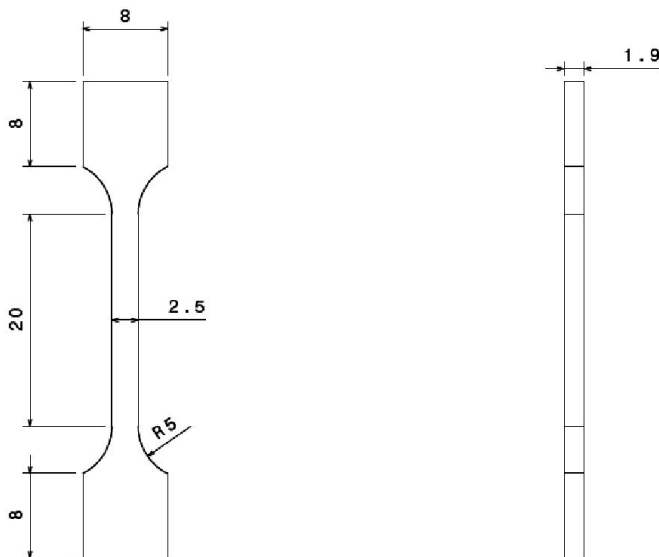
Fig. 1: Dimensions of ASTM D412 specimen (all dimensions in mm)
(Hertzberg, 1996)

Mesh Generation

The element used on the ASTM D412 specimen was SOLID187 which is defined by 10 nodes and there are three degrees of freedom at each node. There are translations in x, y, and z directions. The mesh of the specimens was completed by clicking on the volume and selecting all parts; the display of the mesh generation is shown in *Fig. 2(a)*. The mesh relevance value was set to be 100, as shown in *Fig. 2(b)*. Since the model would undergo large deformation, the "Aggressive Mechanical" in "Shape Checking" was therefore selected.

(b)   (a)
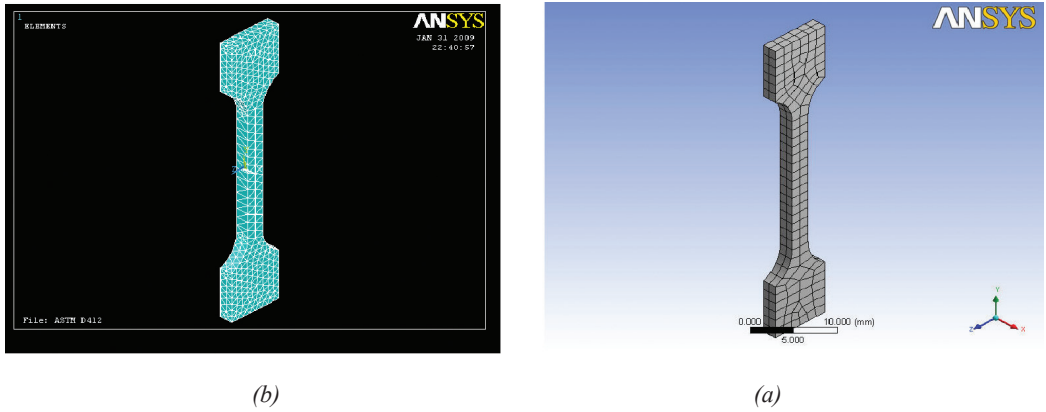
Fig. 2: Mesh generation in (a) ANSYS and (b) ANSYS Workbench

Import Data and Material Curve Fitting

The stress-strain data and stress-life data from the experimental results were imported into ANSYS Multiphysics, while the hyperelastic and material curve fitting was performed as shown in *Fig. 3*. The Ogden model was chosen among other options because it provides the best approximation to a solution at larger strain levels up to 700% (the maximum strain level in the extracted experimental data is up to 385%). From the Ogden Order 1 model, yield α_1= 2.8373 and μ_1=1.6354MPa. In order to set the constraint, the displacement values, ranging from 140 mm - 480 mm (70%-240%), were applied in Area 3. For each value of the strain, the fatigue calculation was performed. After that, the displacement constrain was applied in Area 1 in y-direction and Area 2 in x-direction. *Fig. 4* shows Areas 1, 2, 3, and 4 of the model, respectively. In the experiment, however, both ends were clamped (Area 4) and the upper end of the specimen was displaced in positive y-direction. At the same time, the reduction of thickness also occurred. Generally, the boundary condition applied in Area 2 for both the experiment and simulation are the same.
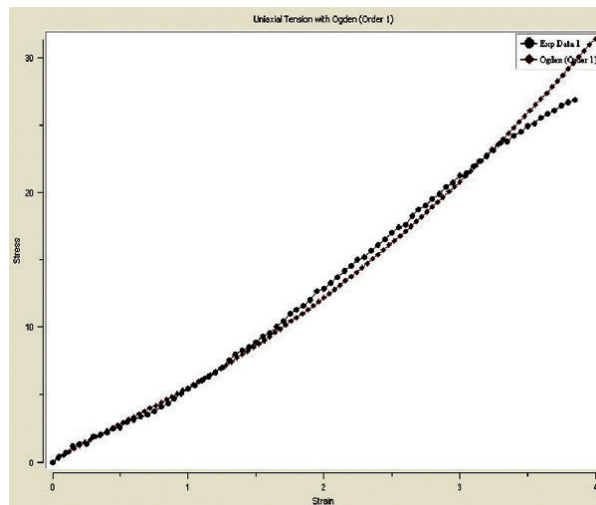
Fig. 3: Hyperelastic material curve fitting
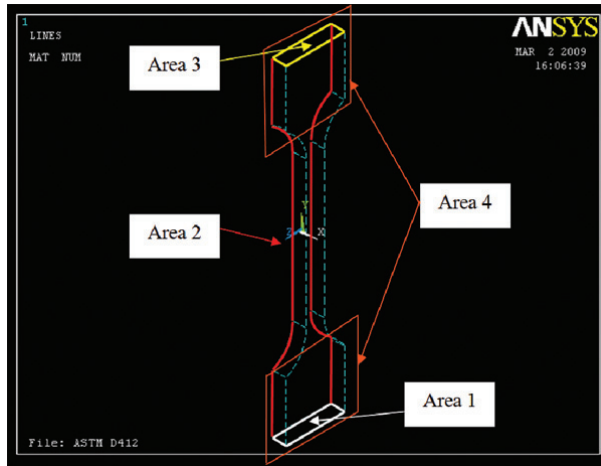
Fig. 4: Areas 1, 2, 3 and 4 of the model
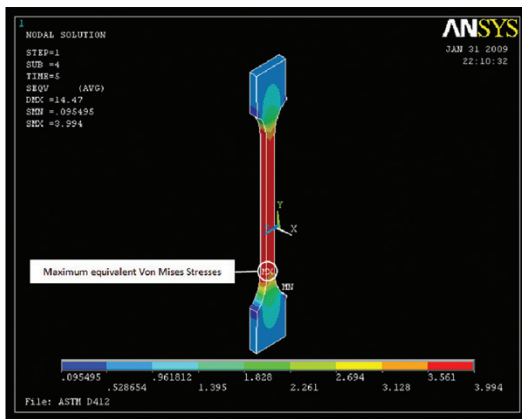
Fig. 5: Maximum SEQV at node 2544   *Fig. 6: Location of the 10 nodes*
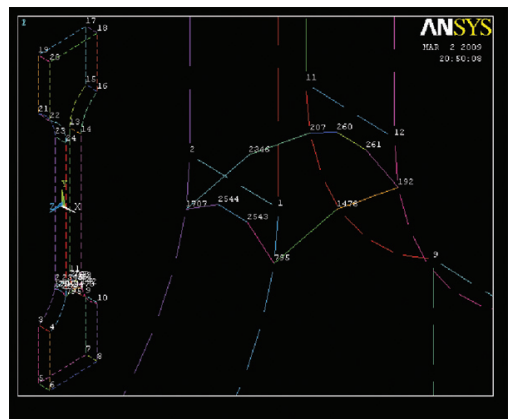
Post-processing

In this section, the nodal solution result was chosen to present the stress results. From the nodal solution, the equivalent Von Mises (SEQV) stresses were used to determine the failure location of the model. *Fig. 5* shows that the maximum SEQV occurred at the same location (node 2544 in ANSYS) for all the values of strain.

In the ANSYS simulation environment, the fatigue life of the model was measured at the shortest life of 10 critical nodes. These nodes are the node of 192, 207, 260, 261, 795, 1478, 1707, 2346, 2543, and 2544 and their positions are shown in *Fig. 6*. On the other hand, the fatigue life which was calculated in the ANSYS Workbench simulation environment is the fatigue life of the whole model rather than of a particular node.
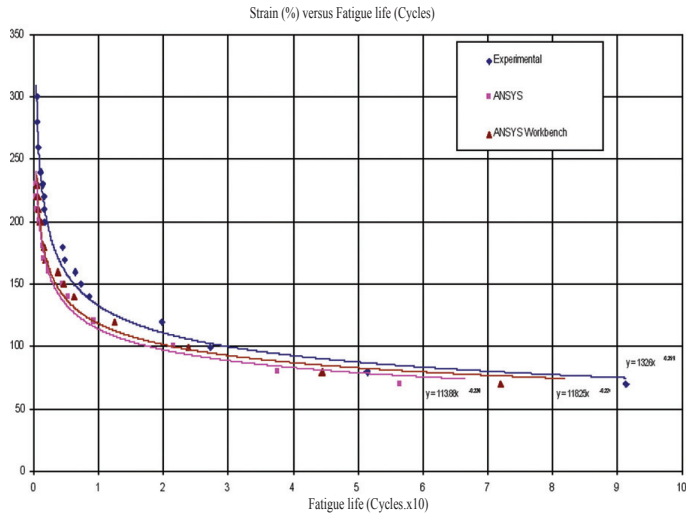
Fig. 7: A comparison between three types of predicted strain-life curve

RESULTS AND DISCUSSION

The fatigue life cycles of the model predicted by ANSYS were obtained and these results were compared with well-documented experimental data for validation. A table of comparison is tabulated in Table 1. In order to compare the simulations and the experimental results, the fatigue life of the model at different strain percentages (i.e. between 70%-240%) was calculated with the software. The negative sign in the percentage difference indicates that the simulation fatigue life is smaller than the experiment fatigue life.

For the ease of comparison, all the fatigue data were plotted in a graph, as shown in *Fig. 7*. From the graph, both the predicted fatigue life cycles of the model are slightly lower than the experimental fatigue life. This state occurs because the experimental fatigue life cycles were taken when the tested specimen was broken into two pieces; however, the fatigue life cycles taken by the ANSYS and ANSYS Workbench the cycles when the failure of a particular node. This is considered as the life of a complete fracture versus the life of an initiated crack.

TABLE 1
A comparison between the simulation and experimental results

Strain (mm)	Strain percentage (%)	Experimental fatigue life (Cycles)	ANSYS predicted fatigue life (Cycles)	Differences in the percentages between ANSYS and experiment (%)	ANSYS Workbench predicted fatigue life (Cycles)	Differences in the percentage between ANSYS Workbench and experiment (%)
14	70	91201	56430	-38	71846	-21
16	80	51310	37570	-27	44365	-14
20	100	27219	21580	-21	23777	-13
24	120	19735	9261	-53	12336	-37
28	140	8438	5328	-37	6188	-27
30	150	7250	4402	-39	4602	-37
32	160	6310	2389	-62	3635	-42
34	170	4671	1580	-66	1720	-63
36	180	4332	1451	-67	1535	-65
40	200	1600	960	-40	898	-44
42	210	1568	552	-65	592	-62
44	220	1468	466	-68	526	-64
46	230	1260	381	-70	424	-66
48	240	1000	-	-	-	-
52	260	602	-	-	-	-
56	280	511	-	-	-	-
60	300	381	-	-	-	-

CONCLUSIONS

A three-dimensional finite element analysis was used to examine the fatigue life cycles of the ASTM D412 specimens and comparisons were made to the well-documented experimental data. These comparisons show similarity in terms of the shape of the plotted strain-life curves and a slight difference in terms of the fatigue life cycles of the specimen. Meanwhile, a finite element model has successfully been developed and it can be applied for the prediction of other materials, load, and size of geometry under cyclic loading. In short, FEM gives a good control of the experimental techniques, confirming, complementing and refining the specimen design before commencing any experiment tests.

ACKNOWLEDGEMENT

REFERENCES

Andriyana, A. and Verron, E. (2007). Prediction of fatigue life improvement in natural rubber using configurational stress. *The International Journal of Solids and Structures*, *44*, 2079-2092.

Andriyana, A. and Verron, E. (2005). Effect of the hysteretic response of elastomers on the fatigue life. In P.E. Austrell and L. Kari (Eds.), *Constitutive models for rubber IV* (pp. 31-36). A.A. Balkema Publishers.

Arruda, E.M. and Boyce, M.C. (1993). Three-dimensional constitutive model for the large stretch behavior of rubber elastic materials. *Journal of the Mechanics and Physics of Solids, 41*(2), 389.

Bea, J.A. and Doblare, M. (2002). Enhanced B-PFEM Model for fatigue life prediction of metals during crack propagation. *Computational Material Sciences, 25*, 14-33.

Bhatti, M.A. (2005). *Fundamental Finite Element Analysis and Applications: With Mathematica and Matlab Computations*. John Wiley & Sons, Inc.

Cadwell, M., Merril, R., Sloman, C. and Yost, F. (1940). Dynamic fatigue life of rubber. *Industrial and Engineering Chemistry Research, 12*(1), 19–23.

Chan, O.B., Elwi, A.E. and Gilbert, G.Y. (2006). Simulation of crack propagation in steel plate with strain softening model. Structural Engineering Report No. 266.

Fatemi, A. and Mars, W.V.A. (2002). Literature survey on fatigue analysis approaches for rubber. *International Journal of Fatigue*, *24*, 949-961.

Green, A.E. and Adkins, J.E. (1970). *Large Elastic Deformations*. Oxford: Clarendon Press.

Griffith, A. (1920). The phenomena of rupture and flow in solids. *Philosophical Transactions of the Royal Society London A, 221*, 163–198.

Hainsworth, S.V. (2007). An environmental scanning electron microsopy investigation of fatigue crack initiation and propagation in elastomers. *Polymer Testing*, *26*, 60-70.

Hall, R.O. (1979). Rubber as an engineering material. *International Journal of Material Engineering Applications, 1*, 295-302.

Hertzberg, R. (1996). *Deformation and Fracture Mechanics of Engineering Materials*. New York: John Wiley and Sons.

Inglis, C.E. (1913). Stresses in plate due to the presence of cracks and sharp corners. *Transaction of the Institution of Naval Architects, 55*(41), 219.

Kilian, H.G., Enderle, H.F. and Unseld, K. (1986). The use of the van der Waals model to elucidate universal aspects of structure property relationships in simply extended dry and swollen rubbers. *Colloid and Polymer Science, 264*, 866–876.

Kim, W.D., Lee, H.J., Kim, J.Y. and Koh, S.K. (2004). Fatigue life estimation of an engine rubber mount. *International Journal of Fatigue*, *26*, 553-560.

Lee, Y.L., Pan, J., Hathaway, R.B. and Barkey, M.E. (2005). *Fatigue Testing and Analysis. Theory and Practice*. Elsevier Inc.

Lira, W.L., Cavalcanti, P.R., Coelho, L.C.G. and Martha, L.F. (2002). A modelling methodology for finite element mesh generation of multi-region models with parameter surfaces. *Journal of Computational and Graphical Statistics, 6*, 907-918.

Liu, Y. and Mahadevan, S. (2005). Multiaxial high-cycle fatigue criterion and life prediction for metals. *International Journal of Fatigue*, *27,* 790-800.

Makkonen, M. (2009). Predicting the total fatigue life in metals. *International Journal of Fatigue*, *31*, 1163-1175.

Marcus, M., Frank, S. and Carsten, M.W. (n.d). *Creation of Finite Element Models of Human Body Based Upon Tissue Classified Voxel Representations*. Germany: University of Karlsruhe.

Mars, W. V., Mars and Fatemi, A. (2002). A literature survey on fatigue analysis approaches for rubber. *International Journal of Fatigue, 24*, 949–961.

Ogden, R. W. (1984). *Non-linear Elastic Deformation*. Ellis Horwood Limited.

Osman, M.H. (2004). *Finite Element Modeling of Sheet Metal Bending*, *2*, 34-36.

Papadopoulos, I.V., Davoli, P., Gorla, C., Filippini, M. and Bernasconi, A. (1997). A comparative study of multiaxial high-cycle fatigue criteria for metals. *International Journal of Fatigue, 19*, 219-235.

Philip, A.S. (2006). *Corrosion of Polymers and Elastomers* (2nd edn.). CRC Press.

Rivlin, R.S. and Thomas, A.G. (1953). Rupture of rubber. I. Characteristic energy for tearing. *Journal of Polymer Science, 10*, 291–318.

Saintier, N., Cailetaud, G. and Piques, R. (2006). Crack initiation and propagation under multiaxial fatigue in a natural rubber. *International Journal of Fatigue*, *28,* 61-72.

Saintier, N., Cailletaud, G. and Piques, R. (2006). Multiaxial fatigue life prediction for a natural rubber. *International Journal of Fatigue*, *28*, 530-539.

Wang, B., Lu, H. and Kim, G. A. (2002). Damage model for the fatigue life of elastomeric materials. *Mechanics of Materials, 34*, 475-483.

Weber, G. and Anand, L. (1990). Finite deformation constitutive equations and a time integration procedure for isotropic, hyperelastic–viscoplastic solids. *Computer Methods in Applied Mechanics and Engineering*, *79*, 173–202.

Wöhler, A. (1867). Wöhler experiments on the strength of metals. *Engineering 2*(1867), 160.

Yeoh, O.H. (1993). Some forms of the strain energy function for rubber. *Rubber Chemistry and Technology, 66*, 754–771.

Pertanika Journal of Science & Technology

Subject Index for Volume 18 Nos. 1 & 2 2010

jacking 155 - 158, 160 - 165
Jawi script 271 - 273, 275 - 277, 284 - 285,
    290 - 291
Johore coastal water 7 - 8, 10

kenaf 433 - 436, 440
keyboard layout 271 - 272, 288

laboratory compaction 13 - 14, 16
LAI *see* Leaf area index
Leaf area index 23
LQR control 61, 67, 70 - 72, 74

machine seeding 95, 98, 101 - 102
manipulator 61 - 62, 69
mechanical properties 433 - 434, 439 - 440
microwave frequencies 122, 137
modelling 33
multiclass 139 - 140
multiclass classification 139 - 141
multi-span 111

n-alkanes 167 - 169, 174 -178
Narmada estuary 293, 295, 298 - 301
natural rubber latex 413
natural ventilation 111
NBRr *see* recycled acrylonitrile butadiene
    rubber
neat polyvinyl alcohol 387
neural network 33
non-parametric 140
nozzle 251
NPVOH *see* neat polyvinyl alcohol
numerical model 293

old palms 23 - 24, 27 - 31
outdoor vision 243

PAHs *see* polycyclic aromatic hydrocarbons
palm plantation 23 - 27
partial budget analysis 95, 98, 100
pattern recognition 139 - 141
PID control 61, 64, 66 - 67
polycyclic aromatic hydrocarbons 167, 169
polyester 433- 440
polypropylene 427
Polyvinyl alcohol 387
PP *see* polypropylene
prevulcanisation 421
purchasing 183, 187 - 188
PVOH *see* Polyvinyl alcohol

RCC dam body 48, 51 - 52
real-time 243 - 244, 247, 250
recycled acrylonitrile butadiene rubber 427
repeated fed-batch cultivation 365 - 366, 373
reservoir inflow 33, 38
RHP *see* rice husk powder
rice husk powder 427
risk factors 321
roller compacted concrete dam 43
roller compactor 13

safety 377 - 384
sago starch 411 - 412, 419
seaweeds 255 - 256, 259 - 260
sediment 43 - 44, 51 - 52, 55 - 57
sedimentation rate 7 - 11
sediment transport 293 - 295, 297 - 298
seismic 43 - 45, 58
slab 13, 15 - 16
SLS *see* soda lime silica
SMA *see* Stone Mastic Asphalt
Syzygium malaccense 1, 3, 5
soda lime silica 223-224
specific heats 387
sprayer 245
Stone Mastic Asphalt 13
supercapacitor 363, 171
surface sediments 170
Symmetrical supercapacitor 351

terpolymer 401, 404 - 408
thermoplastic starch 411
thin layer interface 57
tidal circulation 293
trenchless technology 155
tunnelling 155, 158
Turamesin 15
twin box culvert 155

VEDA *see* Vertical Edge Detection Algorithm
ventilation rate 111 - 117
Vertical Edge Detection Algorithm 303 - 304,
    307
vibration control 61 - 62

wastewater sludge 223
water absorption 433 - 436, 438 - 440
web camera 303, 314
weeds 243, 248
wind effect 111

zinc 83 - 84, 86 - 93

Pertanika Journal of Science & Technology

Author Index for Volume 18 Nos. 1 & 2 2010

REFEREES FOR THE PERTANIKA
JOURNAL OF SCIENCE AND TECHNOLOGY
(JST)

January – July 2010

The Editorial Board of the Journal of Science and Technology wish to thank the following for acting as referees for manuscripts submitted to JST between January and July 2010.

Pertanika

Our goal is to bring high quality research to the widest possible audience

Journal of Science & Technology

INSTRUCTIONS TO AUTHORS
(Manuscript Preparation & Submission Guidelines)
Revised January 2010

We aim for excellence, sustained by a responsible and professional approach to journal publishing.
We value and support our authors in the research community.

Please read the guidelines and follow these instructions carefully; doing so will ensure that the publication of your manuscript is as rapid and efficient as possible. The Editorial Board reserves the right to return manuscripts that are not prepared in accordance with these guidelines.

About the Journal

Pertanika is an international peer-reviewed journal devoted to the publication of original papers, and it serves as a forum for practical approaches to improving quality in issues pertaining to tropical agriculture and its related fields. *Pertanika* began publication in 1978 as Journal of Tropical Agricultural Science. In 1992, a decision was made to streamline *Pertanika* into three journals to meet the need for specialised journals in areas of study aligned with the interdisciplinary strengths of the university. The revamped Journal of Science and Technology (JST) is now focusing on research in science and engineering, and its related fields. Other *Pertanika* series include Journal of Tropical Agricultural Science (JTAS); and Journal of Social Sciences and Humanities (JSSH).

JST is published in **English** and it is open to authors around the world regardless of the nationality. It is currently published two times a year i.e. in **January** and **July**.

Goal of *Pertanika*
Our goal is to bring the highest quality research to the widest possible audience.

Quality
We aim for excellence, sustained by a responsible and professional approach to journal publishing. Submissions are guaranteed to receive a decision within 12 weeks. The elapsed time from submission to publication for the articles averages 5-6 months.

Indexing of *Pertanika*
Pertanika is now over 30 years old; this accumulated knowledge has resulted in *Pertanika* JST being indexed in EBSCO.

Future vision
We are continuously improving access to our journal archives, content, and research services. We have the drive to realise exciting new horizons that will benefit not only the academic community, but society itself.

We also have views on the future of our journals. The emergence of the online medium as the predominant vehicle for the 'consumption' and distribution of much academic research will be the ultimate instrument in the dissemination of the research news to our scientists and readers.

Aims and Scope

Pertanika Journal of Science and Technology aims to provide a forum for high quality research related to science and engineering research. Areas relevant to the scope of the journal include: *bioinformatics, bioscience, biotechnology and bio-molecular sciences, chemistry, computer science, ecology, engineering, engineering design, environmental control and management, mathematics and statistics, medicine and health sciences, nanotechnology, physics, safety and emergency management*, and related fields of study.

Editorial Statement

Pertanika is the official journal of Universiti Putra Malaysia. The abbreviation for *Pertanika* Journal of Science & Technology is *Pertanika J. Sci. Technol.*

Guidelines for Authors

Publication policies

Pertanika policy prohibits an author from submitting the same manuscript for concurrent consideration by two or more publications. It prohibits as well publication of any manuscript that has already been published either in whole or substantial part elsewhere. It also does not permit publication of manuscript that has been published in full in Proceedings.

Editorial process

Authors are notified on receipt of a manuscript and upon the editorial decision regarding publication.

Manuscript review: Manuscripts deemed suitable for publication are sent to the Editorial Advisory Board members and/or other reviewers. We encourage authors to suggest the names of possible reviewers. Notification of the editorial decision is usually provided within to eight to ten weeks from the receipt of manuscript. Publication of solicited manuscripts is not guaranteed. In most cases, manuscripts are accepted conditionally, pending an author's revision of the material.

Author approval: Authors are responsible for all statements in articles, including changes made by editors. The liaison author must be available for consultation with an editor of *The Journal* to answer questions during the editorial process and to approve the edited copy. Authors receive edited typescript (not galley proofs) for final approval. Changes **cannot** be made to the copy after the edited version has been approved.

Please direct all inquiries, manuscripts, and related correspondence to:

The Executive Editor
Pertanika Journals
Research Management Centre (RMC)
IDEA Tower II, UPM-MTDC Technology Centre
Universiti Putra Malaysia
43400 UPM, Serdang, Selangor
Malaysia
Phone: + (603) 8947 1622
ndeeps@admin.upm.edu.my

or visit our website at http://www.pertanika2.upm.edu.my/jpertanika/index.htm for further information.

Manuscript preparation

Pertanika accepts submission of mainly four types of manuscripts. Each manuscript is classified as **regular** or **original** articles, **short communications**, **reviews**, and proposals for **special issues**. Articles must be in **English** and they must be competently written and argued in clear and concise grammatical English. Acceptable English usage and syntax are expected. Do not use slang, jargon, or obscure abbreviations or phrasing. Metric measurement is preferred; equivalent English measurement may be included in parentheses. Always provide the complete form of an acronym/abbreviation the first time it is presented in the text. Contributors are strongly recommended to have the manuscript checked by a colleague with ample experience in writing English manuscripts or an English language editor.

Linguistically hopeless manuscripts will be rejected straightaway (e.g., when the language is so poor that one cannot be sure of what the authors really mean). This process, taken by authors before submission, will greatly facilitate reviewing, and thus publication if the content is acceptable.

The instructions for authors must be followed. Manuscripts not adhering to the instructions will be returned for revision without review. Authors should prepare manuscripts according to the guidelines of *Pertanika*.

1. Regular article
Definition: Full-length original empirical investigations, consisting of introduction, materials and methods, results and discussion, conclusions. Original work must provide references and an explanation on research findings that contain new and significant findings.
Size: Should not exceed 5000 words or 8-10 printed pages (excluding the abstract, references, tables and/or figures). One printed page is roughly equivalent to 3 type-written pages.

2. Short communications
Definition: Significant new information to readers of the Journal in a short but complete form. It is suitable for the publication of technical advance, bioinformatics or insightful findings of plant and animal development and function.
Size: Should not exceed 2000 words or 4 printed pages, is intended for rapid publication. They are not intended for publishing preliminary results or to be a reduced version of Regular Papers or Rapid Papers.

3. Review article
Definition: Critical evaluation of materials about current research that had already been published by organizing, integrating, and evaluating previously published materials. Re-analyses as meta-analysis and systemic reviews are encouraged. Review articles should aim to provide systemic overviews, evaluations and interpretations of research in a given field.

Size: Should not exceed 4000 words or 7-8 printed pages.

4. Special issues
Definition: Usually papers from research presented at a conference, seminar, congress or a symposium.

Size: Should not exceed 5000 words or 8-10 printed pages.

5. Others
Definition: Brief reports, case studies, comments, Letters to the Editor, and replies on previously published articles may be considered.

Size: Should not exceed 2000 words or up to 4 printed pages.

With few exceptions, original manuscripts should not exceed the recommended length of 6 printed pages (about 18 typed pages, double-spaced and in 12-point font, tables and figures included). Printing is expensive, and, for the Journal, postage doubles when an issue exceeds 80 pages. You can understand then that there is little room for flexibility.

Long articles reduce the Journal's possibility to accept other high-quality contributions because of its 80-page restriction. We would like to publish as many good studies as possible, not only a few lengthy ones. (And, who reads overly long articles anyway?) Therefore, in our competition, short and concise manuscripts have a definite advantage.

Format
The paper should be formatted in one column format with the figures at the end. A maximum of eight keywords should be indicated below the abstract to describe the contents of the manuscript. Leave a blank line between each paragraph and between each entry in the list of bibliographic references. Tables should preferably be placed in the same electronic file as the text. Authors should consult a recent issue of the Journal for table layout.

There is no need to spend time formatting your article so that the printout is visually attractive (e.g. by making headings bold or creating a page layout with figures), as most formatting instructions will be removed upon processing.

Manuscripts should be typewritten, typed on one side of the ISO A4 paper with at least 4cm margins and double spacing throughout. Every page of the manuscript, including the title page, references, tables, etc. should be numbered. However, no reference should be made to page numbers in the text; if necessary, one may refer to sections. Underline words that should be in italics, and do not underline any other words.

Authors are advised to use Times New Roman 12-point font. Be especially careful when you are inserting special characters, as those inserted in different fonts may be replaced by different characters when converted to PDF files. It is well known that 'µ' will be replaced by other characters when fonts such as 'Symbol' or 'Mincho' are used.

We recommend that authors prepare the text as a **Microsoft Word** file.

1. Manuscripts in general should be organised in the following order:

   o **Page 1: Running title.** (Not to exceed 60 characters, counting letters and spaces). This page should **only** contain your running title of your paper. In addition, the **Subject areas** most relevant to the study must be indicated on this page. Select one or two subject areas (refer to the *Scope Form).*
   A **list** of number of **black and white / colour figures and tables** should also be indicated on this page**.** Figures submitted in color will be printed in colour. See "*5. Figures & Photographs"* for details.

   o **Page 2: Author(s) and Corresponding author information.** This page should contain the **full title** of your paper with name(s) of all the authors, institutions and corresponding author's name, institution and full address (Street address, telephone number (including extension), hand phone number, fax number and e-mail address) for editorial correspondence. The names of the authors **must** be abbreviated following the international naming convention. e.g. Salleh, A.B., Tan, S.G., or Sapuan, S.M.

   Authors' addresses. Multiple authors with different addresses must indicate their respective addresses separately by superscript numbers:

   George Swan[1] and Nayan Kanwal[2]

[1]Department of Biology, Faculty of Science, Duke University, Durham, North Carolina, USA.
[2]Research Management Centre, Universiti Putra Malaysia, Serdang, Malaysia.

- o **Page 3**: This page should **repeat** the **full title** of your paper with only the **Abstract** (the abstract should be less than 250 words for a Regular Paper and up to 100 words for a Short Communication). **Keywords** must also be provided on this page (Not more than eight keywords in alphabetical order).
- o **Page 4 and subsequent pages**: This page should begin with the **Introduction** of your article and the rest of your paper should follow from page 5 onwards.

Abbreviations. Define alphabetically, other than abbreviations that can be used without definition. Words or phrases that are abbreviated in the introduction and following text should be written out in full the first time that they appear in the text, with each abbreviated form in parenthesis. Include the common name or scientific name, or both, of animal and plant materials.

Footnotes. Current addresses of authors if different from heading.

2. **Text.** Regular Papers should be prepared with the headings **Introduction**, **Materials and Methods**, **Results and Discussion, Conclusions** in this order. Short Communications should be prepared according to "*8. Short Communications.*" below.

3. **Tables.** All tables should be prepared in a form consistent with recent issues of *Pertanika* and should be numbered consecutively with Arabic numerals. Explanatory material should be given in the table legends and footnotes. Each table should be prepared on a separate page. (Note that when a manuscript is accepted for publication, tables must be submitted as data - .doc, .rtf, Excel or PowerPoint file- because tables submitted as image data cannot be edited for publication.)

4. **Equations and Formulae.** These must be set up clearly and should be typed triple spaced. Numbers identifying equations should be in square brackets and placed on the right margin of the text.

5. **Figures & Photographs.** Submit an original figure or photograph. Line drawings must be clear, with high black and white contrast. Each figure or photograph should be prepared on a separate sheet and numbered consecutively with Arabic numerals. Appropriate sized numbers, letters and symbols should be used, no smaller than 2 mm in size after reduction to single column width (85 mm), 1.5-column width (120 mm) or full 2-column width (175 mm). Failure to comply with these specifications will require new figures and delay in publication. For electronic figures, create your figures using applications that are capable of preparing high resolution TIFF files acceptable for publication. In general, we require **300 dpi or higher resolution for coloured and half-tone artwork** and **1200 dpi or higher for line drawings**. For review, you may attach low-resolution figures, which are still clear enough for reviewing, to keep the file of the manuscript under 5 MB. Illustrations may be produced at extra cost in colour at the discretion of the Publisher; the author could be charged Malaysian Ringgit 50 for each colour page.

6. **References.** Literature citations in the text should be made by name(s) of author(s) and year. For references with more than two authors, the name of the first author followed by 'et al.' should be used.

Swan and Kanwal (2007) reported that …
The results have been interpreted (Kanwal et al. 2009).

- o References should be listed in alphabetical order, by the authors' last names. For the same author, or for the same set of authors, references should be arranged chronologically. If there is more than one publication in the same year for the same author(s), the letters 'a', 'b', etc., should be added to the year.

- o When the authors are more than 11, list 5 authors and then et al.

- o Do not use indentations in typing References. Use one line of space to separate each reference. The name of the journal should be written in full. For example:
    - ▪ Jalaludin, S. (1997a). Metabolizable energy of some local feeding stuff. *Tumbuh, 1,* 21-24.
    - ▪ Jalaludin, S. (1997b). The use of different vegetable oil in chicken ration. *Malayan Agriculturist, 11,* 29-31.
    - ▪ Tan, S.G., Omar, M.Y., Mahani, K.W., Rahani, M., Selvaraj, O.S. (1994). Biochemical genetic studies on wild populations of three species of green leafhoppers *Nephotettix* from Peninsular Malaysia. *Biochemical Genetics*, *32,* 415 - 422.

- o In case of citing an author(s) who has published more than one paper in the same year, the papers should be distinguished by addition of a small letter as shown above, e.g. Jalaludin (1997a); Jalaludin (1997b).

- o Unpublished data and personal communications should not be cited as literature citations, but given in the text in parentheses. 'In press' articles that have been accepted for publication may be cited in References. Include in the citation the journal in which the 'in press' article will appear and the publication date, if a date is available.

7. **Examples of other reference citations**:
    Monographs: Turner, H.N. and Yong, S.S.Y. (2006). *Quantitative Genetics in Sheep Breeding*. Ithaca: Cornell University Press.

    Chapter in Book: Kanwal, N.D.S. (1992). Role of plantation crops in Papua New Guinea economy. In Angela R. McLean (Eds.), *Introduction of livestock in the Enga province PNG* (p. 221-250). United Kingdom: Oxford Press.

    Proceedings: Kanwal, N.D.S. (2001). Assessing the visual impact of degraded land management with landscape design software. In N.D.S. Kanwal and P. Lecoustre (Eds.), *International forum for Urban Landscape Technologies* (p. 117-127). Lullier, Geneva, Switzerland: CIRAD Press.

8. **Short Communications** should include **Introduction, Materials and Methods, Results and Discussion, Conclusions** in this order. Headings should only be inserted for Materials and Methods. The abstract should be up to 100 words, as stated above. Short Communications must be 5 printed pages or less, including all references, figures and tables. References should be less than 30. A 5 page paper is usually approximately 3000 words plus four figures or tables (if each figure or table is less than 1/4 page).

    *Authors should state the total number of words (including the Abstract) in the cover letter. Manuscripts that do not fulfill these criteria will be rejected as Short Communications without review.

STYLE OF THE MANUSCRIPT

Manuscripts should follow the style of the latest version of the Publication Manual of the American Psychological Association (APA). The journal uses British spelling and authors should therefore follow the latest edition of the Oxford Advanced Learner's Dictionary.

SUBMISSION OF MANUSCRIPTS

All articles submitted to the journal **must comply** with these instructions. Failure to do so will result in return of the manuscript and possible delay in publication.

The **four copies** of your original manuscript, four sets of photographic figures, as well as a CD with the **electronic copy in MS Word** (including text and figures) together with a **cover letter**, **declaration form**, **referral form A**, **scope form** need to be enclosed. They are available from the *Pertanika*'s home page at http://www.rmc.upm.edu.my/jPertanika/index.htm or from the Executive Editor's office upon request.

Please do **not** submit manuscripts directly to the editor-in-chief or to the UPM Press. All manuscripts must be **submitted through the executive editor's office** to be properly acknowledged and rapidly processed:

Dr. Nayan KANWAL
Executive Editor
Research Management Centre (RMC)
IDEA Tower II, UPM-MTDC Technology Centre
Universiti Putra Malaysia
43400 UPM, Serdang, Selangor, Malaysia
email: ndeeps@admin.upm.edu.my; tel: + 603-8947 1622

Authors should retain copies of submitted manuscripts and correspondence, as materials can not be returned.

Cover letter

All submissions must be accompanied by a cover letter detailing what you are submitting. Papers are accepted for publication in the journal on the understanding that the article is original and the content has not been published or submitted for publication elsewhere. This must be stated in the cover letter.

The cover letter must also contain an acknowledgement that all authors have contributed significantly, and that all authors are in agreement with the content of the manuscript.

The cover letter of the paper should contain (i) the title; (ii) the full names of the authors; (iii) the addresses of the institutions at which the work was carried out together with (iv) the full postal and email address, plus facsimile and telephone numbers of the author to whom correspondence about the manuscript should be sent. The present address of any author, if different from that where the work was carried out, should be supplied in a footnote.

As articles are double-blind reviewed, material that might identify authorship of the paper should be placed on a cover sheet.

Note When your manuscript is received at *Pertanika*, it is considered to be in its final form. Therefore, you need to check your manuscript carefully before submitting it to the executive editor (see also **English language editing** below).

Electronic copy

Preparation of manuscripts on a CD or DVD is preferable and articles should be prepared using MS Word. File name(s), the title of your article and authors of the article must be indicated on the CD. The CD must always be accompanied by four hard-copies of the article, and the content of the two must be identical. The CD text must be the same as that of the final refereed, revised manuscript. CDs formatted for IBM PC compatibles are preferred, as those formatted for Apple Macintosh are not acceptable. Please do not send ASCII files, as relevant data may be lost. Leave a blank line between each paragraph and between each entry in the list of bibliographic references. Tables should be placed in the same electronic file as the text. Authors should consult a recent issue of the Journal for table layout.

Peer review

In the peer-review process, three referees independently evaluate the scientific quality of the submitted manuscripts. The Journal uses a double-blind peer-review system. Authors are encouraged to indicate in **referral form A** the names of three potential reviewers, but the editors will make the final choice. The editors are not, however, bound by these suggestions.

Manuscripts should be written so that they are intelligible to the professional reader who is not a specialist in the particular field. They should be written in a clear, concise, direct style. Where contributions are judged as acceptable for publication on the basis of content, the Editor or the Publisher reserves the right to modify the typescripts to eliminate ambiguity and repetition and improve communication between author and reader. If extensive alterations are required, the manuscript will be returned to the author for revision.

The editorial review process

What happens to a manuscript once it is submitted to *Pertanika*? Typically, there are seven steps to the editorial review process:

1. The executive editor and the editorial board examine the paper to determine whether it is appropriate for the journal and should be reviewed. If not appropriate, the manuscript is rejected outright and the author is informed.

2. The executive editor sends the article-identifying information having been removed, to three reviewers. Typically, one of these is from the Journal's editorial board. Others are specialists in the subject matter represented by the article. The executive editor asks them to complete the review in three weeks and encloses two forms: (a) referral form B and (b) reviewer's comment form along with reviewer's guidelines. Comments to authors are about the appropriateness and adequacy of the theoretical or conceptual framework, literature review, method, results and discussion, and conclusions. Reviewers often include suggestions for strengthening of the manuscript. Comments to the editor are in the nature of the significance of the work and its potential contribution to the literature.

3. The executive editor, in consultation with the editor-in-chief, examines the reviews and decides whether to reject the manuscript, invite the author(s) to revise and resubmit the manuscript, or seek additional reviews. Final acceptance or rejection rests with the Editorial Board, who reserves the right to refuse any material for publication. In rare instances, the manuscript is accepted with almost no revision. Almost without exception, reviewers' comments (to the author) are forwarded to the author. If a revision is indicated, the editor provides guidelines for attending to the reviewers' suggestions and perhaps additional advice about revising the manuscript.

4. The authors decide whether and how to address the reviewers' comments and criticisms and the editor's concerns. The authors submit a revised version of the paper to the executive editor along with specific information describing how they have answered' the concerns of the reviewers and the editor.

5. The executive editor sends the revised paper out for review. Typically, at least one of the original reviewers will be asked to examine the article.

6. When the reviewers have completed their work, the executive editor in consultation with the editorial board and the editor-in-chief examine their comments and decide whether the paper is ready to be published, needs another round of revisions, or should be rejected.

7. If the decision is to accept, the paper is sent to that Press and the article should appear in print in approximately two to three months. The Publisher ensures that the paper adheres to the correct style (in-text citations, the reference list, and tables are typical areas of concern, clarity, and grammar). The authors are asked to respond to any queries by the Publisher. Following these corrections, page proofs are mailed to the corresponding authors for their final approval. At this point, only essential changes are accepted. Finally, the article appears in the pages of the Journal and is posted on-line.

English language editing

Authors are responsible for the linguistic accuracy of their manuscripts. Authors not fully conversant with the English language should seek advice from subject specialists with a sound knowledge of English. The cost will be borne by the author, and a copy of the certificate issued by the service should be attached to the cover letter.

Author material archive policy

Authors who require the return of any submitted material that is rejected for publication in the journal should indicate on the cover letter. If no indication is given, that author's material should be returned, the Editorial Office will dispose of all hardcopy and electronic material.

Contents